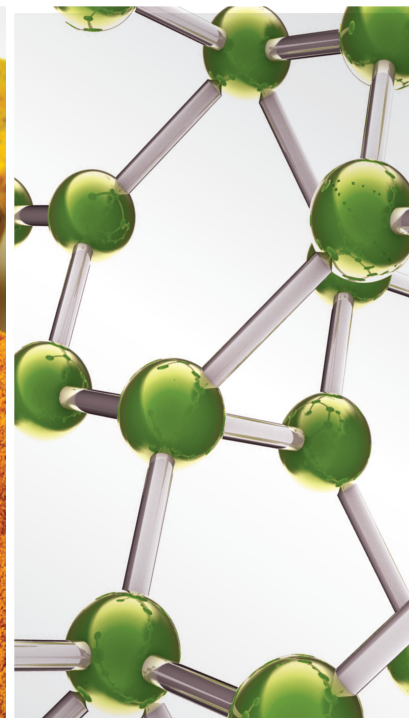# Treatment of Musculoskeletal Diseases with Chinese Medicine

Lead Guest Editor: Jun Jiang
Guest Editors: Chao Liang, Jiake Xu, and Jianping Chen

Treatment of Musculoskeletal Diseases with Chinese Medicine

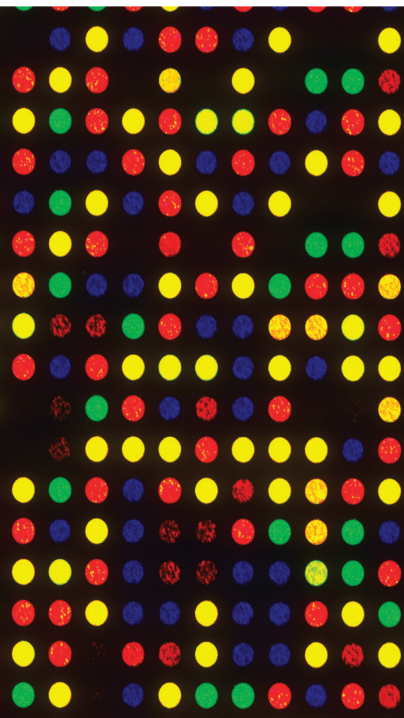# Treatment of Musculoskeletal Diseases with Chinese Medicine

Lead Guest Editor: Jun Jiang
Guest Editors: Chao Liang, Jiake Xu, and Jianping Chen

Arthur De Sá Ferreira (iD), Brazil
Nunziatina De Tommasi (iD), Italy
Marinella De leo (iD), Italy
Gourav Dey (iD), India
Dinesh Dhamecha, USA
Claudia Di Giacomo (iD), Italy
Antonella Di Sotto (iD), Italy
Mario Dioguardi, Italy
Jeng-Ren Duann (iD), USA
Thomas Efferth (iD), Germany
Abir El-Alfy, USA
Mohamed Ahmed El-Esawi (iD), Egypt
Mohd Ramli Elvy Suhana, Malaysia
Talha Bin Emran, Japan
Roger Engel (iD), Australia
Karim Ennouri (iD), Tunisia
Giuseppe Esposito (iD), Italy
Tahereh Eteraf-Oskouei, Iran
Robson Xavier Faria (iD), Brazil
Mohammad Fattahi (iD), Iran
Keturah R. Faurot (iD), USA
Piergiorgio Fedeli (iD), Italy
Laura Ferraro (iD), Italy
Antonella Fioravanti (iD), Italy
Carmen Formisano (iD), Italy
Hua-Lin Fu (iD), China
Liz G Müller (iD), Brazil
Gabino Garrido (iD), Chile
Safoora Gharibzadeh, Iran
Muhammad N. Ghayur (iD), USA
Angelica Gomes (iD), Brazil
Elena González-Burgos, Spain
Susana Gorzalczany (iD), Argentina
Jiangyong Gu (iD), China
Maruti Ram Gudavalli (iD), USA
Jian-You Guo (iD), China
Shanshan Guo, China
Narcís Gusi (iD), Spain
Svein Haavik, Norway
Fernando Hallwass, Brazil
Gajin Han (iD), Republic of Korea
Ihsan Ul Haq, Pakistan
Hicham Harhar (iD), Morocco
Mohammad Hashem Hashempur (iD), Iran
Muhammad Ali Hashmi (iD), Pakistan

Waseem Hassan (iD), Pakistan
Sandrina A. Heleno (iD), Portugal
Pablo Herrero (iD), Spain
Soon S. Hong (iD), Republic of Korea
Md. Akil Hossain (iD), Republic of Korea
Muhammad Jahangir Hossen (iD), Bangladesh
Shih-Min Hsia (iD), Taiwan
Changmin Hu (iD), China
Tao Hu (iD), China
Weicheng Hu (iD), China
Wen-Long Hu, Taiwan
Xiao-Yang (Mio) Hu, United Kingdom
Sheng-Teng Huang (iD), Taiwan
Ciara Hughes (iD), Ireland
Attila Hunyadi (iD), Hungary
Liaqat Hussain (iD), Pakistan
Maria-Carmen Iglesias-Osma (iD), Spain
Amjad Iqbal (iD), Pakistan
Chie Ishikawa (iD), Japan
Angelo A. Izzo, Italy
Satveer Jagwani (iD), USA
Rana Jamous (iD), Palestinian Authority
Muhammad Saeed Jan (iD), Pakistan
G. K. Jayaprakasha, USA
Kyu Shik Jeong, Republic of Korea
Leopold Jirovetz (iD), Austria
Jeeyoun Jung (iD), Republic of Korea
Nurkhalida Kamal (iD), Saint Vincent and the Grenadines
Atsushi Kameyama (iD), Japan
Kyungsu Kang, Republic of Korea
Wenyi Kang (iD), China
Shao-Hsuan Kao (iD), Taiwan
Nasiara Karim (iD), Pakistan
Morimasa Kato (iD), Japan
Kumar Katragunta (iD), USA
Deborah A. Kennedy (iD), Canada
Washim Khan, USA
Bonglee Kim (iD), Republic of Korea
Dong Hyun Kim (iD), Republic of Korea
Junghyun Kim (iD), Republic of Korea
Kyungho Kim, Republic of Korea
Yun Jin Kim (iD), Malaysia
Yoshiyuki Kimura (iD), Japan

Nebojša Kladar, Serbia
Mi Mi Ko, Republic of Korea
Toshiaki Kogure, Japan
Malcolm Koo, Taiwan
Yu-Hsiang Kuan, Taiwan
Robert Kubina, Poland
Chan-Yen Kuo, Taiwan
Kuang C. Lai, Taiwan
King Hei Stanley Lam, Hong Kong
Fanuel Lampiao, Malawi
Ilaria Lampronti, Italy
Mario Ledda, Italy
Harry Lee, China
Jeong-Sang Lee, Republic of Korea
Ju Ah Lee, Republic of Korea
Kyu Pil Lee, Republic of Korea
Namhun Lee, Republic of Korea
Sang Yeoup Lee, Republic of Korea
Ankita Leekha, USA
Christian Lehmann, Canada
George B. Lenon, Australia
Marco Leonti, Italy
Hua Li, China
Min Li, China
Xing Li, China
Xuqi Li, China
Yi-Rong Li, Taiwan
Vuanghao Lim, Malaysia
Bi-Fong Lin, Taiwan
Ho Lin, Taiwan
Shuibin Lin, China
Kuo-Tong Liou, Taiwan
I-Min Liu, Taiwan
Suhuan Liu, China
Xiaosong Liu, Australia
Yujun Liu, China
Emilio Lizarraga, Argentina
Monica Loizzo, Italy
Nguyen Phuoc Long, Republic of Korea
Zaira López , Mexico
Chunhua Lu, China
Ângelo Luís, Portugal
Anderson Luiz-Ferreira, Brazil
Ivan Luzardo Luzardo-Ocampo, Mexico

Michel Mansur Machado, Brazil
Filippo Maggi, Italy
Juraj Majtan, Slovakia
Toshiaki Makino, Japan
Nicola Malafronte, Italy
Giuseppe Malfa, Italy
Francesca Mancianti, Italy
Carmen Mannucci, Italy
Juan M. Manzaneque, Spain
Fatima Martel, Portugal
Carlos H. G. Martins, Brazil
Maulidiani Maulidiani, Malaysia
Andrea Maxia, Italy
Avijit Mazumder, India
Isac Medeiros, Brazil
Ahmed Mediani, Malaysia
Lewis Mehl-Madrona, USA
Ayikoé Guy Mensah-Nyagan, France
Oliver Micke, Germany
Maria G. Miguel, Portugal
Luigi Milella, Italy
Roberto Miniero, Italy
Letteria Minutoli, Italy
Prashant Modi, India
Daniel Kam-Wah Mok, Hong Kong
Changjong Moon, Republic of Korea
Albert Moraska, USA
Mark Moss, United Kingdom
Yoshiharu Motoo, Japan
Yoshiki Mukudai, Japan
Sakthivel Muniyan, USA
Saima Muzammil, Pakistan
Benoit Banga N'guessan, Ghana
Massimo Nabissi, Italy
Siddavaram Nagini, India
Takao Namiki, Japan
Srinivas Nammi, Australia
Krishnadas Nandakumar, India
Vitaly Napadow, USA
Edoardo Napoli, Italy
Jorddy Neves Cruz, Brazil
Marcello Nicoletti, Italy
Eliud Nyaga Mwaniki Njagi, Kenya
Cristina Nogueira, Brazil

Sakineh Kazemi Noureini, Iran
Rômulo Dias Novaes, Brazil
Martin Offenbaecher, Germany
Oluwafemi Adeleke Ojo, Nigeria
Olufunmiso Olusola Olajuyigbe, Nigeria
Luís Flávio Oliveira, Brazil
Mozaniel Oliveira, Brazil
Atolani Olubunmi, Nigeria
Abimbola Peter Oluyori, Nigeria
Timothy Omara, Austria
Chiagoziem Anariochi Otuechere, Nigeria
Sokcheon Pak, Australia
Antônio Palumbo Jr, Brazil
Zongfu Pan, China
Siyaram Pandey, Canada
Niranjan Parajuli, Nepal
Gunhyuk Park, Republic of Korea
Wansu Park, Republic of Korea
Rodolfo Parreira, Brazil
Mohammad Mahdi Parvizi, Iran
Luiz Felipe Passero, Brazil
Mitesh Patel, India
Claudia Helena Pellizzon, Brazil
Cheng Peng, Australia
Weijun Peng, China
Sonia Piacente, Italy
Andrea Pieroni, Italy
Haifa Qiao, USA
Cláudia Quintino Rocha, Brazil
DANIELA RUSSO, Italy
Muralidharan Arumugam Ramachandran,
Singapore
Manzoor Rather, India
Miguel Rebollo-Hernanz, Spain
Gauhar Rehman, Pakistan
Daniela Rigano, Italy
José L. Rios, Spain
Francisca Rius Diaz, Spain
Eliana Rodrigues, Brazil
Maan Bahadur Rokaya, Czech Republic
Mariangela Rondanelli, Italy
Antonietta Rossi, Italy
Mi Heon Ryu, Republic of Korea
Bashar Saad, Palestinian Authority
Sabiu Saheed, South Africa

Mohamed Z.M. Salem, Egypt
Avni Sali, Australia
Andreas Sandner-Kiesling, Austria
Manel Santafe, Spain
José Roberto Santin, Brazil
Tadaaki Satou, Japan
Roland Schoop, Switzerland
Sindy Seara-Paz, Spain
Veronique Seidel, United Kingdom
Vijayakumar Sekar, China
Terry Selfe, USA
Arham Shabbir, Pakistan
Suzana Shahar, Malaysia
Wen-Bin Shang, China
Xiaofei Shang, China
Ali Sharif, Pakistan
Karen J. Sherman, USA
San-Jun Shi, China
Insop Shim, Republic of Korea
Maria Im Hee Shin, China
Yukihiro Shoyama, Japan
Morry Silberstein, Australia
Samuel Martins Silvestre, Portugal
Preet Amol Singh, India
Rajeev K Singla, China
Kuttulebbai N. S. Sirajudeen, Malaysia
Slim Smaoui, Tunisia
Eun Jung Sohn, Republic of Korea
Maxim A. Solovchuk, Taiwan
Young-Jin Son, Republic of Korea
Chengwu Song, China
Vanessa Steenkamp, South Africa
Annarita Stringaro, Italy
Keiichiro Sugimoto, Japan
Valeria Sulsen, Argentina
Zewei Sun, China
Sharifah S. Syed Alwi, United Kingdom
Orazio Taglialatela-Scafati, Italy
Takashi Takeda, Japan
Gianluca Tamagno, Ireland
Hongxun Tao, China
Jun-Yan Tao, China
Lay Kek Teh, Malaysia
Norman Temple, Canada

Kamani H. Tennekoon, Sri Lanka
Seong Lin Teoh, Malaysia
Menaka Thounaojam, USA
Jinhui Tian, China
Zipora Tietel, Israel
Loren Toussaint, USA
Riaz Ullah, Saudi Arabia
Philip F. Uzor, Nigeria
Luca Vanella, Italy
Antonio Vassallo, Italy
Cristian Vergallo, Italy
Miguel Vilas-Boas, Portugal
Aristo Vojdani, USA
Yun WANG, China
QIBIAO WU, Macau
Abraham Wall-Medrano, Mexico
Chong-Zhi Wang, USA
Guang-Jun Wang, China
Jinan Wang, China
Qi-Rui Wang, China
Ru-Feng Wang, China
Shu-Ming Wang, USA
Ting-Yu Wang, China
Xue-Rui Wang, China
Youhua Wang, China
Kenji Watanabe, Japan
Jintanaporn Wattanathorn, Thailand
Silvia Wein, Germany
Katarzyna Winska, Poland
Sok Kuan Wong, Malaysia
Christopher Worsnop, Australia
Jih-Huah Wu, Taiwan
Sijin Wu, China
Xian Wu, USA
Zuoqi Xiao, China
Rafael M. Ximenes, Brazil
Guoqiang Xing, USA
JiaTuo Xu, China
Mei Xue, China
Yong-Bo Xue, China
Haruki Yamada, Japan
Nobuo Yamaguchi, Japan
Junqing Yang, China
Longfei Yang, China

Mingxiao Yang, Hong Kong
Qin Yang, China
Wei-Hsiung Yang, USA
Swee Keong Yeap, Malaysia
Albert S. Yeung, USA
Ebrahim M. Yimer, Ethiopia
Yoke Keong Yong, Malaysia
Fadia S. Youssef, Egypt
Zhilong Yu, Canada
RONGJIE ZHAO, China
Sultan Zahiruddin, USA
Armando Zarrelli, Italy
Xiaobin Zeng, China
Y Zeng, China
Fangbo Zhang, China
Jianliang Zhang, China
Jiu-Liang Zhang, China
Mingbo Zhang, China
Jing Zhao, China
Zhangfeng Zhong, Macau
Guoqi Zhu, China
Yan Zhu, USA
Suzanna M. Zick, USA
Stephane Zingue, Cameroon

Contents

Hindawi

Research Article

Elaborate the Mechanism of Ancient Classic Prescriptions (Erzhi Formula) in Reversing GIOP by Network Pharmacology Coupled with Zebrafish Verification

Zhihui Cai [iD],[1] **Huajun Wang** [iD],[2] **Jun Jiang** [iD],[1] **Shichang Xiao** [iD],[1] **Jianpeng Xiao** [iD],[1] **Jinjin He** [iD],[1] **Zihan Zhao** [iD],[1] and **Jiangning Yin** [iD][3]

[1]*School of Pharmacy, Jiangsu University, No. 301 Xuefu Road, Zhenjiang, Jiangsu 212013, China*
[2]*Affiliated Hospital of Jiangsu University, No. 438 Jiefang Road, Zhenjiang, Jiangsu 212001, China*
[3]*The Affiliated Jiangning Hospital of Nanjing Medical University, Nanjing, Jiangsu 211100, China*

Correspondence should be addressed to Jun Jiang; jiangjuntcm2007@hotmail.com and Jiangning Yin; jsyinjn@163.com

Academic Editor: Shagufta Perveen

Osteoporosis is a degenerative disease that endangers human health. At present, chemical drugs used for osteoporosis have serious side effects. Therefore, it is valuable to search herbs with high safety and good curative effect in antiosteoporosis. Erzhi formula (EZF), an ancient classic compound, has been reported to have a beneficial effect in antiosteoporosis, but its mechanism is unclear. In this paper, the active compounds of EZF were found in Systems Pharmacology Database, and gene targets related to osteoporosis were obtained in GeneCards. The GO functional and KEGG pathway enrichment analysis were performed by Metascape. The network of "components-targets-signal pathway" was constructed by Cytoscape. Next, molecular docking between the active components and hub genes related to the PI3K-Akt signaling pathway was conducted by Autodock. In the verification experiment, the zebrafish induced by prednisolone (PNSL) was used to reproduce glucocorticoid-induced osteoporosis (GIOP) model, and then the reversal effects of EZF were systematically evaluated according to the behavior, skull staining area, bone mineralization area (BMA), average optical density (AOD), and cumulative optical density (COD). Finally, it was shown that 24 components in EZF could regulate 39 common gene targets to exert antiosteoporosis effect. Besides, the main regulatory mechanisms of EZF were 4 signaling pathways: PI3K-Akt, JAK-STAT, AGE-RAGE, and cancer pathway. In PI3K-Akt signaling pathway, wedelolactone, dimethyl wedelolactone, specnuezhenide, ursolic acid, acacetin, beta-sitosterol, apigenin, and kaempferol can bind tightly with EGF, IL-2, and IL-4 genes. Compared with the model group, the moving distance, swimming speed, and cumulative swimming time of zebrafish in EZF group were significantly increased ($P < 0.05$). Meanwhile, the BMA and COD of zebrafish were significantly improved after the intervention of EZF ($P < 0.05$). In summary, the 24 components of EZF exert their antiosteoporosis effects by regulating 39 related gene targets, among which the PI3K signaling pathway is crucial. EZF can promote bone formation and reversed GIOP through "multicomponent/multitarget/multipathway" and the medium dose of EZF may be the most suitable concentration for the treatment of GIOP in zebrafish model.

1. Introduction

Osteoporosis is a silent disorder characterized by reduced bone density and structural deterioration [1], which is caused by the change of bone microstructure and makes patients vulnerable to have brittle fractures. Osteoporosis leads to a remarkable decrease of life quality and increases the mortality and disability rate at the same time. According to the World Health Organization (WHO), more than 200 million people are affected worldwide, and it is more prevalent in postmenopausal women, with about 25 to 30 percent prevalence in the United States and Europe [2]. It is a chronic condition that affects one in three women and one in five men over the age of 50 [3]. Glucocorticoids (GCs) are widely used in chronic noninfectious inflammatory diseases, allergic diseases, and organ transplantation. Even

physiological doses of GCs can cause bone loss, so osteoporosis is one of the most serious side effects of GCs. Generally, this kind of osteoporosis caused by long-term use of GCs is called glucocorticoid-induced osteoporosis (GIOP) [4, 5], which may lead to up to 20% of osteoporosis cases [6]. Generally, it develops in a time-dose-dependent manner, and an increased risk of brittle fractures may be observed within the first month of treatment even at low (<2.5 mg prednisone equivalent) GC daily dose [7]. Published guidelines for the treatment of patients with chronic GCs recommend calcium and vitamin D supplementation, bone mineral density testing, and bisphosphonate therapy [8–10]. However, according to the guidelines for treating GIOP, even if it is treated with the recommended drugs, patients may face the threat of systemic calcium loss, erosive esophagitis, ulcer bleeding, hypocalcemia, decline of renal function, jaw necrosis, or atypical femoral fracture caused by reduced gastrointestinal absorption and renal tubular reabsorption [11–13]. In conclusion, it is urgent to find a relatively safe and effective drug for the treatment of GIOP.

As a well-known formula in China, EZF is mixed of *Fructus Ligustri Lucidi* (FLL) and *Ecliptae herba* (EP) with a ratio of 1 : 1. It has been commonly used for treating menopausal diseases. FLL was first recorded in "The Medical Focus Explanation" in the Qing Dynasty [14]. FLL is the fruit of *Ligustrum lucidum* Ait., which is commonly used to nourish liver and kidney system, improve eyesight, and strengthen muscles and bones in Chinese medicine. EP, the dry aerial part of *Eclipta prostrata* L., has been widely used since ancient times to nourish the liver and kidney, strengthen teeth, darken hair and beard [15, 16]. There have been many studies on EZF in the remedy of GIOP. For example, Yang et al. reported that the combination of EZF and Epimedium can significantly prevent glucocorticoid-induced bone loss, increase the content of BMP-2 which is the bone formation marker, reduce serum TRACP, and inhibit bone resorption [12, 13]. What is more, EZF, as an ancient classic prescription for chronic diseases like GIOP, has been playing an undeniable role since ancient times. Therefore, the advantages of EZF in the treatment of GIOP are not only reflected in its safety and effectiveness but also reflected in the excavation and inheritance of effective classic prescriptions. However, the relationship among its pharmacological effects, therapeutic targets, and signaling pathways for GIOP remains unclear, which limits the wide use of EZF in clinical practice.

Chinese materia medica is a complex system of multi-component, multitarget, and synergistic action among components. Clearly explaining the relationship among these components, targets, and pathways is a hot and difficult problem all the time. Fortunately, network pharmacology, which has been continuously improved and developed since Li's first proposal [17, 18], is a new discipline that systematically reveals the action of Chinese medicine on human body and predicts the potential mechanism by constructing the complex network of "drug-active ingredients-gene targets-disease" [19]. The greatest advantage of the development and application of this technology is that the "network" combines the evaluation of network topology and dynamics, so as to provide visual analysis of complex drug components of EZF [20]. In conclusion, network pharmacology can be applied to the research on the potential mechanism of EZF for GIOP, which provides a new perspective and strategy for the research of ancient classic prescriptions. Besides, zebrafish is a full sequence model organism with highly conserved innate immune system, including cell types and signaling molecules [21]. The advantages of zebrafish such as optical clarity, development speed, and fertility make it a popular vertebrate model for developmental biology research and animal model for studying disease processes [22]; in particular, its bone morphology can be observed directly by staining. In this paper, a network-pharmacology approach was followed to explore the antiosteoporotic mechanism of EZF, and then the medicinal efficacy was confirmed by zebrafish model.

2. Materials and Methods

2.1. Screening Active Components and Corresponding Targets. Active ingredients of EZF were searched based on Traditional Chinese Medicine Systems Pharmacology Database and Analysis Platform (TCMSP, http://tcmspw.com/tcmsp. php, PubChem, https://pubchem.ncbi.nlm.nih.gov, and SwissTargetPrediction database, http://www. swisstargetprediction.ch). Notably, the screening conditions in TCMSP were oral bioavailability (OB) ≥ 30% and drug-likeness (DL) ≥ 0.18 [23]. Immediately, the corresponding drug targets were searched according to the captured active ingredients. Finally, the target proteins reviewed in human were transformed into gene symbols by UniProt database (https://www.uniprot.org/) [24].

2.2. Collection of Osteoporosis-Related Targets. The collection of disease genes depends on the utilization of GeneCards database (https://www.genecards.org/) [25]. "Osteoporosis" and "glucocorticoid osteoporosis" were set as key words in the database and their related targets were obtained.

2.3. Screening the Common Targets between Drug and Disease. The function of COUNTIF was used to capture the common targets between genes related to active components in EZF and the disease target genes of osteoporosis. Then, we imported the common targets into the Bioinformatics platform (bioinformatics.com.cn) [26]. Lastly, a Venn diagram of the EZF-GIOP-related targets was obtained successfully.

2.4. Protein-Protein Interaction (PPI) Network Construction and Hub Gene Screening. PPI is composed of proteins through their interactions to participate in various links of life processes such as biological signal transmission, gene expression regulation, and energy and material metabolism [27]. The STRING database (https://string-db.org) was used to perform a PPI network analysis based on the common targets obtained [28]. The species was limited to "*Homo sapiens*" with parameter of moderate confidence greater than 0.4. Then we obtained a network of PPI. Next, TSV files were

imported into CytoHubba, which is the plug-in unit in Cytoscape (3.6.0). One of the CytoHubba algorithms (Degree, Maximal Clique Centrality (MCC), Clustering Coefficient, Density of Maximum Neighborhood Component (DMNC), BottleNeck, Maximum Neighborhood Component (MNC), Radiality, Edge Percolated Component (EPC), Eccentricity, Closeness, Betweenness, and Stress) was used to find the top 10 hub genes.

2.5. Enrichment Analysis. The enrichment analysis mainly included two parts: Gene Ontology (GO) functional enrichment and the Kyoto Encyclopedia of Genes and Genomes (KEGG) pathway enrichment. Before using Metascape platform (http://metascape.org/gp/index.html#/main/step1) for analysis [29], it is also necessary to import common targets into the "Multiple Gene List" and then click "Custom Analysis." GO functional enrichment analysis contains biological process (BP), cellular component (CC), and molecular function (MF) [30]. Moreover, the top 16 signaling pathways are significantly related to drug disease selected from the results of KEGG enrichment analysis [31].

2.6. Construction of the Network of "Active Components-Gene Targets-Disease". Two Excel files named "Network" and "Type" should be established, respectively, before analysis. Next, the two files were imported into the Cytoscape 3.6. 0 software successively [32]. Finally, the "active components-gene targets-disease" network [33] was successfully constructed by Cytoscape.

2.7. Molecular Docking Verification. On the one hand, we obtained the active components' structure from PunChem website (https://pubchem.ncbi.nlm.nih.gov) and saved it in SDF form. Then we used ChemBio3D software to minimize the binding energy and converted it into 3D structure. On the other side, the protein structures of hub genes were found from PDB database (https://www.rcsb.org/search) and saved as PDB structure. Hydrogenation of proteins and small molecular ligands was performed with PyMOL. Finally, Autodock Vina was used for molecular docking and calculating the binding energy [34].

2.8. Experimental Animals. The wild type AB strain zebrafish embryo with 3 days post fertilization (3 DPF) was supplied by Yi Shu Li Hua company (Nanjing, China) and maintained according to standard conditions (14 : 10 h light/dark cycle at 28°C) [35]. Animal experiments were conducted in accordance with the Guidelines for Animal Experiments of Jiangsu University and approved by the Animal Ethics Committee.

2.9. Preparation of EZF. Firstly, the EP and FLL were crushed, respectively, and passed through a 60-mesh sieve, and then they were mixed according to the ratio of 1 : 1 to prepare EZF. The mixture was refluxed with 10 times ethanol (50%) twice for 1 hour each time, and the two filtrates were combined. After refluxing, the collected extracts were evaporated in a rotary evaporator until there was no alcohol. Lastly, samples were lyophilized in a freeze dryer.

2.10. Animal Grouping and Intervention. Zebrafish embryos with normal morphology were placed in incubator and cultured in 6-well plate containing E_3 culture medium. The culture environment was maintained at 14 h/10 h light/dark cycle, and the room temperature was controlled at 28.5 ± 0.5°C. After 3 days post fertilization (3 DPF), the zebrafish larvae were divided into seven groups: blank control group (E_3), blank DMSO group ($E_3 + 0.5\%$ DMSO), model group ($E_3 + 0.5\%$ DMSO + 25 μM PNSL), EZF low-dose group ($E_3 + 0.5\%$ DMSO + 25 μM PNSL+ 0.1 μg/mL EZF), EZF medium-dose group ($E_3 + 0.5\%$ DMSO + 25 μM PNSL + 1.0 μg/mL EZF), EZF high-dose group ($E_3 + 0.5\%$ DMSO + 25 μM PNSL + 10.0 μg/mL EZF), and positive control group (PC, $E_3 + 0.5\%$ DMSO + 25 μM PNSL+ 15 μM etidronate disodium) randomly ($n = 15$). The specific culture and administration methods were shown in the previous published article [36].

2.11. Observation of Behavior and Bone Mineralization. The groups of zebrafish mentioned above were placed in 6-well plates with 6 fish per hole, and then the data of swimming behavior of zebrafish were recorded and analyzed by animal behavior analyzer. After 10 DPF, zebrafish were anesthetized with MS-222 solution, fixed with 4% paraformaldehyde solution, and dyed with Alizarin Red S. The final step of pretreatment was bleaching and decolorizing [37]. Lastly, the bone staining of zebrafish was observed under the microscope. All zebrafish samples were stored in glycerin solution. After obtaining the image of the ventral side of the skull by microscope, BMA, AOD, and COD of zebrafish skull were quantitatively analyzed by ImageJ software.

2.12. Statistical Analysis. All data were presented as the mean $\pm$ SD and statistically analyzed with statistical software SPSS 19.0 (SPSS, Inc., Chicago, IL). One-way analysis of variance was used for difference analysis, and $P < 0.05$ was considered as significant difference. [38].

3. Results

3.1. Common Targets between "Active Ingredients" and "Osteoporosis". 53 active compounds of EZF were obtained in TCMSP, and their 266 corresponding gene symbols were found. Furthermore, 1276 gene symbols related to the prevention of osteoporosis were acquired from GeneCards database. Venn analysis was used to obtain the common gene targets of "active ingredients" and "glucocorticoid osteoporosis," as shown in Figure 1. Finally, the 24 screened out chemical components corresponding to 39 gene targets of EZF are given in Table 1. The results showed that EZF could regulate 39 of the related targets to intervene in osteoporosis.
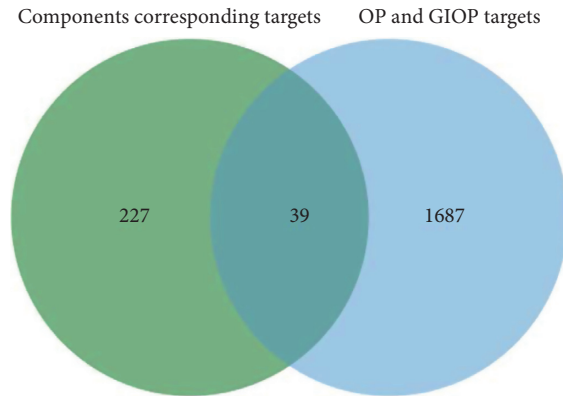
FIGURE 1: Venn diagram of drug targets and disease common targets.

TABLE 1: Chemical components corresponding to gene targets of EZF.

Source	Chemical components	Gene targets
FLL	Luteolin	IL10, RB1, JUN, TOP1, ICAM1, IL2, TYR, IFNG, IL4, INSR, MET
FLL	Apigenin	F7, Bcl-2, PLAU, RB1, JUN, ODC1, IGF1R, ICAM1, IL2, IFNG, IL4, INSR, ALPI
FLL	Alpha-humulene	REN
FLL	Quercetin	F7, Bcl-2, PLAU, IL10, EGF, RB1, JUN, ELK1, ODC1, TOP1, STAT1, CYP1A2, F3, CYP1A1, ICAM1, VCAM1, NOS3, IL2, CYP1B1, PLAT, IFNG, MPO, INSR, IRF1
FLL	Geraniol	HMGCR
FLL	Hydroxytyrosol	PLAU, STAT1, IRF1
FLL	Caffeic acid	PLAU, CYP1A1
FLL	Eugenol	PLAU, CYP1A1, CYP1B1
FLL	Oleanolic acid	ICAM1
FLL	Beta-sitosterol	Bcl-2, JUN
FLL	Daidzein	JUN, NOS3, LDLR, CAT, IGF1R, STAT1, ICAM1, APOB, VCAM1, NOS3, ECE1, IL4, GH1, GHR
FLL	Kaempferol	NOS3, F7, Bcl-2, JUN, STAT1, CYP1A2, CYP1A1, ICAM1, VCAM1, CYP1B1, INSR
FLL	Ursolic acid	PLAU, Bcl-2, JUN, ICAM1, CREB1, NOS3
FLL	DBP	GSK-3β
FLL	Salidroside	Bcl-2
FLL	Taxifolin	ICAM1, APOB
FLL	Lucidumoside D_qt (灵芝苷)	NOS3, GSK-3β
FLL	Oleoside dimethyl ester_qt (油苷二甲酯)	NOS3
FLL	Specnuezhenide	IL2, TYR
EP	Acacetin	NOS3, Bcl-2
EP	3′-O-Methylorobol (3′-O-甲酚)	GSK-3β, NOS3
EP	Pratensein (红三叶草素)	NOS3, GSK-3β
EP	Demethyl wedelolactone (去甲基蟛蜞菊内酯)	GSK-3β
EP	Wedelolactone (蟛蜞菊内酯)	GSK-3β

3.2. PPI Network and Hub Gene. 39 common targets were imported into the STRING website to obtain the interaction relationships with each other. As shown in Figure 2(a), we can get a PPI network diagram by setting parameters. The nodes represent proteins and edges represent protein-protein associations, from which we can learn that there are 39 nodes and 187 edges and the average node degree is 9.59. Using CytoHubba plug-in of Cytoscape, the top 10 core target genes were selected through MCC algorithm calculation (Figure 2(b) and Table 2).

3.3. GO and KEGG Pathway Enrichment Analysis. 39 EZF-GIOP related targets were imported into metascape, and then the results of KEGG pathway analysis and GO-MF, GO-BP, and GO-CC analysis were obtained one by one. According to the results, EZF could regulate GIOP through several signaling pathways, such as PI3K-Akt, cancer, JAK-STAT, AGE-RAGE, HTLV-I infection, Hepatitis C, Epstein-Barr virus infection, ovarian steroidogenesis, C-type lectin receptor, FOXO, complement and coagulation cascades, transcriptional misregulation in cancer, insulin resistance,

(a)

(b)
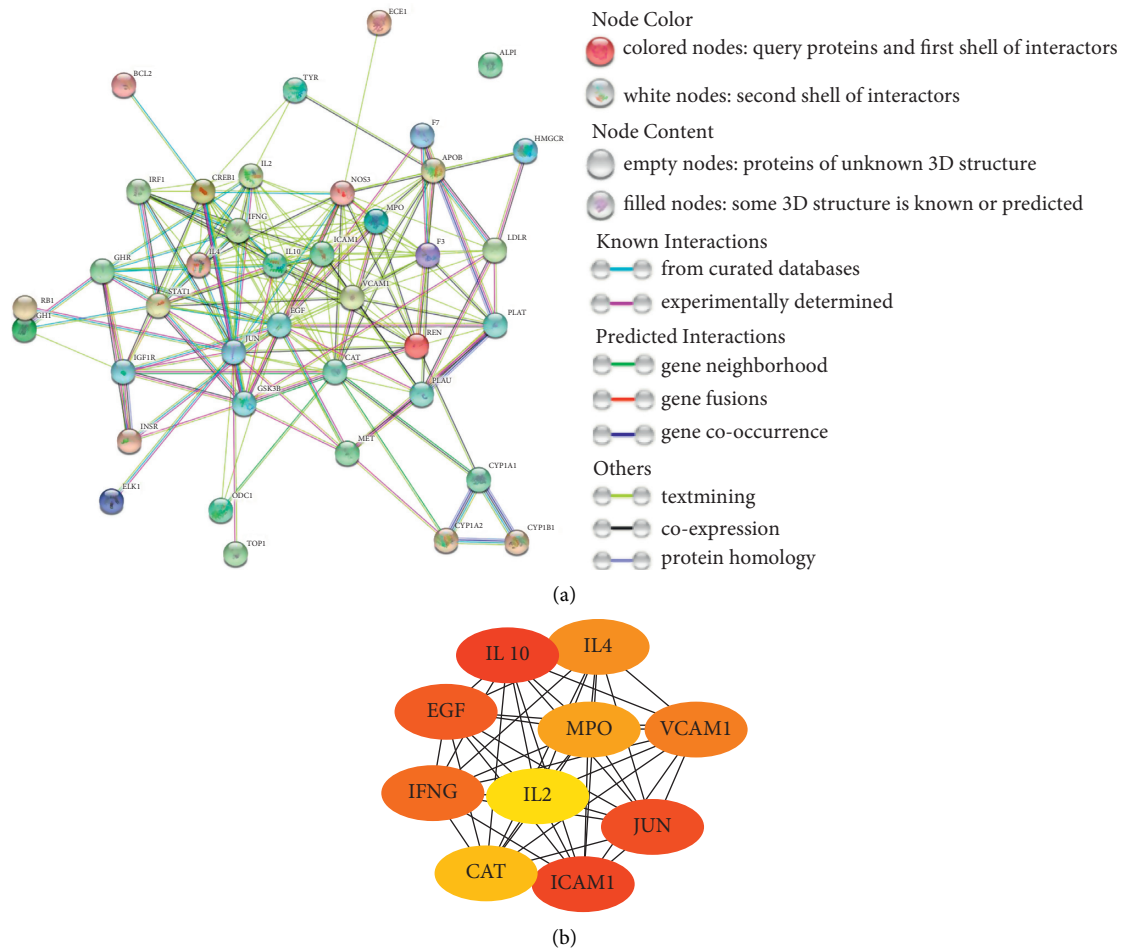
FIGURE 2: Protein-protein interaction (PPI) network and top 10 hub genes. (a) Protein-protein interaction (PPI) network; (b) top 10 hub genes selected by MCC method.

TABLE 2: Top 10 hub genes ranked by MCC method.

Rank	Name	Score
1	IL10	1146366
2	ICAM1	1140888
3	JUN	1135839
4	EGF	1056786
5	IFNG	1049040
6	VCAM1	979608
7	IL4	974160
8	MPO	897120
9	CAT	856930
10	IL2	605522

cushing syndrome, renal cell carcinoma, and microRNAs in cancer. In addition, the main signaling pathways were PI3K-Akt and pathways in cancer, JAK-STAT, and AGE-RAGE (Figure 3).

Interestingly, GO-BP analysis showed that EZF regulated biological process to treat GIOP including response to inorganic substance, reactive oxygen species biosynthetic process, JAK-STAT cascade, response to nutrient levels, response to peptide, positive regulation of cell migration, and response to lipopolysaccharide (Figure 4). Besides, GO-

MF analysis manifested that EZF regulated the molecular functions of heme binding and peptide hormone binding as shown in Figure 5. GO-CC analysis indicated that the regulation of the external side of plasma membrane, lytic vacuole, and receptor complex were beneficial to the therapeutic effect of EZF (Figure 6).

3.4. Network of "Chemical Components-Target Genes-Signaling Pathways". In order to elucidate the internal relationship between the chemical components, key targets, and signaling pathways of EZF clearly, the Cytoscape 3.6.0 software was successfully used to establish the "chemical components-target genes-signaling pathways" network (Figure 7).

PI3k-Akt signaling pathway played an important role in cell signal transduction and metabolism [39]. Protein kinase B (PKB), also known as Akt, was a serine/threonine kinase [40] which protected cells from apoptosis followed by activating PI3K. Moreover, PI3K-Akt signaling pathway could reduce osteoblast apoptosis and prevent osteoporosis by antagonizing oxidative stress [41–43]. This result showed that there were 17 active components in EZF which acted on PI3K-Akt pathway
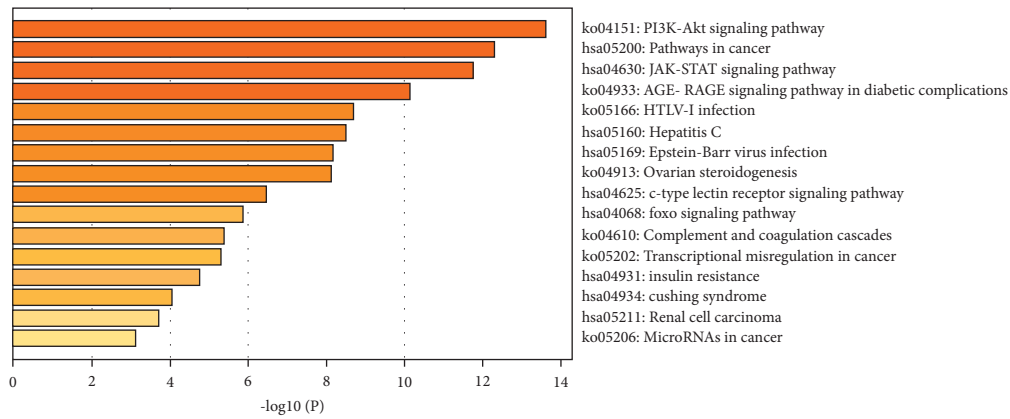
FIGURE 3: KEGG enrichment analysis for signal pathways. The *y*-axis shows top significantly enriched KEGG categories, and the *x*-axis displays the number of enrichment genes of these terms ($P < 0.05$), and the color represents the adjusted *P* value; the redder, the more significant the enrichment. The height of the column is related to *P* value. The higher the column is, the more significant the enrichment is.
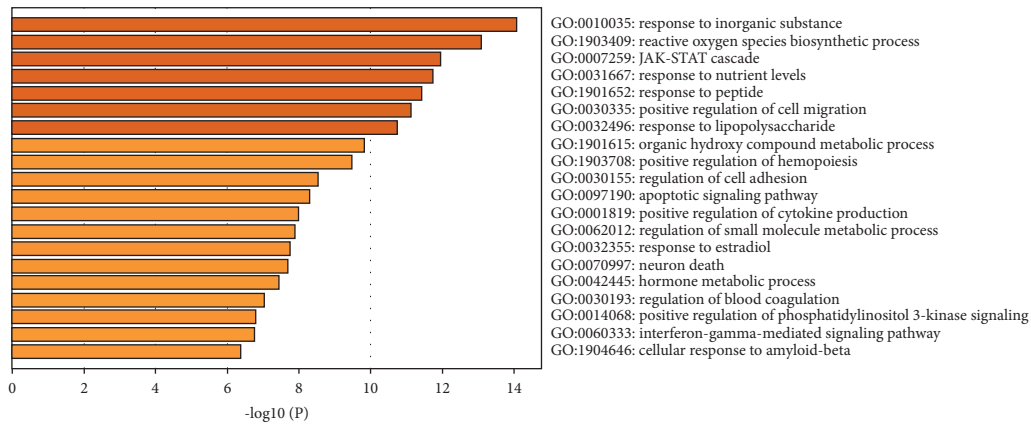
FIGURE 4: GO-BP biological process of enrichment analysis. The *y*-axis shows top significantly enriched GO-BP categories, and the *x*-axis displays the number of enrichment genes of these terms ($P < 0.05$), and the color represents the adjusted *P* value; the redder, the more significant the enrichment. The height of the column is related to *P* value. The higher the column is, the more significant the enrichment is.
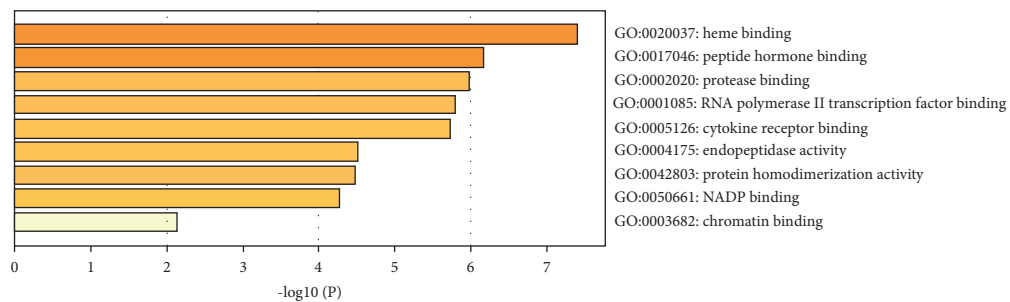
FIGURE 5: GO-MF molecular function of enrichment analysis. The *y*-axis shows top significantly enriched GO-MF categories, and the *x*-axis displays the number of enrichment genes of these terms ($P < 0.05$), and the color represents the adjusted *P* value; the redder, the more significant the enrichment. The height of the column is related to *P* value. The higher the column is, the more significant the enrichment is.

(Figure 8), indicating that PI3K-Akt signaling pathway was one of the important regulatory pathways of EZF in antiosteoporosis.

3.5. *Molecular Docking.* IL2, IL4, and EGF exist in both hub genes and PI3K-Akt signaling pathway (Figure 2(b) and Figure 8), so we selected the corresponding proteins of these

genes as receptors. Similarly, we selected the 17 active components in EZF and PI3K-Akt signaling pathway as ligands. A total of 51 times were docked, and the results were put in Supplementary Files 1 and 2. Then we selected the top ten conformations with the lowest binding energy and optimal conformation to display (Table 3 and Figures 9(a)–9(j)). Through the docking results, we speculate that the components of EZF such as wedelolactone, dimethyl
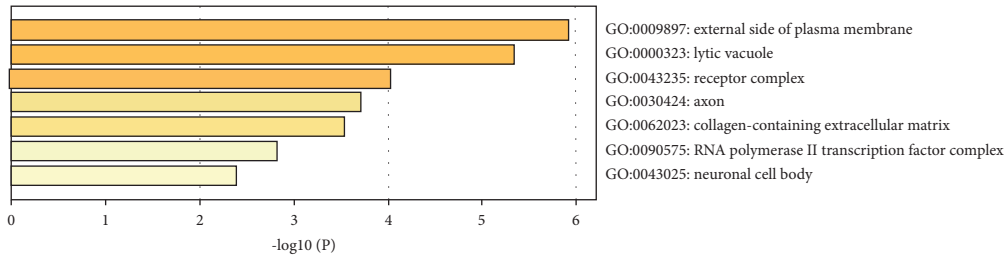
FIGURE 6: GO-CC cellular component of enrichment analysis. The *y*-axis shows top significantly enriched GO-CC categories, and the *x*-axis displays the number of enrichment genes of these terms ($P < 0.05$), and the color represents the adjusted P value; the redder, the more significant the enrichment. The height of the column is related to P value. The higher the column is, the more significant the enrichment is.
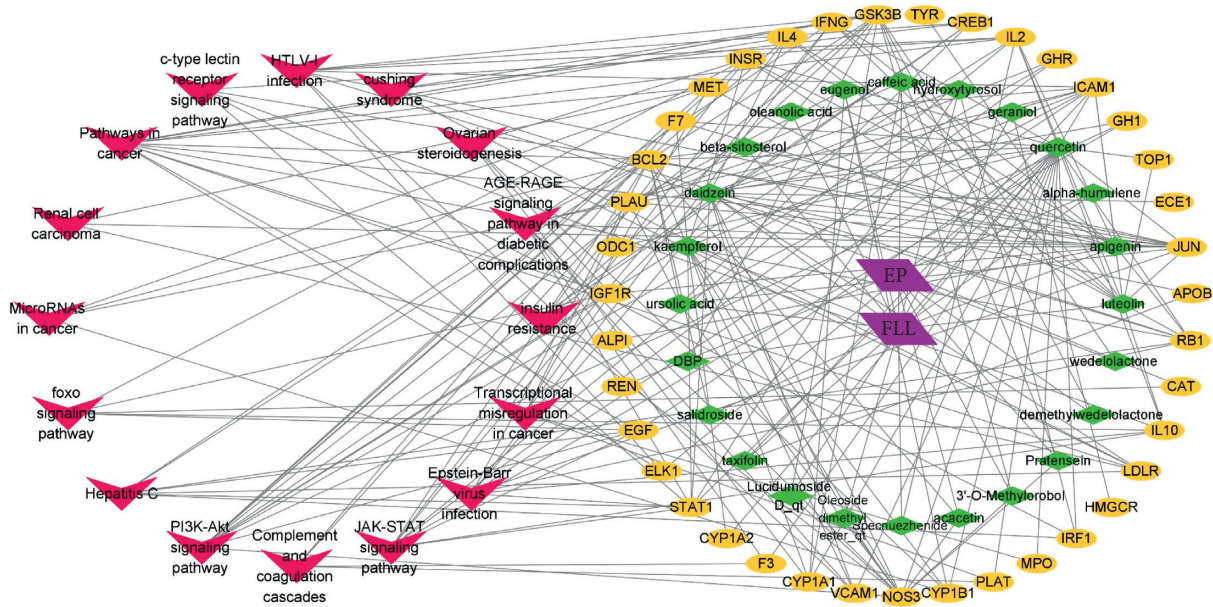
FIGURE 7: The "chemical components-target genes-signal pathway" network of EZF in treating osteoporosis. FLL: Fructus Ligustri Lucidi; EP: *Ecliptae herba*.
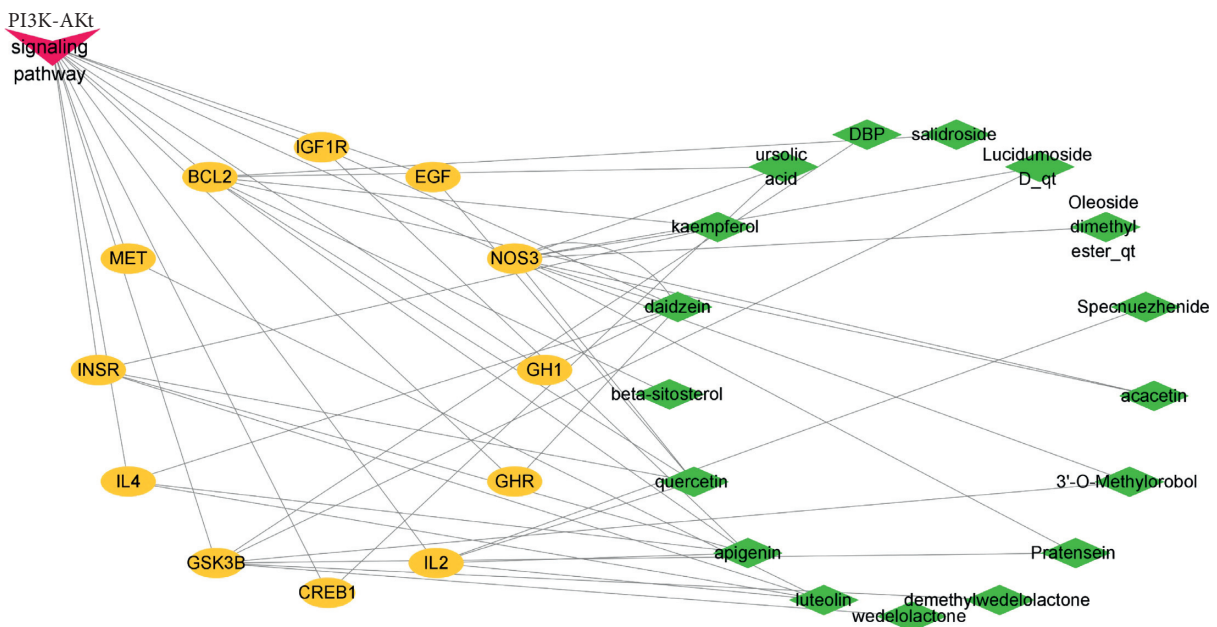
FIGURE 8: PI3K-Akt pathway in preventing osteoporosis mediated by EZF.

TABLE 3: Top 10 molecular dockings optimal binding energy.

Rank	Proteins and compounds	Mode	Affinity (kcal/mol)	Dist from rmsd	Best mode rmsd
1	IL4, wedelolactone	1	−7.6	0.000	0.000
2	EGF, ursolic acid	1	−7.6	0.000	0.000
3	IL2, ursolic acid	1	−7.5	0.000	0.000
4	IL4, acacetin	1	−7.3	0.000	0.000
5	IL2, beta-sitosterol	1	−7.3	0.000	0.000
6	IL4, apigenin	1	−7.2	0.000	0.000
7	IL4, kaempferol	1	−7.2	0.000	0.000
8	EGF, specnuezhenide	1	−7.1	0.000	0.000
9	IL4, demethyl wedelolactone	1	−7.1	0.000	0.000
10	IL4, specnuezhenide	1	−7.1	0.000	0.000

(a)

(b)

(c)

FIGURE 9: Continued.

(d)

(e)

(f)

FIGURE 9: Continued.

(g)

(h)

(i)

FIGURE 9: Continued.

(j)
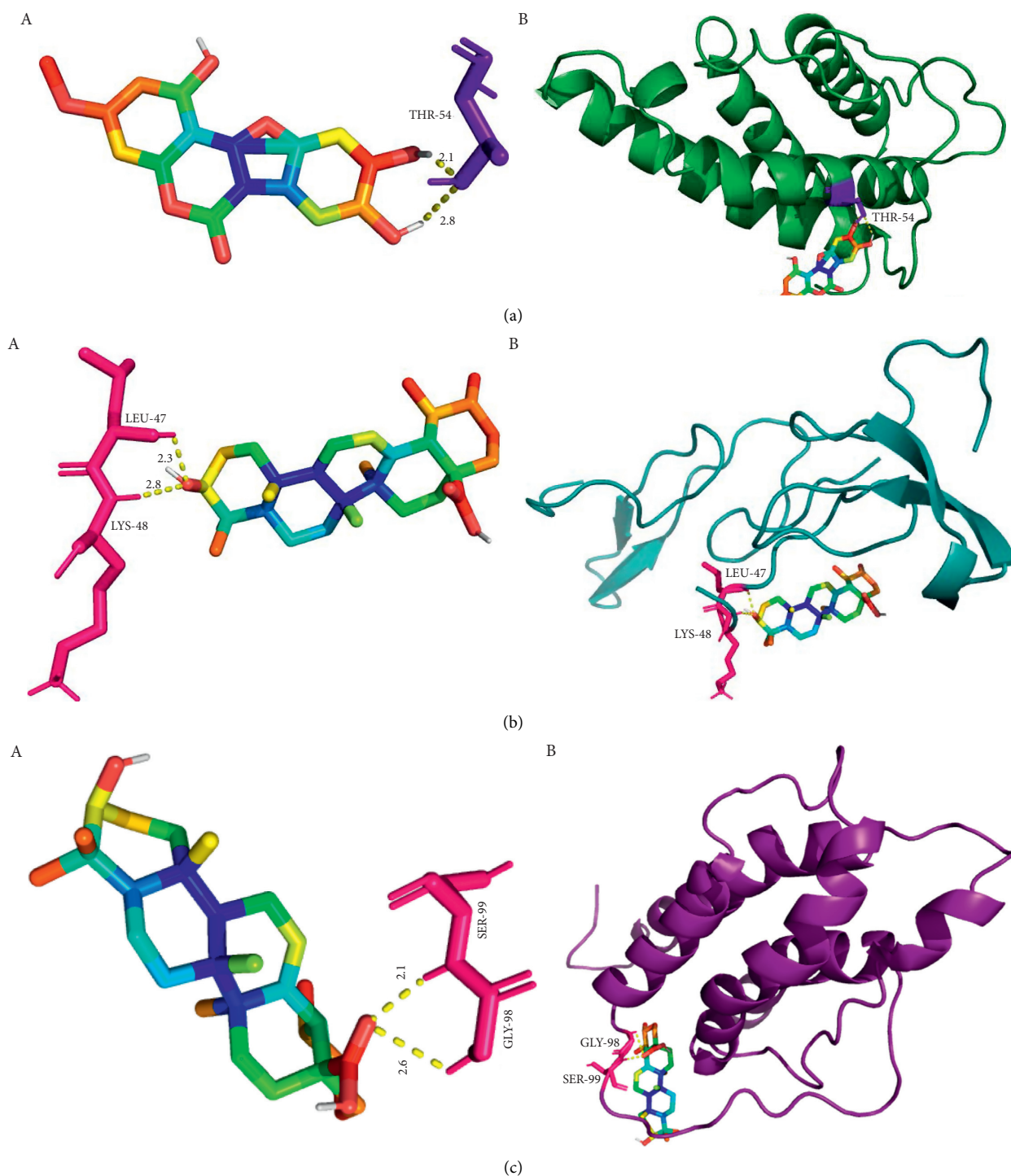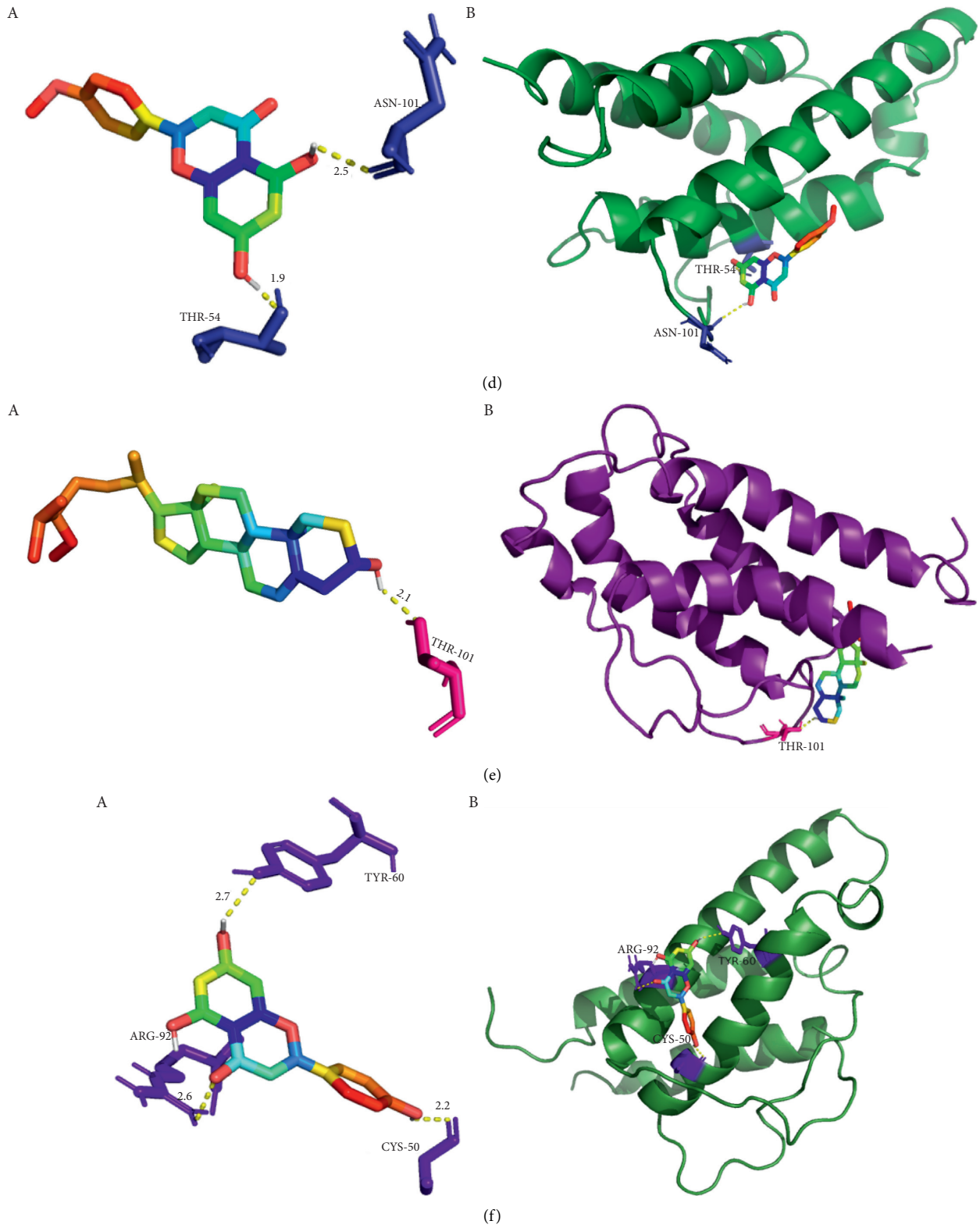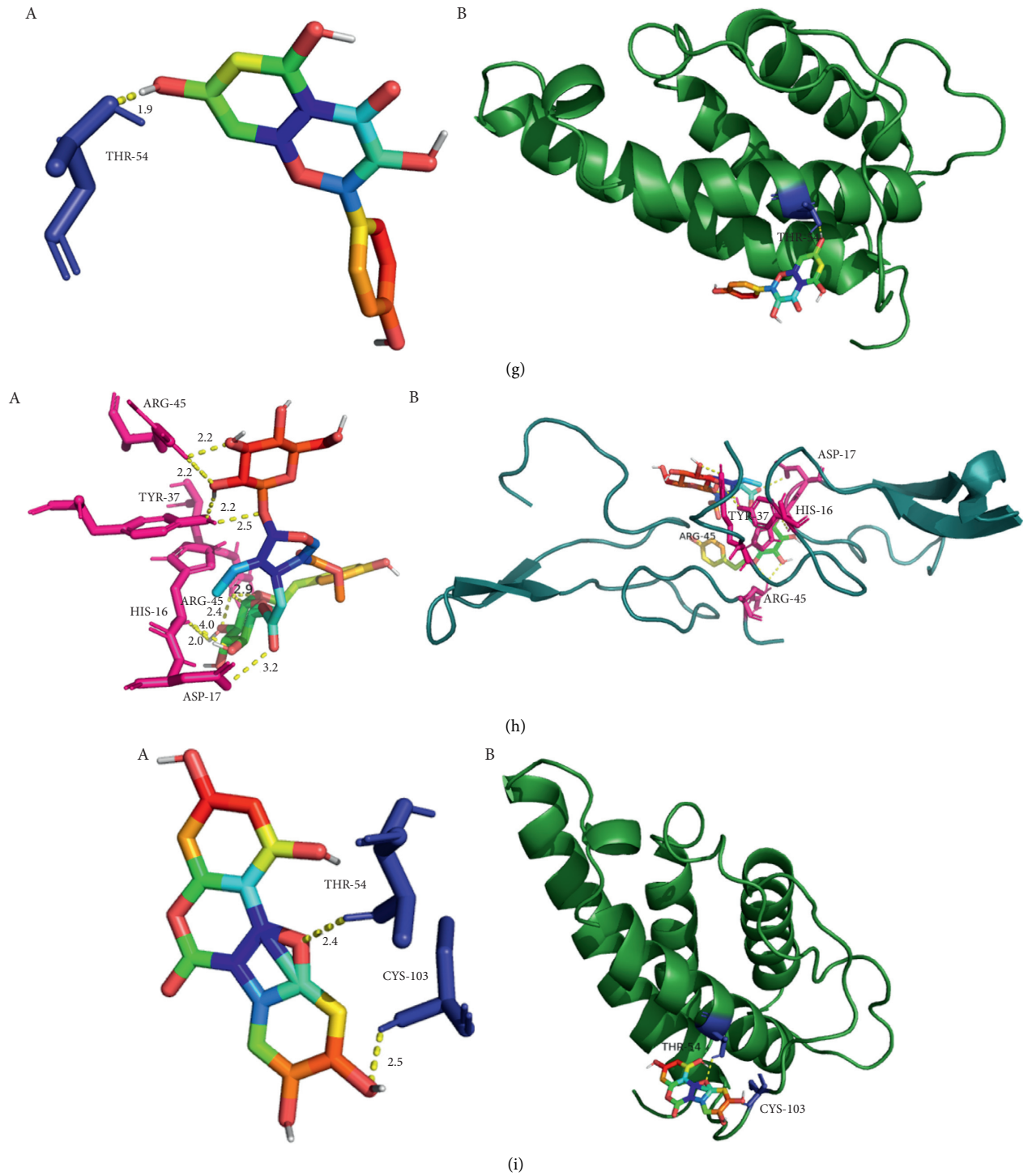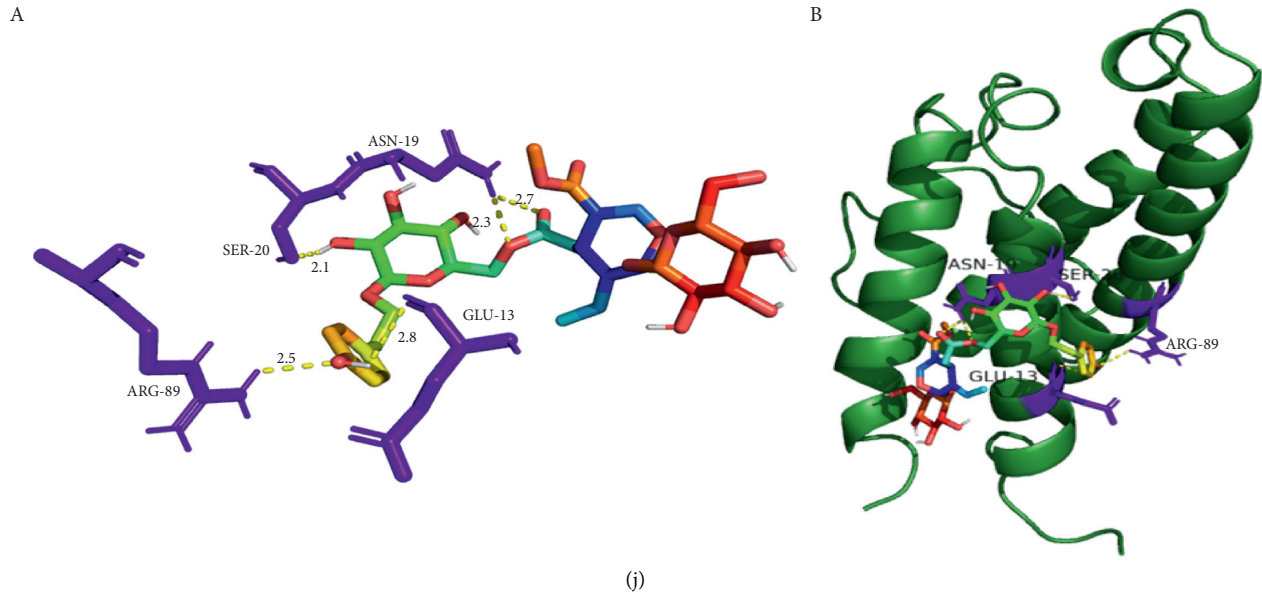
FIGURE 9: Top ten molecular dockings diagram of EZF for treating GIOP. (a) IL4, wedelolactone; (b) EGF, ursolic-acid; (c) IL2, ursolic acid; (d) IL4-, acacetin; (e) IL2, beta-sitosterol; (f) IL4, apigenin; (g) IL4, kaempferol; (h) EGF, specnuezhenide; (i) IL4, dimethyl wedelolactone; (j) IL4, specnuezhenide. "a" shows the amino acid residues and hydrogen bond lengths attached to the active component (ligand), where the colored rainbow represents the ligands and the pure color represents the amino acid residues. "b" is the complete docking of protein and ligand.

wedelolactone, specnuezhenide, ursolic acid, acacetin, beta-sitosterol, apigenin, and kaempferol play an important role in the treatment of GIOP.

3.6. Behavioral Observation of Zebrafish. The moving distance, swimming speed, and cumulative swimming time of each group were obtained by Noldus DanioVision tracking chamber and EthoVision XT (Wageningen, Netherlands) version 8.0 monitoring software. Obviously, the activity of PNSL group more significantly decreased compared to that of the blank group and the blank DMSO group ($P < 0.01$). Compared with the model group, the moving distance, swimming speed, and cumulative swimming time of the EZF medium-dose group, EZF low-dose group, and and positive control group were significantly increased ($P < 0.05$), while there was no significant difference in these indexes between EZF high-dose group and model group. The quantitative results are shown in Figure 10.

3.7. Staining Observation. According to microscopic observation (Olympus IX71/IX81, Olympus Corporation, Japan) of the staining results (Figure 11), the BMA, AOD, and COD were significantly decreased after the intervention of PNSL ($P < 0.001$) compared with the blank group. Compared with the model group, the BMA, AOD, and COD in the positive drug group were significantly improved ($P < 0.01$). Each group of EZF also had significant improvement ($P < 0.05$); in particular, the EZF medium-dose group had the most powerful effect in reversing GIOP ($P < 0.01$, Figure 12). The results suggest that medium dose of EZF may be the most appropriate concentration for the treatment of GIOP in zebrafish model.

4. Discussion

Hormone changes, physical disability, accelerated aging, and inflammation-related osteoclast activation were the main potential factors of osteoporosis [44, 45]. As known to all, the use of GCs was a recognized cause of secondary OP. GIOP led to decreased bone strength and osteoporotic fracture and further aggravated the dysfunction and disability of patients. A meta-analysis from randomized controlled trials and control groups found that the annual incidence of vertebral fractures was 2.8% to 8.2% in patients after taking oral GCs [46]. Zebrafish has many special advantages in establishing osteoporosis model, such as transparent embryo and rapid bone development. Most importantly, it is highly homologous with human related genes, tissues, organs, and development, in which the gene similarity is as high as 87% [47]. Therefore, zebrafish has significant advantages in the establishment of osteoporosis model. The inhibitory effect of GCs on bone formation has been clear, and it can induce an osteoporotic phenotype in many animal models, such as mouse, rat, rabbits, ewes, beagles, pigs, and zebrafish [48]. GCs had little effect on neurological, vascular, and muscular development of zebrafish. Therefore, they can be used to construct many pathological models. For example, sleep deprivation model was induced by light stimulation [49], depression model was induced by reserpine [50], thrombus model was induced by phenylhydrazine (PHZ) [51], epilepsy model was induced by pentylenetetrazol (PTZ) [52], vascular insufficiency model was induced by tyrosine kinase inhibitor [53], vascular defect model was induced by axitinib [54], and *sapje* strain model was always used for muscle atrophy [55]. GCs are only recognized to induce osteoporosis and cannot be used
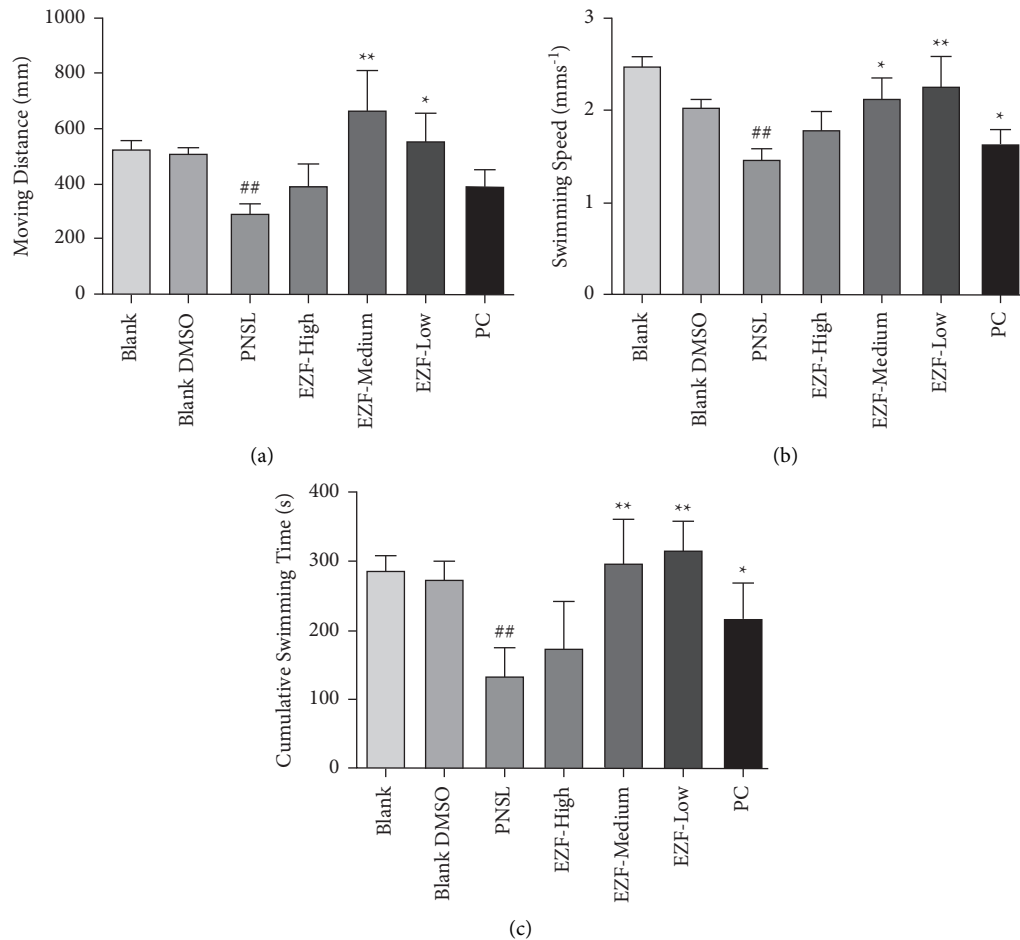
FIGURE 10: Effect of EZF extract on the behavior of GIOP zebrafish ($n = 15$). (a) The moving distance detected by animal behavior analyzer in each group. (b) The swimming speed detected by animal behavior analyzer in each group. (c) Cumulative swimming time detected by animal behavior analyzer in each group. Compared with the blank group, $^{\#\#}P < 0.01$; compared with the model group, $^{*}P < 0.05$ and $^{**}P < 0.01$.

to induce other diseases in zebrafish. Therefore, GC is mainly used as a model drug to induce osteoporosis.

EZF had significantly antiosteoporotic effect on ovariectomized rats [39, 40]. In this paper, we focus on constructing the network of "chemical components-target genes-signaling pathways" through network pharmacology, so as to clarify its main mechanism in treating GIOP. Then the therapeutic effect of EZF was verified by GCs-induced zebrafish model. GCs had multiple pharmacological targets, so they had many advantages, including promoting osteoclast, inhibiting osteoblast, inhibiting the synthesis of sex hormone, and inhibiting the absorption of calcium and phosphorus [56–59]. This study found that the 39 common characteristic targets of EZF and GIOP are as follows: IL10, RB1, JUN, TOP1, ICAM1, IL2, TYR, IFNG, IL4, INSR, MET, F7, Bcl-2, PLAU, ODC1, IGF1R, ALPI REN, EGF, ELK1, STAT1, CYP1A2, F3, CYP1A1, VCAM1, NOS3, CYP1B1, PLAT, MPO, IRF1, HMGCR, LDLR, CAT, APOB, ECE1, GH1, GHR, CREB1, and GSK-3B. Through systematic literature search, it was found that IL10 decreased bone loss in inflammatory diseases [60, 61], the expression of Bcl-2 gene could inhibit the proliferation of osteoblasts and apoptosis of osteoclasts [62], and GSK-3β had an irreplaceable role in

bone metabolism. Therefore, this work is consistent with the existing reports, and, more importantly, we have explored and predicted many targets that have not been reported.

Among the 24 constituents corresponding to 39 common targets, 19 compounds were in FLL and 5 compounds were obtained from EP. It had been reported that luteolin could inhibit the proliferation of osteoblasts by preventing the overproduction of ROS and then enhance the expression of osteoblastic markers to promote the differentiation of osteoblasts [63]. Apigenin could significantly reduce trabecular bone loss in OVX mice [64]. Quercetin widely existed in Chinese herbal medicine, which reduced osteoporosis induced by ovariectomy through regulating autophagy and apoptosis of rat osteoblasts [65]. EP and its component wedelolactone inhibited the proliferation and differentiation of osteoclasts [66]. These potential active ingredients contained in EZF had latent promising clinical application prospect for the curation of GIOP. Besides, the zebrafish experiment we chose further verified the pharmacological effect of EZF in reversing GIOP.

KEGG enrichment analysis screened out 4 signaling pathways with high correlation, which were PI3K-Akt, pathways in cancer, JAK-STAT, and AGE-RAGE signaling
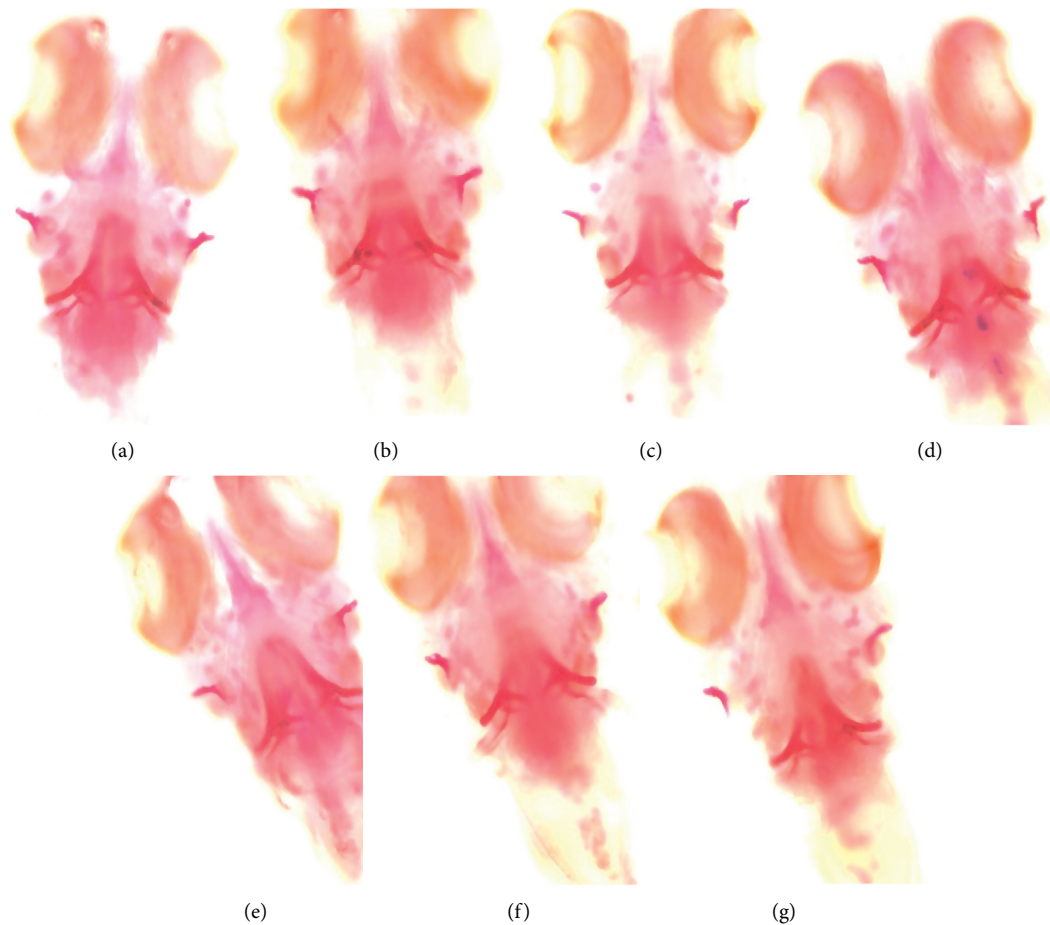
FIGURE 11: Reversal effect of EZF on bone mineralization in GIOP zebrafish ($n = 15$). (a) Blank control group. (b) Blank DMSO group. (c) Model group. (d) EZF high-dose group. (e) EZF medium-dose group. (f) EZF low-dose group. (g) Positive control group.

pathway. Among them, the correlation degree of PI3K-Akt signaling pathway was the highest one, which could be considered as a potential target [67–69]. Revealed research indicated that the protein expression of PI3K, p-AKT, and p-GSK-3 could significantly reverse the GIOP in mice [70]. Moreover, PI3K-Akt pathway could act on specific target genes such as FOXO and GSK-3β to reduce the oxidative damage of osteoblasts and osteoclasts [71]. Our present study listed out the 17 active components of EZF which could adjust 12 gene targets mediated by PI3K-Akt signaling pathway in the treatment of GIOP. Janus kinase (JAK)-signal transduction and activator of transcription (STAT) signaling pathway were important pathway that mediates the signal transduction of many cytokines, growth factors, and hormones [72, 73]. Recent reports indicate that inhibition of JAK-STAT can reconstruct normal bone mineral density in ovariectomized mice [74]. Some clinical diagnosis results of diabetic patients such as decreased bone mineral density, inhibition of bone turnover markers, and bone mass damage may be influenced by AGE-RAGE signaling pathway [75].

Among the 4 signaling pathways, PI3K-Akt signaling pathway shows the most obvious intensity. In this network (Figure 8), there were 17 active components and 3 hub genes (EGF, IL2, and IL4) related to it. By analyzing the results of 51 docking times, we can find that wedelolactone, dimethyl wedelolactone, specnuezhenide, ursolic acid, acacetin, beta-sitosterol, apigenin, and kaempferol had high activity. It had been reported that wedelolactone and dimethyl wedelolactone can enhance BMSC differentiation towards osteoblasts and promote bone formation [76]. Specnuezhenide is one of the iridoid glycosides and plays an important role in promoting the proliferation of bone marrow mesenchymal stem cells in vitro and inhibiting replicative aging [77]. Cao et al. reported that oleanolic acid and ursolic acid, as the active components of FLL, had a beneficial effect on calcium balance and calcium stimulating hormone circulation level, so it is expected to become a candidate drug for the prevention and treatment of osteoporosis [78]. Acacetin, beta-sitosterol, apigenin, and kaempferol, as active components of Chinese medicine, have been screened and reported for many times in the treatment of many diseases [79, 80]. In addition, EZF was quantitatively analyzed by HPLC, and the contents of active components such as specnuezhenide and wedelolactone were detected. The related results are shown in Supplementary File 3. The prediction with network pharmacology helped us accurately locate the molecular mechanism of EZF in antiosteoporosis.

Despite the wide spread of this technology, network pharmacology still has some limitations. Firstly, the existing

(a)

(b)

(c)
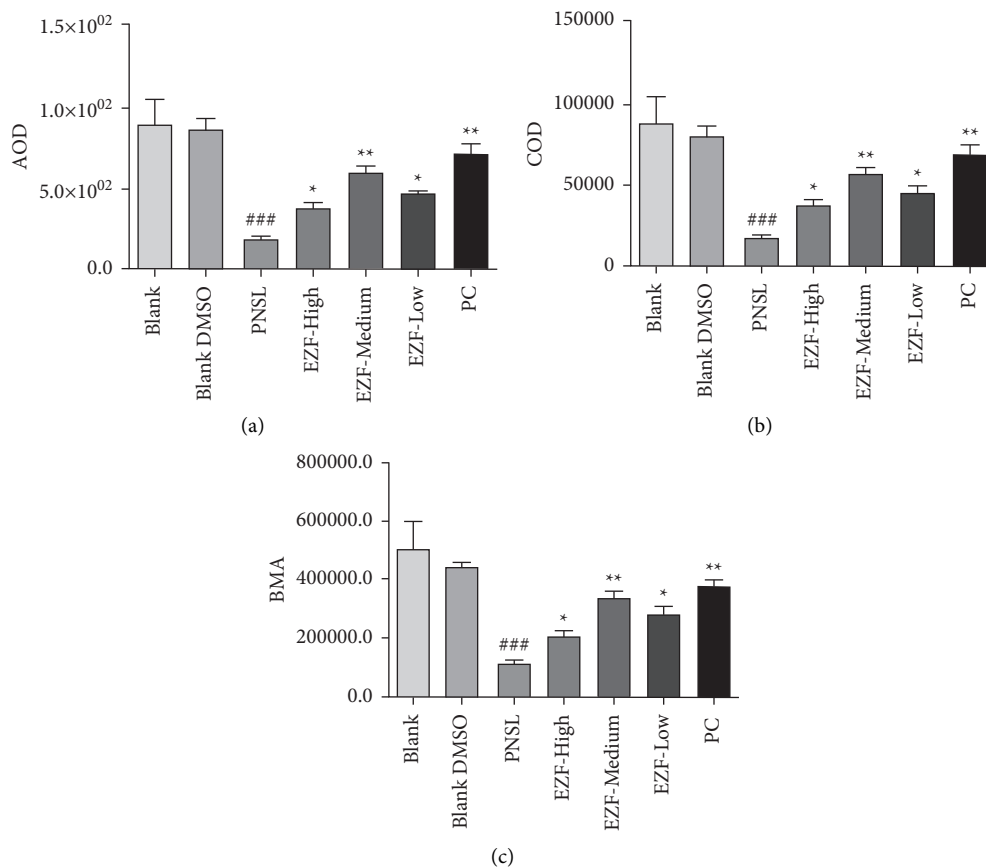
FIGURE 12: Quantitative analysis of the effect of EZF in reversing GIOP in zebrafish ($n = 15$). (a) The average optical density in different groups. (b) Cumulative optical density in different groups. (c) Staining area in different groups. Compared with the blank group, $^{###}P < 0.001$; compared with model group, $^{*}P < 0.05$ and $^{**}P < 0.01$.

databases are not complete enough, so we have to use different platforms to improve the accuracy of researchers' speculation. Secondly, different model algorithms have been formed and developed in Cytoscape and Autodock, which may cause the experiment to be more difficult. Hence, it is necessary to select appropriate algorithms according to different purposes to ensure the accuracy of the results. Thirdly, the method is mainly used in qualitative research. It cannot be ignored that there is a dose-response relationship between drugs and diseases, but the current network pharmacology is still difficult to quantify the target compounds [81]. In the future, combining the development of instrument analysis with data analysis, we hope to find a fast and nondestructive method to effectively solve the above limitations. It is expected to be widely used in the development of ancient classic prescriptions.

5. Conclusion

EZF has a good effect on reversing the inhibition of glucocorticoid-induced bone formation. The 24 components of EZF were found to be the material basis of antiosteoporosis by regulating 39 related gene targets and multiple signaling pathways.

Data Availability

The data used to support the findings of this study are available from the corresponding author upon request.

Disclosure

Zhihui Cai and Huajun Wang are co-first author.

Conflicts of Interest

The authors declare no conflicts of interest.

Authors' Contributions

Zhihui Cai and Huajun Wang contributed equally to this paper.

Acknowledgments

Supplementary Materials

Supplementary File 1: 51 molecular docking results. Supplementary File 2: 51 molecular docking diagrams of EZF for treating GIOP. Supplementary File 3: determination of active components in EZF by HPLC. (*Supplementary Materials*)

References

[1] F. Cosman, S. J. de Beur, M. S. LeBoff et al., "Clinician's guide to prevention and treatment of osteoporosis," *Osteoporosis International*, vol. 25, no. 10, pp. 2359–2381, 2014.

[2] P. Guggenbuhl, "Osteoporosis in males and females: is there really a difference?" *Joint Bone Spine*, vol. 76, no. 6, pp. 595–601, 2009.

[3] L. J. Melton 3rd, E. J. Atkinson, M. K. O'Connor, W. M. O'Fallon, and B. L. Riggs, "Bone density and fracture risk in men," *Journal of Bone and Mineral Research*, vol. 13, no. 12, pp. 1915–1923, 1998.

[4] E. D. Newman, C. K. Matzko, T. P. Olenginski et al., "Glucocorticoid-Induced Osteoporosis Program (GIOP): a novel, comprehensive, and highly successful care program with improved outcomes at 1 year," *Osteoporosis International*, vol. 17, no. 9, pp. 1428–1434, 2006.

[5] J. Compston, "Glucocorticoid-induced osteoporosis: an update," *Endocrine*, vol. 61, no. 1, pp. 7–16, 2018.

[6] R. A. Overman, J. C. Toliver, J.-Y. Yeh, M. L. Gourlay, and C. L. Deal, "United States adults meeting 2010 American College of Rheumatology criteria for treatment and prevention of glucocorticoid-induced osteoporosis," *Arthritis Care & Research*, vol. 66, no. 11, pp. 1644–1652, 2014.

[7] G. Adami and K. G. Saag, "Glucocorticoid-induced osteoporosis: 2019 concise clinical review," *Osteoporosis International*, vol. 30, no. 6, pp. 1145–1156, 2019.

[8] M. de Wit, C. Cooper, P. Tugwell et al., "Practical guidance for engaging patients in health research, treatment guidelines and regulatory processes: results of an expert group meeting organized by the World Health Organization (WHO) and the European Society for Clinical and Economic Aspects of Osteoporosis, Osteoarthritis and Musculoskeletal Diseases (ESCEO)," *Aging Clinical and Experimental Research*, vol. 31, no. 7, pp. 905–915, 2019.

[9] L. Buckley, G. Guyatt, H. A. Fink et al., "2017 American college of rheumatology guideline for the prevention and treatment of glucocorticoid-induced osteoporosis," *Arthritis & Rheumatology*, vol. 69, no. 8, pp. 1521–1537, 2017.

[10] M. Hiligsmann, J.-Y. Reginster, A. N. A. Tosteson et al., "Recommendations for the conduct of economic evaluations in osteoporosis: outcomes of an experts' consensus meeting organized by the European society for clinical and economic aspects of osteoporosis, osteoarthritis and musculoskeletal diseases (ESCEO) and the US branch of the international osteoporosis foundation," *Osteoporosis International*, vol. 30, no. 1, pp. 45–57, 2019.

[11] S. Huybers, T. H. J. Naber, R. J. M. Bindels, and J. G. J. Hoenderop, "Prednisolone-induced Ca^{2+} malabsorption is caused by diminished expression of the epithelial Ca^{2+} channel TRPV6," *American Journal of Physiology-Gastrointestinal and Liver Physiology*, vol. 292, no. 1, pp. G92–G97, 2007.

[12] A. A. Khan, A. Morrison, D. L. Kendler et al., "Case-based review of osteonecrosis of the jaw (ONJ) and application of the international recommendations for management from the international task force on ONJ," *Journal of Clinical Densitometry*, vol. 20, no. 1, pp. 8–24, 2017.

[13] Y. Wei, D.-J. Sui, H.-M. Xu et al., "Atractylodes lancea rhizome water extract reduces triptolide-induced toxicity and enhances anti-inflammatory effects," *Chinese Journal of Natural Medicines*, vol. 15, no. 12, pp. 905–911, 2017.

[14] X.-Y. Qin, Z.-C. Niu, X.-L. Han et al., "Anti-perimenopausal osteoporosis effects of Erzhi formula via regulation of bone resorption through osteoclast differentiation: a network pharmacology-integrated experimental study," *Journal of Ethnopharmacology*, vol. 270, Article ID 113815, 2021.

[15] Y. Zhang, X.-L. Dong, P.-C. Leung, C.-T. Che, and M.-S. Wong, "Fructus ligustri lucidi extract improves calcium balance and modulates the calciotropic hormone level and vitamin D-dependent gene expression in aged ovariectomized rats," *Menopause*, vol. 15, no. 3, pp. 558–565, 2008.

[16] X.-Y. You, Q. Xue, Y. Fang et al., "Preventive effects of Ecliptae Herba extract and its component, ecliptasaponin A, on bleomycin-induced pulmonary fibrosis in mice," *Journal of Ethnopharmacology*, vol. 175, pp. 172–180, 2015.

[17] S. Li, Z. Q. Zhang, L. J. Wu, X. G. Zhang, Y. Y. Wang, and Y. D. Li, "Understanding ZHENG in traditional Chinese medicine in the context of neuro-endocrine-immune network," *IET Systems Biology*, vol. 1, no. 1, pp. 51–60, 2007.

[18] S. Li and B. Zhang, "Traditional Chinese medicine network pharmacology: theory, methodology and application," *Chinese Journal of Natural Medicines*, vol. 11, no. 2, pp. 110–120, 2013.

[19] K. Howe, M. D. Clark, C. F. Torroja et al., "The zebrafish reference genome sequence and its relationship to the human genome," *Nature*, vol. 496, no. 7446, pp. 498–503, 2013.

[20] T.-T. Luo, Y. Lu, S.-K. Yan, X. Xiao, X.-L. Rong, and J. Guo, "Network pharmacology in research of Chinese medicine formula: methodology, application and prospective," *Chinese Journal of Integrative Medicine*, vol. 26, no. 1, pp. 72–80, 2020.

[21] P. Goldsmith, "Zebrafish as a pharmacological tool: the how, why and when," *Current Opinion in Pharmacology*, vol. 4, no. 5, pp. 504–512, 2004.

[22] R. Barrett, C. Chappell, M. Quick, and A. Fleming, "A rapid, high content,in vivo model of glucocorticoid-induced osteoporosis," *Biotechnology Journal*, vol. 1, no. 6, pp. 651–655, 2006.

[23] D. Tsiotas, "Network stiffness: a new topological property in complex networks," *PLoS One*, vol. 14, no. 6, p. e0218477, 2019.

[24] Uniprot, "UniProt: The universal protein knowledgebase," *Nucleic Acids Research*, vol. 45, no. D1, pp. D158–d169, 2017.

[25] G. Stelzer, N. Rosen, I. Plaschkes et al., "The GeneCards suite: from gene data mining to disease genome sequence analyses," *Current protocols in bioinformatics*, vol. 54, pp. 1–33, 2016.

[26] N. J. Mulder, E. Adebiyi, M. Adebiyi et al., "Development of Bioinformatics infrastructure for genomics research," *Global Heart*, vol. 12, no. 2, pp. 91–98, 2017.

[27] J. Gao, B. Song, X. Hu, F. Yan, and J. Wang, "ConnectedAlign: a PPI network alignment method for identifying conserved protein complexes across multiple species," *BMC Bioinformatics*, vol. 19, no. Suppl 9, p. 286, 2018.

[28] C. V. Mering, M. Huynen, D. Jaeggi, S. Schmidt, P. Bork, and B. Snel, "STRING: a database of predicted functional associations between proteins," *Nucleic Acids Research*, vol. 31, no. 1, pp. 258–261, 2003.

[29] K. Yu, P. Zhang, and Z. G. Xie, "A network pharmacology study on the mechanisms of the herbal extract, christina loosestrife, for the treatment of nephrolithiasis," *Medical*

Science Monitor: International Medical Journal of Experimental and Clinical Research, vol. 26, Article ID e919360, 2020.

[30] K. S. Hung, C. C. Hsiao, T. W. Pai et al., "Functional enrichment analysis based on long noncoding RNA associations," *BMC Systems Biology*, vol. 12, no. Suppl 4, p. 45, 2018.

[31] M. Kanehisa and S. Goto, "KEGG: kyoto encyclopedia of genes and genomes," *Nucleic Acids Research*, vol. 28, no. 1, pp. 27–30, 2000.

[32] W.-H. Li, J.-R. Han, P.-P. Ren, Y. Xie, and D.-Y. Jiang, "Exploration of the mechanism of Zisheng Shenqi decoction against gout arthritis using network pharmacology," *Computational Biology and Chemistry*, vol. 90, Article ID 107358, 2021.

[33] M. Sardiello, M. Palmieri, A. di Ronza et al., "A gene network regulating lysosomal biogenesis and function," *Science*, vol. 325, no. 5939, pp. 473–477, 2009.

[34] X. Jiao, X. Jin, Y. Ma et al., "A comprehensive application: molecular docking and network pharmacology for the prediction of bioactive constituents and elucidation of mechanisms of action in component-based Chinese medicine," *Computational Biology and Chemistry*, vol. 90, Article ID 107402, 2021.

[35] Y. Chen, P.-D. Chen, B.-H. Bao et al., "Anti-thrombotic and pro-angiogenic effects of Rubia cordifolia extract in zebrafish," *Journal of Ethnopharmacology*, vol. 219, pp. 152–160, 2018.

[36] J. Jiang, S. Xiao, X. Xu, H. Ma, C. Feng, and X. Jia, "Isomeric flavonoid aglycones derived from Epimedii Folium exerted different intensities in anti-osteoporosis through OPG/RANKL protein targets," *International Immunopharmacology*, vol. 62, pp. 277–286, 2018.

[37] E. M. Katz, D. K. Chu, K. M. Casey, K. Jampachaisri, S. A. Felt, and C. Pacharinsak, "The stability and efficacy of tricaine methanesulfonate (MS222) solution after long-term storage," *Journal of the American Association for Laboratory Animal Science*, vol. 59, no. 4, pp. 393–400, 2020.

[38] L. J. Gleason, E. A. Benton, M. L. Alvarez-Nebreda, M. J. Weaver, M. B. Harris, and H. Javedan, "FRAIL questionnaire screening tool and short-term outcomes in geriatric fracture patients," *Journal of the American Medical Directors Association*, vol. 18, no. 12, pp. 1082–1086, 2017.

[39] L. Xu, X. He, Y. Zhou et al., "Connectivity map analysis identifies fisetin as a treatment compound for osteoporosis through activating the PI3K-AKT signaling pathway in mouse pre-osteoblastic MC3T3-E1 cells," *Current Pharmaceutical Biotechnology*, vol. 22, no. 15, 2021.

[40] B. D. Manning and L. C. Cantley, "AKT/PKB signaling: navigating downstream," *Cell*, vol. 129, no. 7, pp. 1261–1274, 2007.

[41] Y.-X. Gu, J. Du, M.-S. Si, J.-J. Mo, S.-C. Qiao, and H.-C. Lai, "The roles of PI3K/Akt signaling pathway in regulating MC3T3-E1 preosteoblast proliferation and differentiation on SLA and SLActive titanium surfaces," *Journal of Biomedical Materials Research Part A*, vol. 101A, no. 3, pp. 748–754, 2013.

[42] P. Ma, B. Gu, W. Xiong et al., "Glimepiride promotes osteogenic differentiation in rat osteoblasts via the PI3K/Akt/eNOS pathway in a high glucose microenvironment," *PLoS One*, vol. 9, no. 11, Article ID e112243, 2014.

[43] S. Katz, V. Ayala, G. Santillán, and R. Boland, "Activation of the PI3K/Akt signaling pathway through P2Y2 receptors by extracellular ATP is involved in osteoblastic cell proliferation," *Archives of Biochemistry and Biophysics*, vol. 513, no. 2, pp. 144–152, 2011.

[44] E. Legrand, M. Audran, P. Guggenbuhl et al., "Trabecular bone microarchitecture is related to the number of risk factors and etiology in osteoporotic men," *Microscopy Research and Technique*, vol. 70, no. 11, pp. 952–959, 2007.

[45] M. Nie, Q. Zhang, G. Zhang, J. Chen, and Q. Dong, "Synthesis of resveratrol loaded mPEG-PLA nanomicelles for the prevention of osteoporosis in ovariectomized rats," vol. 36, no. 10, pp. 2112–2119, 2017.

[46] M. A. Amiche, J. M. Albaum, M. Tadrous et al., "Fracture risk in oral glucocorticoid users: a Bayesian meta-regression leveraging control arms of osteoporosis clinical trials," *Osteoporosis International*, vol. 27, no. 5, pp. 1709–1718, 2016.

[47] M. Faria, E. Prats, F. Padrós, A. M. V. M. Soares, and D. Raldúa, "Zebrafish is a predictive model for identifying compounds that protect against brain toxicity in severe acute organophosphorus intoxication," *Archives of Toxicology*, vol. 91, no. 4, pp. 1891–1901, 2017.

[48] L. Liu, W. Tao, W. Pan et al., "Hydroxysafflor yellow A promoted bone mineralization and inhibited bone resorption which reversed glucocorticoids-induced osteoporosis," *BioMed Research International*, vol. 2018, Article ID 6762146, 8 pages, 2018.

[49] J. Pinheiro-da-Silva, S. Tran, P. F. Silva, and A. C. Luchiari, "Good night, sleep tight: the effects of sleep deprivation on spatial associative learning in zebrafish," *Pharmacology Biochemistry and Behavior*, vol. 159, pp. 36–47, 2017.

[50] S. Zhang, X. Liu, M. Sun et al., "Reversal of reserpine-induced depression and cognitive disorder in zebrafish by sertraline and Traditional Chinese Medicine (TCM)," *Behavioral and Brain Functions: BBF*, vol. 14, no. 1, 2018.

[51] S.-J. Yin, Y.-Q. Luo, C.-P. Zhao et al., "Antithrombotic effect and action mechanism of Salvia miltiorrhiza and Panax notoginseng herbal pair on the zebrafish," *Chinese Medicine*, vol. 15, no. 1, p. 35, 2020.

[52] G. Tanwar, A. G. Mazumder, V. Bhardwaj et al., "Target identification, screening and in vivo evaluation of pyrrolone-fused benzosuberene compounds against human epilepsy using Zebrafish model of pentylenetetrazol-induced seizures," *Scientific Reports*, vol. 9, no. 1, p. 7904, 2019.

[53] S. Li, Y. Y. Dang, G. Oi Lam Che et al., "VEGFR tyrosine kinase inhibitor II (VRI) induced vascular insufficiency in zebrafish as a model for studying vascular toxicity and vascular preservation," *Toxicology and Applied Pharmacology*, vol. 280, no. 3, pp. 408–420, 2014.

[54] J. Zhang, M. Liu, M. Huang et al., "Ginsenoside F1 promotes angiogenesis by activating the IGF-1/IGF1R pathway," *Pharmacological Research*, vol. 144, pp. 292–305, 2019.

[55] R. Licitra, M. Marchese, L. Brogi, B. Fronte, L. Pitto, and F. M. Santorelli, "Nutraceutical screening in a zebrafish model of muscular dystrophy: gingerol as a possible food aid," *Nutrients*, vol. 13, no. 3, 2021.

[56] Y. Suzuki, "[On "2015 guidelines for prevention and treatment of osteoporosis drug-induced osteoporosis: glucocorticoid-induced osteoporosis]," *Clinical Calcium*, vol. 25, no. 9, pp. 1347–1356, 2015.

[57] M. F. Delaney, "Strategies for the prevention and treatment of osteoporosis during early postmenopause," *American Journal of Obstetrics and Gynecology*, vol. 194, no. 2 Suppl, pp. S12–S23, 2006.

[58] J. A. Dougherty, "Risedronate for the prevention and treatment of corticosteroid-induced osteoporosis," *The Annals of Pharmacotherapy*, vol. 36, no. 3, pp. 512–516, 2002.

[59] H. Liu, Q. Ma, X. Han, and W Huang, "Bone mineral density and its correlation with serum 25-hydroxyvitamin D levels in

patients with hyperthyroidism," *Journal of International Medical Research*, vol. 48, no. 2, Article ID 300060520903666, 2020.

[60] J. M. Owens, A. C. Gallagher, and T. J. Chambers, "IL-10 modulates formation of osteoclasts in murine hemopoietic cultures," *The Journal of Immunology*, vol. 157, no. 2, pp. 936–940, 1996.

[61] H. Shinno, C. Noda, K. Tanaka, and A. Ichihara, "Induction of L-lysine-2-oxoglutarate reductase by glucagon and glucocorticoid in developing and adult rats in vivo and in vitro studies," *Biochimica et Biophysica Acta (BBA) - General Subjects*, vol. 633, no. 3, pp. 310–316, 1980.

[62] T. Pang, M. Gong, J. Han, and D. Liu, "Relationship between osteoporosis and expression of Bcl-2 and CXCL12," *Experimental and Therapeutic Medicine*, vol. 15, no. 2, pp. 1293–1297, 2018.

[63] J. E. Forde and T. C. Dale, "Glycogen synthase kinase 3: a key regulator of cellular fate," *Cellular and Molecular Life Sciences*, vol. 64, no. 15, pp. 1930–1944, 2007.

[64] T. Goto, K. Hagiwara, N. Shirai, K. Yoshida, and H. Hagiwara, "Apigenin inhibits osteoblastogenesis and osteoclastogenesis and prevents bone loss in ovariectomized mice," *Cytotechnology*, vol. 67, no. 2, pp. 357–365, 2015.

[65] S. Vakili, F. Zal, Z. Mostafavi-pour, A. Savardashtaki, and F. Koohpeyma, "Quercetin and vitamin E alleviate ovariectomy-induced osteoporosis by modulating autophagy and apoptosis in rat bone cells," *Journal of Cellular Physiology*, vol. 236, no. 5, pp. 3495–3509, 2021.

[66] Y.-Q. Liu, L.-B. Zhan, T. Liu, M.-C. Cheng, X.-Y. Liu, and H.-B. Xiao, "Inhibitory effect of Ecliptae herba extract and its component wedelolactone on pre-osteoclastic proliferation and differentiation," *Journal of Ethnopharmacology*, vol. 157, pp. 206–211, 2014.

[67] J. Bertacchini, N. Heidari, L. Mediani et al., "Targeting PI3K/AKT/mTOR network for treatment of leukemia," *Cellular and Molecular Life Sciences*, vol. 72, no. 12, pp. 2337–2347, 2015.

[68] M. Zhang and X. Zhang, "The role of PI3K/AKT/FOXO signaling in psoriasis," *Archives of Dermatological Research*, vol. 311, no. 2, pp. 83–91, 2019.

[69] R. L. B. Costa, H. S. Han, and W. J. Gradishar, "Targeting the PI3K/AKT/mTOR pathway in triple-negative breast cancer: a review," *Breast Cancer Research and Treatment*, vol. 169, no. 3, pp. 397–406, 2018.

[70] J. Xi, Q. Li, X. Luo et al., "Celastrol inhibits glucocorticoid-induced osteoporosis in rat via the PI3K/AKT and Wnt signaling pathways," *Molecular Medicine Reports*, vol. 18, no. 5, pp. 4753–4759, 2018.

[71] X.-J. Li, Z. Zhu, S.-L. Han, and Z.-L. Zhang, "Bergapten exerts inhibitory effects on diabetes-related osteoporosis via the regulation of the PI3K/AKT, JNK/MAPK and NF-κB signaling pathways in osteoprotegerin knockout mice," *International Journal of Molecular Medicine*, vol. 38, no. 6, pp. 1661–1672, 2016.

[72] A. V. Villarino, Y. Kanno, and J. J. O'Shea, "Mechanisms and consequences of Jak-STAT signaling in the immune system," *Nature Immunology*, vol. 18, no. 4, pp. 374–384, 2017.

[73] R. Morris, N. J. Kershaw, and J. J. Babon, "The molecular details of cytokine signaling via the JAK/STAT pathway," *Protein Science*, vol. 27, no. 12, pp. 1984–2009, 2018.

[74] S. Adam, N. Simon, U. Steffen et al., "JAK inhibition increases bone mass in steady-state conditions and ameliorates pathological bone loss by stimulating osteoblast function," *Science Translational Medicine*, vol. 12, no. 530, 2020.

[75] K. Asadipooya and E. M. Uy, "Advanced glycation end products (AGEs), receptor for AGEs, diabetes, and bone: review of the literature," *Journal of the Endocrine Society*, vol. 3, no. 10, pp. 1799–1818, 2019.

[76] D. Zhu, X. Deng, X. F. Han et al., "Wedelolactone enhances osteoblastogenesis through ERK- and JNK-mediated BMP2 expression and smad/1/5/8 phosphorylation," *Molecules*, vol. 23, no. 3, 2018.

[77] C. Ma, X. Zhou, K. Xu et al., "Specnuezhenide decreases interleukin-1β-induced inflammation in rat chondrocytes and reduces joint destruction in osteoarthritic rats," *Frontiers in Pharmacology*, vol. 9, p. 700, 2018.

[78] S. Cao, X.-L. Tian, W.-X. Yu et al., "Oleanolic acid and ursolic acid improve bone properties and calcium balance and modulate vitamin D metabolism in aged female rats," *Frontiers in Pharmacology*, vol. 9, p. 1435, 2018.

[79] S. Singh, P. Gupta, A. Meena, and S. Luqman, "Acacetin, a flavone with diverse therapeutic potential in cancer, inflammation, infections and other metabolic disorders," *Food and Chemical Toxicology*, vol. 145, Article ID 111708, 2020.

[80] K. Koc, F. Geyikoglu, O. Cakmak et al., "The targets of β-sitosterol as a novel therapeutic against cardio-renal complications in acute renal ischemia/reperfusion damage," *Naunyn-Schmiedeberg's Archives of Pharmacology*, vol. 394, no. 3, pp. 469–479, 2021.

[81] Y. Yang, K. Yang, T. Hao et al., "Prediction of molecular mechanisms for LianXia NingXin formula: a network pharmacology study," *Frontiers in Physiology*, vol. 9, p. 489, 2018.

Research Article

Study on the Mechanism of Compound Kidney-Invigorating Granule for Osteoporosis based on Network Pharmacology and Experimental Verification

Hao Lv ,[1] **Jiuxiang Wang** ,[1] **Yujun Zhu** ,[2] **and Ting Jiang** [1]

[1]*The First Affiliated Hospital of Anhui University of Chinese Medicine, Hefei 230031, China*
[2]*Anhui University of Chinese Medicine, Hefei 230031, China*

Correspondence should be addressed to Ting Jiang; jiangting70@163.com

Background. This study used a combination of network pharmacology and experimental confirmation to clarify the mechanism of the compound kidney-invigorating granule (CKG) in treating osteoporosis (OP). *Methods*. The main bioactive compounds and corresponding targets of CKG were collected and screened via the Traditional Chinese Medicine Systems Pharmacology Database and Analysis Platform (TCMSP), Yet another Traditional Chinese Medicine (YaTCM), and UniProt databases. Disease targets of OP were summarized in GeneCards and the Comparative Toxicogenomics Database (CTD). Targets of CKG for OP were obtained by Venn diagram. The protein-protein interaction (PPI) network was constructed by the STRING database and then screened for hub genes through Cytoscape 3.7.2 software. The Gene Ontology (GO) and the Kyoto Encyclopedia of Genes and Genomes (KEGG) enrichment were analyzed and visualized by R software. Then, CB-Dock was used for molecular docking verification. Finally, we confirmed the antiosteoporosis effect of CKG through animal and cell experiments. *Results*. A total of 250 putative targets were obtained from 65 bioactive compounds in CKG. Among them, 140 targets were related to OP. Topological analysis of the PPI network yielded 23 hub genes. Enrichment analysis showed the targets of CKG in treating OP might concentrate on the MAPK signaling pathway, the TNF signaling pathway, the PI3K-Akt signaling pathway, etc. The results of molecular docking showed the bioactive components in CKG had good binding ability with the key targets. The experimental results showed that CKG-medicated serum had a promoting effect on proliferating hBMSCs, increasing the expression of AKT, PI3K, ERK1, and IkB in cells and decreasing the expression of IKK in cells. *Conclusion*. CKG has a complex of multicomponent, multitarget, and multipathway. This study lays the theoretical foundation for further *in vitro* and *in vivo* experimental studies and further expands the clinical applications of CKG.

1. Introduction

Osteoporosis (OP) is a systemic metabolic bone disease characterized by low bone mass, low bone density, and bone microstructure destruction, which leads to increased bone fragility and susceptibility to bone fracture. OP is considered a "silent disease" since it progresses without symptoms until a fracture occurs [1]. In the 2010 U.S. census, around 10.2 million adults aged 50 and older were living with OP [2]. An estimated 10.9 million males are suffering from OP in China, while the number of females suffering from OP is 49.3 million [3]. The incidence of OP increases yearly with the aging of the general population. Current treatments for osteoporosis include bisphosphonates, raloxifene, calcium, and vitamin D [4]. Nevertheless, these approved drugs have also shown significant side effects, such as the increased risk of hypercalcemia and hypercalciuria due to long-term vitamin D supplementation [5]. Since bisphosphonates are incorporated within the bone matrix with high affinity, long-term treatment with bisphosphonates may lead to atypical

femur fractures [6]. Raloxifene is associated with adverse effects such as thromboembolism, pulmonary embolism, and cerebrovascular death [7].

Compared with Western medicine, traditional Chinese medicine (TCM) has unique advantages in treating OP, such as low cost, multilevel, and prominent curative effect. Therefore, TCM is gradually attracting considerable attention from the international medical community and is accepted by non-Chinese as an additional and alternative medical treatment for OP due to these characteristics. Clinically, OP is regarded as "bone atrophy" and "lack of bone marrow" in TCM. According to TCM syndrome differentiation, OP is divided into kidney Yang deficiency syndrome, blood stasis syndrome and kidney deficiency syndrome, blood stasis and Qi stagnation syndrome, liver and kidney Yin deficiency syndrome, spleen and kidney Yang deficiency, and asthenia of the spleen and stomach syndrome.

Compound kidney-invigorating granule (CKG) is a TCM formula commonly used at the First Affiliated Hospital of Anhui University of Chinese Medicine. CKG is an effective cure for the OP of blood stasis and kidney deficiency syndrome. It is composed of six kinds of traditional Chinese drugs, namely, Radix Astragali (RA, Huang-qi in Chinese), Radix Paeoniae Alba (RPA, Bai-shao in Chinese), Radix Cyathulae (RC, Chuan-niu-xi in Chinese), Herba Epimedii (HE, Yin-yang-huo in Chinese), Caulis Polygoni Multiflori (CPM, Ye-jiao-teng in Chinese), and Concha Ostreae (CO, Mu-li in Chinese). Preliminary clinical studies have shown that CKG can significantly improve the clinical symptoms, bone mineral density (BMD), and visual analog scale (VAS) in postmenopausal nonelderly patients with OP. There were no adverse reactions that occurred during the study, and there were no significant abnormalities in the safety observation index. Therefore, CKG is safe and effective in treating postmenopausal nonelderly osteoporosis [8]. However, the pharmacological mechanism of CKG in treating OP is unknown.

TCM has become a significant source that provides potential lead compounds for drug development, especially those used to treat complex diseases, owing to its multicomponent and multitarget characteristics [9]. Guided by holistic thinking, TCM exerts unexpected curative effects in difficult and complicated diseases that Western medicine finds difficult to tackle [10]. However, due to the complex components of TCM prescriptions, traditional pharmacological methods to find out their unique actions through experiments may not be suitable for TCM research [11]. Western drug pharmacology molecular research may be stuck in a problem when applied to TCM prescriptions since it clarifies single or limited biological molecules from the perspective of reductionism instead of considering the overall theory of the organism [12]. On the contrary, network pharmacology uses the "target network, multi-components" research model to replace the traditional "one target, one drug" research model. Therefore, network pharmacology conforms to the core of the overall philosophy of TCM

[13]. This combination of pharmacokinetic evaluation and bioinformatics has made a significant contribution to the study of the molecular of TCM [14]. People apply the strategy to the pharmacological research of TCM compounds and explain the complex relationship between biological and herbal prescriptions [12]. Accordingly, regarding the unknown mechanism of CKG, this study adopted the method of network pharmacology to explore the molecular biology mechanism of CKG in treating OP.

The present study uses various platforms, databases, and tools to predict the bioactive compounds, potential targets, and pathways of CKG, aiming to explore the pharmacological network of CKG on OP and verify it through related experiments. Figure 1 shows the detailed technical strategy of the research.

2. Materials and Methods

2.1. Collection and Screening of Bioactive Ingredients.
The bioactive ingredients of CKG were identified by the Traditional Chinese Medicine Systems Pharmacology Database and Analysis Platform (TCMSP) (https://tcmspw.com/tcmsp.php) [15]. It compensates the insufficient information in the Yet another Traditional Chinese Medicine (YaTCM) database (https://cadd.pharmacy.nankai.edu.cn/yatcm/home) [16]. Oral herbal medicines must overcome obstacles in absorption, distribution, metabolism, and excretion (ADME) to be effective. In this process, oral bioavailability (OB) is one of the most important pharmacokinetic parameters [17]. As a qualitative concept, drug-like quality (DL) is used in drug design for the evaluation of the drug ability of a molecule and is utilized to optimize the pharmacokinetics and properties of a drug [18]. This study chose $OB \geq 30\%$ and $DL \geq 0.18$ as the criteria for screening bioactive ingredients. The OB and DL indicators of each ingredient in CKG were retrieved from the TCMSP database.

2.2. Prediction of Drug Targets for CKG.
The protein targets of the screened bioactive ingredients of CKG were obtained from the TCMSP database. The obtained protein targets were converted into gene targets in the Universal Protein Resource (UniProt) database (https://www.uniprot.org/) [19], a comprehensive database of protein sequence and annotation data.

2.3. Construction of Drug-Compound-Target Network.
The obtained bioactive ingredients, gene targets, and herbs were entered into Cytoscape 3.7.2 software (https://www.cytoscape.org/) for data visualization and construction of the "D-C-T" network [20]. The network nodes represent the herbs, gene targets, or bioactive components, and the edges indicate their interaction.

2.4. Collection of Gene Targets for OP.
OP-related human gene targets were obtained from two databases: GeneCards (https://www.genecards.org/) and the comparative
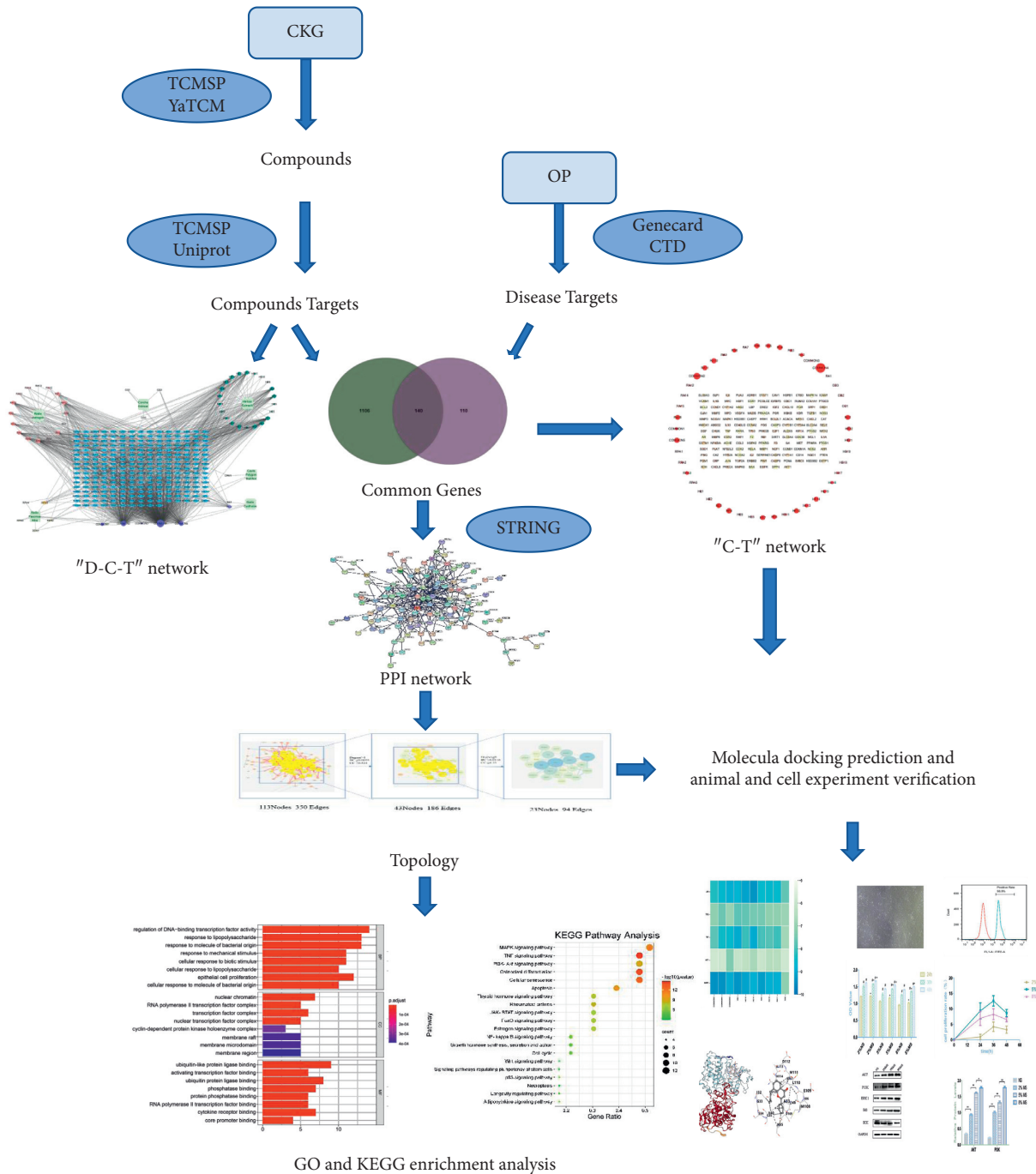
FIGURE 1: The technical strategy of the current study.

toxicogenomics (CTD) database (https://ctdbase.org/). The term "Osteoporosis" was used as the keyword for the search [21, 22].

2.5. Collection of Relevant Targets for Formula Treatment of Diseases. The results of gene targets of CKG were matched with the disease-associated genes of OP. The jvenn (https://www.bioinformatics.com.cn/static/others/jvenn/) was used to realize the visualization of the drug-disease

target and to draw Venn diagrams [23]. Then, the intersecting gene targets of CKG and OP were collected as the relevant targets of CKG for treating OP, which might be the potential target set of CKG in treating OP.

2.6. Construction of a Compound-Target Network That Bioactive Ingredients of Formula with Intersecting Gene Targets. The obtained bioactive ingredients and intersecting gene targets were imported into Cytoscape 3.7.2 software for

data visualization and construction of the "C-T" network. The nodes of the network represented the intersecting gene targets and bioactive components, and the edges indicated their interaction.

2.7. Protein-Protein Interaction (PPI) Network Construction and Core Gene Screening.

The common gene targets of CKG and OP were entered into the STRING database (https://string-db.org/) [24]. The selection parameter was set to "Homo sapiens" for species, the confidence level was set at 0.950 for the minimum required interaction score, and hid disconnected nodes in the network. The PPI network analysis results were downloaded in TSV format. The file was imported into Cytoscape software for topological property analysis. Then, this study evaluated the topological properties of the nodes in the interaction network by calculating three parameters, namely, "degree centrality (DC)," "betweenness centrality (BC)," and "closeness centrality (CC)" via the App CytoNCA [25]. These three parameters measure the importance of nodes in the network and indicate the nature of the nodes in the network. Nodes with high DC, BC, and CC implied that they were playing an essential role in the network. We obtained the core genes in the network by screening above the median value twice based on the results of the topological property analysis of PPI.

2.8. Gene Ontology (GO) and the Kyoto Encyclopedia of Genes and Genomes (KEGG) Enrichment Analysis.

Various bioinformatics analyses and visualization of the results can be achieved through the software R project (https://www.r-project.org/). Firstly, the ENSMBL gene ID of each core gene was obtained from RStudio, AnnotationHub, and org. Hs.eg.db, and then the GO function enrichment (molecular function, MF; biological process, BP; and cellular component, CC) and KEGG enrichment were enriched by RStudio, DOSE, and Cluster Profiler. In the programming language, pvalueCutoff = 0.05 and qvalueCutoff = 0.05 were set. The results of the analysis selected the top 10 items of BP, MF, and CC in GO enrichment and the top 20 filtered pathways most closely related to OP, then displayed the results of the GO enrichment analysis as a bar graph and the results of the KEGG enrichment analysis as a bubble graph.

2.9. Molecular Docking Verification.

Since there is no uniform standard for target screening of bioactive molecules, the 5 proteins with the highest degree of PPI network were selected for molecular docking with the 10 molecules with the highest degree of the "C-T" network. The bioactive compounds were downloaded as 2D structure files using the PubChem database (https://pubchem.ncbi.nlm.nih.gov/), converted into a 3D structure with ChemBio3D Ultra 14.0, and saved as a mol2 format file [26], whereas the RCSB PDB database (https://www.rcsb.org/) was used to retrieve and download the files in "PDB" format of the core target proteins [27]. Then, the proteins and molecules files were imported into the CB-Dock website (https://clab.labshare.cn/cb-dock/php/index.php) for molecular docking. Finally, the docking model with the lowest binding energy was selected and visualized.

2.10. Experimental Verification

2.10.1. Materials

(1) Medicinal Materials. All Chinese medicines of CKG were purchased from the First Affiliated Hospital of Anhui University of Traditional Chinese Medicine. The prescription medicinal materials of each dose of CKG are HE (20 g), RC (15 g), RA (18 g), CO (10 g), RPA (20 g), and CPM (25 g), 30 doses in total.

(2) Antibodies and Reagents. The following antibodies and reagents were used for this study: high-glucose Dulbecco minimum essential medium (HG-DMEM) and fetal bovine serum (FBS) (Gibco, Rockville, MD, USA); 0.25% trypsin-EDTA solution, penicillin-streptomycin, and phosphate-buffered saline (PBS) (Hyclone, Logan, UT, USA); protein extraction kit (KEYGEN, Nanjing, China); AKT, PI3K, ERK1, IkB, IKK antibody, and GAPDH antibody (Wanleibio, Shenyang, China); CD29 antibody, CD34 antibody, and CD44 antibody (Abcam, Cambridge, MA, USA); and cell counting kit-8 (CCK-8) (Beyotime Biotechnology, Shanghai, China).

(3) Instrument. The following instruments were used for this study: CO_2 incubator (NuAire, MN, USA), Multiskan spectrum (BioTek Instruments, VT, USA), flow cytometer (Beckman Coulter, CA, USA), high-performance centrifuge (Eppendorf, Hamburg, German), western blot system (Tanon Science & Technology, Shanghai, China), ice machine (XUEKE ELECTRIC, Changshu, China), inverted microscope (Olympus Corporation, Tokyo, Japan), cell counter (Countstar, Shanghai, China), clean bench (AIRTECH, Suzhou, China), cell culture plates, and cell culture flasks (Corning, NY, USA).

2.10.2. Isolation, Culture, and Identification of Cells.

This investigation was approved by the Ethics Committee of the Anhui University of Chinese Medicine. Written informed consent was obtained from all participants before the study. Bone marrow was obtained from OP patients who underwent surgery in the orthopedics department of the First Affiliated Hospital of Anhui University of Traditional Chinese Medicine and volunteered to participate in this study. Separating and culturing hBMSCs (human bone marrow mesenchymal stem cells) via the method of whole bone marrow adherent. Bone marrow samples applied in cell culture plates were cultured in HG-DMEM containing 10% FBS, 100 U/mL penicillin, and 100 μg/mL streptomycin, then cultured in a 37°C incubator with a 5% CO_2 atmosphere. The medium was changed every 2 days until the cells became confluent, about 80%–90%. The cells were then passaged. The surface marker phenotypes (CD29+, CD44+, and CD34−) were characterized by using flow cytometry.

After the cells were confirmed to be hBMSCs, cells from passages 3 to 5 were used in subsequent experiments.

2.10.3. Preparation and Preservation of CKG-Medicated Serum.

The experiment was approved by the Animal Ethics Committee of the Anhui University of Chinese Medicine. Twenty-four 4-week-old SPF Sprague–Dawley rats weighing 200–250 g, half male and half female, were purchased from the Experimental Animal Center of Anhui Medical University (Experimental Animal Production License Number: SCXK (Wan) 2017-001). Animals were placed in plastic cages at $22 \pm 1°C$ with a 12 h light-dark cycle. Food and water were available ad libitum. They adapted for a week in this environment. The decoction method of the CKG prescription is as follows: after 60 minutes of soaking in sufficient water, the original drugs with the water were decocted in a Chinese herbal medicine decoction machine, then brought to a boil over high heat, and then simmered for 1 hour. The process was repeated three times. The decocting solution was pooled together, added into an electrothermal constant temperature water tank, and concentrated to 2.9 g of the original drugs per mL. The samples were sealed and stored in a refrigerator at 4°C. Animals were randomly divided into medicated serum (MS) ($n = 12$) and nonmedicated serum (NS) ($n = 12$) groups. MS group animals were administered intragastrically with CKG concentrated liquor (20 mL/kg) once a day for 7 days. NS group animals were administered intragastrically saline on the same schedule. 12 h before the final treatment, fasting but not watering. 1 h after the final treatment, rats were weighed and intraperitoneally anesthetized using 1% pentobarbital sodium (60 mg/kg). Blood was collected from the abdominal aorta. The collected blood was allowed to stand at room temperature for one hour, then centrifuged at 3000 r/min for 15 min, and the upper serum was taken from the ultraclean workbench. Serum samples from all individual animals of each group were pooled. Then, it was filtered through a 0.22 μm filter membrane, heat-inactivated at 56°C for 30 min, and stored at $-80°C$ until used.

2.10.4. Detect the Promoting Effect of CKG-Medicated Serum on Cell Proliferation.

Cells were collected in the logarithmic growth phase and a single cell suspension was prepared. Cells were seeded into 96-well microplates at 1×10^4 cells/well in 200 μL medium after counting with a cell counter. NS and MS (at concentrations of 2, 5, and 8%) were added to the culture medium for 24 h. The culture medium was then removed and 100 μL of CKK-8 solution was added to the well and incubated for 24 h, 36 h, and 48 h. Subsequently, the CKK-8 solution was removed, and 100 μL of DMSO was added to dissolve the formazan crystals. The optical density (OD) value was read at 450 nm by using a microplate reader. Cell proliferation rate = $(OD_{MS} - OD_{NS})/OD_{NS}$.

2.10.5. Western Blot.

hBMSCs were plated into 6-well plates. After 12 h, they were treated with MS (at concentrations of 0, 2, 5, and 8%). The treating time is decided by the results of 2.9.3. Total proteins were extracted from the protein extraction kit, separated using SDS-PAGE, and then transferred to polyvinylidene difluoride (PVDF) membranes, which were blocked with 5% nonfat dry milk in TBST buffer. The primary antibodies were added at proper dilution and incubated at 4°C overnight, and the secondary antibody was added and incubated for 60 min, PVDF membranes were washed with precooled PBS three times. Finally, the signals for the immunoreactive proteins were visualized by enhanced chemiluminescence reagents and then analyzed with Quantity One software. The experiment was repeated 3 times independently.

3. Results

3.1. Identification of Bioactive Components in CKG.

The screening criteria were OB $\geq 30\%$ and DL ≥ 0.18. We got 76 bioactive ingredients via the TCMSP database, including 23 of RA, 16 of RPA, 5 of RC, 26 of HE, 3 of CPM, and 3 of CO. 65 bioactive ingredients were obtained after the removal of duplicate components. Results are detailed in Table 1. Sitosterol is the common bioactive ingredient of RA, RPA, and HE. Kaempferol is the common bioactive ingredient of RA, RPA, HE, and CPM. Mairin is the common bioactive component of RA and RPA. Quercetin is the common bioactive component of RA, HE, CPM, and RC. 22, 23-Dihydrostigmasterol is the common bioactive ingredient of RPA, HE, and RC.

3.2. Acquisition of Drug Targets and Construction of the "D-C-T" Network.

By searching targets of the bioactive ingredients in the TCMSP database and performing protein-gene named transformations in the UniProt database, we got 1641 targets in this study. After removing duplicate data, 250 targets were obtained. After removing the bioactive ingredients without targets, they successfully constructed the "D-C-T" network by inputting the files containing drugs, bioactive ingredients with targets, and gene targets into the Cytoscape software. The squares represent drugs, the rounds represent bioactive ingredients, and the diamonds represent various targets. There are 310 nodes and 1705 edges in the "D-C-T" network. Figure 2 shows the network.

3.3. Acquisition of Disease Targets, Intersection Targets, and Construction of the "C-T" Network.

By searching and integrating them in the GeneCards and CTD databases, we got 1246 OP gene targets. By taking the intersection of targets of OP with targets of CKG, we got 140 intersecting genes. Figure 3 shows the drug-disease targets Venn diagram. The "C-T" network was constructed by entering 140 intersecting genes and bioactive ingredients into Cytoscape software. There are 187 nodes and 1028 edges in the "C-T" network. Table 2 shows the degree values of the compounds in the "C-T" network. Results are as detailed in Supplementary Table 1. Figure 4 shows the network.

3.4. Construction, Topology of PPI Network, and Acquisition of Core Genes.

We imported the obtained intersecting genes into the STRING database to acquire the interaction relationships between them and saved the data as a file in TSV format. Figure 5 shows the PPI network diagram. We

TABLE 1: The information of the bioactive compounds of CKG.

Abbreviation	Mol. ID	Molecule name	OB (%)	DL	Herb
COMMON1	MOL000359	Sitosterol	36.91	0.75	RA,RPA,HE
COMMON2	MOL000422	Kaempferol	41.88	0.24	RA,RPA,HE,CPM
COMMON3	MOL000211	Mairin	55.38	0.78	RA,RPA
COMMON4	MOL000098	Quercetin	46.43	0.28	RA,HE,RC,CPM
COMMON5	MOL000358	22,23-Dihydrostigmasterol	36.91	0.75	RPA,HE,RC
CPM1	MOL002259	Physcion diglucoside	41.65	0.63	CPM
RA1	MOL000033	(3S,8S,9S,10R,13R,14S,17R)-10,13-dimethyl-17-[(2R,5S)-5-propan-2-yloctan-2-yl]-2,3,4,7,8,9,11,12,14,15,16,17-dodecahydro-1H-cyclopenta[a]phenanthren-3-ol	36.23	0.78	RA
RA2	MOL000239	Jaranol	50.83	0.29	RA
RA3	MOL000296	Hederagenin	36.91	0.75	RA
RA4	MOL000354	Isorhamnetin	49.6	0.31	RA
RA5	MOL000371	3,9-di-O-methylnissolin	53.74	0.48	RA
RA6	MOL000378	7-O-methylisomucronulatol	74.69	0.3	RA
RA7	MOL000379	9,10-dimethoxypterocarpan-3-O-β-D-glucoside	36.74	0.92	RA
RA8	MOL000380	(6aR,11aR)-9,10-dimethoxy-6a,11a-dihydro-6H-benzofurano[3,2-c]chromen-3-ol	64.26	0.42	RA
RA9	MOL000387	Bifendate	31.1	0.67	RA
RA10	MOL000392	Formononetin	69.67	0.21	RA
RA11	MOL000417	Calycosin	47.75	0.24	RA
RA12	MOL000433	FA	68.96	0.71	RA
RA13	MOL000439	Isomucronulatol-7,2′-di-O-glucosiole	49.28	0.62	RA
RA14	MOL000442	1,7-dihydroxy-3,9-dimethoxy pterocarpene	39.05	0.48	RA
RA15	MOL002565	Calycosin-7-O-beta-D-glucopyranoside	41.6	0.81	RA
RA16	MOL009289	(−)-Medicarpin	49.22	0.34	RA
RA17	MOL000374	5′-hydroxyiso-muronulatol-2′,5′-di-O-glucoside	41.72	0.69	RA
RA18	MOL000398	Isoflavanone	109.99	0.3	RA
RA19	MOL000438	(3R)-3-(2-hydroxy-3,4-dimethoxyphenyl)chroman-7-ol	67.67	0.26	RA
RPA1	MOL001919	(3S,5R,8R,9R,10S,14S)-3,17-dihydroxy-4,4,8,10,14-pentamethyl-2,3,5,6,7,9-hexahydro-1H-cyclopenta[a]phenanthrene-15,16-dione	43.56	0.53	RPA
RPA2	MOL001924	Paeoniflorin	53.87	0.79	RPA
RPA3	MOL000492	(+)-Catechin	54.83	0.24	RPA
RPA4	MOL001918	Paeoniflorgenone	87.59	0.37	RPA
RPA5	MOL002710	Pyrethrin II	48.36	0.35	RPA
RPA6	MOL001930	Benzoyl paeoniflorin	31.27	0.75	RPA
RPA7	MOL001921	Lactiflorin	49.12	0.8	RPA
RPA8	MOL001910	11alpha,12alpha-epoxy-3beta-23-dihydroxy-30-norolean-20-en-28,12beta-olide	64.77	0.38	RPA
RPA9	MOL001928	Albiflorin_qt	66.64	0.33	RPA
RPA10	MOL001925	Paeoniflorin_qt	68.18	0.4	RPA
RPA11	MOL007014	8-debenzoylpaeonidanin	31.74	0.45	RPA
RPA12	MOL007025	Isobenzoylpaeoniflorin	31.14	0.54	RPA
HE1	MOL004427	Icariside A7	31.91	0.86	HE
HE2	MOL001792	DFV	32.76	0.18	HE
HE3	MOL003044	Chryseriol	35.85	0.27	HE
HE4	MOL000006	Luteolin	36.16	0.25	HE
HE5	MOL001771	Poriferast-5-en-3beta-ol	36.91	0.75	HE
HE6	MOL001510	24-epicampesterol	37.58	0.71	HE
HE7	MOL003542	8-Isopentenyl-kaempferol	38.04	0.39	HE
HE8	MOL004380	C-homoerythrinan, 1,6-didehydro-3,15,16-trimethoxy-, (3.beta.)-	39.14	0.49	HE
HE9	MOL004394	Anhydroicaritin-3-O-alpha-L-rhamnoside	41.58	0.61	HE
HE10	MOL004425	Icariin	41.58	0.61	HE
HE11	MOL001645	Linoleyl acetate	42.1	0.2	HE
HE12	MOL004373	Anhydroicaritin	45.41	0.44	HE
HE13	MOL004384	Yinyanghuo C	45.67	0.5	HE
HE14	MOL004391	8-(3-methylbut-2-enyl)-2-phenyl-chromone	48.54	0.25	HE
HE15	MOL004386	Yinyanghuo E	51.63	0.55	HE
HE16	MOL004396	1,2-bis(4-hydroxy-3-methoxyphenyl)propan-1,3-diol	52.31	0.22	HE
HE17	MOL004382	Yinyanghuo A	56.96	0.77	HE

Abbreviation	Mol. ID	Molecule name	OB (%)	DL	Herb
HE18	MOL004388	6-hydroxy-11,12-dimethoxy-2,2-dimethyl-1,8-dioxo-2,3,4,8-tetrahydro-1H-isochromeno[3,4-h]isoquinolin-2-ium	60.64	0.66	HE
HE19	MOL004367	Olivil	62.23	0.41	HE
HE20	MOL000622	Magnograndiolide	63.71	0.19	HE
HE21	MOL002556	7-methoxy-8-(2′-hydroxy-3′-ethoxy-3′-methylbutyl)coumarin	40.36	0.21	HE
HE22	MOL008046	6-demethoxycapillarisin	52.33	0.25	HE
RC1	MOL012298	Rubrosterone	32.69	0.47	RC
RC2	MOL012286	Betavulgarin	68.75	0.39	RC
RC3	MOL012542	β-ecdysterone	44.23	0.82	RC
CO1	MOL010617	5,8,11,14,17-eicosapentaenoic acid	45.66	0.21	CO
CO2	MOL005320	Eicosanetetraenoic acid	45.57	0.2	CO
CO3	MOL010861	Vitamin D3	45.66	0.48	CO
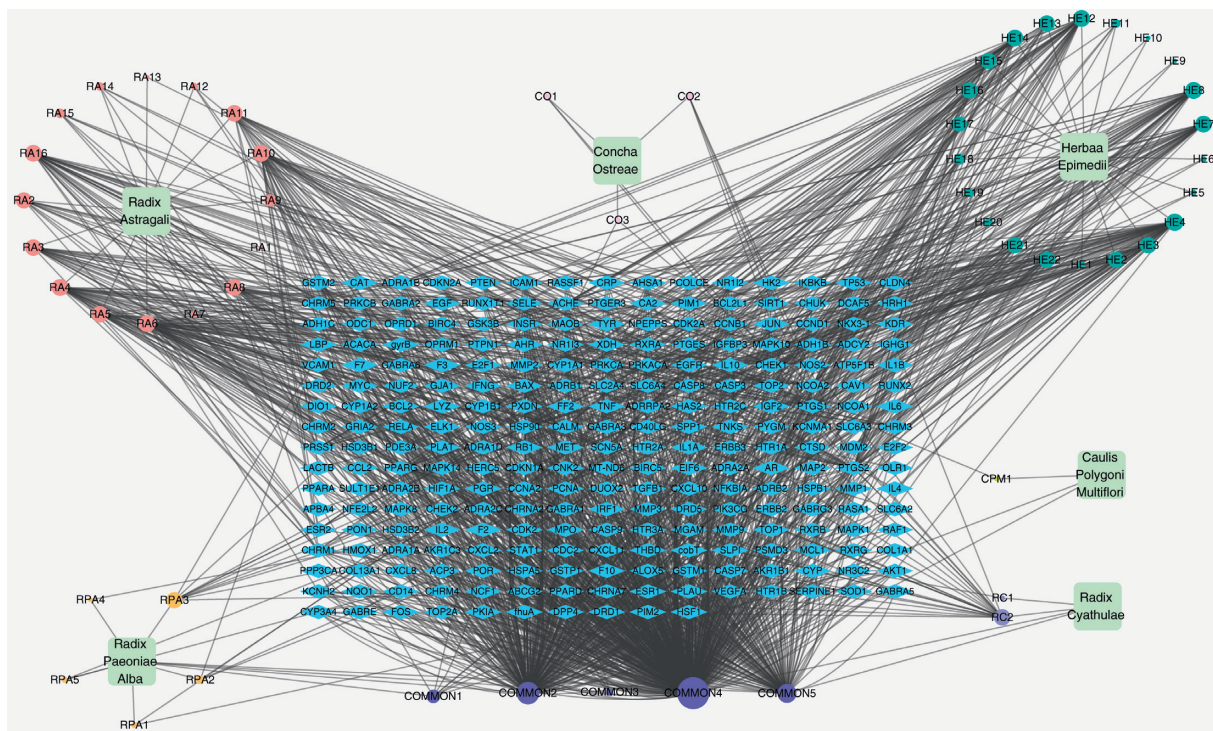
FIGURE 2: drug-compound-target network. Blue diamond nodes indicate targets, cyan square nodes indicate herbs, coral red round nodes indicate bioactive ingredients of RA, chrome yellow round nodes indicate bioactive ingredients of RPA, dark green round nodes indicate bioactive ingredients of HE, lilac round nodes indicate bioactive ingredients of CO, bright yellow round nodes indicate bioactive ingredients of CPM, lavender round nodes indicate bioactive ingredients of RC, and dark purple round nodes indicate bioactive ingredients of herbs together. The size of the compound-related nodes indicates the size of the degree value.
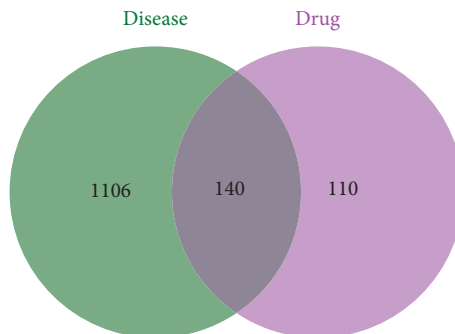
FIGURE 3: Drug-disease targets Venn diagram.

TABLE 2: The abbreviations and degree values of the top 10 bioactive ingredients of the "C-T" network.

Abbreviation	Degree
COMMON4	431
COMMON2	170
COMMON5	51
HE4	46
RA10	27
RA6	23
RA4	22
HE12	20
HE14	20
RA11	16
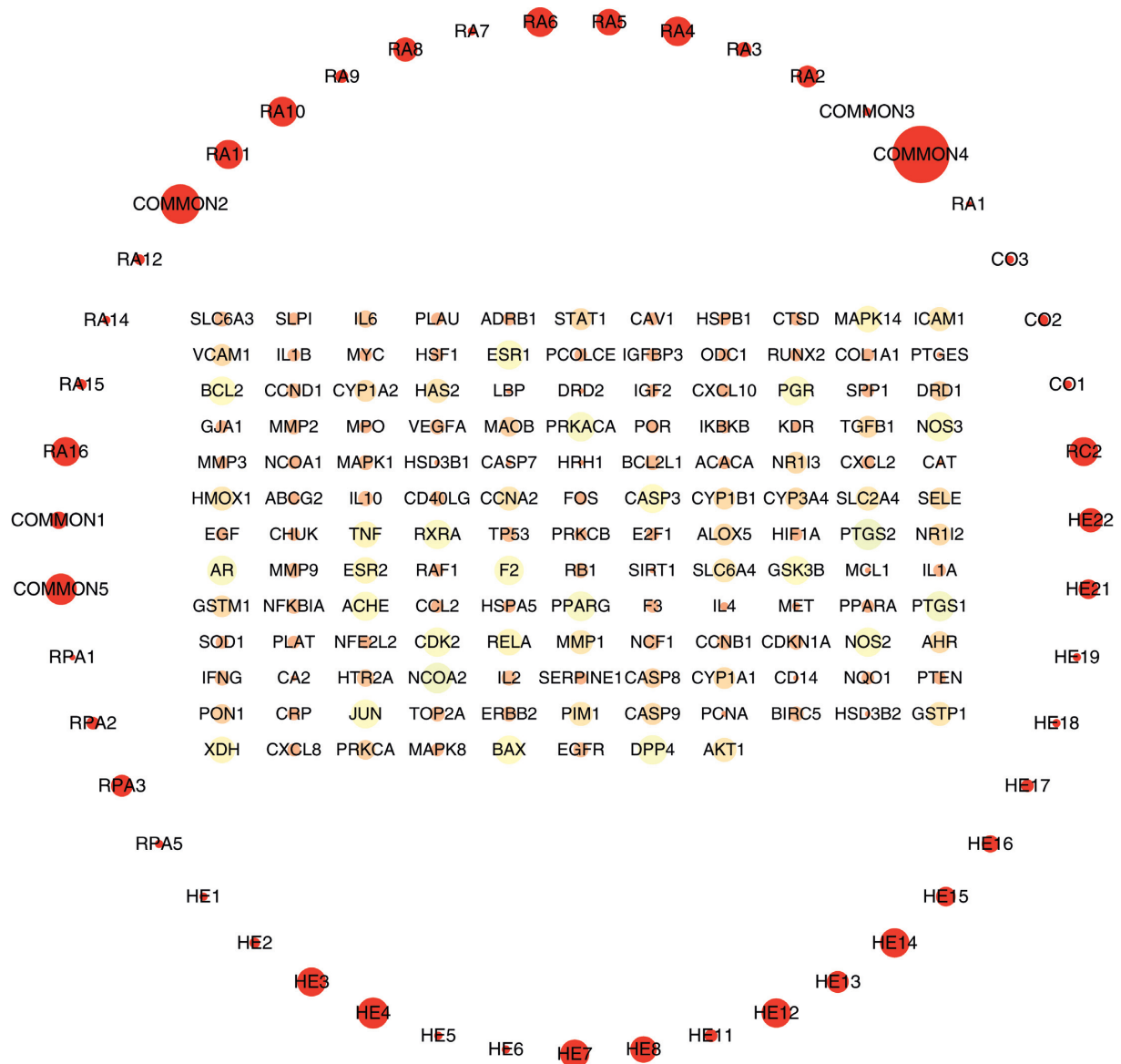
FIGURE 4: The compound-target network. The colored circular nodes indicate the intersecting gene targets, and the red circular nodes indicate the bioactive components of CKG. The size of the nodes indicates the size of the degree value.

imported the TSV data into Cytoscape software. The network has 113 nodes and 350 edges. Then they used CytoNCA to analyze the PPI network based on DC, BC, and CC parameters. The criteria for the first screening were

Degree ≥4, BC ≥ 0.0055, and CC ≥ 0.324. The results showed 43 nodes and 186 edges. The second screening threshold was Degree ≥8, BC ≥ 0.0116, and CC ≥ 0.35. The second screening result was 23 nodes and 94 edges. Figure 6 shows
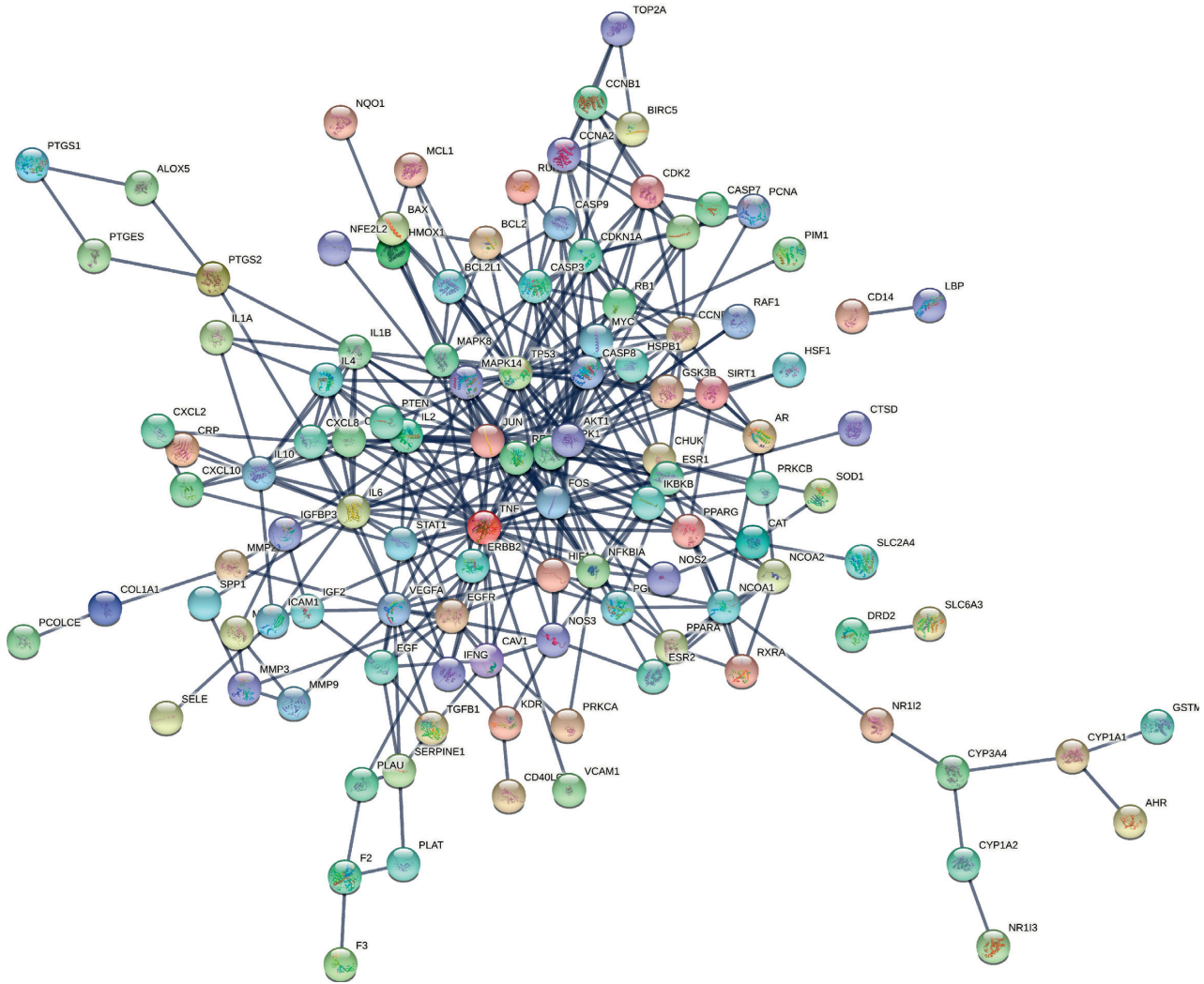
FIGURE 5: The protein-protein interaction network of targets of CKG against OP.

the process of topology. The core genes were JUN, TP53, TNF, AKT1, MAPK1, RELA, IL6, VEGFA, RB1, ESR1, CDKN1A, MYC, CCND1, CASP8, MAPK14, FOS, CXCL8, IL1B, EGFR, NFKBIA, STAT1, PPARG, and NOS3. Figure 7 shows the hub genes. Table 3 shows the top 5 degree values of hub genes.

3.5. Enrichment Analysis of GO and KEGG. GO enrichment analysis got 1723 entries, of which 1621 were BP entries, 20 were CC entries, and 82 were MF entries. BP analysis showed the targets principally relate to regulating DNA-binding transcription factor activity, response to lipopolysaccharide, response to molecules of bacterial origin, response to mechanical stimulus, cellular response to biotic stimulus, cellular response to lipopolysaccharide, epithelial cell proliferation, cellular response to molecules of bacterial origin, response to reactive oxygen species, and muscle cell proliferation. Analysis of the CC category showed the targets mostly within nuclear chromatin, the RNA polymerase II transcription factor complex, the transcription factor complex, the nuclear transcription factor complex, the

cyclin-dependent protein kinase holoenzyme complex, membrane raft, membrane microdomain, membrane region, the serine/threonine-protein kinase complex, the transferase complex, and the transferring phosphorus-containing groups. The MF of these proteins includes ubiquitin-like protein ligase binding, activating transcription factor binding, ubiquitin protein ligase binding, phosphatase binding, protein phosphatase binding, RNA polymerase II transcription factor binding, cytokine receptor binding, core promoter binding, DNA-binding transcription activator activity, RNA polymerase II-specific, and repressing transcription factor binding. The results of the GO analysis are as shown in Figure 8. The KEGG enrichment analysis yielded 180 entries, including the MAPK signaling pathway, the TNF signaling pathway, the PI3K-Akt signaling pathway, osteoclast differentiation, the NF-kappa B signaling pathway, and the Wnt signaling pathway. Figure 9 shows the top 20 filtered pathways most closely related to OP for the KEGG enrichment analysis. According to the KEGG analysis of the hub genes, we obtained the signal pathway diagrams of the MAPK signaling pathway, the PI3K-Akt signaling pathway, and the TNF signaling

Degree≥4
BC ≥0.0055
CC ≥0.324

Degree≥8
BC ≥0.0116
CC ≥0.351

113Nodes 350 Edges   43Nodes 186 Edges   23Nodes 94 Edges
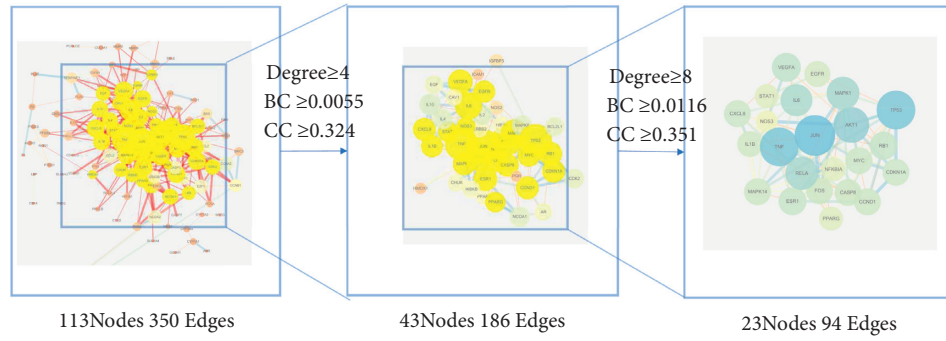
FIGURE 6: The process of topological screening for the PPI network.
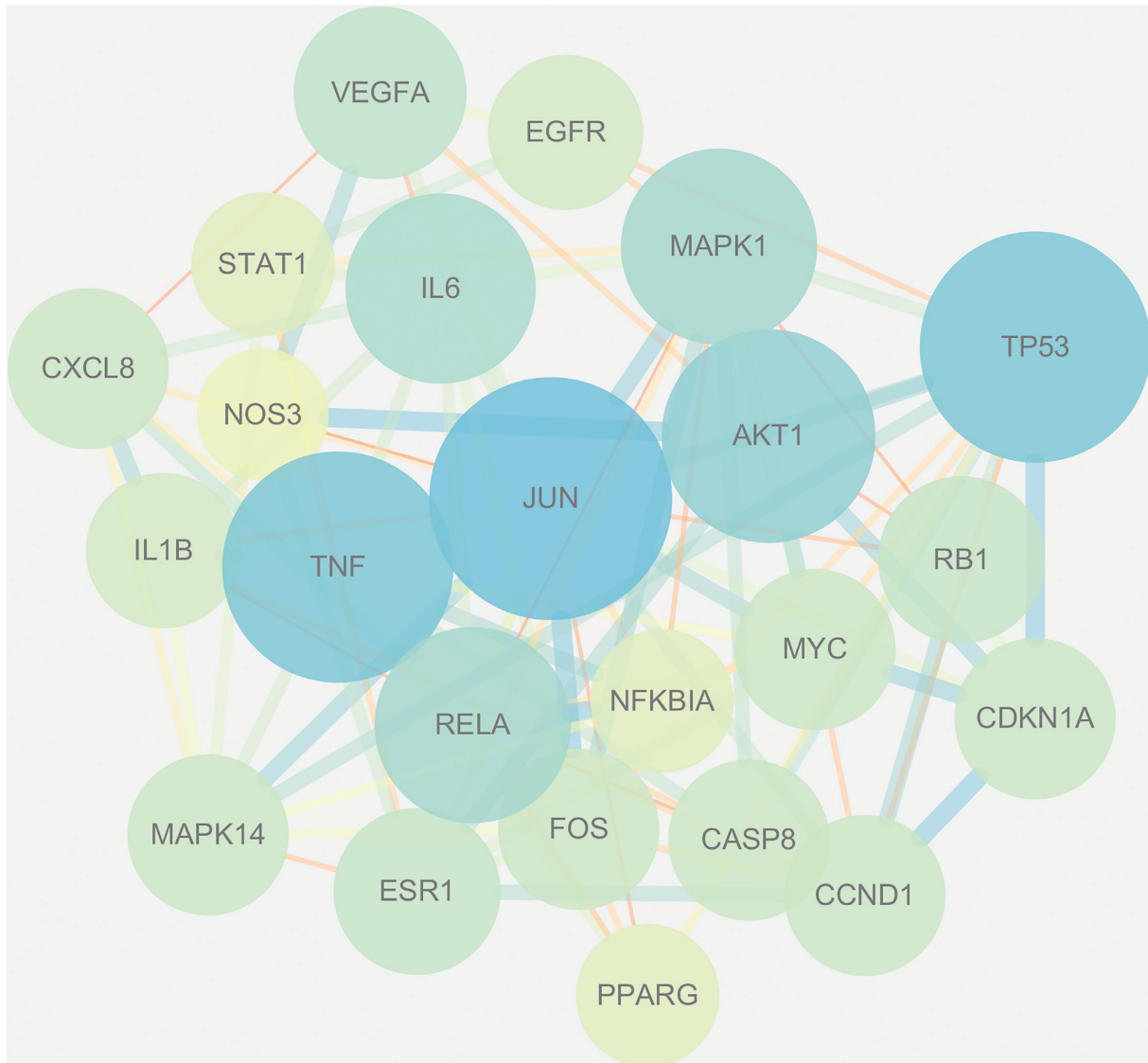
FIGURE 7: The network of the top 23 hub genes.

pathway. Comprehensively analyzing the three pathways, we can conclude that these pathways are all regulated by Akt, which can negatively regulate Raf, thereby affecting the Ras/MAPK signaling pathway. Akt regulates NF-kB by phosphorylating IKK and is directly involved in the regulation of the PI3K-Akt signaling pathway. The diagrams of the three signal pathways and their interconnection are stored in Supplementary Table 5.

TABLE 3: Top 5 hub genes of treating OP of CKG and topological values.

Name	Betweenness centrality	Closeness centrality	Degree
JUN	0.14728269	0.46551724	27
TP53	0.1435125	0.43724696	25
TNF	0.11585625	0.42687747	25
AKT1	0.10719742	0.41698842	22
MAPK1	0.07457652	0.421875	19
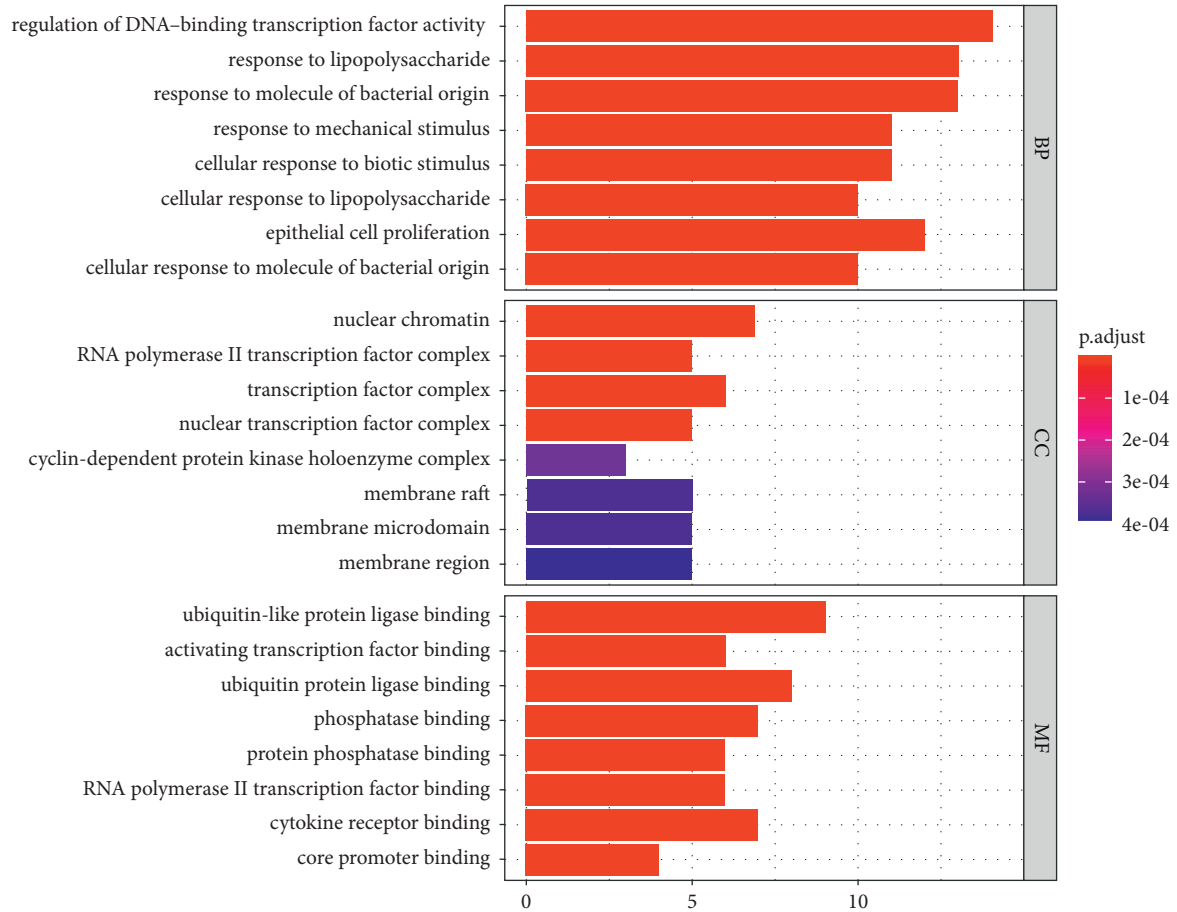
FIGURE 8: GO enrichment analysis.

3.6. Molecular Docking Analysis. Five core targets JUN, TNF, TP53, Akt1, and MAPK1 were selected based on the degree values, and then molecularly docked with the core bioactive ingredients kaempferol, quercetin, 22,23-dihydrostigmasterol, luteolin, anhydroicaritin, 8-(3-methylbut-2-enyl)-2-phenyl-chromone, isorhamnetin, formononetin, calycosin, and 7-O-methylisomucronulatol obtained by swiping the degree values. It is generally accepted that for a protein-ligand complex, the lower the binding energy, the higher the binding affinity. We set binding energy ≤ -5.0 kJ/mol as the standard. Figure 10 shows the results of molecular docking. The results in Figure 10 show that the minimum binding energy of all selected bioactive ingredients to the receptor is much less than -5.0 kJ/mol. Table 4 shows the specific information of the lowest binding energy among the 10 active ingredients docked with each core target. Figure 11 shows the visualization of the docking results. The molecular docking results show the vital bioactive ingredients have excellent binding to the core targets for OP treatment.

3.7. Experimental Verification

3.7.1. Characteristics and Identification of hBMSC Phenotypes. All primary cell cultures were used at early passages (3–5 passage), as shown in Figures 12(a)–12(d)). After 6 days of primary culture, hBMSCs had attached, exhibited spindle and flat shapes, and reached a confluence of around 70%. Passage 2 and 3 hBMSCs reached 85% confluence on day 5 after passaging. Passage 4 hBMSCs reached 85% confluence on day 4 after passaging and resembled a shoal of fish. As shown in Figures 12(e)–12(g), P4 cells were detected with flow cytometry. Notably, the cells
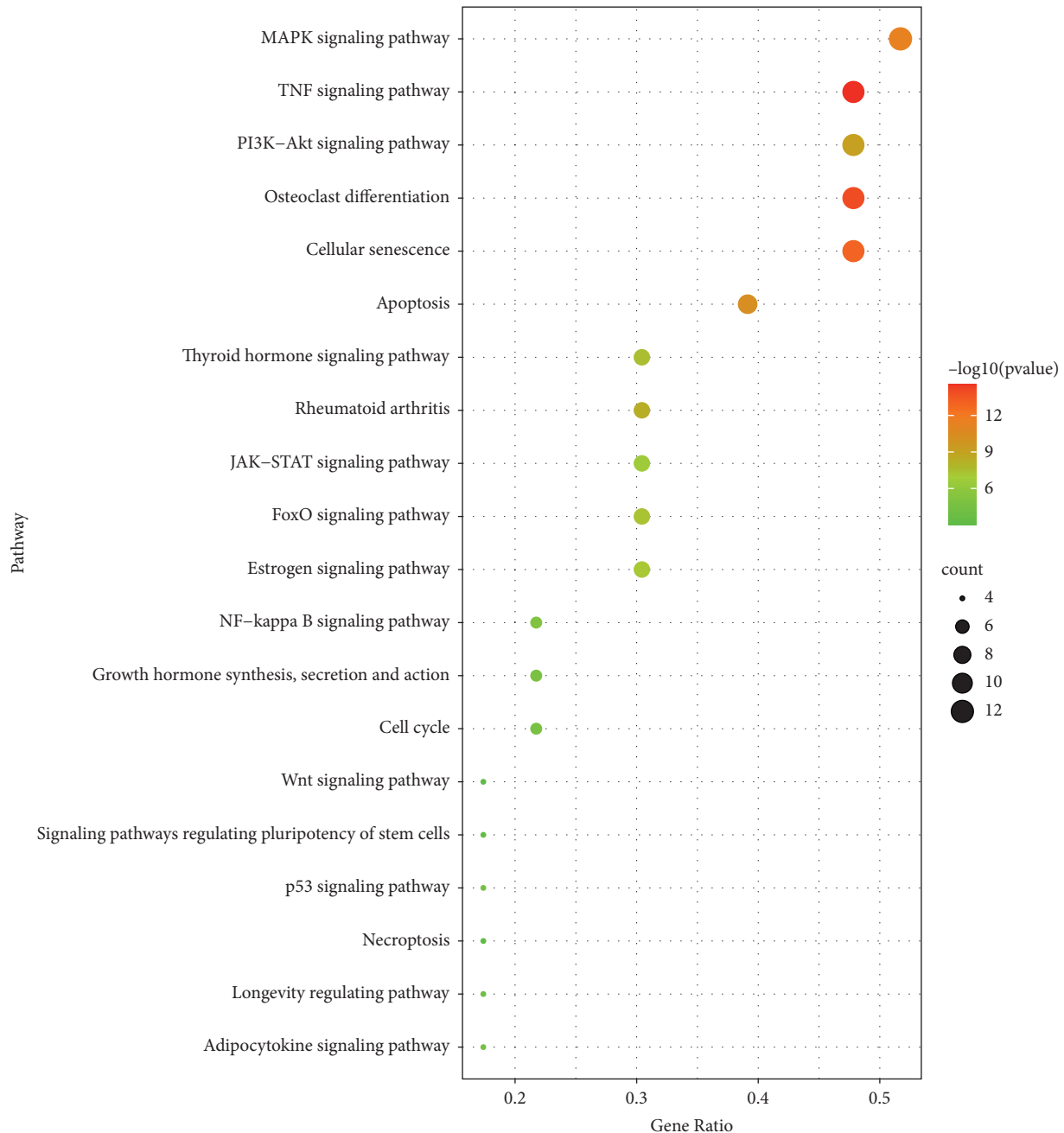
FIGURE 9: KEGG enrichment analysis.

were positive for the typical hBMSCs markers CD29 (98.9%) and CD44 (99%), with concomitant absence of CD34 (0.02%). Therefore, we concluded that most of the isolated and purified cells expressed standard markers of hBMSCs.

3.7.2. The Promoting Effect of CKG-Medicated Serum on Cell Proliferation.
To detect the effect of CKG-medicated serum on hBMSCs' growth, we incubated cells in basic medium with different concentrations of NS and MS (2, 5, or 8%) for 24, 36, and 48 h. According to the results of the CCK-8 assay (Figure 13), the CKG-medicated serum treatment significantly improved hBMSCs growth at different time points. The cell proliferation rate was the highest when cells were treated with 5% MS for 36 h ($P < 0.05$).

3.7.3. Western Blot.
Comprehensively analyzing the screening results of the core targets and the KEGG enrichment analysis results, we can infer that CKG exerts its antiosteoporosis influence through multiple pathways. The top 3 pathways most closely related to OP in KEGG enrichment analysis are the MAPK signaling pathway, the PI3K-Akt signaling pathway, and the TNF signaling pathway. The top 5 core targets of CKG for treating OP are JUN,
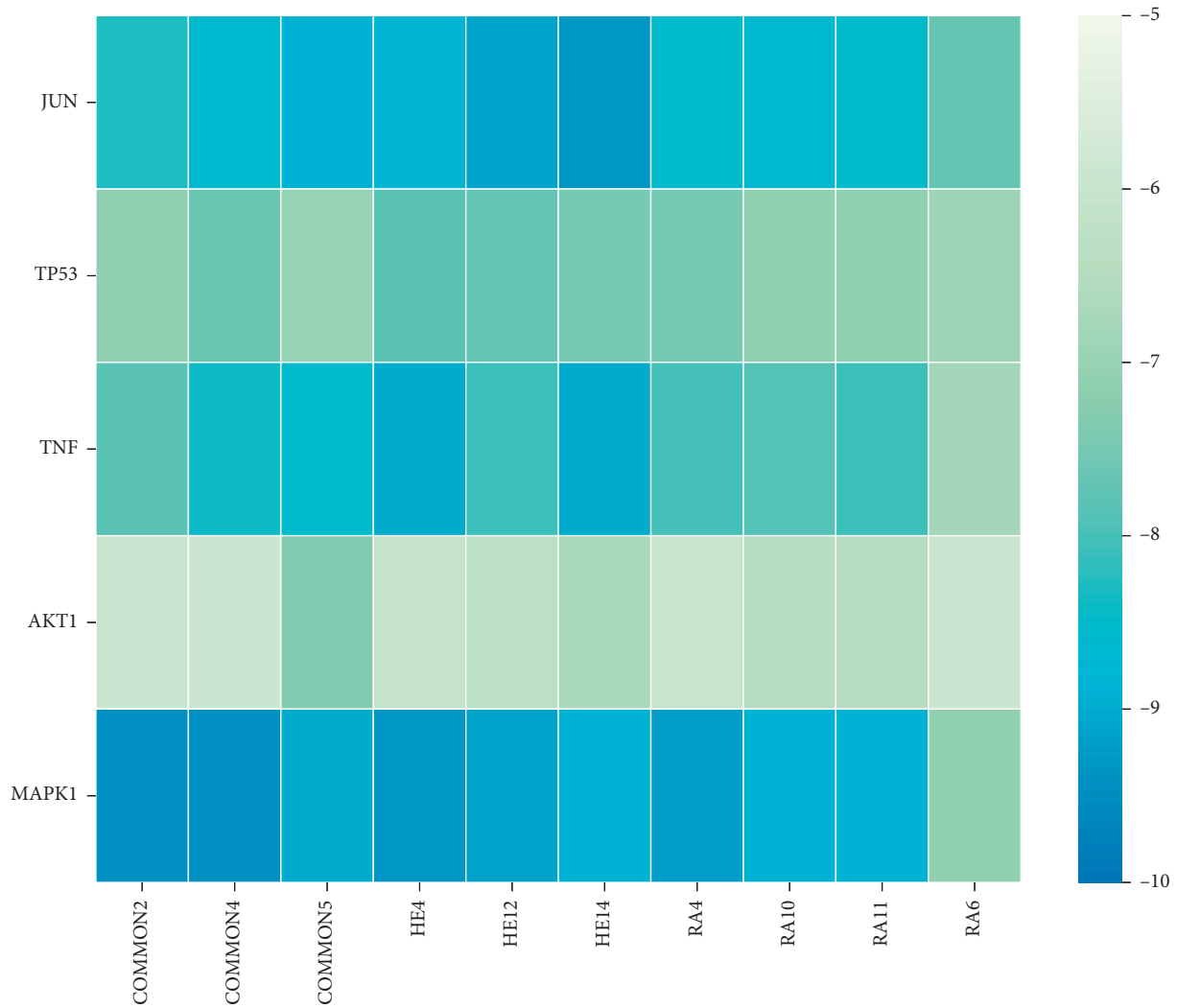
Figure 10: Heat maps of molecular docking between bioactive ingredients of CKG and core targets.

Table 4: Docking scores of the top 10 bioactive ingredients of CKG with 5 core targets.

Target	PDB ID	Compound	Affinity (kcal/mol)
JUN	2g01	8-(3-methylbut-2-enyl)-2-phenyl-chromone	−9.3
TP53	2j21	Luteolin	−7.8
TNF	2az5	Luteolin	−9
AKT1	1unq	22,23-Dihydrostigmasterol	−7.4
MAPK1	3w8q	Kaempferol	−9.4

(a)   (b)   (c)   (d)
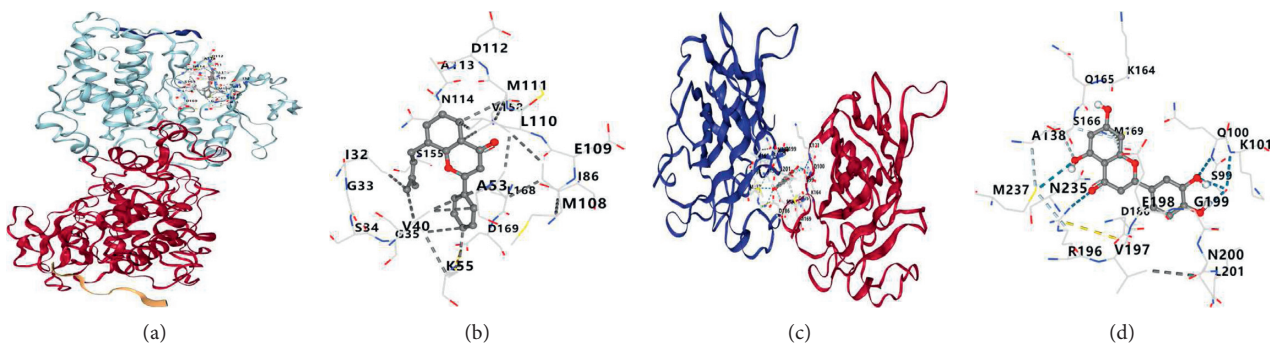
Figure 11: Continued.

(e)   (f)   (g)   (h)

(i)   (j)
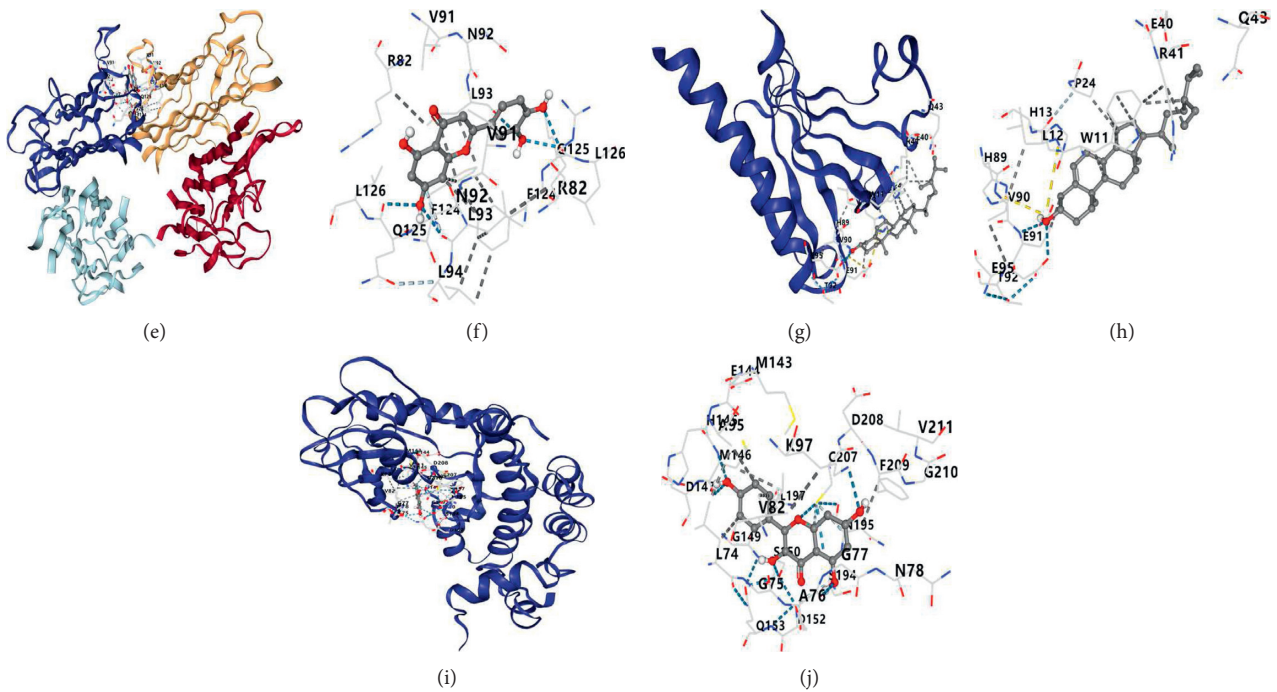
FIGURE 11: Binding mode and a 2D interaction map of compounds with core targets. (a) The binding mode of 8-(3-methylbut-2-enyl)-2-phenyl-chromone with JUN; (b) the 2D interaction map of 8-(3-methylbut-2-enyl)-2-phenyl-chromone with JUN; (c) the docking process of luteolin with TP53; (d) the 2D interaction map of luteolin with TP53; (e) the binding mode of luteolin with TNF; (f) the 2D interaction map of luteolin with TNF; (g) the binding mode of 22,23-dihydrostigmasterol with AKT1; (h) the 2D interaction map of 22,23-dihy-drostigmasterol with AKT1; (i) the binding mode of kaempferol with MAPK1; and (j) the 2D interaction map of kaempferol with MAPK1.

(a)   (b)

(c)   (d)
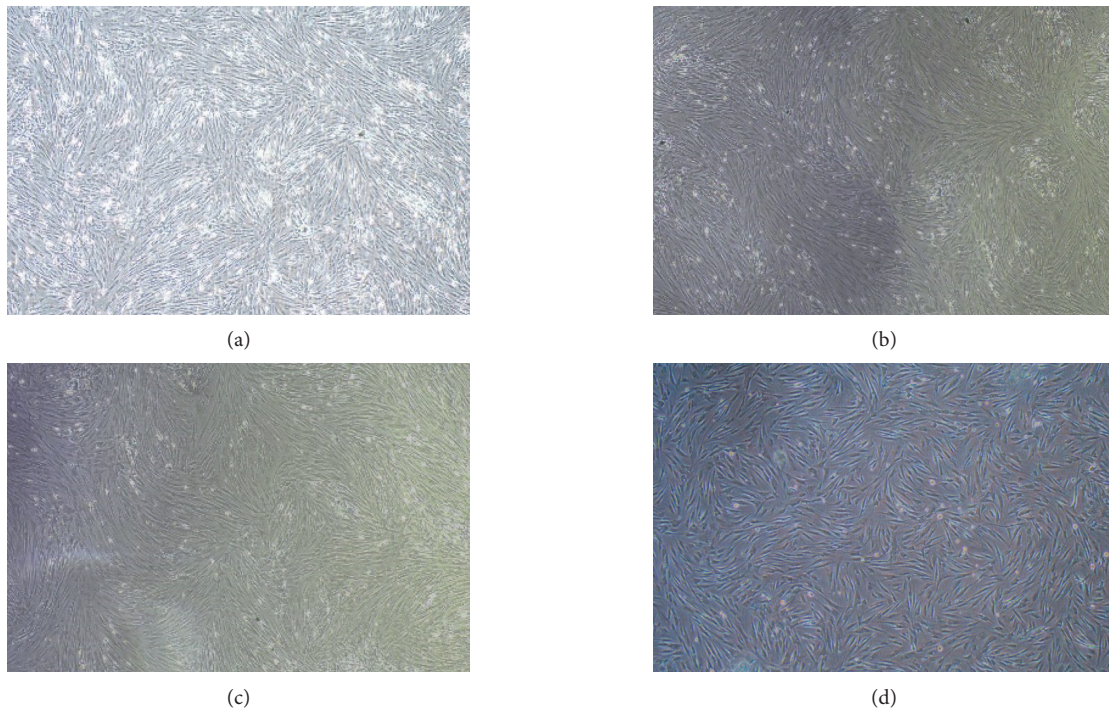
FIGURE 12: Continued.

(e)

(f)

(g)
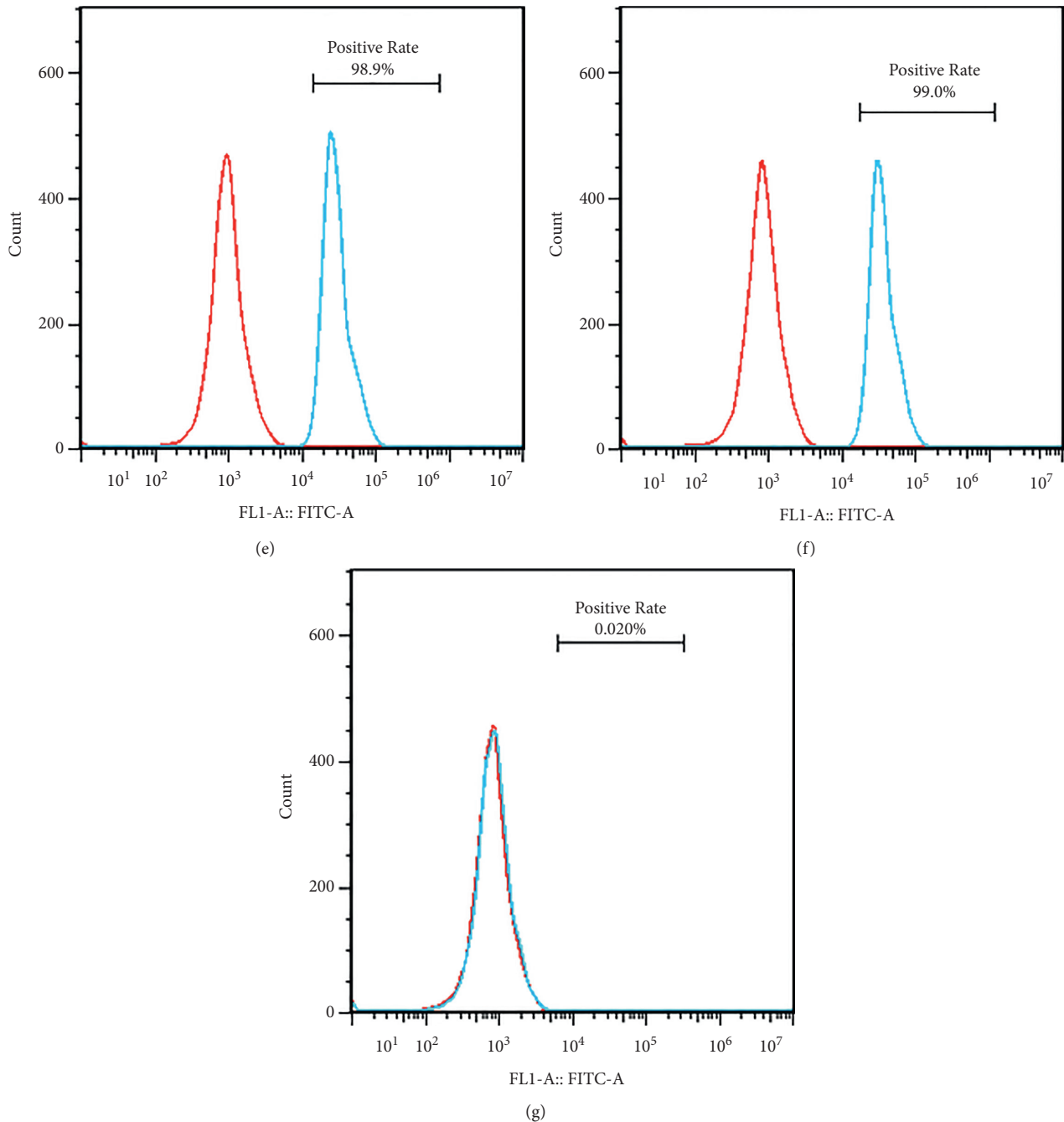
Figure 12: Identification of hBMSCs. hBMSCs at passage 4 were identified with flow cytometry. (a–d) The cell morphology of passage 1 (day 6), 2 (day 5), 3 (day 5), and 4 (day 4), respectively. Flow cytometry was used to analyze the levels of the biomarkers in hBMSCs (e–g). The hBMSCs were positive for CD29 (e), CD44 (f), and negative for CD34 (g).

TNF, TP53, AKT1, and MAPK1. AKT plays an important role in the MAPK signaling pathway, the PI3K-Akt signaling pathway, and the TNF signaling pathway. AKT can negatively regulate B-Raf through phosphorylation of the B-Raf amino-terminal regulatory domain, which in turn affects the Ras/Raf pathway [28]. The inhibition of AKT leads to the enhancement of Ras/MAPK signaling [29]. TNF-α up-regulates several molecules such as the P2X7 receptor through the PI3K-Akt signaling pathway, the intracellular calcium concentration and secondary messengers, the entry of transcription factors into the nucleus, and the differentiation of bone marrow mesenchymal stem cells into osteoclasts [30]. Therefore, this study chose to observe the effect of CKG-medicated serum on the MAPK, PI3K-Akt, and TNF pathway-associated proteins in hBMSCs to verify that CKG participates in the MAPK signaling pathway, the PI3K-Akt signaling pathway, and the TNF signaling pathway by regulating AKT to play its part in treating OP.

Western blot results are shown in Figure 14. The histograms show quantitation of MAPK, PI3K-Akt, and TNF

(a)   (b)
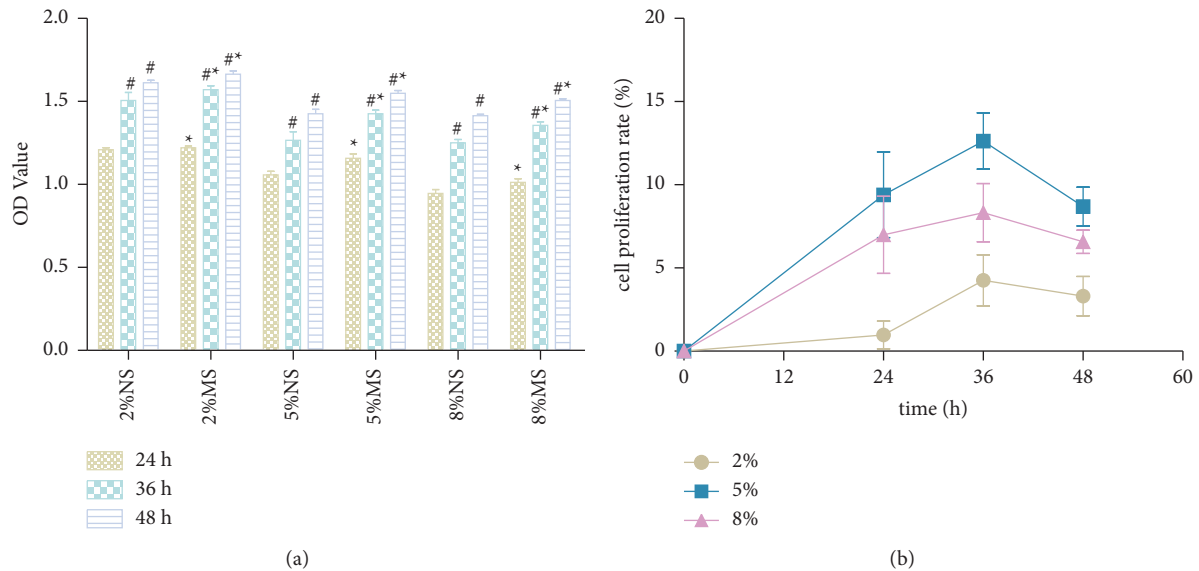
FIGURE 13: CKG-medicated serum treatment increased the proliferation of hBMSCs. (a) The CKG-medicated serum treatment for 24, 36, and 48 h significantly increased the proliferation of hBMSCs ($n = 6$). $^* P < 0.05$, compared to the NS group of the same concentration; $^\# P < 0.05$, compared to the last treatment time. (b) CKG-medicated serum increase hBMSCs proliferation rate, especially when treated with 5% MS for 36 h.

pathway-associated proteins in hBMSCs. Compared with NS, after 36 h of treatment, the AKT, PI3K, ERK1, and IkB protein expression levels in hBMSCs treated with 2, 5, and 8% MS increased. The gradual increase of AKT, PI3K, ERK1, and IkB protein expression levels was detected prominently by western blot as the CKG-MS concentration gradually increased. Compared with NS, after 36 h of treatment, the IKK protein expression levels in hBMSCs treated with 2, 5, and 8% MS decreased. The gradual decrease of IKK protein expression levels was detected prominently by western blot as the CKG-MS concentration gradually increased.

4. Discussion

OP is a metabolic disease caused by various factors, such as age, endocrine, viral infection, and various cytokines [31–33]. Given the multitarget and multipathway pharmacological properties of TCM, we think it is more effective in the treatment of OP. This characteristic of TCM may make it difficult to further study its intrinsic mechanisms. A network pharmacology approach combining systems biology and computer technology may provide a direction for the study of the complex mechanism of TCM [11]. In the present study, we used this approach to clarify the pharmacological mechanisms of OP alleviation by CKG.

In summary, this study analyzed the application of CKG in OP treatment by network pharmacology. We got 69 chemical ingredients, 250 targets of CKG, 1246 disease targets of OP, and 140 intersecting targets of CKG and OP. Topological analysis of the PPI network yielded 23 hub genes. GO enrichment analysis got 1723 entries, of which 1621 were BP entries, 20 were CC entries, and 82 were MF entries. The KEGG enrichment analysis yielded 180 entries. According to enrichment analysis and molecular docking

technique, we inferred that the compounds of CKG (kaempferol, quercetin, 22,23-dihydrostigmasterol, luteolin, anhydroicaritin, 8-(3-methylbut-2-enyl)-2-phenyl-chromone, isorhamnetin, formononetin, calycosin, and 7-O-methylisomucronulatol) could exert antiosteoporosis effects by targeting multiple proteins (JUN, TNF, TP53, AKT1, and MAPK1) and signaling pathways (TNF signaling pathway, osteoclast differentiation, MAPK signaling pathway, PI3K-Akt signaling pathway, NF-kappa B signaling pathway, and Wnt signaling pathway).

The three bioactive compounds in CKG with the highest degree values were 22,23-dihydrostigmasterol, kaempferol, and quercetin, which were obtained from collections of multidatabase information and stringent screening conditions. According to relevant studies, 22,23-dihydrostigmasterol (beta-sitosterol) can play an important role in antiosteoporosis treatment by affecting osteoblasts' activity [34]. Kaempferol promotes bone formation in part via the mTOR signaling pathway [35]. Quercetin inhibits osteoblast apoptosis and inflammatory response, promotes osteogenesis, angiogenesis, and osteoclast apoptosis [36]. The top five core targets in order of degree value are JUN, TNF, TP53, AKT1, and MAPK1. Based on existing relevant literature and studies, JUN accelerates the growth and healing of bone in a drilled defect model [37]. TNF-α directly improves RANKL expression in osteoblasts and promotes osteoclast formation [38]. Related *in vivo* and *in vitro* experiments indicated that TP53 gene expression and serum P53 levels were upregulated in OP patients and OP mouse models; high p53 levels were associated with reduced bone mass, which could be partially reversed by knocking down p53 [39]. Restraint of AKT1 can inhibit BMSC proliferation driven by HB-EGF [40]. MiR-186-5p can reduce IL-1β-induced inflammatory damage of chondrocytes by

(a)

(b)

(c)

(d)

(e)

(f)
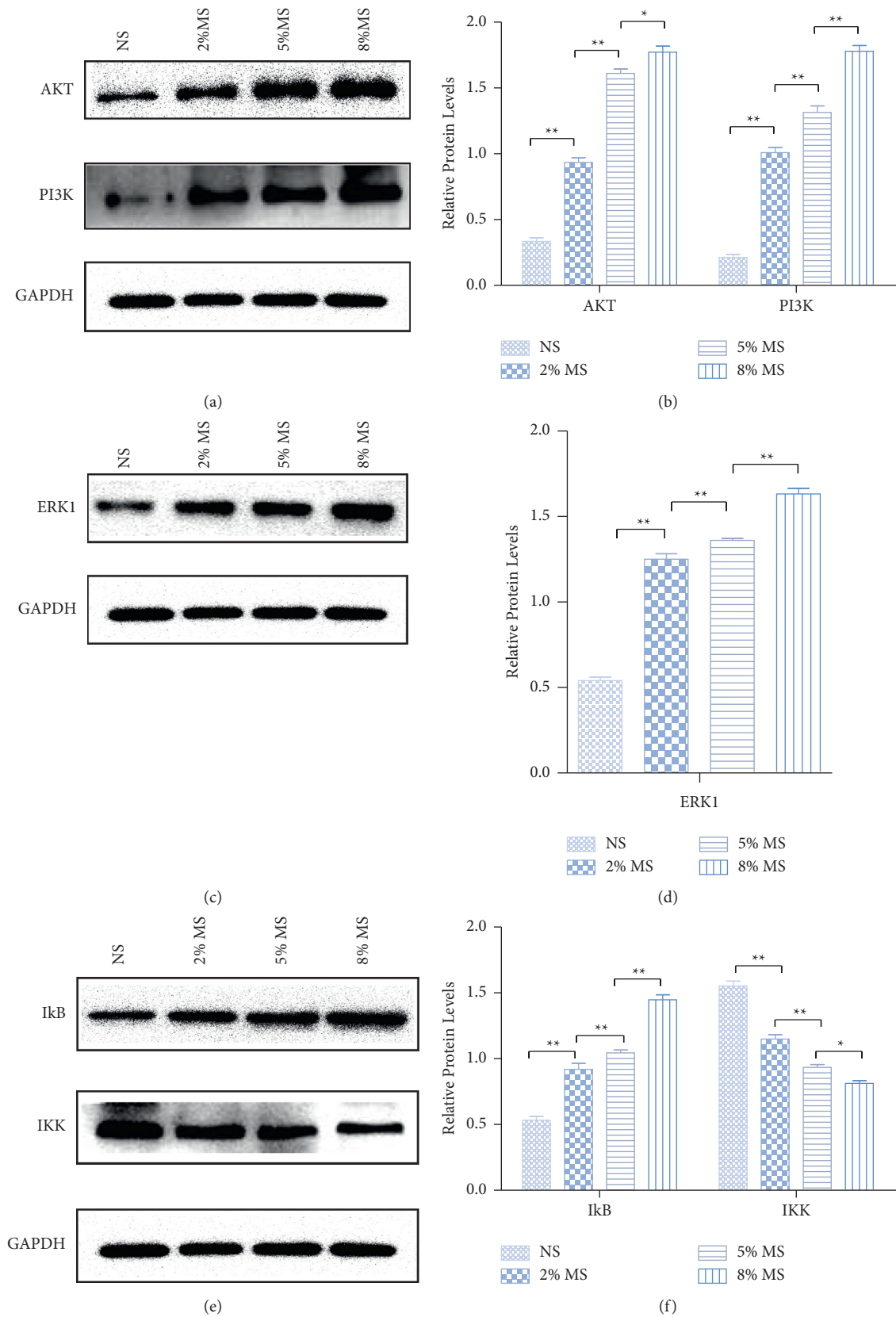
FIGURE 14: Effects of CKG-medicated serum on the expression of MAPK, PI3K-Akt, and TNF pathway-associated proteins. (a, c, e) Western blot was performed to detect AKT, PI3K, ERK1, IkB, and IKK expression levels in CKG-medicated serum-treated hBMSCs. (b, d, f) Quantification of the pathway-related proteins expression. (b) Quantification of the AKT and PI3K expression shown in (a) by normalizing to GAPDH. (d) Quantification of the ERK1 expression shown in C by normalizing to GAPDH. (f) Quantification of the IkB and IKK expression shown in (e) by normalizing to GAPDH. $*P < 0.05$ compared to the previous level group; $**P < 0.01$, compared to the previous level group.

increasing MAPK1 [41]. Enrichment analysis results showed the primary pathways in the therapeutic process include viral-related signaling pathways, bacteria-related signaling pathways, IL-17 signaling pathway, TNF signaling pathway, osteoclast differentiation, MAPK signaling pathway, PI3K-Akt signaling pathway, NF-kappa B signaling pathway, and Wnt signaling pathway. The top 3 pathways most closely related to OP in KEGG enrichment analysis are the MAPK signaling pathway, the PI3K-Akt signaling pathway, and the TNF signaling pathway. PTH induces bone loss through the microbe-dependent expansion of intestinal TNF$^+$ T cells and Th17 cells [42]. Inhibition of NF-kappa B and MAPK signaling can reduce RANKL-induced osteoclastogenesis [43]. The PI3K-Akt signaling pathway involves OP inhibition by promoting osteoblast proliferation, differentiation, and bone formation [44].

The results of molecular docking showed the core bioactive ingredients in CKG had good binding activity to the core targets for treating OP. Comprehensively analyzing the results of PPI, KEGG enrichment analysis, and molecular docking, we speculated that CKG contributes to OP treatment by engaging in multiple pathways. Analyzing the results of KEGG, we concluded that the three most important pathways are the MAPK signaling pathway, the PI3K-Akt signaling pathway, and the TNF signaling pathway. Through comprehensive analysis of the three pathways, we noticed that these pathways are all regulated by AKT, which can negatively regulate Raf, thereby affecting the MAPK signal pathway. AKT regulates the TNF pathway by phosphorylating IKK and is directly involved in the formation of the PI3K-Akt signal pathway. AKT is not only the core target screened by PPI but also the bridging protein between the top 3 pathways in the KEGG enrichment analysis. And related research studies have verified that regulating the AKT protein can affect these three pathways. Therefore, we speculate that CKG exerts an antiosteoporotic effect by affecting the expression of AKT. Then, we conducted related experiments. We used the CCK-8 method to observe the changes in cell proliferation rates after treating them with CKG-containing serum at different concentrations. Western blot was used to observe the changes of MAPK, PI3K-Akt, and TNF pathway-associated protein expression in cells treated with different concentrations of CKG-containing serum. The experimental results showed that CKG-containing serum can promote the proliferation of hBMSCs and that different concentrations of CKG-containing serum can increase the expression of AKT protein in hBMSCs. Therefore, we conclude that the antiosteoporosis effect of CKG may be achieved by regulating AKT and then engaging in the MAPK signaling pathway, the PI3K-Akt signaling pathway, and the TNF signaling pathway.

This study also has some limits, such as the accuracy and timeliness of database data, algorithms, and software characteristics of various analysis platforms. However, based on the completed research, the platforms and algorithms used in this study can meet the research needs. Besides, this study verified the mechanism of CKG in the OP treatment only through molecular docking and animal, cell, and protein experiments. But the results of this study can already

indicate that CKG is involved in the main pathway of antiosteoporosis. Thus, we need to improve related experiments later to support the theory.

5. Conclusion

In this study, the method of combining network pharmacology and experimental confirmation was used to investigate the complexity of multicomponent, multitarget, and multipathway of CKG, which provides essential information for further understanding of the drug-target interaction, a basis for extracting practical drug ingredients from CKG for OP treatment, and a reference for future demonstration of the scientific truth of TCM.

Data Availability

The data used to support the findings of this study are included within the article.

Disclosure

Hao Lv is the first author.

Conflicts of Interest

The authors declare that they have no conflicts of interest.

Authors' Contributions

H. Lv designed the study, analyzed the data, and wrote the manuscript. JX. Wang and YJ. Zhu analyzed the data. T. Jiang revised the manuscript. All the authors read and approved the final manuscript.

Acknowledgments

Supplementary Materials

Supplementary Table 1: the abbreviations and degree values of bioactive ingredients of the "C-T" network. Supplementary Table 2: hub genes of treating OP of CKG. Supplementary Table 3: the results of GO enrichment analysis. Supplementary Table 4: the KEGG enrichment analysis results of the top 20 pathways with high correlation with OP. Supplementary File 5: the diagrams of the MAPK signaling pathway, PI3K-Akt signaling pathway, TNF signaling pathway, and the relationship diagram between them. Supplementary Table 6: docking scores of the top 10 bioactive ingredients of CKG with 5 core targets. Supplementary Table 7: the result of CCK-8. Supplementary Table 8: the results of KEGG enrichment analysis. (*Supplementary Materials*)

References

[1] B. J. Edwards, "Osteoporosis risk calculators," *Journal of Clinical Densitometry*, vol. 20, no. 3, pp. 379–388, 2017.

[2] D. L. Sietsema, "Fighting the epidemic," *Nursing Clinics of North America*, vol. 55, no. 2, pp. 193–202, 2020.

[3] Q. Zeng, N. Li, Q. Wang et al., "The prevalence of osteoporosis in China, a nationwide, multicenter DXA survey," *Journal of Bone and Mineral Research*, vol. 34, no. 10, pp. 1789–1797, 2019.

[4] S. Khosla and L. C. Hofbauer, "Osteoporosis treatment: recent developments and ongoing challenges," *Lancet Diabetes & Endocrinology*, vol. 5, no. 11, pp. 898–907, 2017.

[5] Z. Malihi, Z. Wu, A. W. Stewart, C. M. Lawes, and R. Scragg, "Hypercalcemia, hypercalciuria, and kidney stones in long-term studies of vitamin D supplementation: a systematic review and meta-analysis," *The American Journal of Clinical Nutrition*, vol. 104, no. 4, pp. 1039–1051, 2016.

[6] M. Zhou, Y. Zheng, J. Li et al., "Upper gastrointestinal safety and tolerability of oral alendronate: a meta-analysis," *Experimental and Therapeutic Medicine*, vol. 11, no. 1, pp. 289–296, 2016.

[7] Y. Takeuchi, E. Hamaya, M. Taketsuna, and H. Sowa, "Safety of 3-year raloxifene treatment in Japanese postmenopausal women aged 75 years or older with osteoporosis: a post-marketing surveillance study," *Menopause*, vol. 22, no. 10, pp. 1134–7, 2015.

[8] J. D. Zhao, Y. Q. Shu, J. Liu et al., "Clinical observation on the effect of compound kidney-invigorating granule on visual analog scale and bone mineral density in postmenopausal non-senile osteoporosis patients with kidney deficiency and blood stasis syndrome," *Chinese Journal of Osteoporosis*, vol. 24, no. 1, pp. 98–101, 2018.

[9] P. Xiao-Cong, K. De, F. Jian-Song et al., "Network pharmacology-based analysis of Chinese herbal Naodesheng formula for application to Alzheimer's disease," *Chinese Journal of Natural Medicines*, vol. 16, no. 1, pp. 53–62, 2018.

[10] J. F. Liu, A. N. Hu, J. F. Zan, P. Wang, Q. Y. You, and A. H. Tan, "Network pharmacology deciphering mechanisms of volatiles of wendan granule for the treatment of alzheimer's disease," *Evidence-based Complementary and Alternative Medicine : eCAM*, vol. 2019, Article ID 7826769, 12 pages, 2019.

[11] W. Guo, J. Huang, N. Wang et al., "Integrating network pharmacology and pharmacological evaluation for deciphering the action mechanism of herbal formula zuojin pill in suppressing hepatocellular carcinoma," *Frontiers in Pharmacology*, vol. 10, Article ID 1185, 2019.

[12] T.-T. Luo, Y. Lu, S.-K. Yan, X. Xiao, X.-L. Rong, and J. Guo, "Network pharmacology in research of Chinese medicine formula: methodology, application and prospective," *Chinese Journal of Integrative Medicine*, vol. 26, no. 1, pp. 72–80, 2020.

[13] Y. Chen, T. S. Kern, P. D. Kiser, and K. Palczewski, "Eyes on systems pharmacology," *Pharmacological Research*, vol. 114, pp. 39–41, 2016.

[14] Y. Qu, Z. Zhang, Y. Lu, D. Zheng, and Y Wei, "Network pharmacology reveals the molecular mechanism of cuyux-unxi prescription in promoting wound healing in patients with anal fistula," *Evidence-based Complementary and Alternative Medicine: ECAM*, vol. 2019, Article ID 3865121, 9 pages, 2019.

[15] J. Ru, P. Li, J. Wang et al., "TCMSP: a database of systems pharmacology for drug discovery from herbal medicines," *Journal of Cheminformatics*, vol. 6, Article ID 13, 2014.

[16] B. Li, C. Ma, X. Zhao et al., "YaTCM: yet another traditional Chinese medicine database for drug discovery," *Computational and Structural Biotechnology Journal*, vol. 16, pp. 600–610, 2018.

[17] X. Xu, W. Zhang, C. Huang et al., "A novel chemometric method for the prediction of human oral bioavailability," *International Journal of Molecular Sciences*, vol. 13, no. 6, pp. 6964–6982, 2012.

[18] W. Tao, X. Xu, X. Wang et al., "Network pharmacology-based prediction of the active ingredients and potential targets of Chinese herbal radix curcumae formula for application to cardiovascular disease," *Journal of Ethnopharmacology*, vol. 145, no. 1, pp. 1–10, 2013.

[19] C. UniProt, "UniProt: a worldwide hub of protein knowledge," *Nucleic Acids Research*, vol. 47, no. D1, pp. D506–D515, 2019.

[20] P. Shannon, A. Markiel, O. Ozier et al., "Cytoscape: a software environment for integrated models of biomolecular interaction networks," *Genome Research*, vol. 13, no. 11, pp. 2498–2504, 2003.

[21] G. Stelzer, N. Rosen, I. Plaschkes et al., "The GeneCards suite: from gene data mining to disease genome sequence analyses," *Current protocols in bioinformatics*, vol. 54, pp. 1–33, 2016.

[22] A. P. Davis, C. J. Grondin, R. J. Johnson et al., "Comparative toxicogenomics database (CTD): update 2021," *Nucleic Acids Research*, vol. 49, no. D1, pp. D1138–D1143, 2021.

[23] P. Bardou, J. Mariette, F. Escudié, C. Djemiel, and C. Klopp, "Jvenn: an interactive venn diagram viewer," *BMC Bioinformatics*, vol. 15, Article ID 293, 2014.

[24] C. V. Mering, M. Huynen, D. Jaeggi, S. Schmidt, P. Bork, and B. Snel, "STRING: a database of predicted functional associations between proteins," *Nucleic Acids Research*, vol. 31, no. 1, pp. 258–261, 2003.

[25] Y. Tang, M. Li, J. Wang, Y. Pan, and F.-X. Wu, "CytoNCA: a cytoscape plugin for centrality analysis and evaluation of protein interaction networks," *Biosystems*, vol. 127, pp. 67–72, 2015.

[26] S. Kim, J. Chen, T. Cheng et al., "PubChem in 2021: new data content and improved web interfaces," *Nucleic Acids Research*, vol. 49, no. 1, pp. D1388–D1395, 2021.

[27] S. K. Burley, H. M. Berman, C. Christie et al., "RCSB protein data bank: sustaining a living digital data resource that enables breakthroughs in scientific research and biomedical education," *Protein Science*, vol. 27, no. 1, pp. 316–330, 2018.

[28] K.-L. Guan, C. Figueroa, T. R. Brtva et al., "Negative regulation of the serine/threonine kinase B-Raf by Akt," *Journal of Biological Chemistry*, vol. 275, no. 35, pp. 27354–27359, 2000.

[29] B. Y. Shorning, M. S. Dass, M. J. Smalley, and H. B Pearson, "The PI3K-AKT-mTOR pathway and prostate cancer: at the crossroads of AR, MAPK, and WNT signaling," *International Journal of Molecular Sciences*, vol. 21, no. 12, 2020.

[30] J. Lu, Z. Zhou, J. Ma et al., "Tumour necrosis factor-α promotes BMHSC differentiation by increasing P2X7 receptor in oestrogen-deficient osteoporosis," *Journal of Cellular and Molecular Medicine*, vol. 24, no. 24, pp. 14316–14324, 2020.

[31] K. E. Ensrud and C. J. Crandall, "Osteoporosis," *Annals of Internal Medicine*, vol. 167, no. 3, pp. ITC17–ITC32, 2017.

[32] V. Pavone, G. Testa, S. M. C. Giardina, A. Vescio, D. A. Restivo, and G. Sessa, "Pharmacological therapy of osteoporosis: a systematic current review of literature," *Frontiers in Pharmacology*, vol. 8, Article ID 803, 2017.

[33] M. N. Weitzmann, "Bone and the immune system," *Toxicologic Pathology*, vol. 45, no. 7, pp. 911–924, 2017.

[34] S. Chauhan, A. Sharma, N. K. Upadhyay, G. Singh, U. Ranjan Lal, and R. Goyal, "In-vitro osteoblast proliferation and in-vivo anti-osteoporotic activity of Bombax ceiba with quantification of Lupeol, gallic acid and beta-sitosterol by HPTLC and HPLC," *BMC Complementary and Alternative Medicine*, vol. 18, no. 1, Article ID 233, 2018.

[35] J. Zhao, J. Wu, B. Xu et al., "Kaempferol promotes bone formation in part via the mTOR signaling pathway," *Molecular Medicine Reports*, vol. 20, no. 6, pp. 5197–5207, 2019.

[36] S. K. Wong, K. Y. Chin, and S. Ima-Nirwana, "Quercetin as an agent for protecting the bone: a review of the current evidence," *International Journal of Molecular Sciences*, vol. 21, no. 17, 2020.

[37] T. Lerbs, L. Cui, C. Muscat et al., "Expansion of bone precursors through jun as a novel treatment for osteoporosis-associated fractures," *Stem Cell Reports*, vol. 14, no. 4, pp. 603–613, 2020.

[38] H. Kitaura, A. Marahleh, F. Ohori et al., "Osteocyte-related cytokines regulate osteoclast formation and bone resorption," *International Journal of Molecular Sciences*, vol. 21, no. 14, 2020.

[39] T. Yu, X. You, H. Zhou et al., "p53 plays a central role in the development of osteoporosis," *Aging*, vol. 12, no. 11, pp. 10473–10487, 2020.

[40] P. Li, Q. Deng, J. Liu et al., "Roles for HB-EGF in mesenchymal stromal cell proliferation and differentiation during skeletal growth," *Journal of Bone and Mineral Research*, vol. 34, no. 2, pp. 295–309, 2019.

[41] Q. Li, M. Wu, G. Fang et al., "MicroRNA1865p down-regulation inhibits osteoarthritis development by targeting MAPK1," *Molecular Medicine Reports*, vol. 23, no. 4, 2021.

[42] M. Yu, A. Malik Tyagi, J.-Y. Li et al., "PTH induces bone loss via microbial-dependent expansion of intestinal TNF$^+$ T cells and Th17 cells," *Nature Communications*, vol. 11, no. 1, Article ID 468, 2020.

[43] D. Thummuri, L. Guntuku, V. S. Challa, R. N. Ramavat, and V. G. M. Naidu, "Abietic acid attenuates RANKL induced osteoclastogenesis and inflammation associated osteolysis by inhibiting the NF-KB and MAPK signaling," *Journal of Cellular Physiology*, vol. 234, no. 1, pp. 443–453, 2018.

[44] J. C. Xi, H. Y. Zang, L. X. Guo et al., "The PI3K/AKT cell signaling pathway is involved in regulation of osteoporosis," *Journal of Receptors and Signal Transduction*, vol. 35, no. 6, pp. 640–645, 2015.

Research Article

Exploring the Mechanism of Resveratrol in Reducing the Soft Tissue Damage of Osteoarthritis Based on Network Pharmacology and Experimental Pharmacology

Zhiyong Long,[1] Wang Xiang,[2] Jun Li [ID],[3] Tiejun Yang [ID],[3] and Ganpeng Yu [ID][3]

[1]*Shantou University Medical College, Shantou University, Shantou, Guangdong, China*
[2]*The Affiliated Hospital of Guilin Medical University, Guilin, Guangxi Province, China*
[3]*People's Hospital of Ningxiang City, Ningxiang City, Hunan Province, China*

Correspondence should be addressed to Jun Li; lijun.guke@hotmail.com, Tiejun Yang; yangtiejun321@outlook.com, and Ganpeng Yu; yuganpeng.guke@hotmail.com

Aim. To explore the mechanism of resveratrol in reducing the soft tissue damage of osteoarthritis (OA) based on network pharmacology. *Methods*. Pharmmapper was used to predict the target of resveratrol, OMIM and Genecards were used to collect OA-related disease genes, and David ver 6.8 was used for enrichment analysis. Then, animal experiments were carried out for verification. The rat OA model was established and the rats were randomly divided into 4 groups: model group, resveratrol low-dose group, resveratrol high-dose group, and blank control group for follow-up experiments. Hematoxylin-eosin (HE) staining was used to detect the degree of pathological damage of rat bones and joints. Enzyme-linked immunosorbent assay (ELISA) was used for the content of inflammatory factors. Western blot was used to detect the expression of Toll-like receptor 4 (TLR4), Myeloid differentiation factor 88 (MyD88), nuclear factor kappa B protein (NF-κB), cysteine protease-9 (CASP-9), Bcl-2 protein, and Bax protein. *Results*. Through network pharmacological analysis, this study found that resveratrol may regulate the TLR4 signaling pathway, PI3K-Akt signaling pathway, FoxO signaling pathway, Osteoclast differentiation, Rheumatoid arthritis, etc. Animal experiments showed that compared with the model group, the pathological damage of bone and joint in the resveratrol low-dose and high-dose groups was significantly improved. Compared with the model group, the serum levels of IL-1beta, IL-6, IL-17, TNF-α, and MCP-1 in the resveratrol low-dose and high-dose groups were significantly reduced ($P < 0.05$); protein levels of TLR-4, MyD88, and NF-κB p65 were significantly reduced ($P < 0.05$); caspase-9 and Bax protein levels were significantly reduced ($P < 0.05$), and Bcl-2 was significantly increased ($P < 0.05$). *Conclusion*. Resveratrol may inhibit the activation of the TLR4-mediated NF-κB signaling pathway and has a repairing effect on soft tissue damage in OA.

1. Introduction

Osteoarthritis (OA) is a degenerative joint disease characterized by progressive articular cartilage destruction, subchondral bone changes, osteophyte formation, and synovial inflammation [1]. The clinical symptoms are mainly joint pain, swelling, stiffness, and mobility disorders, which seriously affect the quality of life of patients [2–4]. In the past 20 years, the number of patients with OA has increased dramatically [5, 6]. It is estimated that the current prevalence of OA in people over 50 years old worldwide is as high as

10% to 20%, and in the next 30 years, its prevalence may double [7]. So far, the clinical treatment of OA is mainly to relieve pain and maintain joint function. At present, non-steroidal anti-inflammatory drugs (NSAIDs) have been used as a routine treatment for OA, but their adverse events should not be underestimated [8]. Therefore, it is very important to explore the occurrence and development mechanism of OA and find safer and more effective treatments for the prevention and treatment of OA.

Resveratrol is a natural polyphenol plant compound with a symmetric diphenylethylene structure. Its content is high

in the rhizomes of grapes, cranberries, peanuts, mulberries, and other plants and the traditional Chinese medicine Polygonum cuspidatum [9–11]. It has almost no toxic and side effects on the human body and has been proven to have anti-inflammatory, antitumor, antioxidant, and immune-regulating effects [12]. Studies have shown that resveratrol has anti-inflammatory and chondroprotective effects in a rabbit OA model induced by endotoxin (LPS) [13]. Hua et al. found that resveratrol can prevent sodium nitro-soferricyanide-induced OA-like inflammation [14]. However, the mechanism of resveratrol in the treatment of OA is still unknown.

As a new interdisciplinary developed in recent years, network pharmacology has changed the previous drug discovery model of "single gene, single target, single disease." The emergence of network pharmacology is of great significance for the discovery of new drugs and the multitarget research of drugs, and it is mainly used for drug toxicity prediction and drug readjustment indications [15, 16]. For different kinds of diseases, the location and characteristics of drug targets and disease genes in the network are different. Research shows that the distance between the drug target and the key node of the disease network has certain characteristics in the network. In addition, studies have found that in the process of rational drug design, the network distance between drug targets and corresponding disease genes has a tendency to become smaller and smaller [17]. This suggests that it is of great significance to probe the characteristics of drug targets in biological networks. Therefore, this study would explore the molecular network of resveratrol in the treatment of OA through network pharmacology and further verify the related signaling pathways and biological processes in OA rat models. The idea and process of this research are shown in Figure 1.

2. Materials and Methods

2.1. Potential Targets of Resveratrol Prediction and OA Disease Gene Collection. The relevant chemical information and several potential targets of resveratrol were searched through the PubChem database (https://www.ncbi.nlm.nih.gov) [18], and the chemical structure of resveratrol was drawn using ChemDraw 3D software and saved in sdf format. The SMILES structure of resveratrol was also collected from Pubchem. The "sdf" format of resveratrol was input into Pharmmapper (http://lilab-ecust.cn/pharmmapper/) to predict its potential targets [19]. The SIMES structure of resveratrol was input into Swiss Target Prediction (http://www.swisstargetprediction.ch/) [20], Similarity ensemble approach (SEA) (http://sea.bkslab.org/) [21], and STITCH Database (http://stitch.embl.de/) [22] to obtain the potential targets. The resveratrol targets were imported into UniProt (http://www.uniprot.org/) to obtain the official gene symbol. Finally, those targets were combined and deduplicated to obtain the set of resveratrol potential targets.

OA disease genes were searched and collected using the OMIM database (http://omim.org/) and Genecards (http://www.genecards.org) [23, 24]. The search results of Genecards and OMIM were merged and deduplicated to obtain

OA-related genes set. The resveratrol targets and OA genes are shown in Table S1 (see supplementary materials). The potential target set of resveratrol and the OA target set were compared, and the overlapping part of the two was considered as the target of resveratrol in the treatment of OA (Table S2).

2.2. Resveratrol-OA Protein-Protein Interaction (PPI) Network Construction and Analysis. The String database (https://string-db.org/) is a database for searching protein interactions, including both direct physical interactions between proteins and indirect functional correlations [25]. The targets were input into String to collect the PPI data. Cytoscape 3.7.1 software was utilized for visualization. The node degree and betweenness centrality are used to reflect the importance of the node. The larger the value of the degree and the betweenness centrality, the more important the node in the network.

In order to further understand the functions of core target genes and the main pathways of resveratrol in the treatment of OA, the resveratrol-OA targets in the resveratrol-OA PPI network were input into David database (https://david.ncifcrf.gov/home.jsp) for Gene Ontology (GO) enrichment analysis and KEGG pathway enrichment analysis, and the species was selected as "Homo sapiens" [26].

2.3. Experimental Animals. Eighty (80) 6-week-old, SD male healthy rats were purchased from Guangdong Experimental Animal Center and raised in a standard environment, license number SCXK (Guangdong) 2018–0016. The weight of the rat is (180 ± 10) g. The rats were kept in a temperature-controlled $(22^\circ C \pm 1^\circ C)$ and light-controlled animal facility (200 lux, 12-hour light-dark cycle) for 7 days. The experiment was approved by the Animal Ethics Committee of Shantou University Medical College.

2.4. Reagents and Instruments. Resveratrol was purchased from the National Institute for the Control of Pharmaceutical and Biological Products (batch number: 110742200517, purity 99.9%). Collagenase Type II, (Cat. No.: C2-28, sigma company); BCA protein quantitative kit (batch number Q1220551), phenylmethylsulfonyl fluoride (PMSF, batch number: RE2173411), ethyl iodide Amide (IAA, batch number QL224490), RIPA high-efficiency lysate (batch number TJ272371), Ammonium bicarbonate powder (batch number BCBN6056 V) were purchased from Sigma Inc. The PVDF membrane was purchased from Millipore, USA (Cat. No. IPVH00010). Trypsin-EDTA digestion solution was purchased from Jiangsu KGI Biotechnology Co., Ltd. (Cat. No. KGY0012). HRP goat anti-rabbit secondary antibody IgG (Cat. No. ZB 2306) was purchased from Beijing Zhongshan Jinqiao Biotechnology Co., Ltd. The chemiluminescent substrate (Cat. No. A38555) was purchased from Thermo Company. IL-1β (H002), IL-6 (H007), IL -17 (H014), TNF-α (H052), and MCP-1 (H115) ELISA kits were purchased from Nanjing Jiancheng Institute of

FIGURE 1: The idea and process of this research.

Bioengineering. Antibody TLR-4 (BA1717) and Antibody MyD88 (A00025-1) were purchased from Boster Biological Technology Co, Ltd. Antibody NFκB p65 (ATA33904) was purchased from AtaGenix (Wuhan) Technology Co., Ltd. Antibody Caspase-9 (ab32539), antibody Bcl -2 (ab182858), antibody Bax (ab32503), and antibody β-actin (ab8226) were purchased from Abcam Inc. The desktop high-speed refrigerated centrifuge was purchased from Sigma Inc. The microplate reader was purchased from Thermo Company. The tissue disrupter was purchased from SPEX SamplePrep.

2.5. Animal Modeling, Grouping, and Intervention. The rats were randomly divided into a model group, resveratrol low-dose group, resveratrol high-dose group, and blank control group, with 20 rats in each group. The rats in the model group, resveratrol low-dose group, and resveratrol high-dose group were modeled [27, 28].

After the rats were anesthetized with 3% sodium pentobarbital (40 mg/kg), the right knee joint was disinfected with iodophor 3 times, and then the knee joint was punctured with a 1 mL syringe. 50 μL of Type II collagenase (425 U/mg) with a concentration of 4 mg/mL was injected into the joint cavity. No other special treatment was given after the operation. On the 4th day, the above operation was repeated once, and the animals were raised freely for 3 days after making the model. The rats in the control group were injected with the same volume of normal saline at the same place and time point.

After the model was completed, the drug was started after 3 days of free breeding. Resveratrol low-dose group was given resveratrol 40 mg/kg and the resveratrol high-dose group was given resveratrol 80 mg/kg by gavage, twice daily for 4 weeks. The control group and the model group were given the same amount of normal saline intragastrically.

2.6. Collection, Preparation, and Observation of Knee Joint Specimens. After 4 weeks of intervention, the rats were fasted for 10 hours. After the rats were anesthetized by 3% sodium pentobarbital (40 mg/kg) intraperitoneal injection, about 4 mL of blood was taken from the abdominal aorta and placed in a 5 mL heparin sodium anticoagulation tube. After the blood was taken, the rats were sacrificed by neck dislocation. The entire knee joint was dissected and fixed with 4% paraformaldehyde for 24 h and decalcified with 15% ethylenediaminetetraacetic acid (EDTA) for 4 weeks. The cartilage was cut along the coronal surface of the joint, dehydrated by ethanol, transparent in xylene, embedded in paraffin, and sectioned. The thickness of the section was 7 μm. The isolated cartilage tissue is used to detect protein inflammation and apoptotic protein expression by the Western Bolt method.

2.7. Pathological Observation. The articular cartilage sections were deparaffinized in xylene, then hydrated with gradient alcohol, and stained according to the instructions of the HE staining kit. The sections were stained in hematoxylin for 5 min, dyed in eosin staining solution for 2 min, soaked in distilled water, and then dehydrated in gradient alcohol in turn. Finally, it was made into pathological sections.

2.8. Detection of Serum Inflammatory Factors by ELISA. The rat blood was centrifuged at 3,000 r/min for 10 min, and the supernatant was taken. The antigen is dissolved in 50 mmol/L carbonate coating buffer at 4°C, 100 μL/well is transferred to a 96-well microtiter plate, the antigen is coated overnight, and the coating solution is discarded. After washing, each well was blocked with 150 μL of 1% BSA for 1 hour, washed with PBST 3 times, 100 μL of serum with different dilution ratios was added, and control samples were added and incubated at 37°C for 2 hours. Then it was washed 5 times with PBST, 100 μL of diluted HRP-labeled secondary antibody was added and incubated at 37°C for 1 h. After washing 5 times with PBST, the color developer was added to develop color for 20 min and measured with a microplate reader.

2.9. Detection of Inflammatory Factors by Western Blot. The rat cartilage tissue was prepared as a tissue homogenate, dissolved on ice for 25 min, centrifuged at 12,000 r/min for 10 min, and cell lysate containing protease inhibitors was added for total protein extraction. The BCA kit was used to determine protein content. An equal amount of protein sample (20 mg) was extracted and denatured at 100°C for 5 min. The proteins were then separated using SDS-PAGE gel electrophoresis and transferred to PVDF membranes. At 4°C, the PVDF membrane was added with corresponding monoclonal primary antibodies [TLR4 (1 : 200), MYD88 (1 : 500), NF-KBp65 (1 : 500), Caspase-9 (1 : 100), Bcl- 2, Bax (1 : 100), β-actin (1 : 500)] and incubated overnight. Then the horseradish peroxidase-labeled secondary antibody (1:2 000) was added at 4°C. The color was developed by the chemical substrate luminescence method. ChemiDoc XRS + System gel imager was used for image scanning analysis, Image-QuaNT software was used to measure its absorbance, and each β-actin was used as an internal reference to analyze the relative expression level.

2.10. Statistical Analysis. All the experimental data are statistically analyzed with the statistical software SPSS 20.0. The experimental results are expressed as mean $\pm$ standard deviation. An Independent t-test was used for pairwise comparison, and differences between groups were tested by one-way analysis of variance.

3. Results and Discussion

3.1. Resveratrol-OA PPI Network Analysis. A total of 671 resveratrol potential targets and 3114 OA genes (3114 genes were searched from Genecards and 42 were searched from OMIM) were obtained. There are a total of 302 common targets in the resveratrol potential target set and OA gene set, which are considered as potential targets for resveratrol to treat OA. Among the 302 Resveratrol-OA targets, 297 can

interact with each other. Hence, these 297 were used to construct the Resveratrol-OA PPI network (Figure 2).

3.2. Enrichment Analysis of Resveratrol-OA Targets. The 297 Resveratrol-OA targets in Resveratrol-OA targets PPI network were input into David for enrichment analysis. In the enrichment results of FDR<0.05, the biological processes, cell components, molecular functions, and signal pathways that may be related to OA were screened. Finally, a total of 171 OA-related biological processes, 43 cell components, 90 molecular functions, and 30 signal pathways were obtained (Table S3 and Figure 3). The top 30 biological processes, cell components, molecular functions, and signaling pathways are shown in Figure 4. The relationship between signaling pathways and targets is shown in Figure 5. The targets and genes in the Toll-like receptor signaling pathway and NF-kB signaling pathway are shown in Figure 6 as an example (the Resveratrol-OA targets were marked in pink) [29].

OA is a common degenerative disease that plagues middle-aged and elderly people. The degeneration of articular cartilage caused by the degradation of the cartilage extracellular matrix is the main pathological change of osteoarthritis. The extracellular matrix is mainly composed of type II collagen and Aggrecan. Mature chondrocytes can synthesize and secrete extracellular matrix, which plays a key role in maintaining the dynamic balance between extracellular matrix anabolic and catabolism [30]. Matrix metalloproteinases (MMPs) play an important role in the degeneration of osteoarthritis. MMP-13 is the most effective type II collagen degrading enzyme [31]. In OA pathological process, the secretion of MMP-13 increases and destroys Aggrecan and type II collagen in the extracellular matrix, which ultimately leads to cartilage degeneration and destruction [32].

In the OA model induced by medial meniscus instability surgery, MMP-13 knockout mice inhibited the development of OA by protecting cartilage from proteoglycan loss and structural damage [33]. In clinical samples, MMP-13 is abnormally expressed at different stages of OA: it is upregulated in the cartilage of patients with OA in the early stage and downregulated in the late stage [34]. In addition, MMP-13 is a central node in the cartilage degradation network [35], and its activity can be regulated at multiple levels such as transcription, epigenetic changes, and autophagy [36, 37]. The intervention of resveratrol can decrease the expression of MMP-13, Nuclear factor kappaB (NF-kB) and other inflammatory factors closely related to OA, such as Interleukin-6 (IL-6), Cyclo-oxygenase-2 (COX-2) [38], IL-1β [39], etc. However, the mechanism of resveratrol's anti-OA effect has not been elucidated. Studies have shown that OA may be related to chronic low-grade inflammation, and the expression of a variety of cytokines and inflammatory mediators in the OA state is significantly increased [40], and these inflammatory responses may be related to TLR4. TLR4 can induce synovial cells, chondrocytes, etc., to secrete and release IL-1β and other inflammatory factors, which play a key role in the pathogenesis of OA. The study also found that the expression of TLR4 in OA chondrocytes induced by

IL-1β increased significantly, but after treatment with resveratrol, its expression decreased significantly. Therefore, it is believed that the occurrence and development of OA may be related to the activation of the TLR4 signaling pathway [41], and resveratrol can exert anti-OA effects by inhibiting the Toll-like (TLR4) signaling pathway [42].

TLR4 is one of the important members of the TLRs family and plays a vital role in the process of inducing inflammation [38]. At present, studies have shown that resveratrol can exert anti-OA effects by inhibiting TLR4/MyD88-dependent and independent signaling pathways [43]. Other studies have shown that resveratrol can also exert anti-inflammatory effects through the PI3K/Akt signaling pathway in macrophages [44]. PI3K is an important member of the phospholipid kinase family [45, 46]. Akt is an important direct downstream molecule of PI3K, and activation of PI3K can directly promote Akt phosphorylation and activation. The activation or inhibition of Akt can directly act on its downstream signal molecules and then play a role in regulating cell proliferation, apoptosis, or other important physiological processes [47]. It has been reported in the literature that when LPS acts on human pancreatic cancer cells, it can upregulate the expression of PI3K and Akt. But after adding TLR4 siRNA to silence TLR4, the expression of TLR4 and p-Akt decreased significantly, and after silencing TLR4 and then stimulated by LPS, the expression of TLR4 and p-Akt was still lower than that of the simple LPS group [48]. Xu et al. found that, compared with the hypoxia group, the expression of TNF-a, IL-6, and IL-1β mRNA in the group treated with resveratrol was significantly reduced compared with the hypoxia group. After resveratrol treatment or using LY294002 to inhibit PI3K, the expression of p-Akt decreased significantly. This shows that resveratrol can protect pulmonary artery smooth muscle cells by inhibiting the PI3K/Akt signaling pathway [49]. However, studies have also shown that resveratrol can increase the protein expression of p-Akt in vascular smooth muscle cells while inhibiting the expression of inflammatory factors, that is, by activating the PI3K/Akt signaling pathway to protect vascular smooth muscle [50]. Zong et al. found that when LPS acts on RAW 264.7 cells, the protein expression of p-Akt increases and the PI3K/Akt signaling pathway is activated. Under the combined action of resveratrol and LPS, the activation of the PI3K/Akt signaling pathway was more significant, and the protein expression of p-Akt was further higher than that of the LPS group [51]. It shows that Veratrol may play an anti-LPS-induced inflammatory response in RAW 264.7 cells by activating the PI3K/Akt signaling pathway. The systematic pharmacology part of this study shows that resveratrol can regulate inflammation pathways such as PI3K/Akt signaling pathway, NK-KB signaling pathway, and TNF-α signaling pathway.

3.3. Pathological Changes. The surface of the articular cartilage of the blank control group is flat, the cartilage structure and tidemark of 4 layers are clear, and the chondrocytes are arranged neatly. The cartilage surface in the model group is irregular, cracks are generated, the tidemark recognition is poor, the cartilage structure of 4 layers is unclear, and the cartilage cells proliferate. The cartilage surface of the
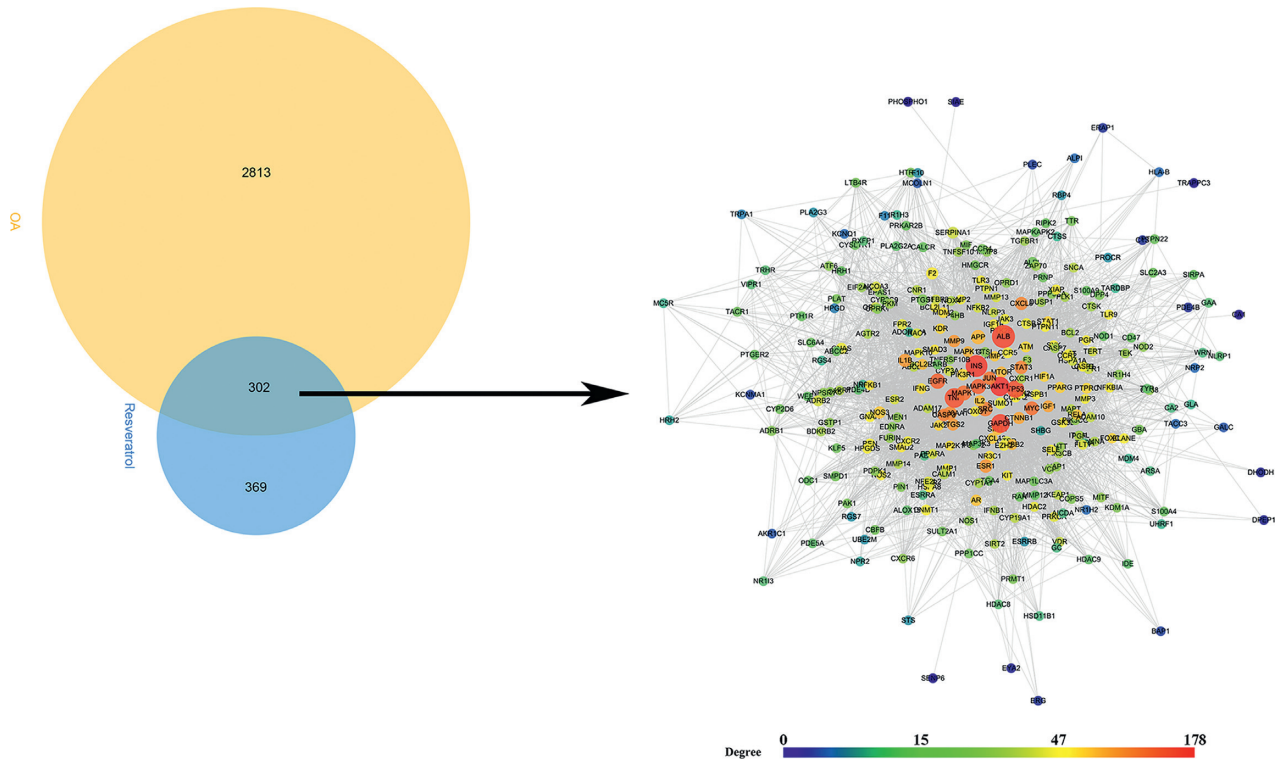
FIGURE 2: Venn diagram and Resveratrol-OA PPI network (the size of the node is positively correlated with its betweenness centrality.).
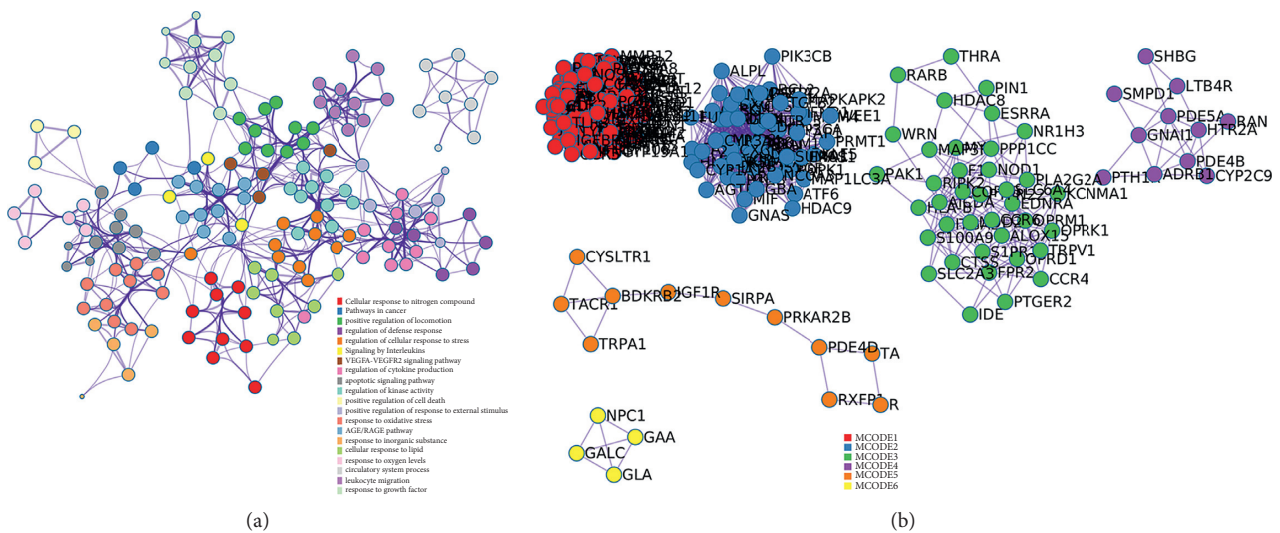
FIGURE 3: Visualizations of functional enrichment and interactome analysis result. (a) PPI network colored by cluster; (b) clusters.

resveratrol low-dose and high-dose groups was more regular, cracks were reduced, a small amount of chondrocyte proliferation was seen, and the tidemark was visible. Compared with the model group, the degree of cartilage pathological damage was reduced (Figure 7).

3.4. Effect of Resveratrol on Serum IL-1β, IL-6, TNF-α, and MCP-1 Content.
Compared with the control group, the levels of IL-1β, IL-6, TNF-α, and MCP-1 in the model group were significantly increased ($P < 0.05$). Compared with the

model group, the levels of IL-1β, IL-6, TNF-α, and MCP-1 in the resveratrol low-dose and high-dose groups were significantly reduced ($P < 0.05$) (Figure 8).

3.5. Effect of Resveratrol on the Expression of TLR-4, MyD88, and NF-Kb p65 Protein.
The expression levels of TLR-4, MyD88, and NF-κB p65 protein in rat cartilage tissue were performed by Western blot. Compared with the control group, the expression of TLR-4, MyD88 and the ratio of NF-κB p65 in the model group were significantly increased
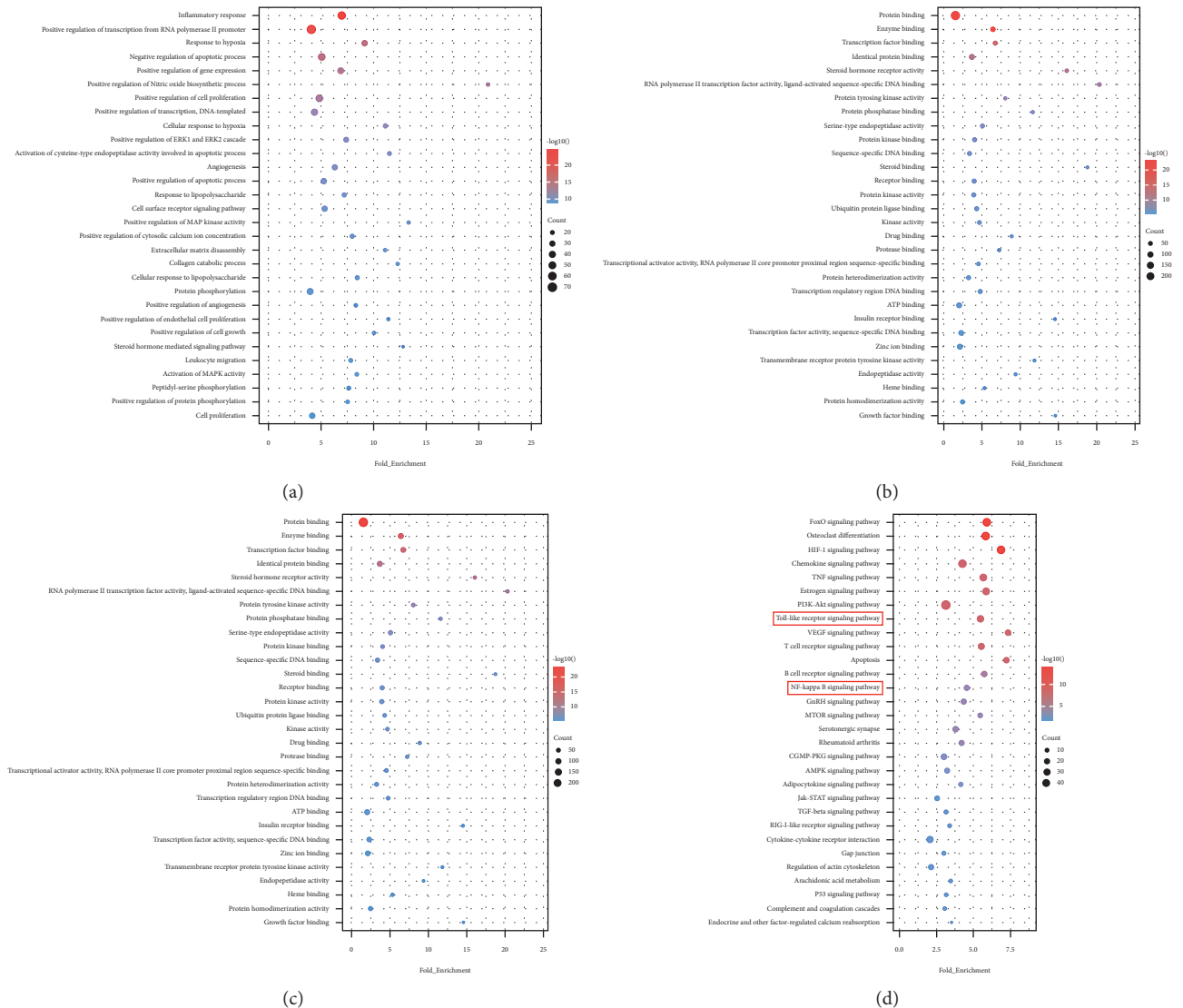
FIGURE 4: Bubble chart of enrichment analysis results. (a) biological processes; (b) cell components; (c) molecular function; (d) signaling pathways. *X*-axis stands for fold enrichment..

($P < 0.05$). Compared with the model group, the expressions of TLR-4, MyD88, and NF-κB p65 in the resveratrol low-dose and high-dose groups were significantly reduced ($P < 0.05$) (Figure 9).

3.6. Effect of Resveratrol on the Expression of Bcl-2, Bax, and Caspase-9 Protein. Compared with the blank control group, the expression of Bcl-2 in the model group decreased ($P < 0.05$), and the expression of Bax and Caspase-9 increased ($P < 0.05$). Compared with the model group, the expression of Bcl-2 in the resveratrol low-dose and high-dose groups increased ($P < 0.05$), and the expression of Bax and Caspase-9 decreased ($P < 0.05$) (Figure 10).

Through network pharmacological analysis, this study found that resveratrol was concentrated in the TLR4 signaling pathway, and animal experiments were used to verify the results. Experimental studies have shown that resveratrol

can improve the degree of pathological damage in OA rats. Apoptosis is positively correlated with the severity of cartilage destruction and matrix depletion in human osteoarthritis tissue specimens. The Caspase family plays an important role in the process of cell apoptosis, and the excessive activation of Caspase-9 and Caspase-3 in the apoptotic cascade can promote cell apoptosis. The anti-apoptotic member Bcl2 can prevent cell apoptosis, while the proapoptotic member Bax is located in the outer mitochondrial membrane or cytoplasm and oligomerizes under stress to promote the release of factors from mitochondria, thereby triggering apoptosis [52]. Burlacu found that the ratio of Bcl-2 to Bax can reflect the relationship between Bcl-2 and Bax in the process of cell apoptosis: an increase in the ratio of Bcl2/Bax inhibits cell apoptosis, and vice versa promotes cell apoptosis [53]. In this experiment, resveratrol can reduce the level of Caspase-9 protein and increase the ratio of Bcl-2/Bax. It shows that resveratrol inhibits the
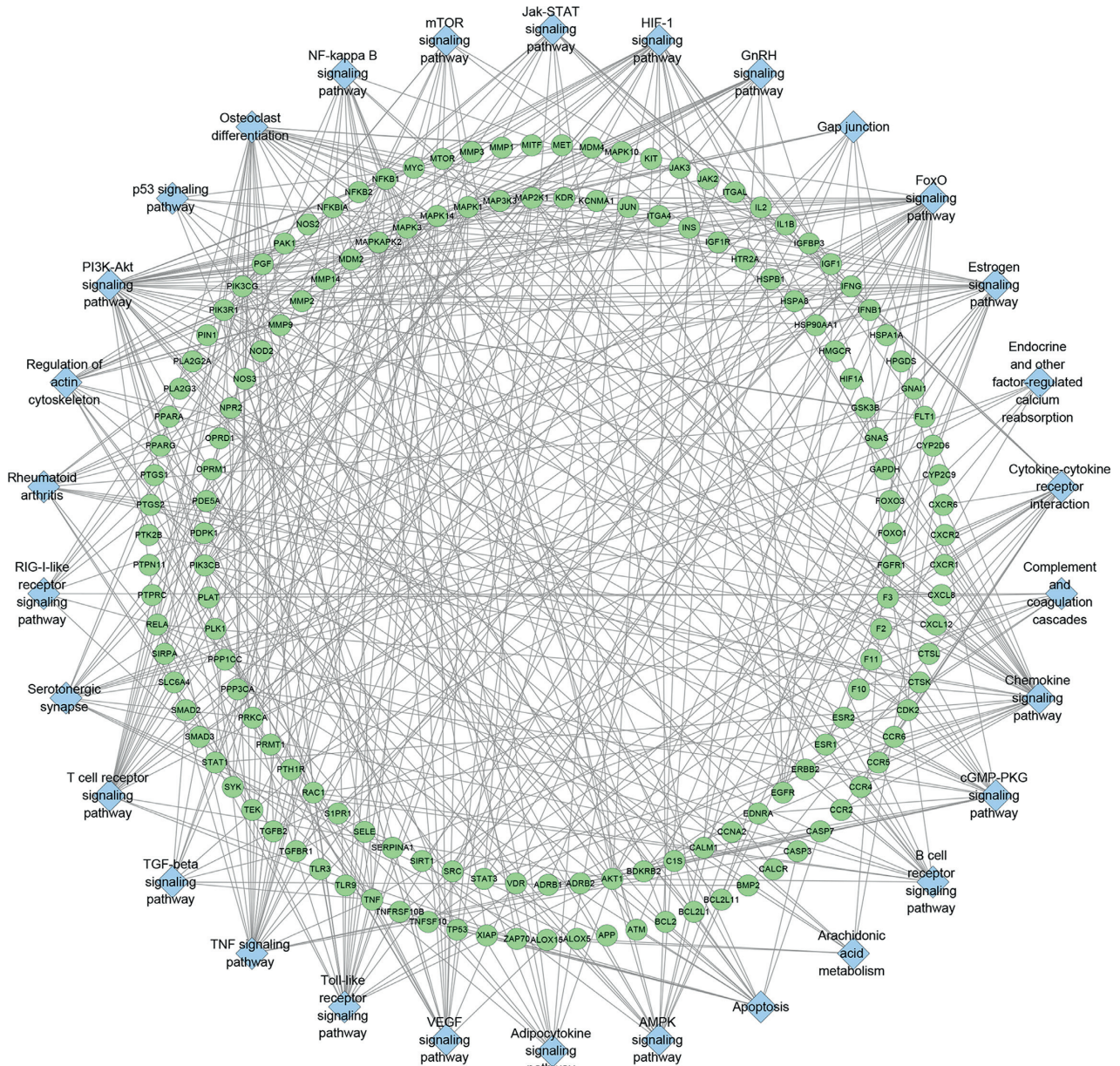
FIGURE 5: Signaling pathway-target network. Blue diamond stands for signaling pathway. Green circles stand for Resveratrol-OA targets.

apoptosis of chondrocytes in OA rats. In the pathology of bone and joint, proinflammatory cytokines play a key role. The levels of TNF-α and IL-6 are recognized cytokines that reflect the degree of inflammation. The high expression of IL-6 can lead to the degradation of articular cartilage and induce pain. TNF-α is an inflammatory response mediator secreted by monocytes and macrophages. Long-term high TNF-α levels may be the main reason for the development of OA in wounded joints. IL-17 is a proinflammatory cytokine secreted by T lymphocytes and monocytes. MCP-1 is a representative of the β subfamily of chemotactic cytokines and an important inflammatory response mediator of OA [54]. This study found that resveratrol can reduce the levels of IL-1β, IL-6, IL17, TNF-α, and MCP-1 in the serum of OA rats. It shows that resveratrol can maintain the normal

structure and function of joints by reducing the content of proinflammatory cytokines.

TLR4/myeloid differentiation factor 88 (My D88) signal transduction pathway is an inflammatory signal pathway that has been studied in the prevention and treatment of knee OA in recent years [55]. TLR4 is an important signal pathway transduction protein, which is closely related to the pathogenesis of OA. It is highly expressed in OA chondrocytes and participates in cartilage destruction. It can activate various inflammatory factors through its downstream MyD88-dependent signal transduction pathway [56]. NF-κB is a primary transcription factor that controls the expression of many proinflammatory genes and plays an important role in cell processes. Literature reports that plant extracts can affect the NF-κB pathway [57]. Studies have
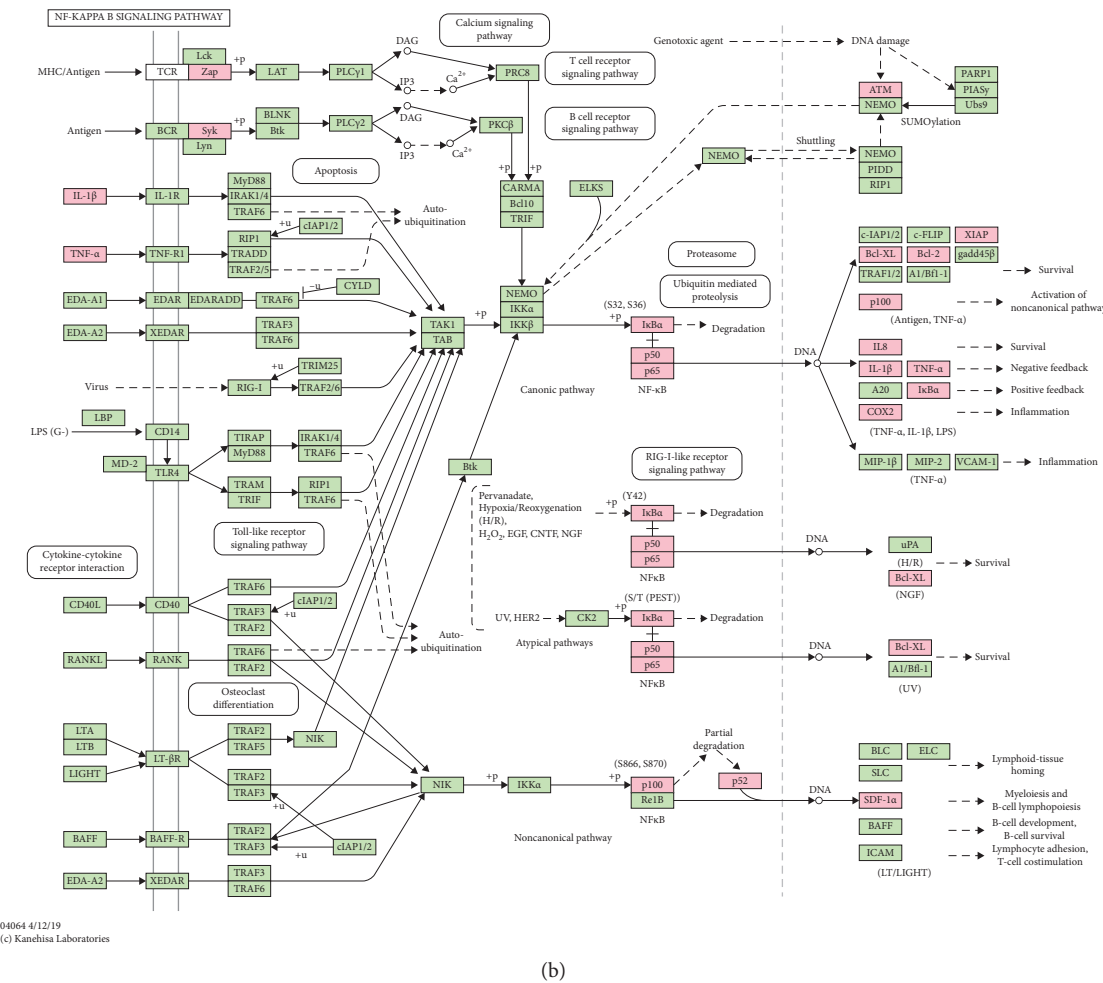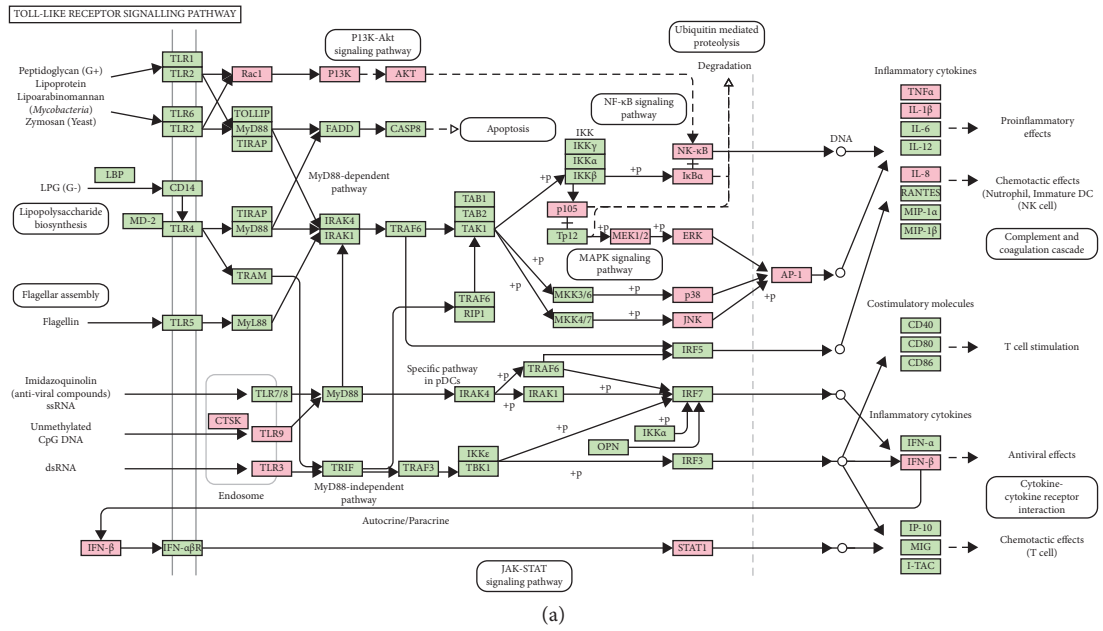
Figure 6: (a) Toll-like receptor signaling pathway adapted from KEGG (ID: hsa04620); (b) NF-kB signaling pathway adapted from KEGG (ID: hsa04064).

(a)

(b)

(c)

(d)
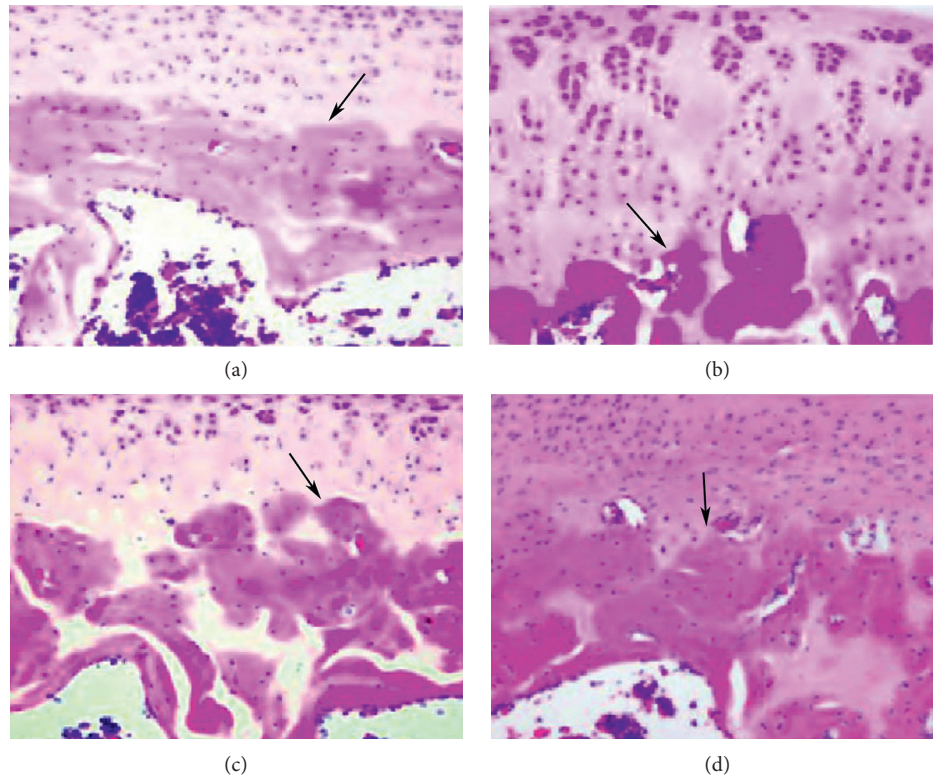
FIGURE 7: Pathological changes (HE staining; X200). (a) Control group; (b) model group; (c) resveratrol low-dose group; (d) resveratrol high-dose group. The black arrow indicates tidemark.
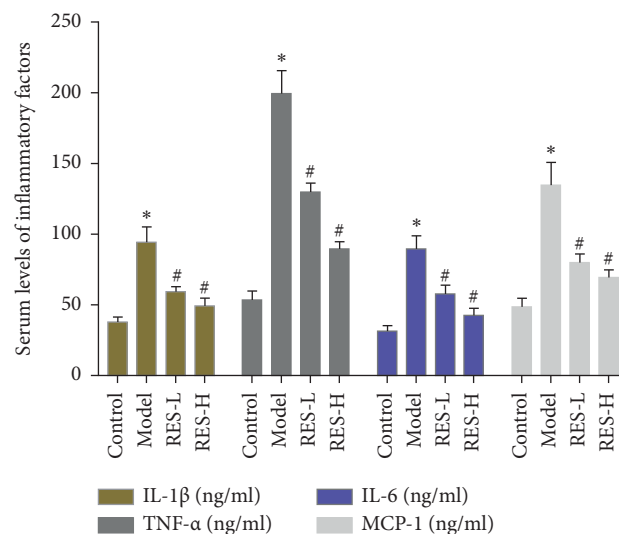
FIGURE 8: Effect of Resveratrol on Serum IL-1β, IL-6, TNF-α, MCP-1 Content (RES-L: resveratrol low-dose group; RES-H: resveratrol high-dose group; *compared with the control group, $P < 0.05$; #compared with model group, $P < 0.05$).

reported that the use of siRNA to interfere with the expression of NFκB p65 can reduce the pathological process of OA in rats, indicating that inhibiting the activity of NF-κB can be used as a target for the treatment of osteoarthritis [58]. This study found that resveratrol downregulated the protein levels of TLR-4, MyD88 and the ratio of pNF-κB p65/NF-κB p65 in osteoarthritis rats. This shows that

resveratrol can treat OA rats by inhibiting TLR-4/MyD88 and NF-κB signaling pathways.

In summary, resveratrol improves the degree of pathological damage in rats with bone OA, reduces cartilage tissue apoptosis, increases the proportion of trabecular bone and the proportion of cartilage, inhibits the degradation of extracellular matrix, promotes the synthesis of extracellular
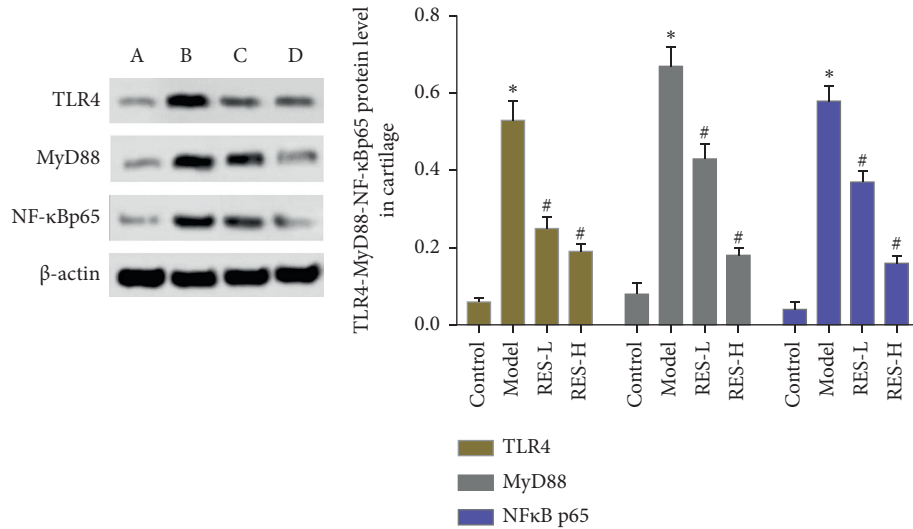
FIGURE 9: Effect of resveratrol on the expression of TLR-4, MyD88, NF-κB p65 protein (A) control group; (B) model group; (C) resveratrol low-dose group; (D) resveratrol high-dose group. *Compared with the control group, $P < 0.05$; #compared with model group, $P < 0.05$.
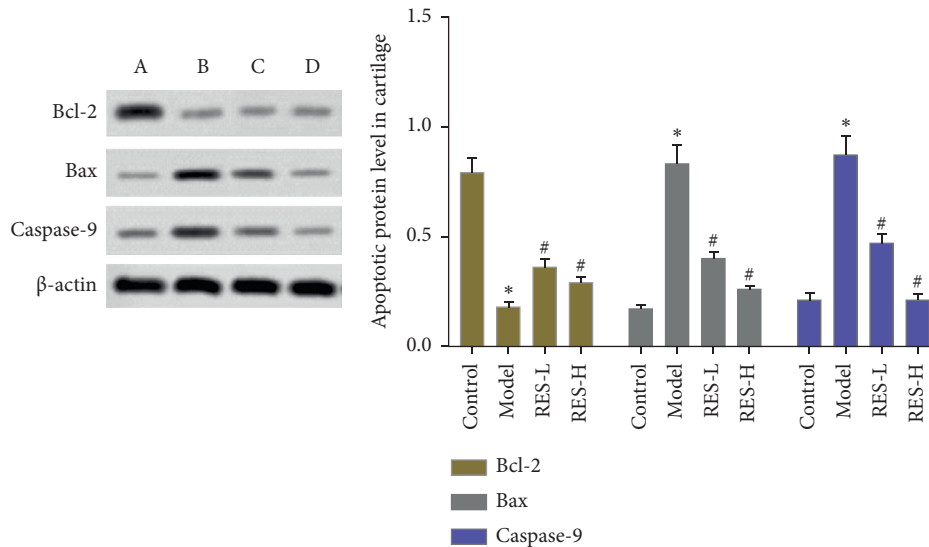
FIGURE 10: Effect of resveratrol on the expression of Bcl-2, Bax, Caspase-9 protein; (A) control group; (B) model group; (C) resveratrol low-dose group; (D) resveratrol high-dose group. *Compared with control group, $P < 0.05$; #compared with model group, $P < 0.05$.

matrix, and reduces the content of proinflammatory cytokines. This may be achieved through the NF-κB signaling pathway mediated by TLR4. This study provides a theoretical basis for the clinical application of resveratrol in the treatment of OA.

4. Conclusion

Resveratrol may inhibit the activation of the TLR4-mediated NF-κB signaling pathway and has a repairing effect on soft tissue damage in OA.

Data Availability

The data that support the findings of this study are available in supplementary materials.

Disclosure

Zhiyong Long, Wang Xiang, and Ganpeng Yu are considered as joint first authors.

Conflicts of Interest

The authors declare that there are no conflicts of interest.

Authors' Contributions

Zhiyong Long, Wang Xiang, Ganpeng Yu, Jun Li, and Tiejun Yang are responsible for the study concept and design. Zhiyong Long, Wang Xiang, Ganpeng Yu, Jun Li, and Tiejun Yang are responsible for the data collection, data analysis, and interpretation. Zhiyong Long and Wang Xiang drafted

the paper; Q Ganpeng Yu, Jun Li, and Tiejun Yang supervised the study; all the authors participated in the analysis and interpretation of data and approved the final paper.

Acknowledgments

Supplementary Materials

Table S1: Resveratrol Potential Targets. Table S2: OA genes. Table S3: Enrichment Analysis of Resveratrol-OA PPI Network. (*Supplementary Materials*)

References

[1] J. B. SnellingS, S. Bas, and J. PuskasG, "Presence of IL-17 in synovial fluid identifes a potential inflammatory osteathitic phenotype," *PloS One*, vol. 12, no. 4, 2017.

[2] D. T. Felson, A. Naimark, J. Anderson, L. Kazis, W. Castelli, and R. F. Meenan, "The prevalence of knee osteoarthritis in the elderly. the framingham osteoarthritis study," *Arthritis & Rheumatism*, vol. 30, no. 8, pp. 914–918, 1987.

[3] J. L. Van Saase, L. K. Van Romunde, A. Cats, J. P. Vandenbroucke, and H. A. Valkenburg, "Epidemiology of osteoarthritis: zoetermeer survey. Comparison of radiological osteoarthritis in a Dutch population with that in 10 other populations," *Annals of the Rheumatic Diseases*, vol. 48, no. 4, pp. 271–280, 1989.

[4] G. Peat, R. McCamney, and P. Croft, "Knee pain and osteoarthritis in older adults: a review of community burden and current use of primary health care," *Annals of the Rheumatic Diseases*, vol. 60, no. 2, pp. 91–97, 2001.

[5] L. Busija, L. Bridgett, S. R. M. Williams, R. Buchbinder, L. March, and M. Fransen, "Osteoarthritis," *Best Practice & Research Clinical Rheumatology*, vol. 24, no. 6, pp. 757–768, 201 0.

[6] I. Osborne, C. K. Kwoh, A. Guermazi et al., "Synovitis in knee osteoarthritis: a precursor of disease?" *Annals of the Rheumatic Diseases*, vol. 75, no. 2, pp. 390–395, 2016.

[7] K. D 'Lima, D. D. D'Lima, S. Hashimoto, and M. Lotz, "Cell death in cartilage," *Osteoarthritis and Cartilage*, vol. 12, no. 1, pp. 1–16, 2004.

[8] M. Kapoor, J. Martel-Pelletier, D. Lajeunesse, J. P Pelletier, and H Fahmi, "Role of proinflammatory cytokines in the pathophysiology of osteoarthritis," *Nature Reviews. Rheumatology*, vol. 7, no. 1, pp. 33–42, 2011.

[9] O. Bruyere, C. Cooper, and N. Arden, "Can we identify patients with high nisk of osteoathrtisprogresson who will resp ond to treatment? A focus on epidemiology and phenotype of osteoarthritis," *Drugs & Aging*, vol. 32, no. 3, pp. 179–187, 2015.

[10] D. Huang, Q. Zhao, H. Liu, Y. Guo, and H. Xu, "PPAR-α agonist WY-14643 inhibits LPS-induced inflammation in synovial fibroblasts via NF-kB pathway," *Journal of Molecular Neuroscience*, vol. 59, no. 4, pp. 544–553, 2016.

[11] P. A. Dieppe and L. S. Lohmander, "Pathogenesis and management of pain in osteoarthritis," *The Lancet*, vol. 365, no. 9463, pp. 965–973, 2005.

[12] G. A. Hawker, "Osteoarthritis is a serious disease," *Clinical & Experimental Rheumatology*, vol. 37, no. 5, pp. 3–6, 2019.

[13] A. E. M. Jargensen, M. Kjer, and K. M. Heinemeier, "The effect of A ging and mechanical loading on the metabolism of

[14] J. A. Martin and J. A. Buckwalter, "Aging, articular cartilage chondrocytesenescence and osteoarthritis," *Biogerontology*, vol. 3, no. 5, pp. 257–264, 2002.

[15] X. Liang, H. Li, and S. Li, "A novel network pharmacology approach to analyse traditional herbal formulae: the Liu-Wei-Di-Huang pill as a case study," *Molecular BioSystems*, vol. 10, no. 5, pp. 1014–1022, 2014.

[16] J. Gu and S. Li, "Towards integrative annotation of the cell-type specific gene functional and signaling map in vascular endothelial cells," *Molecular BioSystems*, vol. 8, no. 8, pp. 2041–2049, 2012.

[17] S. Li, T. P. Fan, W. Jia, A. Lu, and W. Zhang, "Network pharmacology in traditional Chinese medicine," *Evidence-based Complementary and Alternative Medicine*, vol. 2014, Article ID 138460, 2 pages, 2014.

[18] D. Gfeller, A. Grosdidier, M. Wirth, A. Daina, O. Michielin, and V. Zoete, "SwissTargetPrediction: a web server for target prediction of bioactive small molecules," *Nucleic Acids Research*, vol. 42, no. W1, pp. W32–W38, 2014.

[19] X. F. Liu, S. S. Ouyang, and Y. Biao, "PharmMapper server: a web server for potential drug target identification using pharmacophore mapping approach," *Nucleic Acids Research*, vol. 38, pp. W609–W614., 2017.

[20] M. J. Keiser, B. L. Roth, B. N. Armbruster, P. Ernsberger, J. J. Irwin, and B. K. Shoichet, "Relating protein pharmacology by ligand chemistry," *Nature Biotechnology*, vol. 25, no. 2, pp. 197–206, 2007.

[21] M. Kuhn, D. Szklarczyk, A. Franceschini et al., "Stitch 2: an interaction network database for small molecules and proteins," *Nucleic Acids Research*, vol. 38, no. suppl_1, pp. D552–D556, 2010.

[22] S. Kim, J. Chen, T. Cheng et al., "PubChem 2019 update: improved access to chemical data," *Nucleic Acids Research*, vol. 47, no. D1, pp. D1102–D1109, 2019.

[23] G. Stelzer, R. Rosen, I. Plaschkes et al., "The GeneCards suite: from gene data mining to disease genome sequence analysis," *Current Protocols in Bioinformatics*, vol. 54, pp. 1301–1303, 2016.

[24] A. Hamosh, A. F. Scott, and J. S. Amberger, "Online Mendelian Inheritance in Man (OMIM), a knowledgebase of human genes and genetic disorders," *Nucleic Acids Research*, vol. 33, pp. D514–D517, 2014.

[25] D. Szklarczyk, A. Franceschini, S. Wyder et al., "STRING v10: protein-protein interaction networks, integrated over the tree of life," *Nucleic Acids Research*, vol. 43, no. D1, pp. D447–D452, 2015.

[26] D. W. Huang, B. T. Sherman, and R. A. Lempicki, "Systematic and integrative analysis of large gene lists using DAVID Bioinformatics Resources," *Nature Protocols*, vol. 4, no. 1, pp. 44–57, 2009.

[27] X. Gao, D. Deeb, J. Media et al., "Immunomodulatory activity of resveratrol: discrepant in vitro and in vivo immunological effects," *Biochemical Pharmacology*, vol. 66, no. 12, pp. 2427–2435, 2003.

[28] Y. Wei, J. Jia, X. Jin, W. Tong, and H. Tian, "Resveratrol ameliorates inflammatory damage and protects against osteoarthritis in a rat model of osteoarthritis," *Molecular Medicine Reports*, vol. 17, no. 1, pp. 1493–1498, 2018.

[29] M. Kanehisa, Y. Sato, and M. Kawashima, "KEGG mapping tools for uncovering hidden features in biological data," *Protein Science*, 2021.

[30] F. K. Nielsen, N. Egund, A. Jørgensen, and A. G. Jurik, "Risk factors for joint replacement in knee osteoarthritis; a 15-year

follow-up study," *BMC Musculoskeletal Disorders*, vol. 18, no. 1, p. 510, 2017.

[31] W. Hideto, "Aggrecan and its chondroitin sulfate in cartilage," *Seikagaku*, vol. 80, no. 1, p. 28, 2008.

[32] L. Pulsatelli, O. Addimanda, V. Brusi, B. Pavloska, and R. Meliconi, "New findings in osteoarthritis pathogenesis: therapeutic implications," *Therapeutic Advances in Chronic Disease*, vol. 4, no. 1, pp. 23–43, 2013.

[33] C. B. Little, A. Barai, D. Burkhardt et al., "Matrix metalloproteinase 13â"deficient mice are resistant to osteoarthritic cartilage erosion but not chondrocyte hypertrophy or osteophyte development," *Arthritis & Rheumatism*, vol. 60, no. 12, pp. 3723–3733, 2009.

[34] T. Sato, K. Konomi, S. Yamasaki et al., "Comparative analysis of gene expression profiles in intact and damaged regions of human osteoarthritic cartilage," *Arthritis & Rheumatism*, vol. 54, no. 3, pp. 808–817, 2006.

[35] D. Philipot, D. Guérit, D. Platano et al., "p16INK4a and its regulator miR-24 link senescence and chondrocyte terminal differentiation-associated matrix remodeling in osteoarthritis," *Arthritis Research and Therapy*, vol. 16, no. 1, p. R58, 2014.

[36] H. Li, D. Wang, Y. Yuan, and J. Min, "New insights on the MMP-13 regulatory network in the pathogenesis of early osteoarthritis," *Arthritis Research and Therapy*, vol. 19, no. 1, p. 248, 2017.

[37] Y. Wan, W. Li, Z. Liao, M. Yan, X. Chen, and Z. Tang, "Selective MMP-13 inhibitors: promising agents for the therapy of osteoarthritis," *Current Medicinal Chemistry*, vol. 27, no. 22, pp. 3753–3769, 2020.

[38] C. Csali, N. Kes his hzadeh, and K. Fise her, "Regulation of iflamnatnonsigalling by resveratrol in ku man c hondrocytes in vntro," *Biochemical phaIaology*, vol. 75, no. 3, pp. 677–687, 2008.

[39] M. Shakibaei, C. Csaki, S. Nebrich, and A. Mobasheri, "Resveratrol suppresses interleukin-1β-induced inflammatory signaling and apoptosis in human articular chondrocytes: potential for use as a novel nutraceutical for the treatment of osteoarthritis," *Biochemical Pharmacology*, vol. 76, no. 11, pp. 1426–1439, 2008.

[40] E. Limagne, A. Lancon, and D. Delmas, "Resveratrol interferes with IL 1-b eta -induced pro -inflammatory paracrine interacti on between primary chondrocytes and macrophages," *Nutrients*, no. 5, p. 8, 20 16.

[41] L. Liu, H. Gu, H. Liu et al., "Protective effect of resveratrol against IL-1β-induced inflammatory response on human osteoarthritic chondrocytes partly via the TLR4/MyD88/NF-κB signaling pathway: an "in vitro study"," *International Journal of Molecular Sciences*, vol. 15, no. 4, pp. 6925–6940, 2014.

[42] K. Bobacz, I. G. Sunk, J. G. Hofstaetter et al., "Toll-like receptors and chondrocytes: the lipopolysaccharide-induced decrease in cartilage matrix synthesis is dependent on the presence of toll-like receptor 4 and antagonized by bone morphogenetic protein 7," *Arthritis & Rheumatism*, vol. 56, no. 6, pp. 1880–1893, 2007.

[43] H. Gu, Y. Jiao, and X. Yu, "Resveratrol inhibits the IL- 1b eta -induced expression of MMP-13 and IL-6 in human articular chondrocytes via TLR4/MyD 88-dependent and-independent signaling ca sca des," *Intermational journal of molecular medi cine*, 2017.

[44] J. Y. Lee and G. Z. YeJ, "Reciproalmodulation of Tl-1ke receptor-4 signaling pathways inv olvingMyD 88 and pho sphatidylinositol 3-kinase/AKT by saturated and polyunsaturated fatty acids," *Journal of Biological Chemistry*, vol. 278, no. 39, pp. 3704 1–37051, 2003.

[45] E. Aksamitiene, B. N. Kiyatkin, and B. N. Kholodenko, "Cross-talk between mitogenic Ras/MAPK and survival PI3K/Akt pathways: a fine balance," *Biochemical Society Transactions*, vol. 40, no. 1, pp. 139–146, 2012.

[46] M. Y. Zhu, J. L. Guo, and H. Xia, "[The anti-apoptotic effect of cytoplasmic alpha- fetoprotein in hepatoma cells induced by all trans retinoic acid involves activation of the PI3K/AKT signaling pathway]," *Zhonghuaganzangbing za zhi = Zhonghuaganzangbingzazhi = Chinese joumalofhepatology*, vol. 22, no. 1 1, pp. 837–842, 2014.

[47] R. J. Atkins, L. Dimou, A. P. Morokoff, A. H. Kaye, K. J. Drummond, and C. M. Hovens, "Regulation of glycogen synthase kinase-3 beta (GSK-3β) by the Akt pathway in gliomas," *Journal of Clinical Neuroscience*, vol. 19, no. 11, pp. 1558–1563, 2012.

[48] Y. Sun, C. Wu, J. Ma et al., "Toll-like receptor 4 promotes angiogenesis in pancreatic cancer via PI3K/AKT signaling," *Experimental Cell Research*, vol. 347, no. 2, pp. 274–282, 201 6.

[49] D. Xu, Y. Li, B. Zhang et al., "Resveratrol alleviate hypoxic pulmonary hypertension via anti-inflammation and anti-oxidant pathways in rats," *International Journal of Medical Sciences*, vol. 13, no. 12, pp. 942–954, 2016.

[50] A. M. Th omp son, K. A. Martin, and E. M. Rzucidlo, "Resveratro1 induces vascularsmooth musclecell differentiati on through stimulation of SirT1 and AMPK," *P1oS one*, vol. 9, no. 1, pp. e8–95, 2014.

[51] Y. Zong, L. Sun, B. Liu et al., "Resveratrol inhibits LPS-induced MAPKs activation via activation of the phosphatidylinositol 3-kinase pathway in murine RAW 264.7 macrophage cells," *PloS One*, vol. 7, no. 8, Article ID e44107, 2012.

[52] P. E. Czabotar, G. Lessene, A. Strasser, and J. M. Adams, "Control of apoptosis by the bcl-2 protein family: implications for physiology and therapy," *Nature Reviews Molecular Cell Biology*, vol. 15, no. 1, pp. 49–63, 2014.

[53] A. Burlacu, "Regulation of apoptosis by bcl-2 family proteins," *Journal of Cellular and Molecular Medicine*, vol. 7, no. 3, pp. 249–257, 2010.

[54] H. M. Ismail, K. Yamamoto, T. L. Vincent, H. Nagase, L. Troeberg, and J. Saklatvala, "Interleukin-1 acts via the jnk-2 signaling pathway to induce aggrecan degradation by human chondrocytes," *Arthritis & Rheumatology*, vol. 67, no. 7, pp. 1826–1836, 2015.

[55] J. Liu, C. Z. Qu, and P. J. Xie, "Changes in cartilage Toll-like receptor 4/myeloid differentiation factor 88 signal transduction pathway in knee osteoarthritis model rats after receiving massage treatment," *Chinese Tissue Engineering Research*, vol. 19, pp. 3019–3024, 2019, [in chinese].

[56] F. Hua, T. Ha, J. Ma et al., "Blocking the MyD88-dependent pathway protects the myocardium from ischemia/reperfusion injury in rat hearts," *Biochemical and Biophysical Research Communications*, vol. 338, no. 2, pp. 1118–1125, 2005.

[57] Y. Ding, S. Yuan, X. Liu et al., "Protective effects of astragaloside IV on db/db mice with diabetic retinopathy," *PloS One*, vol. 9, no. 11, Article ID e112207, 2014.

[58] L. X. Chen, L. Lin, H. J. Wang et al., "Suppression of early experimental osteoarthritis by in vivo delivery of the adenoviral vector-mediated NF-κBp65-specific siRNA," *Osteoarthritis and Cartilage*, vol. 16, no. 2, pp. 174–184, 2008.

Research Article

Application of Implantable Polylactic-Co-Glycolic Acid Microcapsule in Repairing Alveolar Bone Defects

Jun Jiang ⓘ,[1] **Jianpeng Xiao** ⓘ,[1] **Dongqing Wang** ⓘ,[2] **and Huazhong Cai** ⓘ[1,2,3]

[1]*School of Pharmacy, Jiangsu University, 301# Xuefu Road, Zhenjiang 212013, Jiangsu Province, China*
[2]*Affiliated Hospital of Jiangsu University, Department of Medical Imaging, Zhenjiang 212001, Jiangsu Province, China*
[3]*Affiliated Hospital of Jiangsu University, Department of Emergency, Zhenjiang 212001, Jiangsu Province, China*

Correspondence should be addressed to Jun Jiang; jiangjuntcm2007@hotmail.com

Alveolar bone defects (ABDs) were a perennial problem, especially in the aged. Bisphosphonates, especially etidronate sodium (ET), were frequently used in clinical treatment of ABD. However, the oral administration of ET had poor absorption (<1%). Therefore, optimization of a suitable dosage form substituted with ET to locally repair the ABD was a straightforward approach. Polylactide-co-glycolide (PLGA) is a biodegradable material and had been used in locally implanted medical devices. Therefore, an ET-PLGA microcapsule may help local delivery and prolong the activity of healing ABD. In this paper, a preparation method of ET-PLGA microcapsule was optimized by the single-factor investigation and response surface method. Subsequently, the rat ABD model was used to evaluate the enhancement effect of these microcapsules. Finally, the optimum parameters were determined as follows: 40% dichloromethane, 160 mg/mL PLGA, 10% internal aqua/oil phase, 4% PVA, and emulsifying for 10 min. These microcapsules were spherical in shape and fairly monodisperse in a particle size of 27,51 μm (PDI = 0.3), encapsulation rate 96.6%, and drug loading 4.58%. Compared with the ET groups, the total healing volume of ABD in ET-PLGA groups was significantly increased ($P < 0.05$). ET-PLGA microcapsules significantly enhanced the effect of ET on ABD. This study provided important technical support for the treatment of ABD with bisphosphonates by local administration. This paper has an exploratory significance for the development of water-soluble bioactive components with low bioavailability for ABD.

1. Introduction

Alveolar bone defects (ABDs) continue to be a perennial problem, especially in the aged [1]. ABD is mainly caused by trauma, infection, periodontal disease, or congenital alveolar fenestration, which affected the mastication ability and quality of life [2, 3]. Bisphosphonates, antibiotics, or anti-inflammatory compounds have been wildly used to cure the ABD, but their ability to effectively achieve alveolar regeneration remains elusive [4, 5], especially the bisphosphonates.

In clinical treatment, bisphosphonates are the most commonly prescribed for antiresorptive drugs [6, 7]; for example, etidronate sodium (ET) was frequently chosen to increase bone mineral density and reduce the risk of fracture and was well tolerated [8, 9] by oral administration.

However, its excretion levels by the renal system reached 38% to 73% in 24 h [10]. Furthermore, the poor absorption from the gastrointestinal tract was its major disadvantage, generally less than 1% [11]. Therefore, optimization of synthetic bone substitutes with ET to locally adjust the imbalance in bone remodeling seemed a straightforward approach to aid bone regeneration in ABD.

Among the available synthetic bone substitutes, poly-lactide-co-glycolide (PLGA) is an FDA-approved biodegradable material and had been used in locally implanted medical devices, including scaffolds [12–15]. PLGA composites could maintain the structural integrity of in situ placement, provide micro-/macropore space, and stabilize the bioadhesion of clots and quick biodegradation for rapid clearance [16]. PLGA microcapsule is an effective way to locally control drug release and can be easily adapted to

complex defects in a less-invasive manner compared to conventional surgery [17]. Compared to the conventional drug delivery vector, PLGA also had been extensively applied to other delivery systems such as nanocrystals and microspheres [18–20].

According to the internal structure, PLGA microparticles are classified into microspheres and microcapsules [21]. In microcapsules, vesicular particles consist of a polymer shell surrounding a single core (mononuclear) or multicores which mainly appropriate for encapsulating hydrophilic drugs. PLGA implants gradually released encapsulated drug in situ as they were degradated and prolonged the drug bioactivity through control degradation time [22, 23]. Theoretically, PLGA should be able to encapsulate water-soluble ET and increase its bioavailability and tissue repair by controlling release.

ABD repair generally lasts several months, so it is necessary to prolong the drug efficacy in the treatment of this disease [24]. An ET-loaded PLGA may help local delivery and prolong the activity of ABD healing in rats for a long period. However, there have been few reports on the fabrication of this delivery system. In this paper, a preparation method of Water$_1$ (W$_1$)/O (Oil)/W$_2$ ET-PLGA microcapsule was optimized by the single-factor investigation and response surface method. Subsequently, the rats' ABD model was used to evaluate the enhancement effect of these microcapsules.

2. Materials and Methods

2.1. Ethics Statement.
All animal experiments strictly comply with the Guidelines for Animal Experimentation of Jiangsu University (Zhenjiang, China), and the protocol was approved by the Animal Ethics Committee of this institution.

2.2. Materials and Chemicals.
Etidronate sodium (purity > 99.8%) was purchased from Jizhi Biochemical Technology Co., Ltd. (Shanghai, China). PLGA (75/25) was purchased from Jinan Daigang Bioengineering Co., Ltd. (Jinan, Shanghai, China). The chromatographic distilled water was made in our laboratory. Chloral hydrate, polyvinyl alcohol (PVA), dichloromethane (DCM), ethyl acetate (EAC), and KOH were purchased from Titan Technology Co., Ltd. (Shanghai, China).

2.3. Preparation of ET-PLGA Microcapsules.
The ET-PLGA microcapsules were prepared by improved double emulsion solvent—an evaporation method to form W$_1$/O/W$_2$ complex emulsion. The customized preparation parameters were set as follows: 40% DCM (DCM: EAC), 160 mg/mL PLGA, 10% internal aqua/oil phase, 4% PVA, and emulsifying for 10 min. The operation flow is shown in Figure 1.

2.4. Quality Evaluation of Microcapsules.
The encapsulation efficiency (EE) of microcapsules was chosen as the main index to evaluate microcapsules, and the drug loading yield (DL) and particle size distribution (PSD) were also considered. EE (%) = [(amount of drug used in the formulation−Amount of residue in the supernatant)/Amount of drug used in the formulation] × 100%. Actual drug loading = (Total amount of drugs in microcapsules/Microcapsule weight) × 100%.

2.5. Determination of Drug Content.
We accurately weighed etidronate sodium, prepared 5 mg/mL standard solution, diluted to 10 μg/mL, 40 μg/mL, 80 μg/mL, 160 μg/mL, 320 μg/mL, and 400 μg/mL standard solution. An Ics 600 ion chromatograph (Thermo Fisher Scientific Co., Ltd., Shanghai, China) was used to detect the peak area as the ordinate and the concentration as the abscissa, and linear regression was used to obtain the standard curve equation. In order to determine the residual amount of ET in the supernatant as described in Figure 1, 5 mL of the supernatant of ET-PLGA microcapsule preparation was obtained, successively filtrated by using a C$_{18}$ SPE column and 0.22 μm aqueous membrane, and then, injected into an ion chromatograph for analysis.

2.6. Single-Factor Experiment.
The entrapment rate as the main index and the main factors affecting the formation of microcapsules, such as oil phase composition (DCM: EAC), PLGA concentration, volume ratio of internal water phase to oil phase (RWO), emulsification time, and PVA concentration, were investigated. During the single-factor investigation, the encapsulation rate and particle size were measured as evaluation indicators.

2.7. Response Surface Experiment.
Based on single-factor experiment, response surface experiment was designed by selecting 3 factors (Proportion of DCM, PLGA concentration and RWO) which have an obvious influence on the quality of microcapsules. The response surface was designed by Box–Behnken, and the encapsulation rate was taken as the index.

2.8. Animals and Administration.
Thirty SD rats (220 ± 20 g) were supplied by the Laboratory Animal Center of Jiangsu University. Before the experiment, all rats were given 14 days of adaptation period with a standard laboratory rodent diet (calcium content 0.5%) and tap water under climate-controlled conditions (55% humidity, 25°C, and 12 hours alternating day and night). After the accommodation period, the rats were anesthetized with 10% urethane (10 mL/kg) by intraperitoneal injection. After fixation, the alveolar bone of rat was exposed and a round hole bone defect was made by using a dental drill (T$_3$, Sirona Dental Systems Co., Ltd., Shanghai, China) near the first molar. In order to prevent the high temperature of the operation area, the rats' ABD was made by intermittent and low-speed drilling. After establishing the ABD model, the ET powder or prepared ET-PLGA microcapsule were implanted into the bone defect immediately, and the gingiva was sutured carefully. Rats were divided into 6 groups ($n = 5$); they were the blank control group (CON), ABD model group (ABD), ET low-
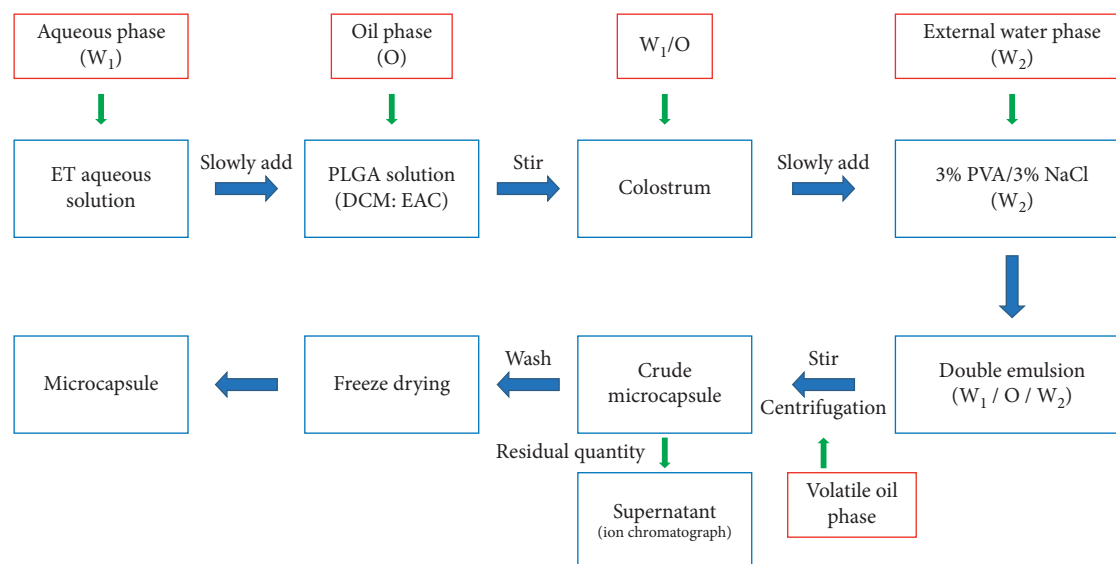
FIGURE 1: Preparation flow chart of ET-PLGA microcapsules.

dose group (ET-L, 2 mg), ET high-dose group (ET-H, 10 mg), ET-PLGA low-dose group (ET-PLGA-L, 2 mg), and ET-PLGA high-dose group (ET-PLGA-L-H, 10 mg). In the CON group, no diaphragm was implanted and the wound was sutured directly. All the experimental protocols were approved by the Animal Ethics Committee of Jiangsu University.

2.9. Collection and Analysis of Alveolar Bone Samples.
Within one month after the operation, cone-beam computed tomography (CB-CT, kawa i-cat 17–19, Imaging science international LLC, USA) was used to scan the ABD of rats every week. The main parameters of CB-CT were as follows: reconstruction solvent size was 8 cm × 8 cm (diameter × height), resolution was 125 pixels, exposure was mAs = 37.07, KVP = 120, and acquisition time = 26.9 seconds. Mimics Research 20.0 software was applied to analyze the CT image and calculate defect volume.

2.10. Statistical Analysis of Data.
Statistical analyses were conducted by one-way ANOVA followed by Tukey's test (GraphPad Prism 5.0) for comparing all groups. Data were presented as mean value ± SD. The P value < 0.05 was considered as statistically significant.

3. Results

3.1. Methodological Validation.
Ion chromatography was established for the determination of ET residue in the supernatant by an external standard method (Figure 2). The mobile phase was 30 mmol/L KOH solution with isocratic elution. The regression equation was obtained by linear regression of concentration Y with peak area X. The standard curve was $Y = 0.251, X−0.184, R^2 = 0.9996$. The results showed that there is a good linear relationship between 10 μg/mL and 400 μg/mL. The 3 or 10 times of the relative standard deviation of the analytical blank values was calculated as the limit of detection

(LOD) and limit of quantitation (LOQ). The LOD and LOQ were 0.6 ng and 2.1 ng, respectively. One sampling solution was treated according to Section 2.5 and then injected into an ion chromatograph for 6 times continuously to record the peak area of ET. The RSD was 2.34% which indicated that the precision is fine (Table S1). Similarly, when the sample solution was injected at 0, 2, 4, 8, 16, and 24 h, the RSD of the peak area of ET was 0.27%, indicating that ET was stable within 24 h under room temperature (Table S2). For repeatability, six samples with the same concentration were determined and the RSD of their contents was 0.37% (Table S3), indicating a good repeatability. The sample with known concentration was chosen, and, respectively, added into ET according to 1 : 1, 1 : 2, and 1 : 4 times, and the recovery rate was calculated ([Measured quantity – Original quantity] × 100/Amount added, %). The recovery was 99.6% with the RSD of 1.81% (Table S4). All these results showed that the ion chromatography method established in this paper can be well applied to optimize the preparation of ET-PLGA microcapsules.

3.2. Single-Factor Results.
The oil phases (30%, 45%, 60%, and 75% dichloromethane, Table 1), PLGA concentrations (80, 120, 160, and 200 mg/mL, Table 2), PVA concentrations (1%, 2%, 3%, and 4%, Table 3), emulsification times (5, 10, 15, and 20 min, Table 4), and RWO (v/v 5%, 10%, 15%, and 20%, Table 5) were investigated by EE (%) and particle size (nm). The single factor results indicated that the best encapsulation efficiency was obtained when the proportion of DCM, PLGA, PVA, emulsification time, and RWO was 30%, 200 mg/mL, 4%, 10 min, and 5%, respectively.

3.3. Response Surface Test Results.
The proportion of DCM and the concentration of PLGA and RWO were the three factors that had an obvious influence on the quality of microcapsules. The Box–Behnken software was used to design response surface experiment (Table 6), and the encapsulation

(a)

(b)
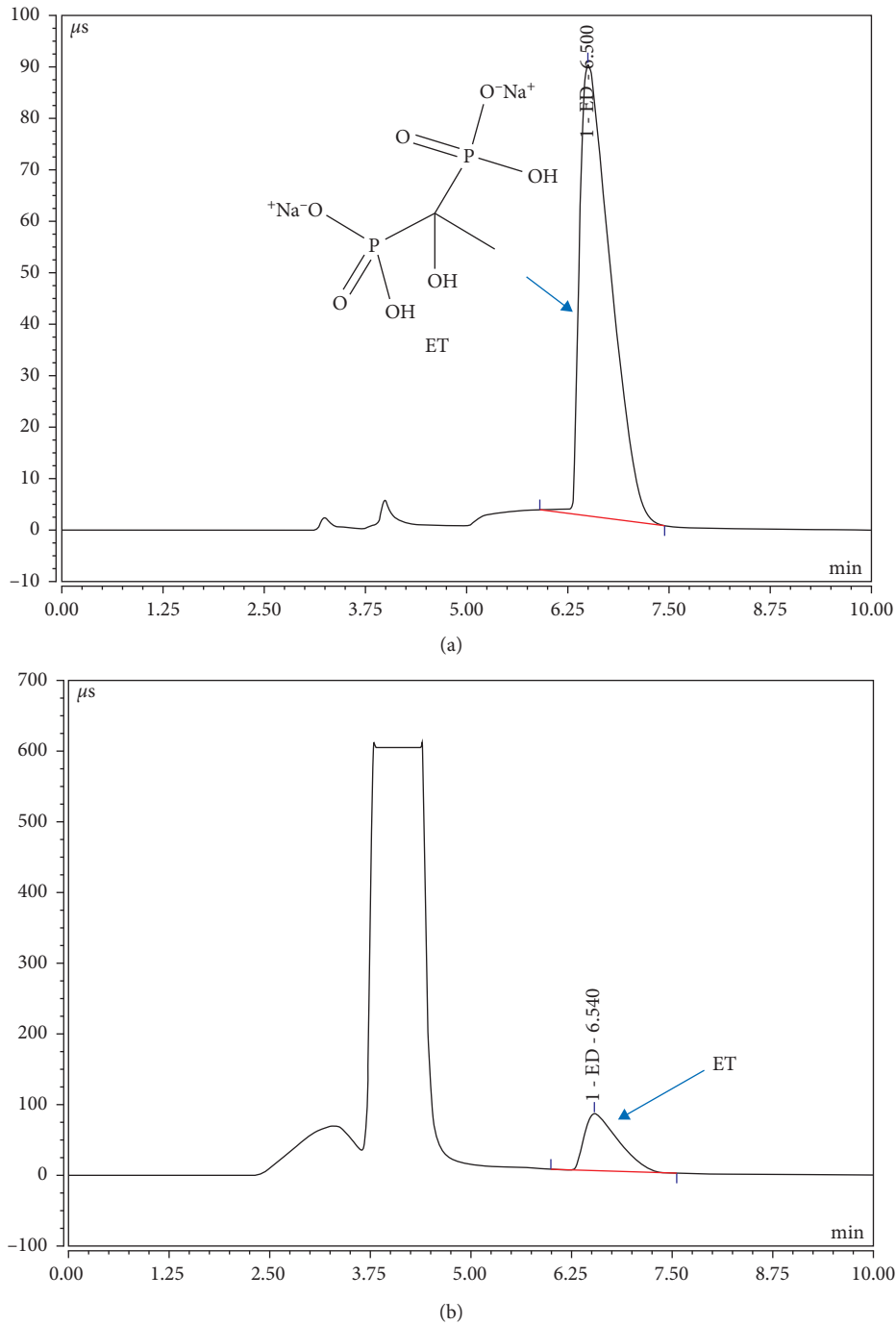
FIGURE 2: Determination of sodium etidronate by ion chromatography. (a) Chromatogram of the ET standard solution; (b) chromatogram of ET detection in samples.

rate was taken as the evaluation index. The predicted results of response surface showed that when the oil phase composition (DCM: EAC) was 40%, PLGA was 160 mg/mL and RWO was 10%, and the EE% was up to 97.83% (Figure 3).

3.4. Validation of Optimum Preparation. According to the results of single-factor and response surface experiments, the optimum parameters were determined as follows: 40%

DCM, 160 mg/mL PLGA, 10% RWO, 4% PVA, and emulsifying time 10 min. Based on the optimized results, 3 batches of ET-PLGA microcapsules were prepared in parallel, and their EE, DL, particle size, and morphology were detected in turn. The results demonstrated that the average encapsulation rate was 96.6% (RSD, 0.46%) and the average DL was 4.58% (RSD, 0.98%). Under the microscope and scanning electron microscope, the surface of ET-PLGA microcapsules was smooth without adhesion (Figure 4). The

TABLE 1: The effect of oil phase composition on the preparation of PLGA microcapsules.

Proportion of DCM (%)	EE (%)	Particle size (nm)
30	87.11	12085.61
45	84.94	21872.26
60	84.59	27462.43
75	80.92	27174.97

TABLE 2: Effect of PLGA concentration on the preparation of PLGA microcapsules.

PLGA concentration (mg/mL)	EE (%)	Particle size (nm)
80	74.94	7784.28
120	87.55	9500.88
160	84.74	25136.59
200	92.94	25732.73

TABLE 3: Effect of PVA concentration on the preparation of PLGA microcapsules.

PVA concentration (%)	EE (%)	Particle size (nm)
1	90.88	56577.15
2	89.67	95270.58
3	82.65	19958.97
4	98.79	11593.56

TABLE 4: Effect of emulsification time on the preparation of PLGA microcapsules.

Emulsification time (min)	EE (%)	Particle size (nm)
5	83.53	18711.51
10	86.88	82029.78
15	84.94	13068.48
20	84.94	18896.24

TABLE 5: Effect of volume ratio of the internal water phase to oil phase on the preparation of PLGA microcapsules.

Proportion of the internal water phase (%)	EE (%)	Particle size (nm)
5	93.47	38459.89
10	78.37	19318.54
15	85.03	20178.52
20	78.23	20780.43

TABLE 6: Response surface experiment design.

Std	Run	A	B	C	EE%
2	1	1	−1	0	96.88
7	2	−1	0	1	93.49
1	3	−1	−1	0	94.90
16	4	0	0	0	95.78
15	5	0	0	0	96.88
10	6	0	1	−1	96.78
6	7	1	0	−1	96.88
4	8	1	1	0	96.78
11	9	0	−1	1	96.94
5	10	−1	0	−1	96.95
3	11	−1	1	0	96.93
14	12	0	0	0	95.28
9	13	0	−1	−1	96.97
17	14	0	0	0	96.92
8	15	1	0	1	96.97
13	16	0	0	0	96.91
12	17	0	1	1	96.94

"−1": 20% DCM, PLGA 160 mg/mL, 5% proportion of the internal water phase; "−0": 30% DCM, PLGA 180 mg/mL, 7.5% proportion of the internal water phase; "1": 40% DCM, PLGA 200 mg/mL, 10% proportion of the internal water phase.

particle size was 27.51 μm (RSD, 1.2%), and the polydispersity index (PDI) was below 0.3, indicating that the distribution of the particles was narrow. After measuring zeta potential, it was found that the average potential of the particle was below −38 mV, indicating that its property was relatively stable (Table 7).

3.5. Healing Effect on ABD. After administration, the healing volume was calculated once a week for 4 consecutive times. When measuring the healing volume (HV) of bone defect weekly, the calculation method was to subtract the volume of defect (VD) in the previous week from the VD in the current

FIGURE 3: Response surface optimization results. (a) The effect of DCM ratio on EE%; (b) the effect of PLGA concentration on EE%; (c) the influence of the ratio of internal water phase to EE%; (d) 2D panel of PLGA-DCM; (e) 2D panel of internal water phase-DCM; (f) 2D panel of internal water phase-PLGA; and (g)–(i) 3D response surface plots.

week, such as $HV_n = VD_{n-1} - VD_n$, $n = 1, 2, 3, 4$. The total healing volume (THV) was calculated as $THV = HV_1 + HV_2 + HV_3 + HV_4$. The effects of ET and ET-PLGA microcapsules on the healing of ABD were compared by total healing volume (Figure 5). Compared with the ABD group $(0.478 \pm 0.100 \, \text{mm}^3)$, the total healing volume in all treatment groups was significantly increased $(P < 0.01)$. Compared with the ET-L group $(0.828 \pm 0.075 \, \text{mm}^3)$, the total healing volume of ET-PLGA-L $(1.133 \pm 0.175 \, \text{mm}^3)$ was enhanced significantly $(P < 0.05)$. Compared with the ET-H group $(1.223 \pm 0.083 \, \text{mm}^3)$, the total healing volume of ET-PLGA-H $(1.528 \pm 0.113 \, \text{mm}^3)$ was also significantly improved $(P < 0.05)$. Additionally, there was no abnormal infection, ulceration, or death in the ET-PLGA microcapsule group during the whole experiment.

4. Discussion

Compared with the traditional PLGA microspheres, the preparation of PLGA microcapsules with water-phase nuclei has higher technical difficulties [25]. PLGA microspheres have shortcomings in drug loading, encapsulation efficiency, and drug release, especially for water-soluble drugs and hydrophilic macromolecules [26–28]. In this paper, ET-PLGA microcapsules were prepared by double emulsion—solvent evaporation $(W_1/O/W_2)$. PLGA polymers were dissolved in a mixture of DCM and EAC (volatile), and then, ET aqueous solution was slowly dripped into it to form an internal aqueous phase, thus forming a W_1/O colostrum. Then, the W_1/O colostrum was slowly dripped into the aqueous solution containing 3% PVA and 3% NaCl to form
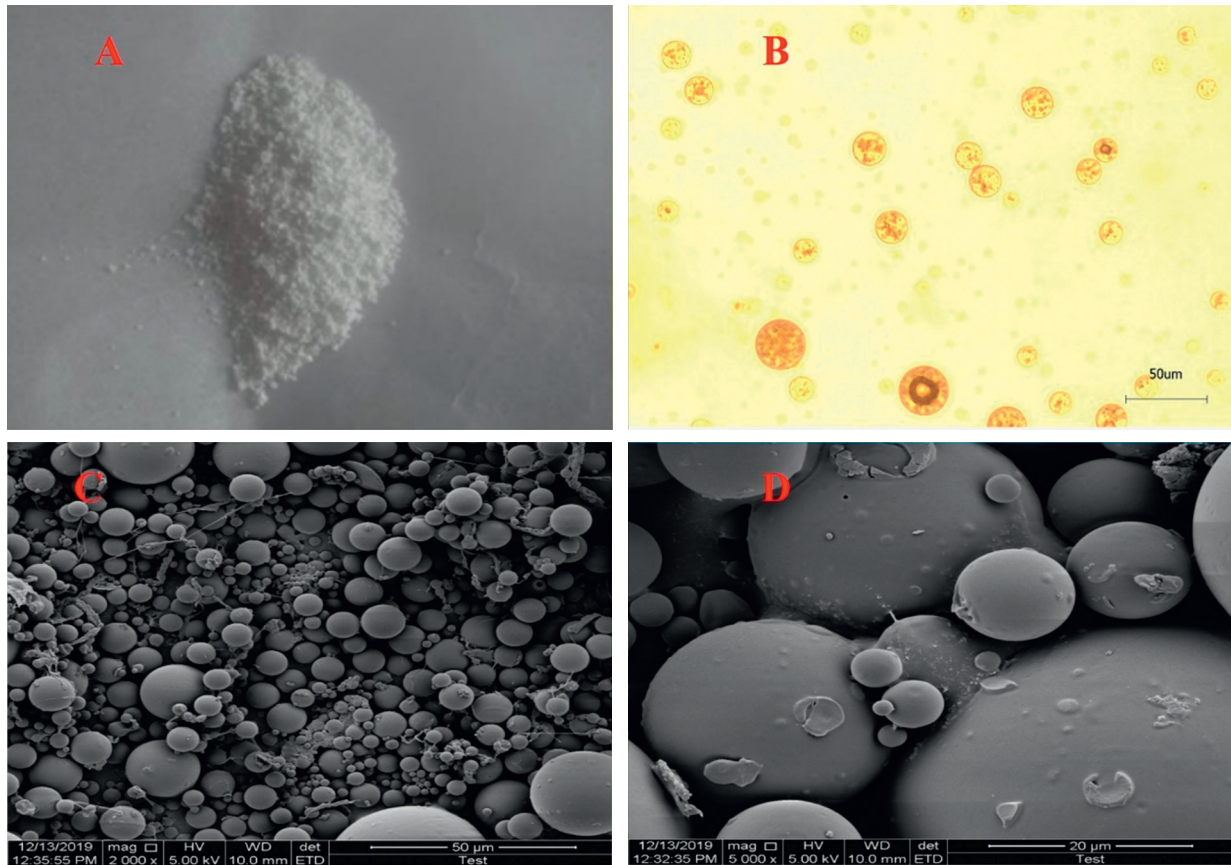
Figure 4: The morphology of ET-PLGA microcapsules. (a) Freeze-dried powder of ET-PLGA microcapsules; (b) the morphology of ET-PLGA microcapsules under an upright microscope; and (c) the morphology of ET-PLGA microcapsules under a scanning electron microscope.

Table 7: Particle size and potential of ET-PLGA microcapsules.

Batch	Particle size (nm)	Polydispersity	Zeta potential (mV)	EE%	DL%
1	2740	0.26	−38.29	96.65	4.64
2	2717	0.30	−38.63	97.12	4.57
3	2795	0.29	−38.33	96.03	4.53
Average value	2751	0.28	−38.42	96.60	4.58

the W_1/O/W_2 composite emulsion. Finally, upon DCM and EAC evaporation from the internal oil phase droplets, the solubility of PLGA polymers decreased gradually leading to phase separation and migration to the interface surrounding water droplets.

It was found that the amount of PLGA had a significant impact on the particle size of microcapsules [29]. With the increase of PLGA concentration, the size of microcapsules decreased from several microns to several hundred nanometers. PLGA not only acted as a drug carrier but also played the role of an emulsifier when the internal water phase was encapsulated into the oil phase [30–32]. It could be inferred that the stability of the colostrum was one of the key factors affecting the EE of microcapsules. In addition, due to the presence of PVA in the external water phase, it had the function of a surfactant. When the colostrum was added into

the external aqueous phase to prepare the compound emulsion, the outer wall of this prepared microcapsule was compact and uniform [33–35].

Determination of ET and calculation of bone defect volume were the other two technical difficulties in this paper. Fortunately, an ion chromatography method was successfully established, which completed the analysis of a single sample within 10 min with high precision. This powerful analysis method provided important technical support for the optimization of microcapsules. On the other hand, evaluation of the enhancement effect of microcapsules on ABD repair lasted for 1 months and the scanning by CB-CT was needed every week. CB-CT, as a modern noninvasive imaging technique, was widely used in radiology, orthopedics, dentistry, and image-guided radiation therapy [36, 37]. Compared with micro-CT and high-resolution CT,
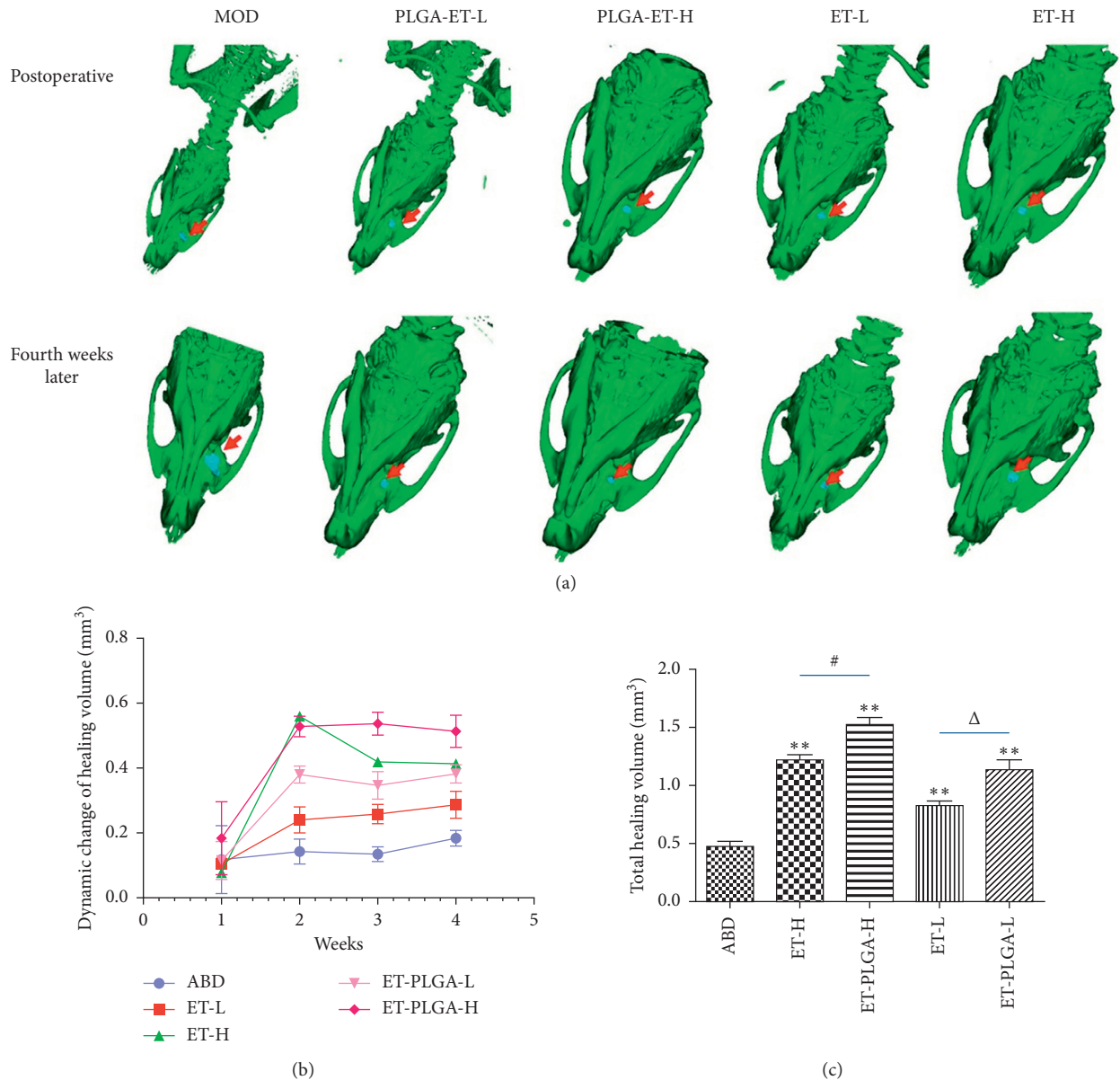
FIGURE 5: The effect of ET-PLGA microcapsules on alveolar bone defects by CB-CT ($n = 5$). (a) CB-CT images of ABD in rats at different time periods; (b) dynamic changes of healing volume (mm^3) of ET-PLGA microcapsules in ABD rats; and (c) the total healing volume (mm^3) of ABD in each group. **, compared with the ABD model group, $P < 0.01$; #, compared with the ET-H group, $P < 0.05$; and Δ, compared with the ET-L group, $P < 0.05$.

CB-CT recovered imaging parameters accurately, leading to superior image quality [38]. CB-CT provided strong technical support for the evaluation of synergism of ET-PLGA microcapsules in this study.

5. Conclusions

An improved double emulsion/solvent evaporation approach was employed to prepare ET-PLGA microcapsules successfully. These microcapsules were spherical in shape and fairly monodisperse in size with a mean particle size of 27.51 μm (PDI = 0.3). The results demonstrated that the average encapsulation rate was 96.6% and the average DL

was 4.58%. ET-PLGA microcapsules significantly enhanced the effect of ET on alveolar bone defects. This study provided an important research foundation for the local use of bisphosphonates. More importantly, the implantable PLGA microcapsule system constructed in this study was especially suitable for water-soluble active ingredients (polysaccharides or peptides) with low oral bioavailability in natural medicine.

Data Availability

The data used to support the findings of this study are available from the corresponding author upon request.

Conflicts of Interest

All authors had no conflicts of interest regarding the publication of this study.

Authors' Contributions

Jun Jiang and Jianpeng Xiao contributed equally to this paper.

Acknowledgments

Supplementary Materials

Table S1. The precision of ET by ion chromatography. Table S2. The stability of ET by ion chromatography. Table S3. The repeatability of ET by ion chromatography. Table S4. The Recovery test of ET by ion chromatography. (*Supplementary Materials*)

References

[1] L. Wang, W. Xu, Y. Chen, and J. Wang, "Alveolar bone repair of rhesus monkeys by using BMP-2 gene and mesenchymal stem cells loaded three-dimensional printed bioglass scaffold," *Scientific Reports*, vol. 9, no. 1, Article ID 18175, 2019.

[2] H. H. Tüz, O. Koç, S. E. Meral, and A. S. El, "Reconstruction and implant-supported rehabilitation of an iatrogenically caused maxillary alveolar defect," *Implant Dentistry*, vol. 28, no. 5, pp. 510–513, 2019.

[3] J. Pan, J. Deng, Y. Luo et al., "Thermosensitive hydrogel delivery of human periodontal stem cells overexpressing platelet-derived growth factor-BB enhances alveolar bone defect repair," *Stem Cells and Development*, vol. 28, no. 24, pp. 1620–1631, 2019.

[4] G. Bhattarai, S. B. Poudel, S.-H. Kook, and J.-C. Lee, "Anti-inflammatory, anti-osteoclastic, and antioxidant activities of genistein protect against alveolar bone loss and periodontal tissue degradation in a mouse model of periodontitis," *Journal of Biomedical Materials Research Part A*, vol. 105, no. 9, pp. 2510–2521, 2017.

[5] P. Goes, N. A. Lima, J. A. G. Rodrigues, N. M. B. Benevides, G. A. C. Brito, and V. Lima, "Anti-inflammatory and anti-resorptive effects of atorvastatin on alveolar bone loss in wistar rats," *Brazilian Dental Journal*, vol. 27, no. 3, pp. 267–272, 2016.

[6] L. Liu, W. Tao, W. Pan et al., "Hydroxysafflor yellow A promoted bone mineralization and inhibited bone resorption which reversed glucocorticoids-induced osteoporosis," *Biomed Research International*, vol. 2018, Article ID 6762146, 2018.

[7] J. Jiang, S. Xiao, X. Xu, H. Ma, C. Feng, and X. Jia, "Isomeric flavonoid aglycones derived from epimedii folium exerted different intensities in anti-osteoporosis through OPG/RANKL protein targets," *International Immunopharmacology*, vol. 62, pp. 277–286, 2018.

[8] R. R. Recker and J. Barger-Lux, "Risedronate for prevention and treatment of osteoporosis in postmenopausal women,"

[9] M. P. Ettinger, "Aging bone and osteoporosis," *Archives of Internal Medicine*, vol. 163, no. 18, pp. 2237–2246, 2003.

[10] R. G. G. Russell, N. B. Watts, F. H. Ebetino, and M. J. Rogers, "Mechanisms of action of bisphosphonates: similarities and differences and their potential influence on clinical efficacy," *Osteoporosis International*, vol. 19, no. 6, pp. 733–759, 2008.

[11] A. Ezra and G. Golomb, "Administration routes and delivery systems of bisphosphonates for the treatment of bone resorption," *Advanced Drug Delivery Reviews*, vol. 42, no. 3, pp. 175–195, 2000.

[12] F. Danhier, E. Ansorena, J. M. Silva, R. Coco, A. Le Breton, and V. Préat, "PLGA-based nanoparticles: an overview of biomedical applications," *Journal of Controlled Release*, vol. 161, no. 2, pp. 505–522, 2012.

[13] P. Gentile, V. Chiono, I. Carmagnola, and P. Hatton, "An overview of poly (lactic-co-glycolic) acid (PLGA)-based biomaterials for bone tissue engineering," *International Journal of Molecular Sciences*, vol. 15, no. 3, pp. 3640–3659, 2014.

[14] H. K. Makadia and S. J. Siegel, "Poly lactic-co-glycolic acid (PLGA) as biodegradable controlled drug delivery carrier," *Polymers*, vol. 3, no. 3, pp. 1377–1397, 2011.

[15] J. Naghipoor and T. Rabczuk, "A mechanistic model for drug release from PLGA-based drug eluting stent: a computational study," *Computers in Biology and Medicine*, vol. 90, pp. 15–22, 2017.

[16] J.-C. Park, U. M. E. Wikesjö, K.-T. Koo et al., "Maturation of alveolar bone following implantation of an rhGDF-5/PLGA composite into 1-wall intra-bony defects in dogs: 24-week histometric observations," *Journal of Clinical Periodontology*, vol. 39, no. 6, pp. 565–573, 2012.

[17] Y. Yao, F. Kauffmann, S. Maekawa et al., "Sclerostin antibody stimulates periodontal regeneration in large alveolar bone defects," *Scientific Reports*, vol. 10, no. 1, p. 16217, 2020.

[18] L. Chen, L. Mei, D. Feng et al., "Anhydrous reverse micelle lecithin nanoparticles/PLGA composite microspheres for long-term protein delivery with reduced initial burst," *Colloids and Surfaces B: Biointerfaces*, vol. 163, pp. 146–154, 2018.

[19] Q. Yang, Y. Wu, F. Lan et al., "Hollow superparamagnetic PLGA/Fe_3O_4 composite microspheres for lysozyme adsorption," *Nanotechnology*, vol. 25, no. 8, Article ID 085702, 2014.

[20] V. M. Gaspar, A. F. Moreira, E. C. Costa et al., "Gas-generating TPGS-PLGA microspheres loaded with nanoparticles (NIMPS) for co-delivery of minicircle DNA and anti-tumoral drugs," *Colloids and Surfaces B: Biointerfaces*, vol. 134, pp. 287–294, 2015.

[21] M. S. Shive and J. M. Anderson, "Biodegradation and biocompatibility of PLA and PLGA microspheres," *Advanced Drug Delivery Reviews*, vol. 28, no. 1, pp. 5–24, 1997.

[22] O. A. Sindeeva, O. I. Gusliakova, O. A. Inozemtseva et al., "Effect of a controlled release of epinephrine hydrochloride from PLGA microchamber array: in vivo studies," *ACS Applied Materials & Interfaces*, vol. 10, no. 44, pp. 37855–37864, 2018.

[23] M. J. Dorta, A. Oliva, O. Munguía, M. Llabrés, and J. B. Fariña, "In-vitro release of fluoropyrimidines from PLGA film implants," *The Journal of Pharmacy and Pharmacology*, vol. 54, no. 6, pp. 757–763, 2002.

[24] S. K. Boda, Y. Almoshari, H. Wang et al., "Mineralized nanofiber segments coupled with calcium-binding BMP-2 peptides for alveolar bone regeneration," *Acta Biomaterialia*, vol. 85, pp. 282–293, 2019.

Expert Opinion on Pharmacotherapy, vol. 6, no. 3, pp. 465–477, 2005.

[25] T. Watanabe, Y. Kimura, and T. Ono, "Microfluidic fabrication of monodisperse polylactide microcapsules with tunable structures through rapid precipitation," *Langmuir*, vol. 29, no. 46, pp. 14082–14088, 2013.

[26] T. Govender, S. Stolnik, M. C. Garnett, L. Illum, and S. S. Davis, "PLGA nanoparticles prepared by nanoprecipitation: drug loading and release studies of a water soluble drug," *Journal of Controlled Release*, vol. 57, no. 2, pp. 171–185, 1999.

[27] X. Yu, Z. Zhao, W. Nie et al., "Biodegradable polymer microcapsules fabrication through a template-free approach," *Langmuir*, vol. 27, no. 16, pp. 10265–10273, 2011.

[28] S. R. Abulateefeh and A. M. Alkilany, "Synthesis and characterization of PLGA shell microcapsules containing aqueous cores prepared by internal phase separation," *AAPS PharmSciTech*, vol. 17, no. 4, pp. 891–897, 2016.

[29] P. Blasi, S. Giovagnoli, A. Schoubben et al., "Preparation and in vitro and in vivo characterization of composite microcapsules for cell encapsulation," *International Journal of Pharmaceutics*, vol. 324, no. 1, pp. 27–36, 2006.

[30] R. L. McCall and R. W. Sirianni, "PLGA nanoparticles formed by single- or double-emulsion with vitamin E-TPGS," *Jove-Journal of Visualized Experiments*, vol. 82, Article ID 51015, 2013.

[31] A. Sahin, F. Spiroux, I. Guedon et al., "Using PVA and TPGS as combined emulsifier in nanoprecipitation method improves characteristics and anticancer activity of ibuprofen loaded PLGA nanoparticles," *Die Pharmazie*, vol. 72, no. 9, pp. 525–528, 2017.

[32] S. K. Paswan and T. R. Saini, "Purification of drug loaded PLGA nanoparticles prepared by emulsification solvent evaporation using stirred cell ultrafiltration technique," *Pharmaceutical Research*, vol. 34, no. 12, pp. 2779–2786, 2017.

[33] A. S. Ahmed, U. K. Mandal, M. Taher, D. Susanti, and J. M. Jaffri, "PVA-PEG physically cross-linked hydrogel film as a wound dressing: experimental design and optimization," *Pharmaceutical Development and Technology*, vol. 23, no. 8, pp. 751–760, 2018.

[34] N. Y. Martinez, P. F. Andrade, N. Durán, and S. Cavalitto, "Development of double emulsion nanoparticles for the encapsulation of bovine serum albumin," *Colloids and Surfaces B: Biointerfaces*, vol. 158, pp. 190–196, 2017.

[35] K. Shi, F. Cui, H. Yamamoto, and Y. Kawashima, "Optimized preparation of insulin-lauryl sulfate complex loaded poly (lactide-co-glycolide) nanoparticles using response surface methodology," *Die Pharmazie*, vol. 63, no. 10, pp. 721–725, 2008.

[36] R. Tanaka, T. Hayashi, M. Ike, Y. Noto, and T. K. Goto, "Reduction of dark-band-like metal artifacts caused by dental implant bodies using hypothetical monoenergetic imaging after dual-energy computed tomography," *Oral Surgery, Oral Medicine, Oral Pathology and Oral Radiology*, vol. 115, no. 6, pp. 833–838, 2013.

[37] A. C. Oenning, R. Jacobs, R. Jacobs et al., "Cone-beam CT in paediatric dentistry: DIMITRA project position statement," *Pediatric Radiology*, vol. 48, no. 3, pp. 308–316, 2018.

[38] G. Li, S. Luo, C. You et al., "A novel calibration method incorporating nonlinear optimization and ball-bearing markers for cone-beam CT with a parameterized trajectory," *Medical Physics*, vol. 46, no. 1, pp. 152–164, 2019.

Research Article

Integrated Molecular Docking with Network Pharmacology to Reveal the Molecular Mechanism of Simiao Powder in the Treatment of Acute Gouty Arthritis

Yihua Fan [ID],[1,2] **Wei Liu** [ID],[1,2] **Yue Jin** [ID],[1,2] **Xu Hou**,[3] **Xuewu Zhang**,[4] **Hudan Pan**,[5] **Hang Lu**,[1,2] **and Xiaojing Guo**[1,2]

[1]*First Teaching Hospital of Tianjin University of Traditional Chinese Medicine, Tianjin 300193, China*
[2]*National Clinical Research Center for Chinese Medicine Acupuncture and Moxibustion, Tianjin 300381, China*
[3]*Department of Endocrinology and Metabolic Diseases, Shandong Provincial Hospital*
 Affiliated to Shandong First Medical University, Jinan 250021, Shandong Province, China
[4]*Department of Rheumatology, People Hospital of Beijing University, Bejing 100044, China*
[5]*Dr. Neher's Biophysics Laboratory for Innovative Drug Discovery,*
 State Key Laboratory of Quality Research in Chinese Medicine, Macau University of Science and Technology,
 Macao 999078, China

Correspondence should be addressed to Wei Liu; fengshiliuwei@163.com

Received 14 January 2021; Revised 12 March 2021; Accepted 16 April 2021; Published 28 April 2021

Academic Editor: Jun Jiang

Background. The incidence of gout has been rapidly increasing in recent years with the changing of diet. At present, modern medications used in the clinical treatment of gout showed several side effects, such as gastrointestinal damage and the increased risk of cardiovascular disease. The traditional Chinese prescription Simiao Powder (SMP) has a long history in the treatment of acute gouty arthritis (AGA) and has a good curative effect. However, the mechanism and target of its therapeutic effects are still not completely understood. *Methods.* Potential active compounds (PACs) and targets of SMP were found in the TCMSP database, and the disease target genes related to AGA were obtained by searching CTD, DisGeNET, DrugBank, GeneCards, TTD, OMIM, and PharmGKB disease databases with "acute gouty arthritis" and "Arthritis, Gouty" as keywords, respectively. The network of "Traditional Chinese medicine (TCM)-PACs-potential targets of acute gouty arthritis" was constructed with the Cytoscape 3.7.2 software, and the target genes of acute gouty arthritis were intersected with genes regulated by active compounds of SMP. The resultant common gene targets were input into Cytoscape 3.7.2 software, and the BisoGenet plug-in was used to construct a PPI network. The GO functional enrichment analysis and KEGG pathway enrichment analysis of the intersecting target proteins were performed using R software and corresponding program packages. The molecular docking verification was carried out between the potentially active compounds of SMP and the core target at the same time. *Results.* 40 active components and 203 targets were identified, of which 95 targets were common targets for the drugs and diseases. GO function enrichment analysis revealed that SMP regulated several biological processes, such as response to lipopolysaccharide and oxidative stress, RNA polymerase II transcription regulator complex, protein kinase complex, and other cellular and molecular processes, including DNA-binding transcription factor binding. Results of KEGG pathway analysis showed that SMP was associated with AGA-related pathways such as interleukin-17 (IL-17), tumor necrosis factor (TNF), p53, and hypoxia-inducible factor 1 (HIF-1) signaling pathways. The results of molecular docking showed that active compounds in SMP exhibited strong binding to five core protein receptors (TP53, FN1, ESR1, CDK2, and HSPA5). *Conclusions.* Active components of SMP, such as quercetin, kaempferol, wogonin, baicalein, beta-sitosterol, and rutaecarpine, showed therapeutic effects on AGA. These compounds were strongly associated with core target proteins (such as TP53, FN1, ESR1, CDK2, and HSPA5). This study reveals that IL-17, TNF, p53, and HIF-1 signaling pathways mediate the therapeutic effects of SMP on AGA. These findings expand our understanding of the mechanism of SMP in the treatment of AGA.

1. Introduction

Gouty arthritis (GA) is characterized by acute onset of single joint redness, swelling, heat, and pain at night or in the morning. The pain progressively worsens, and in severe cases, patients often suffer from cutting pain, which often reaches a peak within 24 hours [1]. The number of gout patients has increased drastically due to dietary changes and high intake of high-purine foods and beer [2]. According to the gout epidemic survey in Hong Kong, the prevalence of gout increased from 1.56% in 2006 to −2.92% in 2016 [3]. In the United States, the prevalence of gout was about 3.9% in 2016, with an estimated 9.2 million gout patients [4]. Acute gouty arthritis (AGA) is the first symptom of gout. Severe pain can reduce the quality of life of patients. Recurrent acute arthritis can destroy joints and damage internal organs [5]. Gout treatment guidelines issued in 2012 by the American College of Rheumatology (ACR) recommend nonsteroidal anti-inflammatory drugs (NSAIDs) or oral colchicine for acute attacks of gout [6]. It has been reported that NSAIDs are harmful to the gastrointestinal tract, liver, and kidney, central nervous system, etc. [7]. Colchicine is an anti-inflammatory drug commonly used in the treatment of acute gout. However, when taken in large doses, it easily causes gastrointestinal tract discomfort, liver and kidney damage, or heart disease. Meanwhile, it may lead to poisoning in elderly patients [8]. Therefore, safer and more effective drugs for the treatment of AGA are urgently needed.

Simiao Powder (SMP) is a well-known prescription used in ancient China for the treatment of joint pain [9]. This prescription originated from *Chengfang Biandu* in the Qing Dynasty (1904 A.D.). SMP is composed of *Rhizoma Atractylodis* (Cang Zhu), *Cortex Phellodendri* (Huang Bo), *Radix Vladimiriae* (Niu Xi), and *Semen Coicis* (Yi Yi Ren), and it could clear heat, dry dampness, and promote blood circulation to invigorate the tendons. In the gouty arthritis model, Lin et al. revealed that SMP treatment could effectively relieve joint symptoms and improve laboratory indexes (e.g., serum uric acid content or inflammatory cytokines IL-1b, IL-9, IFN-g, and so on). Moreover, the anti-inflammatory effect of SMP was stronger than febuxostat [10]. A systematic review and meta-analysis demonstrated that SMP possesses anti-inflammatory, analgesic, and uric acid-lowering effects and hence can treat AGA. Jiawei reported that SMP is superior to other anti-inflammatory drugs or combined uric acid-lowering drugs. Compared to modern medications, SMP is associated with fewer adverse events [11]. However, the mechanism and the therapeutic target of SMP in the management of AGA are vague and are the main limiting factors for its widespread clinical application [11].

The entire human body is a complex network, and the occurrence and progression of a disease are the results of the comprehensive action of multiple factors. Single-targeted therapy cannot meet the needs of multitarget and multipathway treatment of diseases. The network pharmacology concept put forward by Hopkins in 2007 [12] provides a "multiway" and "multitarget" approach to drug analysis. It is similar to the thoughts of TCM compound prescription, as well as the characteristics of the overall TCM compatibility and comprehensive and multipathway treatment of diseases.

The present study employed network pharmacology and molecular docking techniques to establish the active components of SMP in AGA treatment and predicted the potential target and drug action pathways of SMP. Collectively, we aimed to explore the potential mechanism of action of SMP and provide a reference for pharmacological research and clinical application of this prescription. The specific flow chart is shown in Figure 1.

2. Methods

2.1. Screening of Drug Components and SMP Targets.
Rhizoma Atractylodis (Cang Zhu), *Cortex Phellodendri* (Huang Bo), *Radix Vladimiriae* (Niu Xi), and *Semen Coicis* (Yi Yi Ren), SMP components, were acquired from the traditional Chinese medicine systems pharmacology database and analysis platform (TCMSP, http://tcmspw.com/tcmsp.php), capturing all the potential active components of drugs in SMP. We screened the active compounds in SMP following the standards of oral bioavailability (OB) ≥30% and drug-likeness (DL) ≥0.18. Then, a search was undertaken for corresponding targets of active compounds on the TCMSP platform. The identified drug targets were input into the UniProt database (https://www.uniprot.org/). To obtain the abbreviation of the human gene for each target, we set the protein type as "Homo sapiens."

2.2. Search and Screening of AGA-Related Genes.
The search for target genes related to AGA was achieved using the terms "acute gouty arthritis" and "Arthritis, Gouty" in the Human Gene Database (GeneCards, https://www.genecards.org/), Online Mendelian Inheritance in Man (OMIM, https://www.omim.org/), the Pharmacogenomics Knowledge Base database (PharmGKB, https://www.pharmgkb.org/), DrugBank database (https://www.drugbank.ca/), DisGeNET database (https://www.disgenet.org/), the Therapeutic Target Database (TTD, http://db.idrblab.net/ttd/), and Comparative Toxicogenomics Database (CTD, http://ctdbase.org/). The results of the above databases were integrated to obtain the target genes of AGA after deleting the repeated genes.

2.3. Potential SMP Targets in the Treatment of AGA.
We intersected the targets regulated by active compounds in SMP with the disease target genes of AGA. After that, common targets were obtained. The R 4.0.2 software and its Venn diagram package were employed to generate a Venn diagram of the SMP-AGA-related target.

2.4. Network Construction of Potential Active Compound-Potential Target.
The potential targets and active compounds corresponding to the potential targets of SMP in
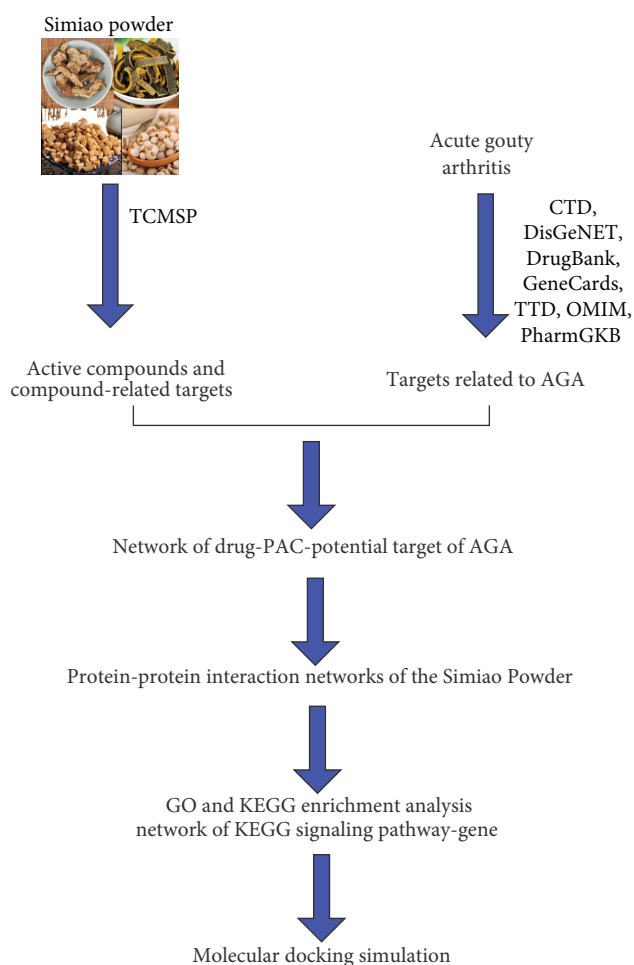
Figure 1: Flow diagram of the study.

AGA treatment were introduced into Cytoscape 3.7.2 software. Then, we constructed the network of "TCM-active compound-potential targets" and conducted the visualization display.

2.5. Construction of the Protein-Protein Interaction (PPI) Network and Screening of Core Targets. The intersection target was imported into Cytoscape 3.7.2 software. The PPI network was constructed via its plug-in BisoGenet with the following data sources: DIP, BIOGRID, HPRD, BIND, MINT, and INTACT. The plug-in CytoNCA was employed for topology analysis. Then, the degree centrality (DC) betweenness centrality (BC) of each node was calculated. A larger DC and BC of the node at the protein location implied that the protein was more important in the constructed PPI network [13]. Because we screened out various important target proteins, other protein interaction parameters, such as closeness centrality (CC) and eigenvector centrality (EC), were further applied to screen core target proteins.

2.6. Gene Ontology (GO) Functional Enrichment and the Kyoto Encyclopedia of Genes and Genomes (KEGG) Pathway Enrichment Analyses. The ID of the intersection target was obtained using R4.2.0 software and its "org.Hs.eg.db" package. Then, the "clusterProfiler" and other program packages were adopted for GO functional enrichment analysis of the target. A histogram was constructed after screening out the first 10 functional categories of biological process (BP), cellular component (CC), and molecular function (MF). The target proteins were subjected to the KEGG enrichment analysis, whereby the first 30 KEGG pathways were selected to construct the histogram. Information of the first 20 KEGG pathways was introduced into Cytoscape 3.7.2 to draw the KEGG pathway-gene network map. After that, we selected a signal pathway closely related to GA for visual display.

2.7. SMP Potential Active Compounds and Protein Molecular Docking. The 2D structure of the potential compound was retrieved from PubChem (https://pubchem.ncbi.nlm.nih.gov/). For small molecules, their energy was minimized using ChemBio3D 2014 software. The 2D structure was converted into a 3D structure. We downloaded the 3D structure of the core target protein from the Protein Data Bank (PDB) database (http://www.rcsb.org). Using the Pymol software, the target protein receptor molecules were processed, including dehydration and removal of ligand small molecules. The target protein receptor molecule was hydrogenated using Autodock Tools 4.2.6 software. The center coordinate and size of the box were set based on the position of the active site of the protein molecule and the area where it potentially acted on the ligand small molecule. Molecular docking was achieved using AutoDock Vina, whereby lower binding energy depicted a better affinity between the receptor and the ligand. The binding energy ≤0 kcal/mol indicated that the compound could bind and interact with the target, whereas the binding energy <−5 kcal/mol demonstrated a very strong binding force. The docking results with the best binding force between each core target protein and active compound were simultaneously presented in 2D images and 3D structures.

3. Results

3.1. Target Screening of SMP and AGA. In total, 403 compounds of SMP were obtained from the TCMSP database, including 49 from *Rhizoma Atractylodis* (Cang Zhu), 140 from *Cortex Phellodendri* (Huang Bo), 176 from *Radix Vladimiriae* (Niu Xi), and 38 from *Semen Coicis* (Yi Yi Ren). Besides, 52 active compounds were screened according to OB ≥ 30% and DL ≥ 0.18, including 4 from *Rhizoma Atractylodis* (Cang Zhu), 25 from *Cortex Phellodendri* (Huang Bo), 17 from *Radix Vladimiriae* (Niu Xi), and 6 from *Semen Coicis* (Yi Yi Ren). After eliminating repeated active compounds, 40 active compounds were obtained. From the TCMSP platform, 916 targets of the 40 active compounds were obtained, including 60 from *Rhizoma Atractylodis* (Cang Zhu), 430 from *Cortex Phellodendri* (Huang Bo), 384 from *Radix Vladimiriae* (Niu Xi), and 42 from *Semen Coicis* (Yi Yi Ren). After eliminating repeated targets, 203 targets

and their abbreviations were obtained. Information of active compounds and the number of action targets of TCM in SMP are outlined in Table 1. Through a search in GeneCards, OMIM, PharmGKB, DrugBank, DisGeNET, TTD, and CTD databases, 1,204 target genes associated with AGA were obtained (Figure 2).

3.2. Potential Targets and Corresponding Active Compounds of SMP in the Treatment of AGA. The drug-disease intersection target (the potential target of SMP in AGA treatment) was obtained by intersecting the 203 drug targets with 1204 disease targets using R software, with 95 potential targets (Figure 3). Notably, 33 active compounds corresponded to the 95 potential targets. They were the active compounds of SMP in AGA treatment.

3.3. Construction of TCM-PACs-Potential Target of AGA Network. We drew and analyzed the potential targets of SMP in the treatment of AGA using Cytoscape 3.7.2 network drawing software. Then, a PAC-potential target network diagram of SMP for AGA treatment was constructed (Figure 4). The network diagram comprised 133 nodes (including 95 target genes, 33 drug active components, 4 TCM, and 1 disease name) and 250 edges. We further calculated the degree of the compound in the figure. Notably, a higher degree implied that the compound played a more critical role in the network. The top six active compounds included MOL000098-quercetin, MOL000422-kaempferol, MOL000173-wogonin, MOL002714-baicalein, MOL000358beta-sitosterol, and MOL002662-rutaecarpine, with 79, 30, 21, 18, 12, and 7 as the corresponding target numbers, respectively.

3.4. Construction of PPI Network, Topological Analysis, and Determination of Core Targets. After obtaining the potential target genes, they were imported into Cytoscape 3.7.2 software. We then drew the PPI network diagram using the Bisogent plug-in and obtained 5,264 nodes and 133,011 connections (Figure 5(a)). For the first topology analysis, $DC \geq 74$ and 982 nodes and 43,726 connections were obtained (Figure 5(b)). The second topology analysis was conducted with $BC \geq 925.611$ (average), $CC \geq 0.581$ (average), and $EC \geq 0.096$ (average) to identify the crucial target genes; eventually, 54 nodes and 829 lines were obtained. Target proteins with the top five degree values were selected as the core target proteins in the protein network (Figure 5(c)), where TP53 protein, FN1 protein, ESR1 protein, CDK2 protein, and HSPA5 protein corresponded to 946 edges, 781 edges, 1,762 edges, 687 edges, and 445 edges, respectively.

3.5. GO Functional Enrichment and KEGG Pathway Enrichment Analyses. For GO analysis, BP, CC, and MF were included, and 1,938 items were obtained via BP enrichment analysis (including response to lipopolysaccharide, oxidative stress, reactive oxygen species (ROS), etc.); 36 items via CC enrichment analysis (including RNA polymerase II

transcription regulator complex, protein kinase complex, and membrane raft); 145 items via MF enrichment analysis (including DNA-binding transcription factor binding, heme binding, and RNA polymerase II-specific DNA-binding transcription factor binding). To draw the GO function histogram of SMP in AGA treatment, we selected the top 10 BP, CC, and MF results at $P < 0.05$ (Figure 6).

To further elucidate the pathways regulated by the therapeutic target genes, we did a KEGG pathway analysis. Results revealed that these target genes were distributed in 155 pathways. To construct a histogram, the pathways with the top 30 enriched genes were selected (Figure 7). GA-related pathways were mainly associated with IL-17, TNF, p53, and HIF-1 signaling pathways. We also analyzed the association of the top 20 pathways with their corresponding target genes by constructing a KEGG pathway-gene network diagram (Figure 8). There were 83 nodes (including 20 pathways and 63 target genes) and 403 lines. Based on the number of regulatory pathways, the top five genes were RELA, TP53, MAPK1, IKBKB, and CHUK with 16, 15, 15, 15, and 15 regulatory pathways, respectively. A strong relationship existed between GA and inflammation (the IL-17 pathway is closely related to inflammation). Therefore, we constructed a diagram to demonstrate the association of the regulatory target of SMP with the IL-17 pathway (Figure 9).

3.6. Molecular Docking. Using the AutoDock Vina software, PACs in the network map of "TCM-PAC-potential targets of AGA" were docked with five core target proteins (TP53, FN1, ESR1, CDK2, and HSPA5) in PPI. A higher binding activity between the compound and the target protein receptor implied lower binding energy. Results demonstrated that the docking of 33 active compounds with the 5 core target protein receptors was less than 0 kcal/mol (a majority was less than −5 kcal/mol) (Table 2). The molecular docking results of the compounds with the highest binding energy corresponding to the five targets are displayed in 2D images and 3D structures (Figure 10).

4. Discussion

The repeated attacks and protracted course of acute gouty arthritis can lead to joint swelling, deformity, and destruction of bone and joint cartilage. Tophi can be formed in many parts of the body, and it could seriously invade joints, kidneys, and even aorta and heart valves in severe cases [14–16]. For the treatment of gout, anti-inflammatory analgesics are mainly used in the acute stage. After the pain of patients is completely relieved, the use of uric acid-lowering drugs to correct the serum uric acid level is adopted [7, 17, 18]. Studies have found that although febuxostat and allopurinol can effectively reduce blood uric acid levels, they can also increase the risk of cardiovascular disease [19]. Traditional Chinese medicine compounds could function in anti-inflammatory analgesics and lowering uric acid at the same time, which has certain advantages compared with anti-inflammatory analgesics alone [20–22]. Besides, its relatively fewer adverse reactions and lower price have attracted more and more scholars' attention.

Table 1: Active compounds and their number of targets of SMP.

No.	Source	ID	Compound	OB	DL	Number
1	Huangbo, Niuxi	MOL000098	quercetin	46.43	0.28	138
2	Niuxi	MOL000422	kaempferol	41.88	0.24	55
3	Cangzhu, Niuxi	MOL000173	wogonin	30.68	0.23	41
4	Niuxi	MOL002714	baicalein	33.52	0.21	33
5	Huangbo	MOL000790	Isocorypalmine	35.77	0.59	31
6	Huangbo, Niuxi	MOL000358	beta-sitosterol	36.91	0.75	28
7	Huangbo	MOL001455	(S) -Canadine	53.83	0.77	28
8	Huangbo, Niuxi, Yiyiren	MOL000449	Stigmasterol	43.83	0.76	27
9	Huangbo	MOL002670	Cavidine	35.64	0.81	24
10	Huangbo	MOL000787	Fumarine	59.26	0.83	22
11	Huangbo	MOL002651	Dehydrotanshinone II A	43.76	0.4	18
12	Cangzhu	MOL000188	3β-acetoxyatractylone	40.57	0.22	17
13	Huangbo, Niuxi	MOL000785	palmatine	64.6	0.65	16
14	Huangbo	MOL002662	rutaecarpine	40.3	0.6	14
15	Huangbo, Niuxi	MOL001454	berberine	36.86	0.78	14
16	Huangbo	MOL006422	thalifendine	44.41	0.73	12
17	Huangbo	MOL002894	berberrubine	35.74	0.73	11
18	Huangbo	MOL002644	Phellopterin	40.19	0.28	9
19	Niuxi	MOL002897	piberberine	43.09	0.78	9
20	Huangbo, Niuxi	MOL001458	coptisine	30.67	0.86	8
21	Huangbo	MOL001131	phellamurin_qt	56.6	0.39	7
22	Niuxi	MOL003847	Inophyllum E	38.81	0.85	6
23	Huangbo	MOL002668	Worenine	45.83	0.87	6
24	Yiyiren	MOL001323	Sitosterol alpha1	43.28	0.78	5
25	Huangbo	MOL002666	Chelerythrine	34.18	0.78	5
26	Yiyiren	MOL000953	CLR	37.87	0.68	3
27	Niuxi	MOL004355	Spinasterol	42.98	0.76	3
28	Huangbo	MOL002663	Skimmianin	40.14	0.2	3
29	Yiyiren	MOL000359	sitosterol	36.91	0.75	3
30	Niuxi	MOL001006	poriferasta-7	42.98	0.76	3
31	Huangbo	MOL002641	Phellavin_qt	35.86	0.44	3
32	Yiyiren	MOL001494	Mandenol	42	0.19	3
33	Huangbo	MOL001771	poriferast-5-en-3beta-ol	36.91	0.75	2
34	Huangbo	MOL000622	Magnograndiolide	63.71	0.19	2
35	Cangzhu	MOL000184	NSC63551	39.25	0.76	1
36	Huangbo, Niuxi	MOL002643	delta 7-stigmastenol	37.42	0.75	1
37	Huangbo	MOL005438	campesterol	37.58	0.71	1
38	Cangzhu, Niuxi	MOL000085	beta-daucosterol_qt	36.91	0.75	1
39	Yiyiren	MOL008121	2-Monoolein	34.23	0.29	1
40	Niuxi	MOL012461	28-norolean-17-en-3-ol	35.93	0.78	1

According to Figure 4, the key active components of SMP in the treatment of GA were quercetin, kaempferol, wogonin, baicalein, beta-sitosterol, and rutaecarpine. Quercetin is the active compound of *Cortex Phellodendri* (Huang Bo) and *Radix Vladimiriae* (Niu Xi), kaempferol is the active compound of *Radix Vladimiriae* (Niu Xi), wogonin is the active compound of *Rhizoma Atractylodis* (Cang Zhu) and *Radix Vladimiriae* (Niu Xi), baicalein is the active compound of *Radix Vladimiriae* (Niu Xi), beta-sitosterol is the active compound of *Cortex Phellodendri* (Huang Bo) and *Radix Vladimiriae* (Niu Xi), and rutaecarpine is the active compound of *Cortex Phellodendri* (Huang Bo). Among them, quercetin and wogonin are the common active components of two traditional Chinese medicines, which is similar to the compatibility and synergism of TCM compounds. Considering *Semen Coicis* (Yi Yi Ren) as an indispensable TCM in this prescription, the active ingredient stigmasterol, characterized by a great degree value in Figure 4, was established as one of the crucial active compounds.

These PACs in SMP have a certain curative effect on inhibiting inflammation and lowering blood uric acid level [23]. Among them, quercetin, baicalein, wogonin, and rutaecarpine showed strong anti-inflammatory effects [19–21]. Baicalein could inhibit the activity of NF-κB and some inflammatory factors, such as monocyte chemotactic protein-1 (MCP-1), interleukins, tumor necrosis factor, and cellular adhesion molecules. In addition, it also clears the reactive oxygen species (ROS) to show anti-inflammatory and antioxidant effects [24]. Moreover, wogonin, a flavonoid from medicinal plants, has shown various biological activities. It potentially inhibits the production of inflammatory mediators by macrophages and lymphocytes [25]. Inhibition of NF-κB and mitogen-activated protein kinase (MAPK) pathways in rutaecarpine-derivative R3 inhibits the NLRP3 inflammasome activation, which

FIGURE 2: Venn diagram of disease targets.

FIGURE 3: Venn diagram of drug targets and disease targets.

FIGURE 4: A network of the drug-PAC-potential target of AGA. The left circle represents the active ingredients. Different colors distinguish drug sources of each ingredient; blue represents the active ingredient from Cortex Phellodendri (Huang Bo), yellow represents the active ingredient from Rhizoma Atracylodis (Cang Zhu), orange represents the active ingredient from Semen Coicis (Yi Yi Ren), green represents the active ingredient from Radix Vladimiriae (Niu Xi), and purple represents the common ingredient of various drugs. The square node on the right denotes the target.
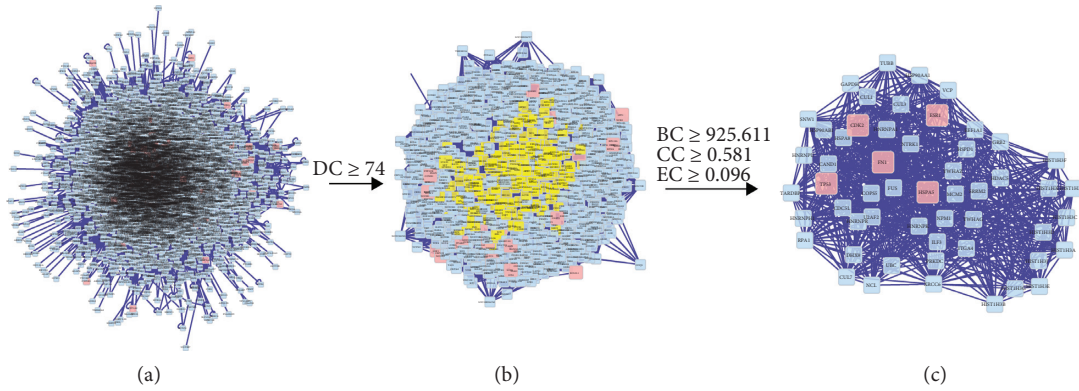
(a) (b) (c)

FIGURE 5: Protein-protein interaction network of the Simiao Powder.
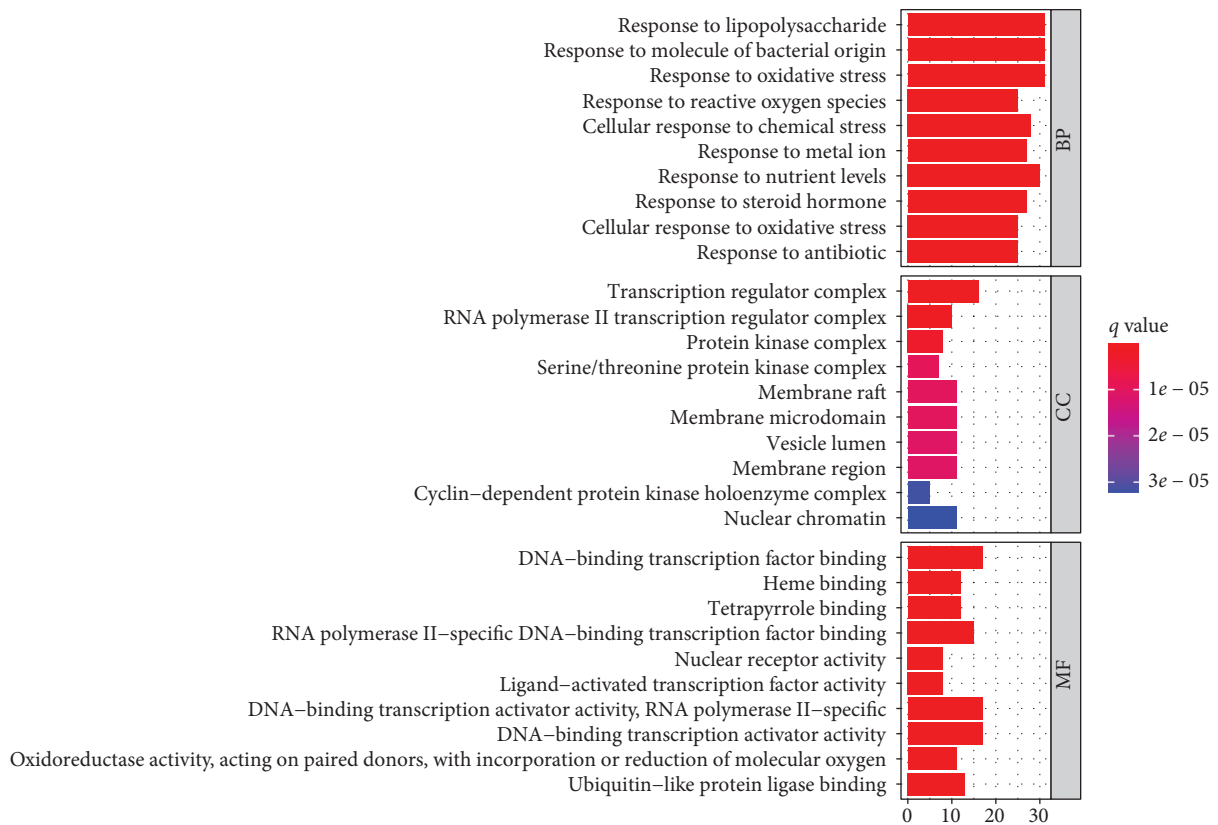
FIGURE 6: GO functional enrichment analysis.GO analysis of putative targets. The *y*-axis demonstrates the top 10 significantly enriched BP, CC, and MF categories, whereas the *x*-axis displays the number of enrichment genes of these terms ($P < 0.05$). The color denotes the different *P* value range, and the redder it is, the more significant enrichment.

consequently lowers the expression of proinflammatory cytokine IL-1β [26, 27]. The pathogenesis of GA is highly associated with the inflammatory cascade induced by the activation of the inflammatory bodies of NLRP3 [2]. Thus, the inhibitory effect of rutaecarpine on the inflammatory body activation of NLRP3 may influence GA treatment. Besides, quercetin and kaempferol may significantly elevate the total antioxidant capacity and inhibit the xanthine oxidase (XOD) effect in hyperuricemia rats [28]. In another study, inhibition of XOD activity could reduce the serum

uric acid level and the formation of ROS, consequently reducing the deposition of gout urate crystals [29]. Additional studies found that quercetin could reduce serum uric acid levels in hyperuricemia mice and impede renal insufficiency. This was achieved via the regulation of renal organic ion transport protein and uromodulin, and demonstrated fewer side effects than allopurinol [30, 31]. Beta-sitosterol (SIT), the main compound among various phytosterols, can reduce the expression of chemokines and inflammatory cytokines. It then regulates various biological
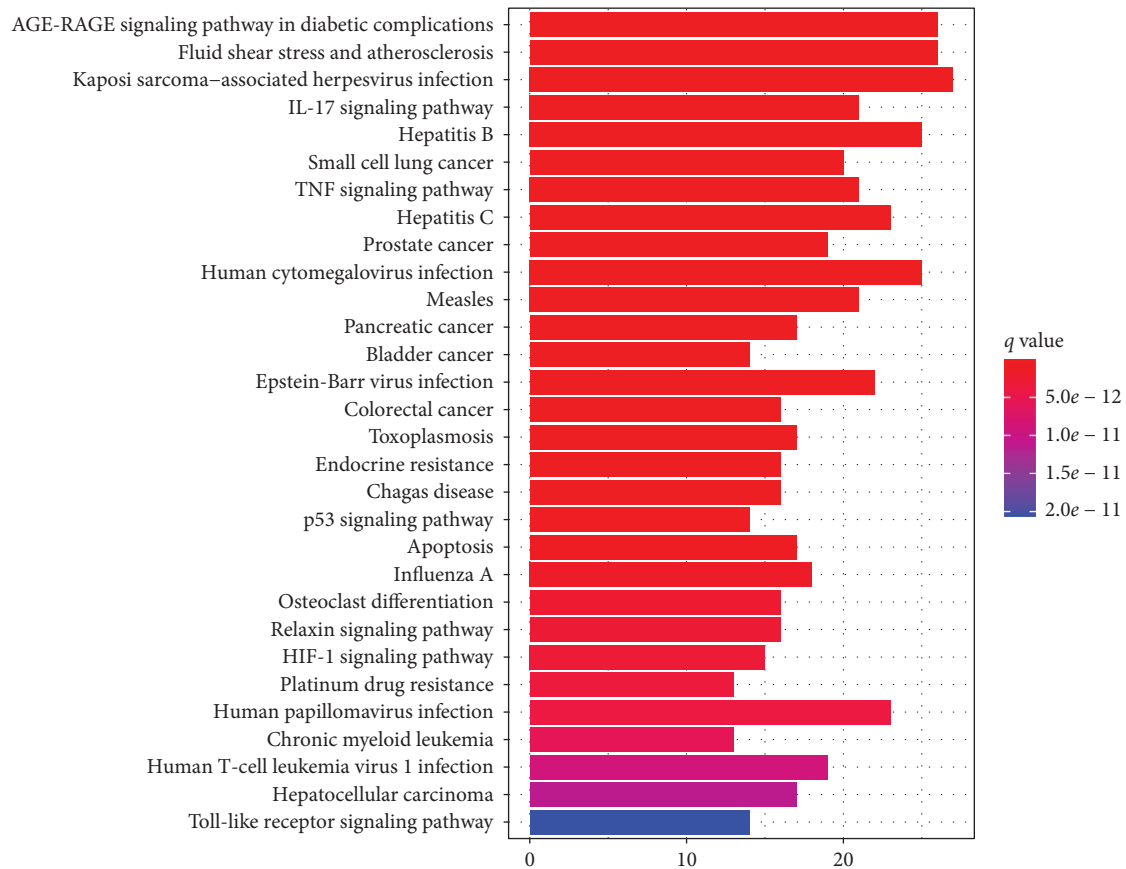
FIGURE 7: KEGG pathway enrichment analysis. *Note.* KEGG enrichment analysis of putative targets. The *y*-axis outlines the top 30 significantly enriched KEGG pathways, whereas the *x*-axis displays the number of enrichment genes of these terms ($P < 0.05$). The color denotes the different *P* value range; the redder it is, the more significant enrichment.

functions, including anti-inflammatory, analgesic, immunomodulatory, and antimicrobial functions [32, 33]. Also, stigmasterol can inhibit the inflammation induced by sodium urate crystals and XOD activity in mice, a phenomenon that validates its antigout effect [34].

Herein, to obtain the core target proteins of SMP in the treatment of GA disease, the PPI network of intersecting target proteins was constructed. Also, we performed two topological screens on the SMP target for GA treatment based on DC, BC, CC, and EC. TP53, FN1, ESR1, CDK2, and HSPA5 were the five core target proteins. Based on the existing reports, TP53, also known as p53, contributes to transcriptional regulation of the cell cycle, DNA repair, cell survival, and cell metabolism [35]. Inhibition of p53 exerts a substantial effect on promoting the senescence of IL-1β-induced chondrocytes [36]. The potential role of TP53 in the regulation of inflammation has been described, whereby it significantly inhibits the production of proinflammatory factor IL-6 [37]. The overexpression of FN1 can activate TGF-Akt/PI3K/Akt signal pathway to promote cell viability and differentiation capacity [38]. Cyclin-dependent kinase (CDK) is the main regulator of cell division. It can be potentially triggered by different cyclins at different cell cycle stages [39], and it can regulate the secretion of inflammatory cytokines in macrophages [40] and inhibit

CDK2. In consequence, a reduction in chemotaxis of primary neutrophils outlines the role of CDK2 in regulating inflammation [39]. Estrogen receptor 1 (ESR1) is a subtype of human ESR, expressed in chondrocytes, stromal cells, and osteoblasts [41]. In particular, ESR can induce the transcription of related target genes to promote the proliferation and differentiation of tissue cells as they bind to estrogen [42]. Heat shock protein family A member 5 (HSPA5) gene can also participate in the inflammatory process of various types of osteoarthritis as it encodes the binding immunoglobulin protein (BiP) of the endoplasmic reticulum Hsp70 family [43].

Following the KEGG signal pathway analysis, the mechanisms of SMP in the treatment of AGA were mainly anti-inflammation and protection of the cartilage. The critical inflammatory signaling pathways included TNF and IL-17, whereas the apoptosis signaling pathways included p53 and HIF.

Current pieces of research on the mechanism of gout have reported that the phagocytosis of MSU crystal triggers the change of inflammatory cell state of synovial cells in GA pathogenesis [14]. For instance, the deposition of MSU crystals promotes the local release of TNF-α and IL-1β, which causes persistent gout episodes [44]. IL-17 also stimulates macrophages and monocytes to produce
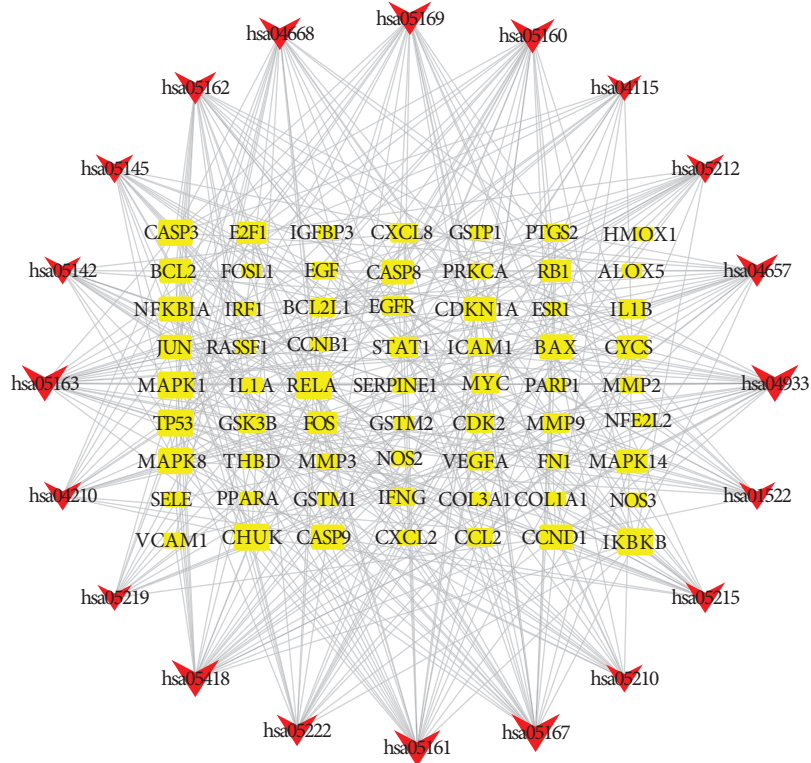
FIGURE 8: A network of KEGG signaling pathway-gene. Red triangles denote pathways, whereas yellow square nodes denote genes. The larger the shape of the node is, the more genes or pathways are connected to it.
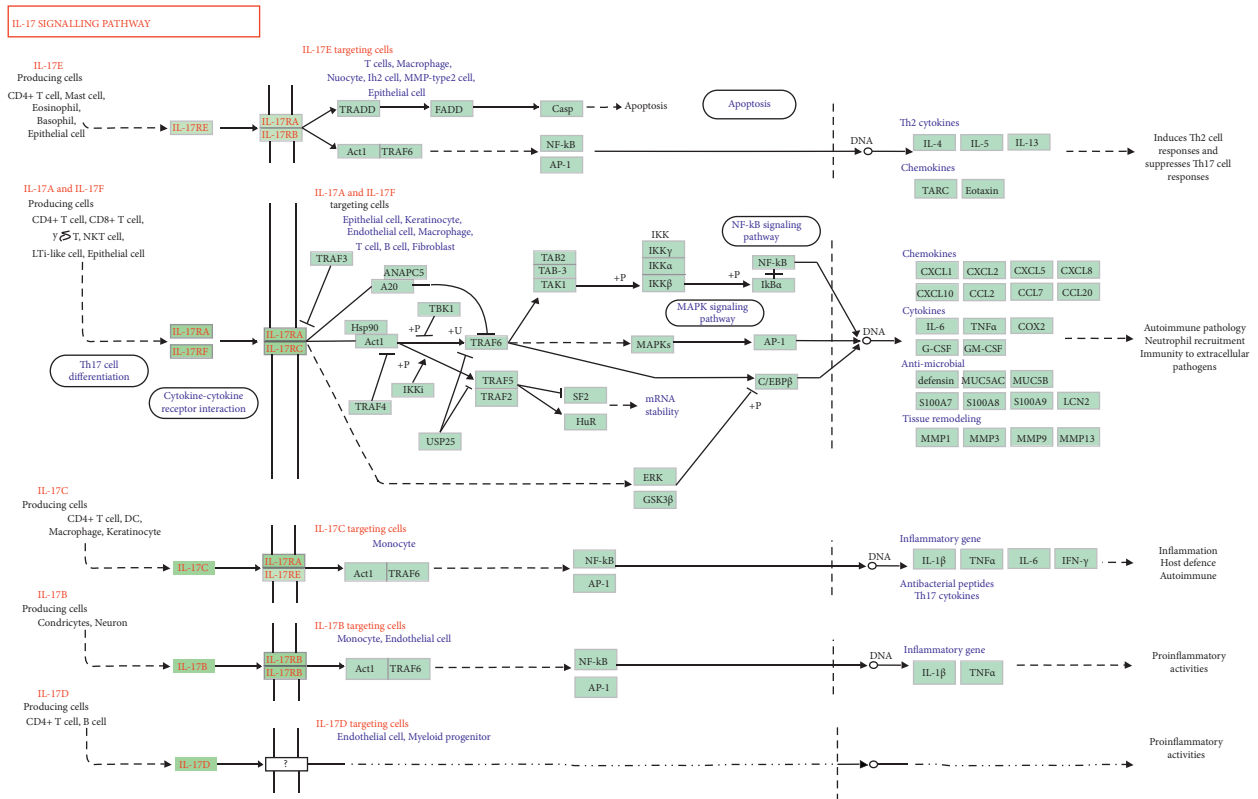

FIGURE 9: The IL-17 signaling pathway. The green nodes in the road map denote the genes existing in our SMP network.

TABLE 2: The affinity of the putative compounds with core targets.

Compound	Affinity -TP53 (kcal/mol)	Affinity-FN1 (kcal/mol)	Affinity-ESR1 (kcal/mol)	Affinity-CDK2 (kcal/mol)	Affinity -HSPA5 (kcal/mol)
Dehydrotanshinone II A	−7.6	−4.0	−8.7	−11.5	−8.3
3β-acetoxyatractylone	−6.8	−3.3	−8.7	−8.6	−6.9
baicalein	−6.6	−4.0	−8.4	−8.7	−9.7
kaempferol	−6.4	−3.9	−8.3	−8.4	−8.8
wogonin	−6.9	−3.9	−8.3	−8.7	−7.9
quercetin	−6.5	−3.9	−8.1	−8.8	−8.2
Phellopterin	−6.6	−3.4	−7.9	−8.5	−7.0
phellamurin_qt	−7.4	−3.8	−7.2	−9.4	−7.8
Mandenol	−4.3	−1.6	−7.1	−6.4	−4.2
rutaecarpine	−8.3	−4.2	−7.0	−10.5	−9.6
2-Monoolein	−4.9	−2.1	−6.6	−6.5	−4.7
Spinasterol	−7.9	−3.8	−6.5	−9.1	−8.3
beta-sitosterol	−7.3	−3.4	−6.5	−10.6	−7.6
Phellavin_qt	−7.1	−3.7	−6.2	−9.5	−7.7
CLR	−7.0	−3.2	−6.1	−9.9	−8.1
poriferast-5-en-3beta-ol	−7.6	−3.1	−6.1	−9.9	−7.0
sitosterol	−6.8	−3.1	−6.0	−10.2	−7.7
Stigmasterol	−7.8	−3.9	−5.9	−9.8	−8.1
Sitosterol alpha1	−7.2	−3.6	−5.6	−9.8	−8.4
Fumarine	−7.4	−3.9	−5.5	−9.5	−8.9
Chelerythrine	−7.6	−3.6	−5.5	−10.4	−8.2
Worenine	−7.7	−4.3	−5.4	−10.9	−9.0
poriferasta-7	−7.1	−3.5	−5.3	−10.4	−7.6
epiberberine	−6.8	−3.8	−5.1	−9.4	−8.6
Cavidine	−6.9	−3.9	−4.9	−8.7	−8.1
berberine	−7.3	−3.8	−4.8	−9.6	−8.0
thalifendine	−6.8	−4.0	−4.7	−9.6	−8.3
(S)-Canadine	−6.7	−3.8	−4.7	−9.1	−8.1
berberrubine	−6.9	−3.8	−4.7	−9.5	−7.6
Inophyllum E	−8.6	−4.4	−4.2	−11.7	−9.7
coptisine	−7.4	−4.0	−4.2	−10.1	−8.9
Isocorypalmine	−6.5	−3.9	−4	−8.7	−7.5
palmatine	−6.5	−3.6	−3.6	−8.8	−7.2

proinflammatory factors, including IL-1β, TNF-α, and IFN-γ (Figure 9). As a powerful proinflammatory cytokine, IL-17 can increase serum IL-17 levels 8 hours following the acute attack of gout [45]. Moreover, in several arthritic animal models, the inhibition of IL-17 expression was found to limit inflammation and reduce joint erosion [46]. The TNF signaling pathway has also proved to be a crucial inflammatory signal pathway. Signal transduction is mediated by TNF receptor 1 (TNFR1) and receptor-2 (TNFR2). TNFR2 is, in most cases, expressed in immune cells. It binds to TNF-α and TNF-β to regulate immune response [47]. TNF-α is a proinflammatory cytokine produced by different cell types, such as macrophages, lymphocytes, and fibroblasts, and reflects inflammation, infection, and other environmental stresses [48]. Previous reports showed that inhibition of TNF-α expression in synovial cells during AGA could effectively inhibit local inflammation [49, 50].

The physiological dose of soluble uric acid exerts a specific protective effect on cartilage [51]. However, following repeated attacks by GA, the articular cartilage edge is damaged, the articular surface becomes irregular, the joint space becomes narrow, and MSU deposition occurs [52]. A study found that reduced articular cartilage matrix secretion in patients with GA was associated with chondrocyte apoptosis [53]. p53 can regulate cell differentiation and senescence. The inhibition of p53 expression potentially improves senescence and affects the destruction of IL-1β-induced chondrocytes [36]. Compared to the inflammatory signaling pathway, the HIF-1 signaling pathway is slightly less in gout studies. As a transcription factor, activation of HIF-1α expression in synovial cells may be induced during hypoxia. Synovial hyperplasia follows the repeated infiltration of inflammatory cells in the joint. On the other hand, hypoxia is associated with immune cell infiltration and synovial hyperplasia. Therefore, the upregulation of synovium-derived HIF-1α occurs in the pathogenesis of rheumatoid arthritis (RA) and osteoarthritis (OA), which are hypoxia-associated diseases [54, 55]. HIF-1α exerts a regulatory role in the function of immune cells. Activated LPS-induced macrophages can also express HIF-1α, which is crucial in glycolysis and the induction of proinflammation [56]. The therapeutic effect of SMP on AGA may be derived through the regulation of the inflammatory signal pathway, p53 apoptosis signal, and HIF-1signaling pathway. And other top-ranked signaling pathways, such as the AGE-RAGE signaling pathway in diabetic complications, fluid shear stress, and atherosclerosis, etc., still lack their gout-related studies, which are
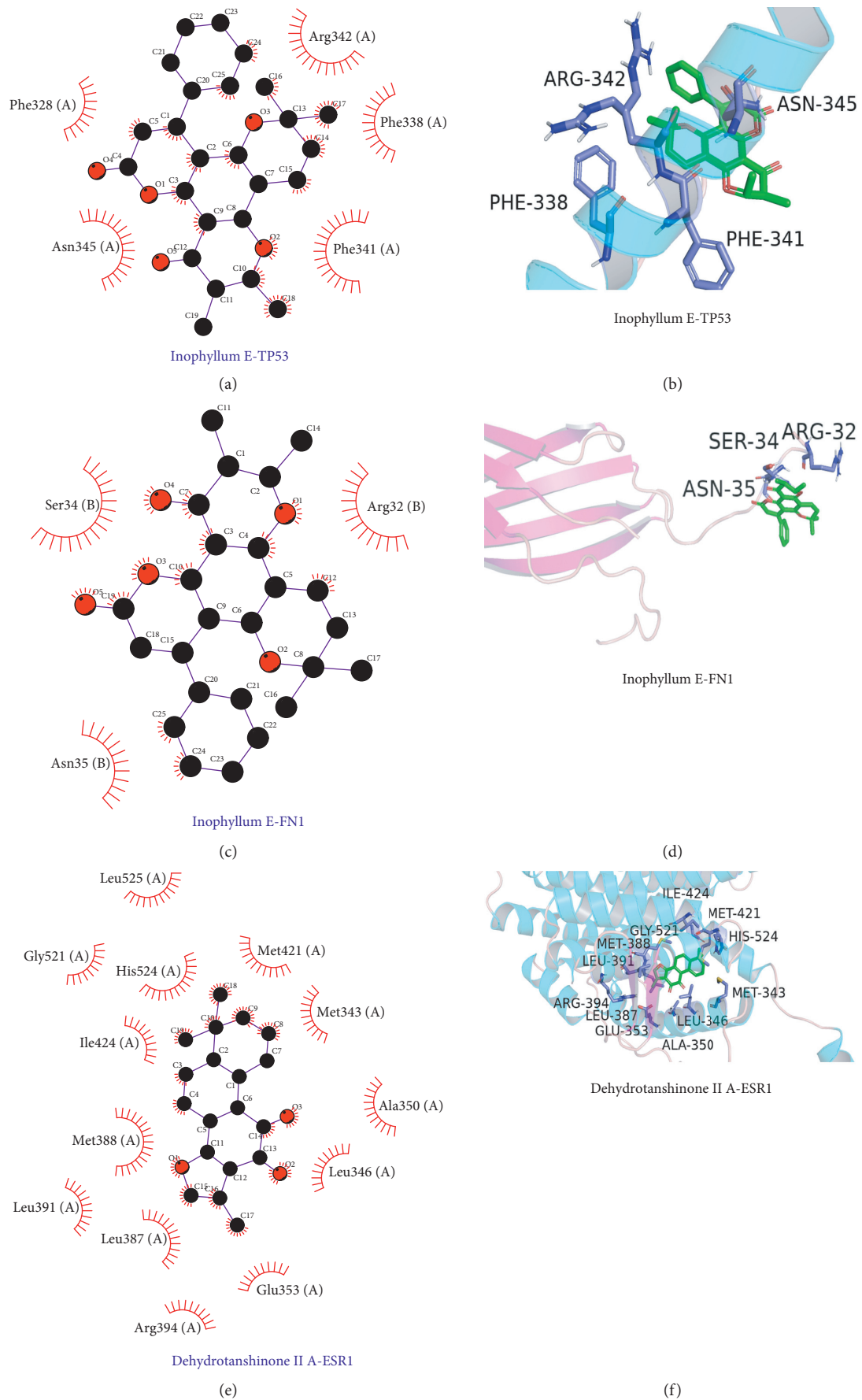
Inophyllum E-TP53

(a)

Inophyllum E-TP53

(b)

Inophyllum E-FN1

(c)

Inophyllum E-FN1

(d)

Dehydrotanshinone II A-ESR1

(e)

Dehydrotanshinone II A-ESR1

(f)

FIGURE 10: Continued.

Inophyllum E-CDK2

(g)

Inophyllum E-CDK2

(h)

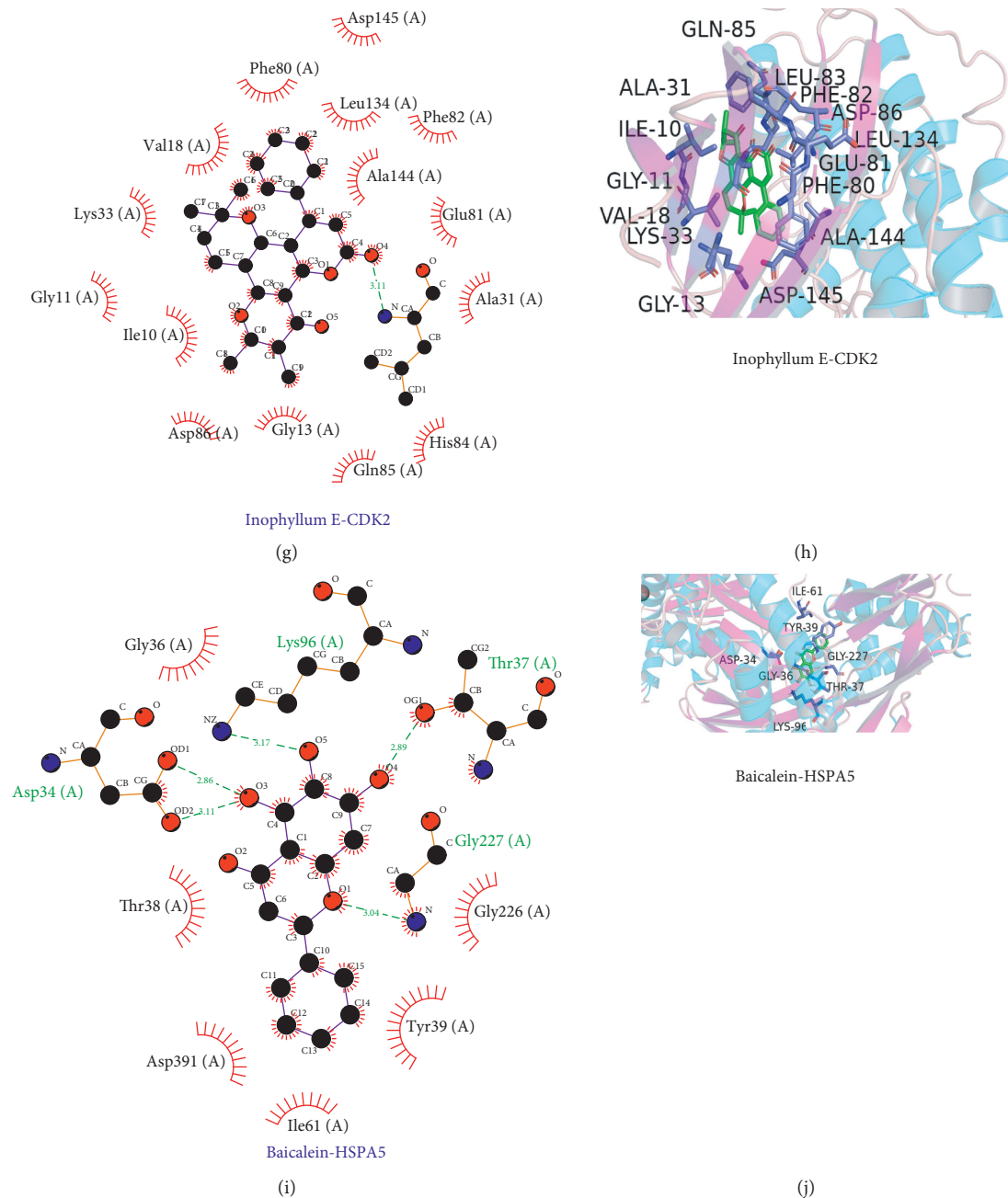
Baicalein-HSPA5

(i)

Baicalein-HSPA5

(j)

FIGURE 10: A diagram for the five core targets molecular docking of SMP gouty arthritis treatment.

likely to be the future direction of gout mechanism research.

According to the space matching and energy matching relationship between molecules, the core target protein of SMP in AGA treatment was docked with active compounds. This provides a reference for the subsequent research and development of targeted drugs. The 2D image of molecular docking depicts the binding mode between the core target protein and the compound as well as the interaction with the surrounding amino acid residues. Hydrophobic interaction best describes the main association of target protein TP53, FN1, and ESR1

with Inophyllum E. The target protein CDK2 residue Leu83 (A) forms a hydrogen bond with Inophyllum E, whereas the residues Asp34 (A), Lys96 (A), Thr37 (A), and Gly227 (A) of the target protein HSPA5 form five hydrogen bonds with baicalein. The main forces between ligand and protein are hydrophobic force and hydrogen bond, which both are chemical bonds with strong binding force. According to Table 2, key components of SMP have strong binding activity with core target proteins, such as TP53, FN1, ESR1, CDK2, and HSPA5, suggesting that SMP may play its pharmacological role by regulating these key targets. However, there are still some

shortcomings in this study, and the conclusions need to be further verified by in vivo, in vitro, and clinical trials.

5. Conclusion

The present study systematically expounds the core compounds and molecular action mechanism of SMP in the treatment of AGA. The core compounds of SMP, including quercetin, kaempferol, wogonin, baicalein, and beta-sitosterol, were screened via network pharmacology, whereas the core targets of AGA including TP53, FN1, ESR1, CDK2, and HSPA5 were screened out via PPI. These core compounds are characterized by stable binding activity to the core targets. Also, SMP could regulate signal pathways related to AGA disease, for example, TNF, IL-17, p53, and HIF signaling pathways. These findings suggest the potential synergistic role of SMP in treating AGA via multiple components, multitargets, multiple biological functions, and multiple signal pathways.

Abbreviations

SMP:	Simiao Powder
AGA:	Acute gouty arthritis
TCM:	Traditional Chinese medicine
IL-17:	Interleukin-17
TNF:	Tumor necrosis factor
HIF-1:	Hypoxia-inducible factor 1
GA:	Gouty arthritis
ACR:	American College of Rheumatology
NSAIDs:	Nonsteroidal anti-inflammatory drugs
TCMSP:	Traditional Chinese medicine systems pharmacology database and analysis platform
OB:	Oral bioavailability
DL:	Drug-likeness
OMIM:	Online Mendelian Inheritance in Man
PharmGKB:	Pharmacogenomics Knowledge Base database
TTD:	Therapeutic Target Database
CTD:	Comparative Toxicogenomics Database
PACs:	Potential active compounds
PPI:	Protein-protein interaction
DC:	Degree centrality
BC:	Betweenness centrality
CC:	Closeness centrality
EC:	Eigenvector centrality
GO:	Gene ontology
KEGG:	Kyoto Encyclopedia of Genes and Genomes
BP:	Biological process
CC:	Cellular component
MF:	Molecular function
PDB:	Protein Data Bank
ROS:	Reactive oxygen species
MSU:	Monosodium urate
NF-κB:	Nuclear factor-kappa B
MAPK:	Mitogen-activated protein kinase
XOD:	Xanthine oxidase
SIT:	Beta-sitosterol
XO:	Xanthine oxidase
CDK:	Cyclin-dependent kinase
ESR1:	Estrogen receptor 1
HSPA5:	Heat shock protein family A (Hsp70) member 5
BiP:	Binding immunoglobulin protein
TNFR1:	TNF receptor 1
TNFR2:	TNF receptor-2
RA:	Rheumatoid arthritis
OA:	Osteoarthritis.

Data Availability

The data for this study can be provided by the corresponding author (Wei Liu: fengshiliuwei@163.com).

Conflicts of Interest

There are no conflicts of interest between these authors.

Authors' Contributions

Yihua Fan, Wei Liu, and Yue Jin have contributed equally to this work and are co-first authors.

Acknowledgments

References

[1] R. Terkeltaub, "What makes gouty inflammation so variable?" *BMC Medicine*, vol. 15, no. 1, p. 158, 2017.

[2] T. Pascart and F. Lioté, "Gout: state of the art after a decade of developments," *Rheumatology (Oxford, England)*, vol. 58, no. 1, pp. 27–44, 2019.

[3] M. Tsoi, "Epidemiology of gout in Hong Kong: a population-based study from 2006 to 2016," *Arthritis Research & Therapy*, vol. 22, no. 1, p. 204, 2020.

[4] M. Chen-Xu, "Contemporary prevalence of gout and hyperuricemia in the United States and decadal trends: the national health and nutrition examination survey, 2007–2016," *Arthritis & Rheumatology (Hoboken, N.J.)*, vol. 71, no. 6, pp. 991–999, 2019.

[5] L. Staurengo-Ferrari, "Trans-chalcone attenuates pain and inflammation in experimental acute gout arthritis in mice," *Frontiers in Pharmacology*, vol. 9, p. 1123, 2018.

[6] D. Khanna, P. P. Khanna, J. D. Fitzgerald et al., "2012 American College of Rheumatology guidelines for management of gout. Part 2: therapy and antiinflammatory

prophylaxis of acute gouty arthritis," *Arthritis Care & Research*, vol. 64, no. 10, pp. 1447–1461, 2012.

[7] S. Bindu, S. Mazumder, and U. Bandyopadhyay, "Non-steroidal anti-inflammatory drugs (NSAIDs) and organ damage: a current perspective," *Biochemical Pharmacology*, vol. 180, Article ID 114147, 2020.

[8] Y. Jiang, "Colchicine: risk of severe toxicity and death from drug overdose," *Chinese Journal of Pharmacoepidemiology*, vol. 20, no. 2, p. 102, 2011.

[9] M. A.-O. Tang, "Integrating network pharmacology with molecular docking to unravel the active compounds and potential mechanism of simiao pill treating rheumatoid arthritis," *Evidence-Based Complementary and Alternative Medicine*, vol. 2020, Article ID 5786053, 16 pages, 2020.

[10] X. Lin, "Simiao decoction alleviates gouty arthritis by modulating proinflammatory cytokines and the gut ecosystem," *Frontiers in Pharmacology*, vol. 11, 2020.

[11] Y.-F. Liu, Y. Huang, C.-Y.-Z. Wen et al., "The effects of modified simiao decoction in the treatment of gouty arthritis: a systematic review and meta-analysis," *Evidence-Based Complementary and Alternative Medicine*, vol. 2017, p. 12, 2017.

[12] A. L. Hopkins, "Network pharmacology," *Nature Biotechnology*, vol. 25, no. 10, pp. 1110-1111, 2007.

[13] Y. Wang, "Drug target prediction based on the herbs components: the study on the multitargets pharmacological mechanism of qishenkeli acting on the coronary heart disease," *Evidence-Based Complementary and Alternative Medicine*, vol. 2012, Article ID 698531, 10 pages, 2012.

[14] B. N. Cronstein and P. Sunkureddi, "Mechanistic aspects of inflammation and clinical management of inflammation in acute gouty arthritis," *JCR: Journal of Clinical Rheumatology*, vol. 19, no. 1, pp. 19–29, 2013.

[15] M. H. Pillinger and B. F. Mandell, "Therapeutic approaches in the treatment of gout," *Seminars in Arthritis and Rheumatism*, vol. 50, no. 3, pp. S24–S30, 2020.

[16] C. Yokose, N. Lu, H. Xie et al., "Heart disease and the risk of allopurinol-associated severe cutaneous adverse reactions: a general population-based cohort study," *Canadian Medical Association Journal*, vol. 191, no. 39, pp. E1070–E1077, 2019.

[17] Y.-F. Huang, C. Bai, F. He, Y. Xie, and H. Zhou, "Review on the potential action mechanisms of Chinese medicines in treating coronavirus disease 2019 (COVID-19)," *Pharmacological Research*, vol. 158, Article ID 104939, 2020.

[18] X. Zheng, F. Wu, X. Lin, L. Shen, and Y. Feng, "Developments in drug delivery of bioactive alkaloids derived from traditional Chinese medicine," *Drug Delivery*, vol. 25, no. 1, pp. 398–416, 2018.

[19] L. Li, "Insights into the action mechanisms of traditional Chinese medicine in osteoarthritis," *Evidence-based Complementary and Alternative Medicine*, vol. 2017, Article ID 5190986, 13 pages, 2017.

[20] X. He, X. Wang, J. Fang et al., "The genus Achyranthes: a review on traditional uses, phytochemistry, and pharmacological activities," *Journal of Ethnopharmacology*, vol. 203, pp. 260–278, 2017.

[21] H.-C. Ko, Y.-H. Wang, K.-T. Liou et al., "Anti-inflammatory effects and mechanisms of the ethanol extract of *Evodia rutaecarpa* and its bioactive components on neutrophils and microglial cells," *European Journal of Pharmacology*, vol. 555, no. 2-3, pp. 211–217, 2007.

[22] W. Yan-Hang and K.-W. Zeng, "Natural products as a crucial source of anti-inflammatory drugs: recent trends and advancements," *Traditional Medicine Research*, vol. 4, no. 5, p. 257, 2019.

[23] H. Wang, H. Duan, S. Chen et al., "Chinese herbal medicine si-miao-san decoction for acute gouty arthritis: a protocol for systematic review and meta-analysis of randomized controlled trials," *Medicine*, vol. 99, no. 32, Article ID e21510, 2020.

[24] L. Baandrup, S. Dinda, S. DasSharma, R. Banik, A. Chakraborty, and M. Dinda, "Therapeutic potentials of baicalin and its aglycone, baicalein against inflammatory disorders," *European Journal of Medicinal Chemistry*, vol. 131, pp. 68–80, 2017.

[25] D. L. Huynh, T. H. Ngau, N. H. Nguyen, G.-B. Tran, and C. T. Nguyen, "Potential therapeutic and pharmacological effects of Wogonin: an updated review," *Molecular Biology Reports*, vol. 47, no. 12, pp. 9779–9789, 2020.

[26] Q. Qin, H. Liu, J. Shou, Y. Jiang, H. Yu, and X. Wang, "The inhibitor effect of RKIP on inflammasome activation and inflammasome-dependent diseases," *Cellular & Molecular Immunology*, vol. 18p. 992, 1004.

[27] J. Luo, X. Wang, X. Jiang et al., "Rutaecarpine derivative R3 attenuates atherosclerosis via inhibiting NLRP3 inflammasome-related inflammation and modulating cholesterol transport," *The FASEB Journal*, vol. 34, no. 1, pp. 1398–1411, 2020.

[28] F. Haidari, "Effects of parsley (*Petroselinum crispum*) and its flavonol constituents, kaempferol and quercetin, on serum uric acid levels, biomarkers of oxidative stress and liver xanthine oxidoreductase aactivity in Oxonate-induced hyperuricemic rats," *Iranian Journal of Pharmaceutical Research: IJPR*, vol. 10, no. 4, pp. 811–819, 2011.

[29] S. Ahmad, "Therapeutic efficacy of urinile against gouty arthritis," *Dose-Response*, vol. 18, no. 4, 2020.

[30] Q.-H. Hu, X. Zhang, X. Wang, R.-Q. Jiao, and L.-D. Kong, "Quercetin regulates organic ion transporter and uromodulin expression and improves renal function in hyperuricemic mice," *European Journal of Nutrition*, vol. 51, no. 5, pp. 593–606, 2012.

[31] J. X. Zhu, Y. Wang, L. D. Kong, C. Yang, and X. Zhang, "Effects of *Biota orientalis* extract and its flavonoid constituents, quercetin and rutin on serum uric acid levels in oxonate-induced mice and xanthine dehydrogenase and xanthine oxidase activities in mouse liver," *Journal of Ethnopharmacology*, vol. 93, no. 1, pp. 133–140, 2004.

[32] Q. Yang, D. Yu, and Y. Zhang, "β-sitosterol attenuates the intracranial aneurysm growth by suppressing TNF-α-mediated mechanism," *Pharmacology*, vol. 104, pp. 303–311, 2019.

[33] S. Babu and S. Jayaraman, "An update on β-sitosterol: a potential herbal nutraceutical for diabetic management," *Biomedicine & Pharmacotherapy*, vol. 131, Article ID 110702, 2020.

[34] C. Martins de Sá Müller, G. B. Coelho, M. Carolina de Paula Michel Araújo, and D. A. Saúde-Guimarães, "*Lychnophora pinaster* ethanolic extract and its chemical constituents ameliorate hyperuricemia and related inflammation," *Journal of Ethnopharmacology*, vol. 242, Article ID 112040, 2019.

[35] E. M. Pinto and G. P. Zambetti, "What 20 years of research has taught us about the TP53 p.R337H mutation," *Cancer*, vol. 126, no. 21, pp. 4678–4686, 2020.

[36] H. Lu, D. Wang, H. Li et al., "GPR39 agonist TC-G 1008 ameliorates IL-1β-induced chondrocyte senescence," *Artificial Cells, Nanomedicine, and Biotechnology*, vol. 47, no. 1, pp. 2612–2617, 2019.

[37] T. Zhang, "p53 predominantly regulates IL-6 production and suppresses synovial inflammation in fibroblast-like synoviocytes and adjuvant-induced arthritis," *Arthritis Research & Therapy*, vol. 18, no. 1, p. 271, 2016.

[38] H. Zhang, X. Chen, P. Xue, X. Ma, and J. Li, "FN1 promotes chondrocyte differentiation and collagen production via TGF-β/PI3K/Akt pathway in mice with femoral fracture," *Gene*, Article ID 145253, 2020.

[39] A. Y. Hsu, D. Wang, S. Liu et al., "Phenotypical microRNA screen reveals a noncanonical role of CDK2 in regulating neutrophil migration," *Proceedings of the National Academy of Sciences*, vol. 116, no. 37, pp. 18561–18570, 2019.

[40] P. Laphanuwat and S. Jirawatnotai, "Immunomodulatory roles of cell cycle regulators," *Frontiers in Cell and Developmental Biology*, vol. 7, p. 23, 2019.

[41] Y. Oshima, K.-i. Matsuda, A. Yoshida, N. Watanabe, M. Kawata, and T. Kubo, "Localization of estrogen receptors alpha and beta. In the articular surface of the rat femur," *Acta Histochemica et Cytochemica*, vol. 40, no. 1, pp. 27–34, 2007.

[42] W. Liu, F. M. Shao, L. Yan, H. X. Cao, and D. Qiu, "Polymorphisms in the gene encoding estrogen receptor alpha are associated with osteoarthritis in Han Chinese women," *International Journal of Clinical and Experimental Medicine*, vol. 7, no. 12, pp. 5772–5777, 2014.

[43] J. Wang, J. Lee, D. Liem, and P. Ping, "HSPA5 Gene encoding Hsp70 chaperone BiP in the endoplasmic reticulum," *Gene*, vol. 618, pp. 14–23, 2017.

[44] Y. Zamudio-Cuevas, J. Fernández-Torres, G. A. Martínez-Nava et al., "Phagocytosis of monosodium urate crystals by human synoviocytes induces inflammation," *Experimental Biology and Medicine*, vol. 244, no. 5, pp. 344–351, 2019.

[45] Y. Liu, Q. Zhao, Y. Yin, M. A. McNutt, T. Zhang, and Y. Cao, "Serum levels of IL-17 are elevated in patients with acute gouty arthritis," *Biochemical and Biophysical Research Communications*, vol. 497, no. 3, pp. 897–902, 2018.

[46] M. I. Koenders, E. Lubberts, B. Oppers-Walgreen et al., "Blocking of interleukin-17 during reactivation of experimental arthritis prevents joint inflammation and bone erosion by decreasing RANKL and interleukin-1," *The American Journal of Pathology*, vol. 167, no. 1, pp. 141–149, 2005.

[47] M. K. McCoy and M. G. Tansey, "TNF signaling inhibition in the CNS: implications for normal brain function and neurodegenerative disease," *Journal of Neuroinflammation*, vol. 5, no. 1, p. 45, 2008.

[48] S. Abramson and Y. Yazici, "Biologics in development for rheumatoid arthritis: relevance to osteoarthritis," *Advanced Drug Delivery Reviews*, vol. 58, no. 2, pp. 212–225, 2006.

[49] Z. Wang, X. Fan, Y. Xu, K. Chen, X. Yu, and G. Sun, "Efficacy of Xixiancao (Herba Siegesbeckiae Orientalis) on interactions between nuclear factor kappa-B and inflammatory cytokines in inflammatory reactions of rat synovial cells induced by sodium urate," *Journal of Traditional Chinese Medicine = Chung I Tsa Chih Ying Wen pan*, vol. 40, no. 5, pp. 774–781, 2020.

[50] A. Liu, "The effects of carvacrol on inflammatory cytokines and the apoptosis of cartilage in rats with gouty arthritis," *Journal of Clinical and Experimental Medicine*, vol. 16, no. 6, pp. 531–534, 2017.

[51] J. Lai, "Physiological concentrations of soluble uric acid are chondroprotective and anti-inflammatory," *Scientific Reports*, vol. 7, no. 1, p. 2359, 2017.

[52] F. Oliviero, A. Scanu, and L. Punzi, "Metabolism of crystals within the joint," *Reumatismo*, vol. 63, no. 4, pp. 221–229, 2012.

[53] F. Zhu, L. Yin, and L. Ji, "Suppressive effect of sanmiao formula on experimental gouty arthritis by inhibiting cartilage matrix degradation: an in vivo and in vitro study," pp. 36–42, 2016.

[54] G. George, G. L. Shyni, and K. G. Raghu, "Current and novel therapeutic targets in the treatment of rheumatoid arthritis," *Inflammopharmacology*, vol. 28, no. 6, pp. 1457–1476, 2020.

[55] Y. Yu, W. Cai, J. Zhou et al., "Anti-arthritis effect of berberine associated with regulating energy metabolism of macrophages through AMPK/HIF-1α pathway," *International Immunopharmacology*, vol. 87, Article ID 106830, 2020.

[56] M. Wu, "Chaetocin attenuates gout in mice through inhibiting HIF-1α and NLRP3 inflammasome-dependent IL-1β secretion in macrophages," *Archives of Biochemistry and Biophysics*, vol. 670, pp. 94–103, 2019.

Research Article

Exploring the Pharmacological Mechanism of Duhuo Jisheng Decoction in Treating Osteoporosis Based on Network Pharmacology

Zhencheng Xiong [ID],[1,2] **Can Zheng** [ID],[3] **Yanan Chang,**[4] **Kuankuan Liu,**[4] **Li Shu,**[4] **and Chi Zhang** [ID][1,3,4,5,6]

[1]*Institute of Medical Technology, Peking University Health Science Center, Beijing, China*
[2]*Peking University Third Hospital, Beijing, China*
[3]*Biomedical Engineering Department, Peking University, Beijing, China*
[4]*Central Laboratory, Peking University International Hospital, Beijing, China*
[5]*Department of Orthopedics, Peking University International Hospital, Beijing, China*
[6]*School of Chinese Materia Medica, Beijing University of Chinese Medicine, Beijing, China*

Correspondence should be addressed to Chi Zhang; chi.zhang@case.edu

Objective. The purpose of this work is to study the mechanism of action of Duhuo Jisheng Decoction (DHJSD) in the treatment of osteoporosis based on the methods of bioinformatics and network pharmacology. *Methods*. In this study, the active compounds of each medicinal ingredient of DHJSD and their corresponding targets were obtained from TCMSP database. Osteoporosis was treated as search query in GeneCards, MalaCards, DisGeNET, Therapeutic Target Database (TTD), Comparative Toxicogenomics Database (CTD), and OMIM databases to obtain disease-related genes. The overlapping targets of DHJSD and osteoporosis were identified, and then GO and KEGG enrichment analysis were performed. Cytoscape was employed to construct DHJSD-compounds-target genes-osteoporosis network and protein-protein interaction (PPI) network. CytoHubba was utilized to select the hub genes. The activities of binding of hub genes and key components were confirmed by molecular docking. *Results*. 174 active compounds and their 205 related potential targets were identified in DHJSD for the treatment of osteoporosis, including 10 hub genes (AKT1, ALB, IL6, MAPK3, VEGFA, JUN, CASP3, EGFR, MYC, and EGF). Pathway enrichment analysis of target proteins indicated that osteoclast differentiation, AGE-RAGE signaling pathway in diabetic complications, Wnt signaling pathway, MAPK signaling pathway, PI3K-Akt signaling pathway, JAK-STAT signaling pathway, calcium signaling pathway, and TNF signaling pathway were the specifically major pathways regulated by DHJSD against osteoporosis. Further verification based on molecular docking results showed that the small molecule compounds (Quercetin, Kaempferol, Beta-sitosterol, Beta-carotene, and Formononetin) contained in DHJSD generally have excellent binding affinity to the macromolecular target proteins encoded by the top 10 genes. *Conclusion*. This study reveals the characteristics of multi-component, multi-target, and multi-pathway of DHJSD against osteoporosis and provides novel insights for verifying the mechanism of DHJSD in the treatment of osteoporosis.

1. Introduction

Osteoporosis is characterized by low bone mass, impaired bone microstructure, increased bone fragility, and susceptibility to fracture and is also a systemic bone disease [1]. Osteoporosis can occur in different genders and ages, but it is more common in postmenopausal women and elderly men [2]. The serious consequences of osteoporosis are fragility fractures that can occur during minor trauma or daily activities, leading to an increase in disability and mortality [3]. Moreover, the treatment and nursing of osteoporosis and osteoporotic fracture need to invest huge

manpower and material resources, and the cost is high, resulting in heavy family, social, and economic burden [4]. Therefore, early adoption of scientific prevention strategies and standardized treatment is very necessary. Among these, drug therapies such as bisphosphonates and denosumab are commonly used to treat osteoporosis by inhibiting the development, formation, and survival of osteoclasts [1]. Although these drugs are effective, high-dose or long-term use may cause serious adverse effects, such as gastrointestinal tolerance, atypical long bone fracture, jaw osteonecrosis, and acute renal failure [1]. Therefore, continuing to search for potential drugs with significant efficacy and high safety has become a consistent hot spot for the treatment of osteoporosis.

As we all know, traditional Chinese medicine (TCM) plays an important role in health maintenance in China and other Asian countries [5]. For a long time, TCM has been used as a complementary and alternative treatment option for patients with osteoporosis [6]. Systematic reviews and experimental studies have explored the efficacy and safety of TCM prescriptions in the treatment of osteoporosis, including Duhuo Jisheng Decoction (DHJSD), Xianling Gubao capsules, Liuwei Dihuang Decoction, and Erxian Decoction [2, 7–9].

DHJSD is a TCM recorded in Bei Ji Qian Jin Yao Fang of the Tang Dynasty for the treatment of "Bi Zheng," usually consisting of the following 15 herbs, including Du Huo (*Radix Angelicae Pubescentis*), Sang Ji Sheng (*Herba Taxilli*), Qin Jiao (*Radix Gentianae Macrophyllae*), Fang Feng (*Radix Saposhnikoviae*), Xi Xin (*Herba Asari*), Fu Ling (*Poria Cocos*), Chuan Xiong (*Rhizoma Chuanxiong*), Bai Shao (*Radix Paeoniae Alba*), Du Zhong (*Cortex Eucommiae Ulmoidis*), Ren Shen (*Panax Ginseng*), Gan Cao (*Radix Glycyrrhizae*), Dang Gui (*Radix Angelicae Sinensis*), Niu Xi (*Radix Achyranthis Bidentatae*), Shu Di Huang (*Radix Rehmanniae Preparata*), and Rou Gui (*Cortex Cinnamomi*) [10]. Among them, Du Huo has the good effects of relieving the pain of "Bi Zheng," dispelling cold and dehumidification, nourishing blood and Qi; Xi Xin, Fang Feng, and Qin Jiao dispel rheumatism, relax tendons and muscles, and benefit joints; Sang Ji Sheng, Du Zhong, Rou Gui, and Niu Xi nourish liver and kidney and strengthen bones and muscles; Dang Gui, Bai Shao, Shu Di Huang, and Chuan Xiong promote blood circulation; Ren Shen, Gan Cao, and Fu Ling strengthen spleen and supplement Qi [11]. The combination of the above herbs forms DHJSD, the classic bone injury prescription in TCM, it has the effect of nourishing the liver and kidney, benefiting Qi and blood, and stopping the pain of "Bi Zheng", which obviously improves the microcirculation of the body [2]. According to the theory of Chinese medicine, "Bi Zheng" refers to the symptoms of numbness, soreness, and poor flexion of muscles and joints caused by external factors (wind, dampness, cold, heat) on the body surface, tendons, and veins [12]. Osteoporosis belongs to the category of "Gu Bi" and "Gu Lou" in TCM theory [13]. And the cause of osteoporosis is the deficiency of Qi and blood in the liver and kidney and the loss of nutrition in the tendons and bones, so the treatment should be to nourish the liver and kidney and strengthen the tendons and bones as the

primary treatment [14]. Therefore, DHJSD has been widely used in China to treat rheumatoid arthritis, intervertebral disc disease, knee osteoarthritis, and osteoporosis, especially postmenopausal osteoporosis [2, 11, 14–17]. However, due to the ingredients contained, the mechanism of action of TCM is often elusive.

The network pharmacology of TCM is a part of bioinformatics, and it is still a priori analysis method for studying the relationship between drugs, compounds, diseases, and targets [18]. Due to the characteristics of multi-component, multi-target, and multi-pathway of TCM, network pharmacology has been widely used to clarify the mechanism of action of TCM and provide researchers with new directions and strategies. In this work, we tried to use the network pharmacology method to reveal the active compounds of DHJSD, and the key genes and pathways of DHJSD against osteoporosis, which facilitated further research and development (Figure 1).

2. Materials and Methods

2.1. Screening of Potential Active Compounds and Related Targets in DHJSD. We used the Traditional Chinese Medicine Systems Pharmacology (TCMSP, Version: 2.3, https://tcmspw.com/tcmsp.php) database and the analysis platform [19], and input the names of 15 Chinese herbal medicines in DHJSD to obtain the corresponding compounds and related information. According to the absorption, distribution, metabolism, and excretion (ADME) protocols, the active compounds were screened, and the criteria were oral bioavailability (OB) ≥30 and drug-likeness (DL) ≥0.18 [20, 21]. Then, the potential target proteins of the selected active compounds were mined in TCSMP database to construct the potential target gene set of DHJSD. UniProt database (https://www.uniprot.org/) was used to obtain the unique corresponding gene names and UniProt ID of drug or disease-related targets [22]. The species was selected as "*Homo sapiens.*"

2.2. Mining of Osteoporosis-Related Targets. Osteoporosis-related targets were obtained through retrieving GeneCards (https://www.genecards.org/) [23], MalaCards (https://www.malacards.org/) [24], DisGeNet database (https://www.disgenet.org/, v7.0) [25], Therapeutic Target Database (TTD) (http://db.idrblab.net/ttd/) [26], Comparative Toxicogenomics Database (CTD) (http://ctdbase.org/, Last update by June, 2020) [27], and Online Mendelian Inheritance in Man (OMIM) (https://omim.org/, updated November 25, 2020) [28] using the keyword "osteoporosis." GeneCards is a comprehensive, user-friendly database providing information on all annotated and predicted human genes, and we screen out targets with the relevance score ≥10 [23]. DisGeNET is a discovery platform that contains one of the largest public collections of genes and variants related to human diseases; targets with the score ≥0.1 were screened [25]. CTD is a powerful public database designed to improve people's understanding of how environmental exposure affects human health; targets with the
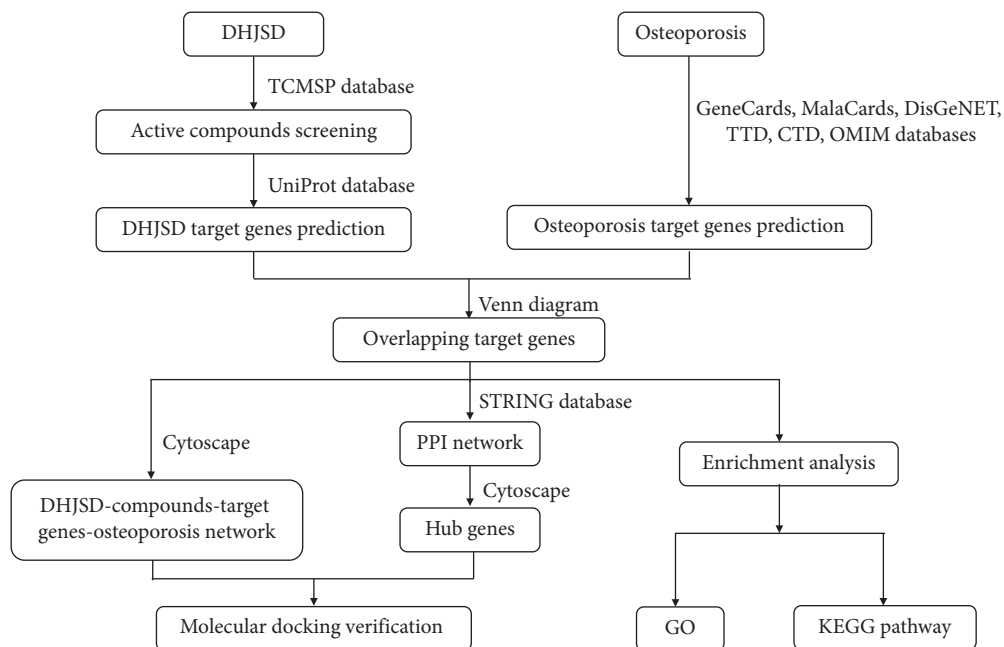
FIGURE 1: The schematic diagram of the present study to investigate potential mechanisms of DHJSD against osteoporosis.

inference score ≥20 were screened [27]. Finally, the potential targets obtained from the six databases mentioned above were integrated and de-duplicated to construct a set of targets relevant to osteoporosis.

2.3. Network Construction and Analysis.
DHJSD-related targets and osteoporosis-related targets were entered separately into the Venn online tool (http://www.bioinformatics. com.cn/) for common targets, which were candidate targets of DHJSD against osteoporosis. The interaction between "DHJSD-active compounds-target genes-osteoporosis" was constructed by Cytoscape software (version 3.7.2) [29].

2.4. Protein-Protein Interaction (PPI) Analysis.
PPI underlies most biological processes in living cells and is essential for understanding cell physiology in normal and disease states [10]. In this study, PPI network analysis of the obtained common targets was performed using the STRING database (http://string-db.org/; version 11) with the species limited to "*Homo sapiens*" and a confidence score >0.4 [30]. The PPI networks were constructed by Cytoscape software (version 3.7.2). Additionally, the plug-in 12 CytoHubba algorithms of Cytoscape software (Degree, Maximal Clique Centrality (MCC), Density of Maximum Neighborhood Component (DMNC), Maximum Neighborhood Component (MNC), Edge Percolated Component (EPC), Closeness, Betweenness, ClusteringCoefficient, EcCentricity, Radiality, Stress, BottleNeck) were used to select the first 10 nodes for finding the hub genes [31, 32].

2.5. Gene Ontology (GO) and Kyoto Encyclopedia of Genes and Genomes (KEGG) Pathway Enrichment Analysis.
We performed GO and KEGG pathway enrichment analysis using the clusterProfiler package in *R* (R 4.0.2 for Windows) to identify the biological processes and signaling pathways involved in DHJSD in treating osteoporosis [33–35]. An adjusted *P* value of <0.05 was considered to identify the enriched terms.

2.6. Molecular Docking.
The plug-in CytoHubba of Cytoscape software was used to screen top 10 hub genes [32]. In addition, Sankey diagram (http://sankeymatic.com/) was built with top 10 hub genes and relative active ingredients of DHJSD to find out key active ingredients. Sankey diagram discloses the relationship among herb, ingredients, and targets. Subsequently, molecular docking between top 10 hub genes and key active ingredients was carried out to predict the accuracy of the pivotal components and prediction targets using AutoDock Vina [36]. PubChem database (https://pubchem.ncbi.nlm.nih.gov/) and RCSB protein data (http://www.rcsb.org/) were selected to download the MOL2 format of ligands and PDB format of proteins [4]. Crystal of proteins were introduced to Pymol software (https://pymol.org/2/; version 2.4.1) to conduct dehydration and separation of ligands [37]. Subsequently, the crystal conducted was introduced to AutoDockTools to build a docking grid box of targets [1]. Molecular dockings were achieved via AutoDock Vina [37]. The lower Vina scores, one of the results of molecular docking, represent a more stable binding affinity of protein and ligand [38]. Eventually, the complexes of protein and compound were visualized by Pymol software.

3. Results

3.1. Screening of Active Compounds in DHJSD.
A total of 1939 compounds in DHJSD were retrieved through the

TCMSP database, of which 99 were from Du Huo, 46 were from Sang Ji Sheng, 27 were from Qin Jiao, 173 were from Fang Feng, 192 were from Xi Xin, 34 were from Fu Ling, 189 were from Chuan Xiong, 85 from Bai Shao, 147 from Du Zhong 190 from Ren Shen, 280 from Gan Cao, 125 from Dang Gui, 176 from Niu Xi, 76 from Shu Di Huang, and 100 from Rou Gui. According to the criteria of OB ≥30% and DL ≥0.18, a total of 240 (after removing duplication: 209) active compounds of DHJSD were screened, of which 9 were from Du Huo, 2 were from Sang Ji Sheng, 2 were from Qin Jiao, 18 were from Fang Feng, and 8 were from Xi Xin, 15 from Fu Ling, 7 from Chuan Xiong, 13 from Bai Shao, 28 from Du Zhong, 22 from Ren Shen, 92 from Gan Cao, 2 from Dang Gui, 20 from Niu Xi, and 2 from Shu Di Huang. However, there is no compound in Rou Gui that meets the screening criteria. Table 1 shows the basic information of some active compounds in DHJSD.

3.2. Mining of the Putative Target Genes for DHJSD.
By using the compound-target search function of TCMSP database, it was confirmed that 179 of the 209 active compounds in DHJSD possess target proteins. Subsequently, UniProt database was used to convert the target protein predicted by the biologically active compound of DHJSD into gene name. Finally, 267 putative target genes were identified.

3.3. Mining of the Potential Therapeutic Targets of DHJSD in Treating Osteoporosis.
A total of 3131 potential therapeutic targets of osteoporosis were obtained by searching Gene-Cards, MalaCards, DisGeNET, TTD, CTD, and OMIM databases. The Venn diagram was drawn by using Venn online platform, which is derived from the targets regulated by the active ingredients of DHJSD and the potential targets of osteoporosis. Subsequently, a total of 205 core targets were obtained, which were the potential therapeutic targets of DHJSD in the treatment of osteoporosis, as shown in Figure 2. The "DHJSD-active compounds-target genes-osteoporosis" network of DHJSD against osteoporosis was constructed by Cytoscape software (Figure 3). In this case, the sub-network of "active compounds-target genes" includes 379 nodes and 1856 edges. We ranked the target genes according to the number of targeting nodes. Table 2 shows the basic information of some key targets of DHJSD against osteoporosis.

3.4. Construction of the PPI Network and Mining of the Hub Genes of DHJSD in Treating Osteoporosis.
A total of 205 potential target genes of DHJSD in the treatment of osteoporosis were input into STRING database to obtain PPI network. The network involves 205 nodes and 4078 edges. Then, the obtained data was imported into Cytoscape 3.7.2 version for further visualization (Figure 4(a)). Subsequently, according to the 12 CytoHubba algorithms of Cytoscape software, including Degree, MCC, DMNC, MNC, EPC, Closeness, Betweenness, ClusteringCoefficient, EcCentricity, Radiality, Stress, and BottleNeck, the top 10 hub genes of DHJSD for treating osteoporosis were selected based on the

above results. The top 10 genes calculated based on 12 algorithms contain a total of 41 different genes. We showed the relationship between these genes and the corresponding algorithms in the form of Chord diagrams (Figure 4(b)). Then, we sorted the genes according to the number of algorithms corresponding to them and got the top 10 hub genes, and the results were consistent with the results of the Degree algorithm (Figure 4(c)). The top 10 hub genes contained AKT1, ALB, IL6, MAPK3, VEGFA, JUN, CASP3, EGFR, MYC, and EGF. In addition, the Sankey diagram was constructed using the top 10 hub genes and the relative active compounds of DHJSD, of which MOL000098 (Quercetin) targets most hub genes (Figure 5).

3.5. GO and KEGG Pathway Enrichment Analysis.
In order to elucidate the biological mechanisms of DHJSD against osteoporosis, GO and KEGG pathway enrichment analysis was performed by using clusterProfiler in R. The 205 potential targets of DHJSD for treating osteoporosis were input into the R, and a total of 2590 GO terms (adjusted, $P < 0.05$) were obtained, including 2320 biological process (BP) terms and 179 molecular function (MF) terms and 91 cellular component (CC) terms. Based on the adjusted P value from small to large, the top 10 GO-BP terms were mainly enriched in cellular response to chemical stress (GO:0062197), response to metal ion (GO:0010038), response to antibiotic (GO:0046677), response to lipopolysaccharide (GO: 0032496), response to alcohol (GO:0097305), response to steroid hormone (GO:0048545), response to molecule of bacterial origin (GO:0002237), response to oxidative stress (GO:0006979), response to reactive oxygen species (GO: 0000302), and response to nutrient levels (GO:0031667). The top 10 GO-CC terms were mainly enriched in membrane raft (GO:0045121), membrane microdomain (GO:0098857), membrane region (GO:0098589), transcription regulator complex (GO:0005667), vesicle lumen (GO:0031983), RNA polymerase II transcription regulator complex (GO: 0090575), cyclin-dependent protein kinase holoenzyme complex (GO:0000307), serine/threonine protein kinase complex (GO:1902554), mitochondrial outer membrane (GO:0005741), and cytoplasmic vesicle lumen (GO: 0060205). The top 10 GO-MF terms were mainly enriched in nuclear receptor activity (GO:0004879), ligand-activated transcription factor activity (GO:0098531), steroid hormone receptor activity (GO:0003707), RNA polymerase II-specific DNA-binding transcription factor binding (GO:0061629), DNA-binding transcription factor binding (GO:0140297), "DNA-binding transcription activator activity, RNA polymerase II-specific" (GO:0001228), DNA-binding transcription activator activity (GO:0001216), phosphatase binding (GO:0019902), heme binding (GO:0020037), and NADP binding (GO:0050661). Finally, the top 10 GO enrichment terms were selected and visualized using bar diagram, as shown in Figure 6. Table 3 shows the top 10 GO enrichment items.

Additionally, a total of 170 enriched KEGG pathways (adjusted, $P < 0.05$) were obtained, the top 10 including AGE-RAGE signaling pathway in diabetic complications

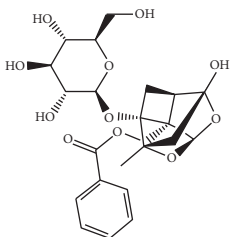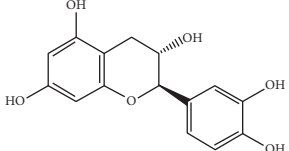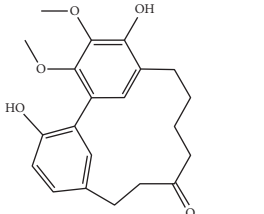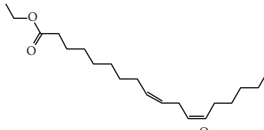TABLE 1: Basic information of some active compounds in DHJSD.
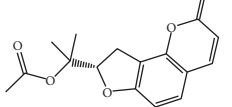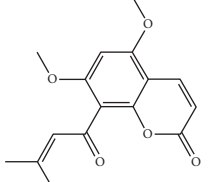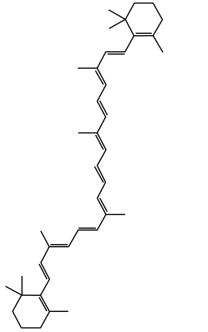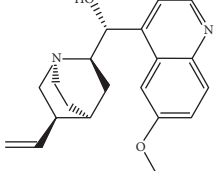
Molecule ID	Molecule name	OB (%)	DL	2D structure	Source	PubChem CID
MOL001924	Paeoniflorin	53.87	0.79		Bai Shao (*Radix Paeoniae Alba*)	442534
MOL000492	Cianidanol	54.83	0.24		Bai Shao	9064
MOL002135	Myricanone	40.60	0.51		Chuan Xiong (*Rhizoma Chuanxiong*)	161748
MOL001494	Ethyl linoleate	42.00	0.19		Chuan Xiong	5282184
MOL003608	O-acetylcolumbianetin	60.04	0.26		Du Huo (*Radix Angelicae Pubescentis*)	161409
MOL004780	Angelicone	30.99	0.19		Du Huo	616303
MOL002773	Beta-carotene	37.18	0.58		Du Zhong (*Cortex Eucommiae Ulmoidis*)	5280489
MOL009031	Epiquinidine	68.22	0.40		Du Zhong	94175

Table 1: Continued.
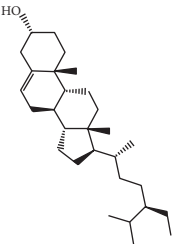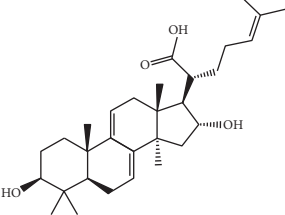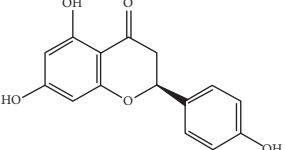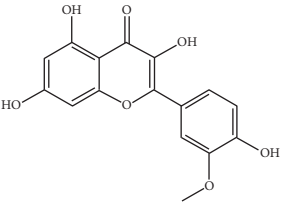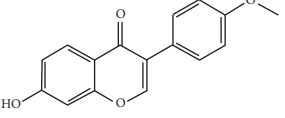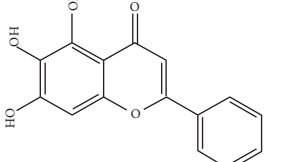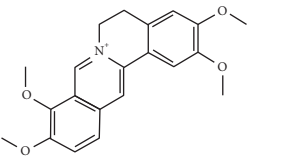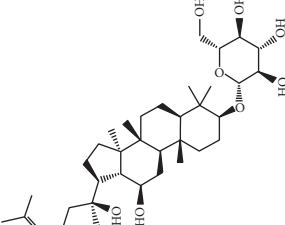
Molecule ID	Molecule name	OB (%)	DL	2D structure	Source	PubChem CID
MOL000296	Hederagenin	36.91	0.75		Fu Ling (*Poria Cocos*)	NA
MOL000273	16alpha-Hydroxydehydrotrametenolic acid	30.93	0.81		Fu Ling	10743008
MOL004328	Naringenin	59.29	0.21		Gan Cao (*Radix Glycyrrhizae*)	439246
MOL000354	Isorhamnetin	49.60	0.31		Gan Cao	5281654
MOL000392	Formononetin	69.67	0.21		Gan Cao	5280378
MOL002714	Baicalein	33.52	0.21		Niu Xi (*Radix Achyranthis Bidentatae*)	5281605
MOL000785	Palmatine	64.60	0.65		Niu Xi	19009
MOL005344	Ginsenoside rh2	36.32	0.56		Ren Shen (*Panax Ginseng*)	119307

TABLE 1: Continued.
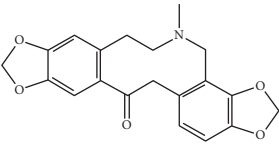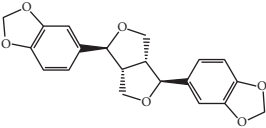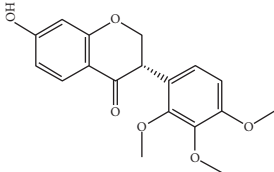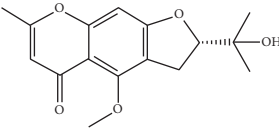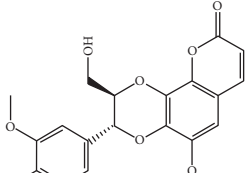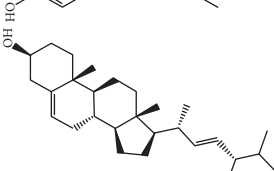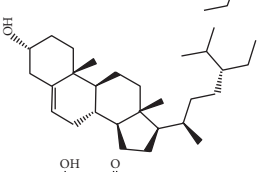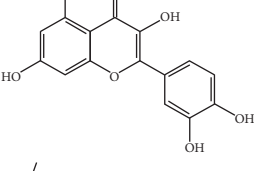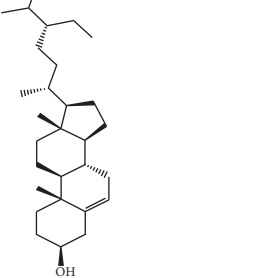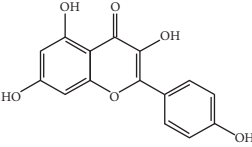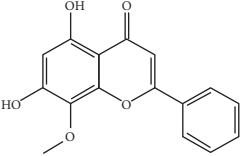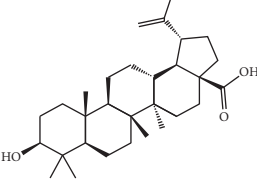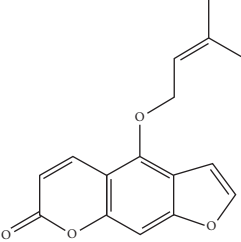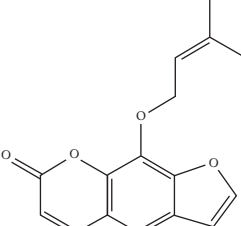
Molecule ID	Molecule name	OB (%)	DL	2D structure	Source	PubChem CID
MOL000787	Fumarine	59.26	0.83		Ren Shen	4970
MOL001558	Sesamin	56.55	0.83		Xi Xin (*Herba Asari*)	72307
MOL002962	3-O-Methylviolanone	48.23	0.33		Xi Xin	10019512
MOL011753	5-O-Methylvisamminol	37.99	0.25		Fang Feng (*Radix Saposhnikoviae*)	441970
MOL000011	Cleomiscosin A	68.83	0.66		Fang Feng	442510
MOL000449	Stigmasterol	43.83	0.76		Dang Gui (*Radix Angelicae Sinensis*), Niu Xi, Ren Shen, Shu Di Huang	5280794
MOL000359	3-Epi-beta-Sitosterol	36.91	0.75		Bai Shao, Chuan Xiong, Fang Feng, Gan Cao, Qin Jiao, Sang Ji Sheng, Shu Di Huang (*Radix Rehmanniae Preparata*)	12303645
MOL000098	Quercetin	46.43	0.28		Du Zhong, Gan Cao, Sang Ji Sheng (*Herba Taxilli*), Niu Xi	5280343
MOL000358	Beta-sitosterol	36.91	0.75		Bai Shao, Dang Gui, Du Huo, Du Zhong, Fang Feng, Niu Xi, Qin Jiao, Ren Shen	222284

TABLE 1: Continued.

Molecule ID	Molecule name	OB (%)	DL	2D structure	Source	PubChem CID
MOL000422	Kaempferol	41.88	0.24		Bai Shao, Du Zhong, Gan Cao, Niu Xi, Ren Shen, Xi Xin	5280863
MOL000173	Wogonin	30.68	0.23		Fang Feng, Niu Xi	5281703
MOL000211	Mairin	55.38	0.78		Bai Shao, Du Zhong, Gan Cao	64971
MOL001942	Isoimperatorin	45.46	0.23		Du Huo, Fang Feng	68081
MOL001941	Ammidin	34.55	0.22		Du Huo, Fang Feng	10212

Abbreviations: DHJSD, Duhuo Jisheng Decoction; OB, oral bioavailability; DL, drug-likeness.
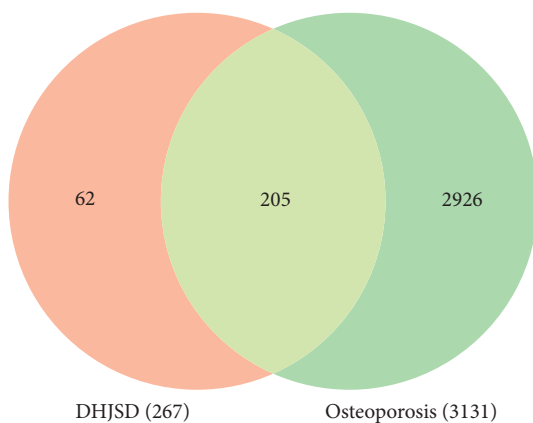
FIGURE 2: Venn diagram of DHJSD-related targets and osteoporosis-related targets.

(hsa04933), Kaposi sarcoma-associated herpesvirus infection (hsa05167), fluid shear stress and atherosclerosis (hsa05418), hepatitis B (hsa05161), prostate cancer (hsa05215), hepatitis C (hsa05160), pancreatic cancer (hsa05212), human cytomegalovirus infection (hsa05163), IL-17 signaling pathway (hsa04657), and TNF signaling pathway (hsa04668). The top 20 KEGG pathway enrichment terms were selected and visualized using bar diagram, as shown in Figure 7. Next, we searched the KEGG pathway database for osteoporosis, looking for potential pathways related to osteoporosis in the enriched 170 pathways. A total of 50 pathways were selected that may be associated with osteoporosis, and then we proceeded to build a network map of target genes and pathways using Cytoscape software (Figure 8). These include 13 of the pathways most strongly associated with osteoporosis, including osteoclast differentiation (hsa04380), AGE-RAGE signaling pathway in diabetic complications (hsa04933), Wnt signaling pathway (hsa04310), MAPK signaling pathway (hsa04010), apoptosis (hsa04210), chemokine signaling pathway (hsa04062), T cell receptor signaling pathway (hsa04660), B cell receptor signaling pathway (hsa04662), PI3K-Akt signaling pathway (hsa04151), JAK-STAT signaling pathway (hsa04630),
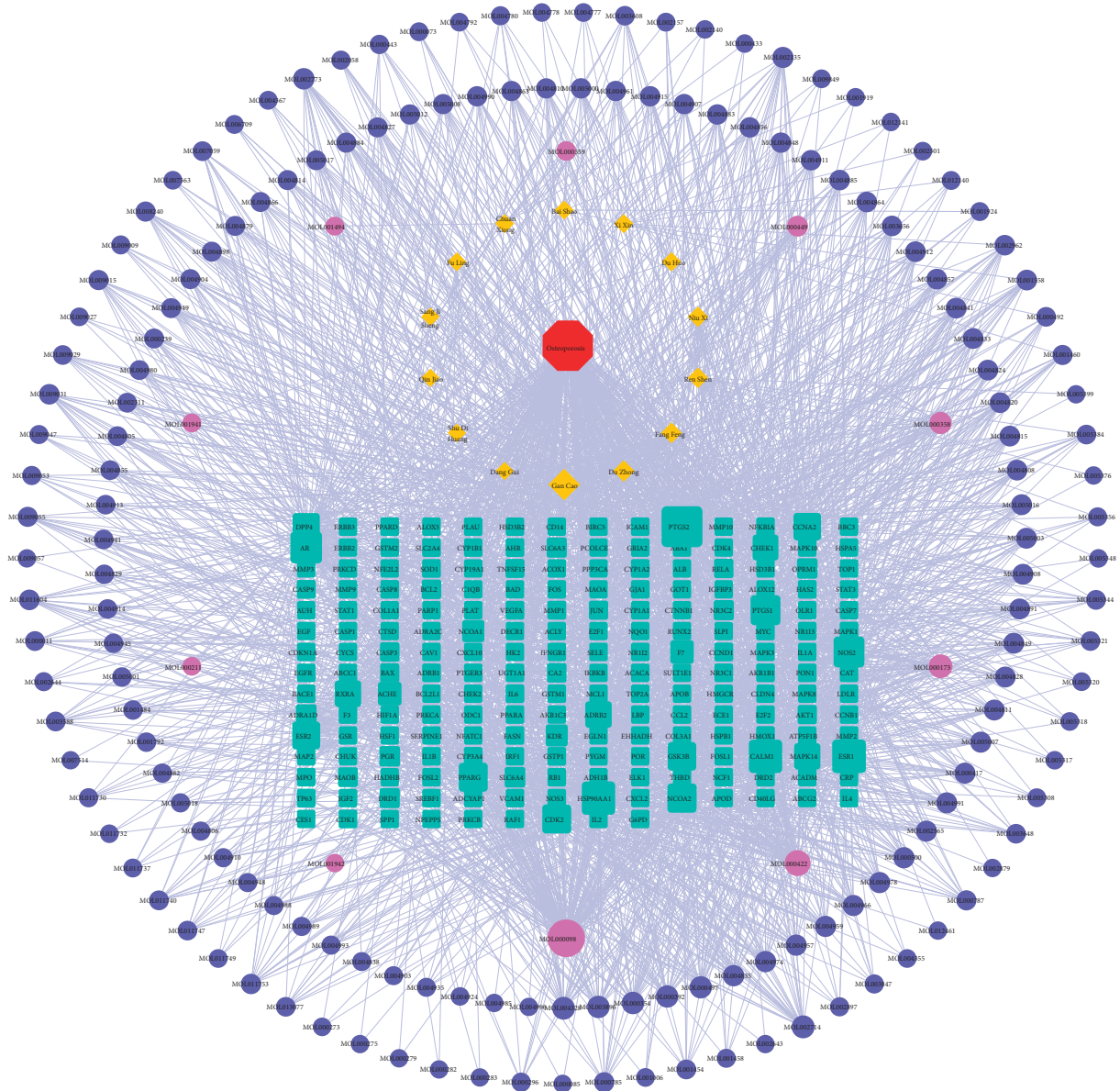
FIGURE 3: "DHJSD-active compounds-target genes-osteoporosis" network. The red octagon represents the disease; the brown diamond represents the herbs contained in DHJSD; the cyan rectangle represents the potential targets; the blue ellipse belongs to the herbs contained in DHJSD; and the purple ones are common ingredients. The line between two nodes represents the interaction; the size of each node represents the number of connections.

calcium signaling pathway (hsa04020), NF-kappa B signaling pathway (hsa04064), and TNF signaling pathway (hsa04668). Table 4 shows the enriched 50 possible related pathways of osteoporosis.

3.6. Molecular Docking Results.

According to the results of the Sankey diagram, we carried out molecular docking of the core target protein and active compound involved. Molecular docking between top 10 target proteins (AKT1, ALB, IL6, MAPK3, VEGFA, JUN, CASP3, EGFR, MYC, EGF) and key active compounds (Quercetin, Kaempferol, Beta-sitosterol, Wogonin, Beta-carotene, Baicalein, Naringenin, Formononetin, Paeoniflorin, Ginsenoside Rh2,

and Epiquinidine) was carried out using AutoDock Vina. The docking scores of the strongest affinity of 10 core target proteins and 11 key active compounds were visualized using the heatmap, as shown in Figure 9. The binding energy between target proteins and the active compounds was approximately between -5.8 and $-10.9\,\text{kcal mol}^{-1}$. AKT1, ALB, MAPK3, JUN, CASP3, and EGFR have stronger docking energy. The remaining target proteins also have relatively strong docking energy, which means that the compounds in DHJSD bind well to 10 core target proteins. Eventually, we chose the top 4 target protein macromolecules and small compound molecules with the best docking affinity for visualization with Pymol (Figure 10).

Table 2: Basic information of some key targets of DHJSD against osteoporosis.

UniProt ID	Gene symbol	Protein names	Degree
P35354	PTGS2	Prostaglandin G/H synthase 2	144
P03372	ESR1	Estrogen receptor	98
P0DP23	CALM1	Calmodulin-1	96
P07900	HSP90AA1	Heat shock protein HSP 90-alpha	96
P10275	AR	Androgen receptor	85
P35228	NOS2	Nitric oxide synthase, inducible	80
P23219	PTGS1	Prostaglandin G/H synthase 1	74
Q15596	NCOA2	Nuclear receptor coactivator 2	70
P24941	CDK2	Cyclin-dependent kinase 2	68
P37231	PPARG	Peroxisome proliferator-activated receptor gamma	68
P49841	GSK3B	Glycogen synthase kinase-3 beta	65
Q92731	ESR2	Estrogen receptor beta	62
P20248	CCNA2	Cyclin-A2	59
P27487	DPP4	Dipeptidyl peptidase 4	57
P07550	ADRB2	Beta-2 adrenergic receptor	52
P19793	RXRA	Retinoic acid receptor RXR-alpha	52
Q16539	MAPK14	Mitogen-activated protein kinase 14	51
O14757	CHEK1	Serine/threonine-protein kinase Chk1	48
P22303	ACHE	Acetylcholinesterase	34
P08709	F7	Coagulation factor VII	33
Q15788	NCOA1	Nuclear receptor coactivator 1	25
P35968	KDR	Vascular endothelial growth factor receptor 2	24
P25100	ADRA1D	Alpha-1D adrenergic receptor	15
P06401	PGR	Progesterone receptor	15
P31645	SLC6A4	Sodium-dependent serotonin transporter	15
P35372	OPRM1	Mu-type opioid receptor	14
P21728	DRD1	D (1A) dopamine receptor	12
P08235	NR3C2	Mineralocorticoid receptor	12
Q01959	SLC6A3	Sodium-dependent dopamine transporter	12
P27338	MAOB	Amine oxidase [flavin-containing] B	10
Q92934	BCL2	Bcl2-associated agonist of cell death	8
P00918	CA2	Carbonic anhydrase 2	8
P42574	CASP3	Caspase-3	8
Q04206	RELA	Transcription factor p65	7
P31749	AKT1	RAC-alpha serine/threonine-protein kinase	6
Q07812	BAX	Apoptosis regulator BAX	6
P05412	JUN	Transcription factor AP-1	6
O95150	TNFSF15	Tumor necrosis factor ligand superfamily member 15	5
P55211	CASP9	Caspase-9	4
P24385	CCND1	G1/S-specific cyclin-D1	4
P03956	MMP1	Interstitial collagenase	4
P08588	ADRB1	Beta-1 adrenergic receptor	3
P35869	AHR	Aryl hydrocarbon receptor	3
P15121	AKR1B1	Aldo-keto reductase family 1 member B1	3
Q14790	CASP8	Caspase-8	3
P06493	CDK1	Cyclin-dependent kinase 1	3
P05177	CYP1A2	Cytochrome P450 1A2	3
P08684	CYP3A4	Cytochrome P450 3A4	3
P09211	GSTP1	Glutathione S-transferase P	3
Q92819	HAS2	Hyaluronan synthase 2	3
P09601	HMOX1	Heme oxygenase 1	3
P05231	IL6	Interleukin-6	3
P28482	MAPK1	Mitogen-activated protein kinase 1	3
P04150	NR3C1	Glucocorticoid receptor	3
Q03181	PPARD	Peroxisome proliferator-activated receptor delta	3
P14672	SLC2A4	Solute carrier family 2, facilitated glucose transporter member 4	3
P00441	SOD1	Superoxide dismutase [Cu-Zn]	3
Q9H3D4	TP63	Tumor protein 63	3
P15692	VEGFA	Vascular endothelial growth factor A	3
Q13085	ACACA	Acetyl-CoA carboxylase 1	2

TABLE 2: Continued.

UniProt ID	Gene symbol	Protein names	Degree
P00533	EGFR	Epidermal growth factor receptor	2
P01106	MYC	Myc proto-oncogene protein	2
P02768	ALB	Albumin	1
P01133	EGF	Pro-epidermal growth factor	1
P27361	MAPK3	Mitogen-activated protein kinase 3	1
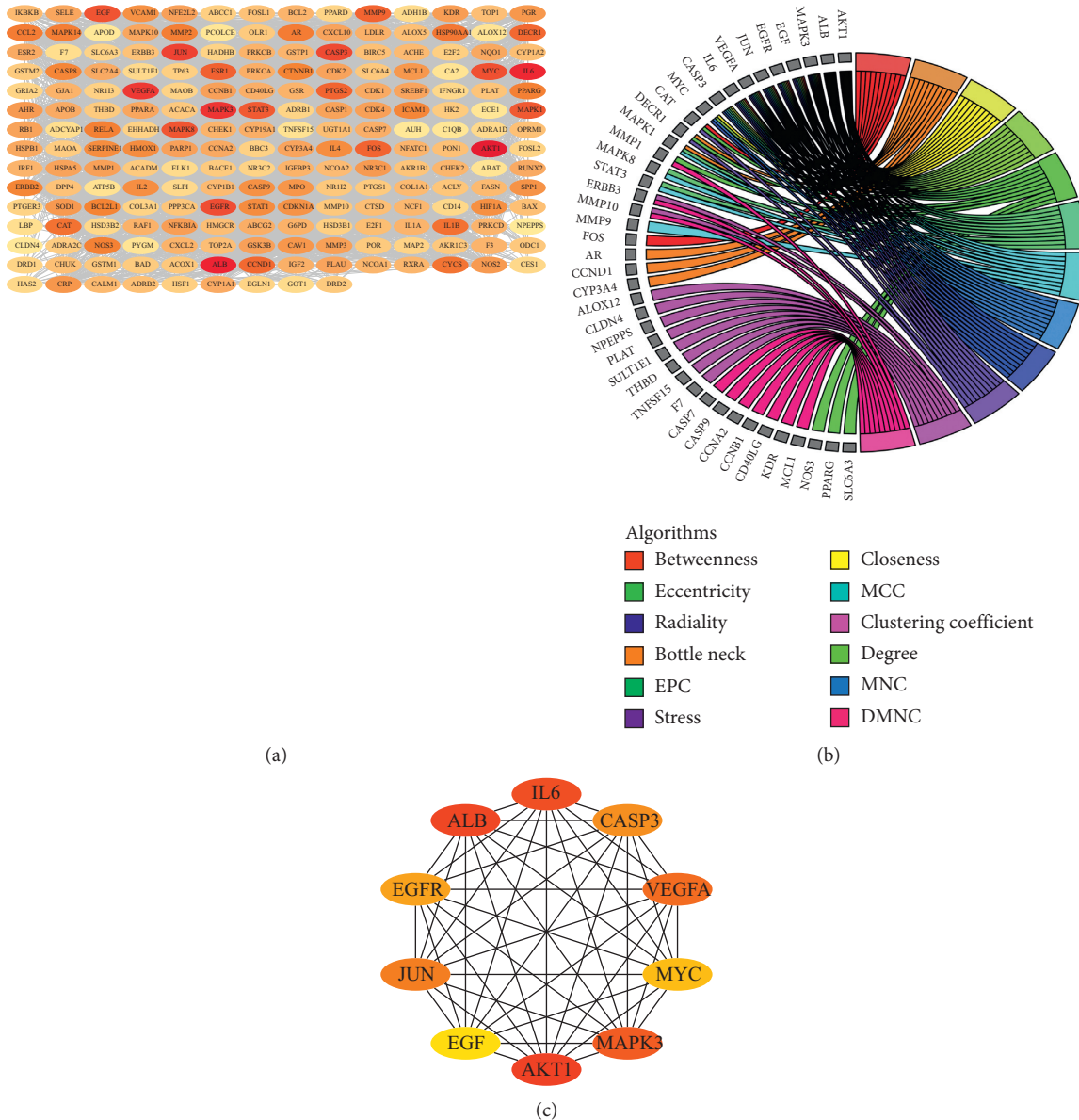
FIGURE 4: The PPI network of potential targets of DHJSD in the treatment of osteoporosis. (a) The PPI network from STRING was further analyzed using Cytoscape software (the line between two nodes indicates the interaction. The darker the color of the node, the better the relationship between them). (b) Chord diagram of the corresponding relationship between the top 10 genes and 12 CytoHubba algorithms. (c) The top 10 hub genes were identified by Degree (the darker the color of the node, the greater the degree).

4. Discussion

Osteoporosis is a degenerative disease, which increases with age. With the prolongation of human life and the coming of aging society, osteoporosis has become an important health problem [1]. Considering the threat of the aging of the global population and the increasing side effects of clinical drugs, finding potential drugs for the prevention and treatment of osteoporosis from natural products is a novel treatment strategy [2]. DHJSD is an extremely common TCM that has
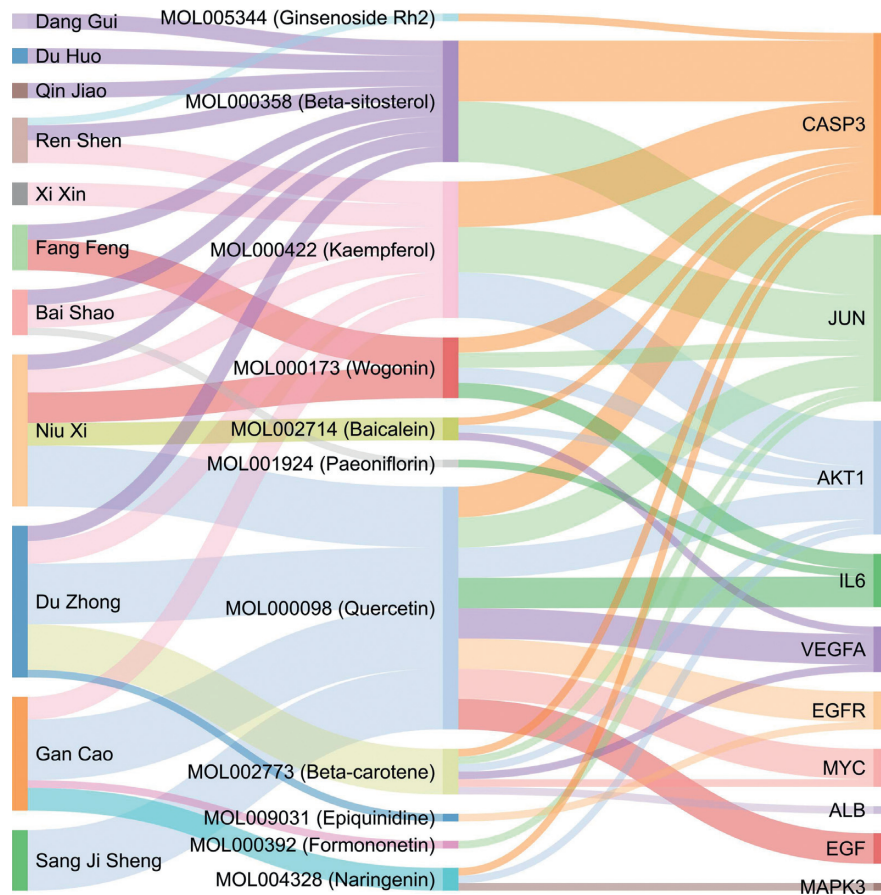
FIGURE 5: Sankey diagram. The colored vertical bars on the left represent the different herbs contained in DHJSD, the middle bars represent the active ingredients of the herbs, and the right bars represent the target genes. The size of the bars and the thickness of the lines represent the number of interactions.

been used in China to treat patients with osteoporosis, especially postmenopausal osteoporosis [2]. However, the mechanism of action of TCM is usually elusive due to the ingredients it contains. It is of great significance to explore the molecular mechanism of TCM by using systematic and normative bioinformatics methods to mine multiple databases to integrate and analyze the information of target proteins and compounds [4]. A systematic network pharmacological method for determining molecular biological networks has been developed, which may be used to discover new therapeutic effects of drugs derived from medicinal plants. In this study, based on systematic network pharmacology, including ADME system assessment, PPI network analysis, GO and KEGG pathway analysis, and molecular docking verification, the active ingredients and potential targets of DHJSD in the treatment of osteoporosis were evaluated.

According to the principle of ADME (setting OB ≥30 and DL ≥0.18) [20], we searched the TCMSP database and screened a total of 209 active compounds (after deduplication) from the 15 herbs contained in DHJSD (Rou Gui did not find a compound that meets the requirements). By using the compound-target search function of the TCMSP database, 267 target proteins were finally found from 209 active compounds (30 of which did not find the corresponding target protein). Then, we transformed the full name of the

target protein into the gene ID through UniProt database. Through searching 6 disease-target databases (GeneCards, MalaCards, DisGeNET, TTD, CTD, and OMIM), a total of 3131 potential osteoporosis treatment targets were obtained. Finally, we obtained 205 potential target genes of DHJSD in the treatment of osteoporosis. The network of DHJSD against osteoporosis was built, which was involved in 394 nodes and 2265 interactions. Furthermore, PPI network has been constructed involved in 205 nodes and 4078 edges. Top 10 hub genes were revealed by weighing the CytoHubba 12 algorithms of Cytoscape software (Degree, MCC, DMNC, MNC, EPC, Closeness, Betweenness, ClusteringCoefficient, EcCentricity, Radiality, Stress, and BottleNeck), including AKT1, ALB, IL6, MAPK3, VEGFA, JUN, CASP3, EGFR, MYC, and EGF.

AKT1 is one of three closely related serine/threonine protein kinases (AKT1, AKT2, and AKT3), which regulates many physiological processes including metabolism, proliferation, cell survival, and angiogenesis [39]. A study published in 2012 showed that AKT1 may be a regulator of the differentiation and function of osteoblasts and osteoclasts [40]. IL6 is an important inflammatory factor, and its function involves a variety of inflammation-related disease states, including diabetes mellitus susceptibility and systemic juvenile rheumatoid arthritis [41]. A study published in 2018
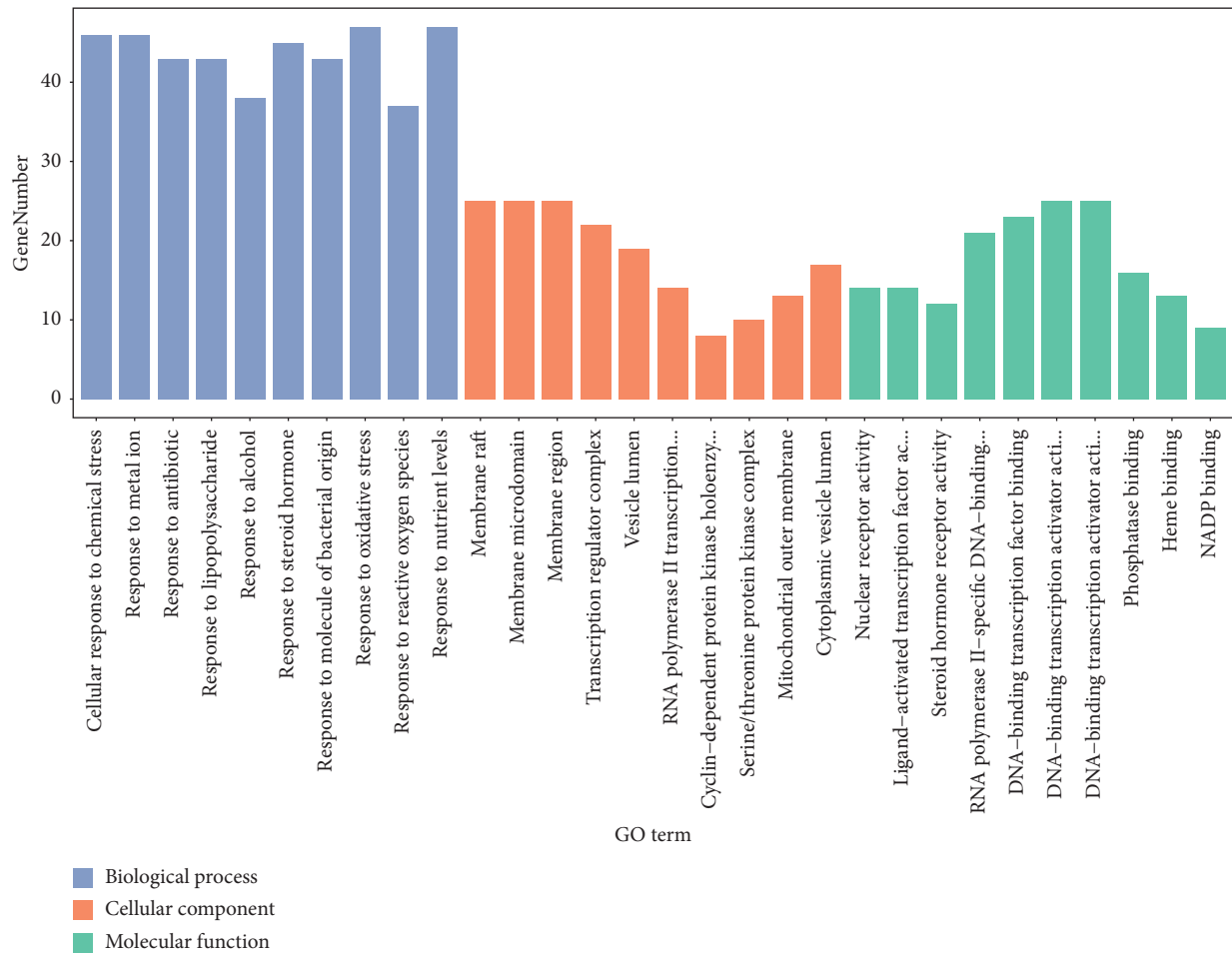
FIGURE 6: Barplot of the top 10 GO enrichment items. The GO enrichment items (BP, CC, MF) are arranged from left to right according to the adjusted *P* value.

showed that the upregulation of IL6 expression is an important factor in promoting the osteogenic differentiation of adipose-derived stem cells [42]. ALB is the most important protein in human plasma, which maintains the body's nutrition and osmotic pressure, and acts as a carrier protein for a variety of endogenous molecules (including hormones, fatty acids, and metabolites) and exogenous drugs [43]. A retrospective study suggested that preoperative ALB levels may help predict complications after osteoporotic vertebral compression fractures [43]. MAPK3 is a member of the MAP kinase family and plays a role in the signal cascade that responds to various extracellular signals to regulate various cellular processes, such as proliferation, differentiation, and cell cycle progression [44]. Studies have shown that MAPK3 promotes the expression of RUNX2, and targeting MAPK3 can affect osteoblast differentiation [44]. VEGFA is a member of the PDGF/VEGF growth factor family, which is active in angiogenesis, angiogenesis, and endothelial cell growth, and induces endothelial cell proliferation, promotes cell migration, and inhibits cell apoptosis [45]. By inhibiting the expression of VEGFA, miR-16-5p could exert an anti-osteogenesis effect [45]. The human JUN gene encodes a protein that is highly similar to the viral protein, which

directly interacts with specific target DNA sequences to regulate gene expression [46]. By activating the c-Fos/c-Jun pathway, IL-7/IL-7R could promote RANKL-mediated osteoclast formation and bone resorption and induce bone loss in ovariectomized mice [46]. The protein encoded by the CASP3 gene is a cysteine-aspartic acid protease, which plays a vital role in the execution-phase of cell apoptosis [47]. By targeting CASP3 and activating the PI3K-Akt signaling pathway, the overexpression of miR-378 could attenuate the osteogenic differentiation inhibited by high glucose [47]. The protein encoded by the EGF gene is a member of the epidermal growth factor superfamily, which acts as an effective mitogenic factor and plays an important role in the growth, proliferation, and differentiation of various cell types [48]. EGFR gene encodes a protein that is a receptor for members of the epidermal growth factor family [48]. Studies have shown that inhibition of the EGFR signaling pathway inhibits the expression of the enhancer of zeste homolog 2 (Ezh2) through the ERK1/2 pathway, thereby promoting the senescence of osteoprogenitor cells [48]. MYC is a proto-oncogene and encodes a nuclear phosphoprotein, which plays a role in cell cycle progression, apoptosis, and cell transformation [49]. In a mouse model of osteoporosis, both

TABLE 3: The top 10 Gene Ontology (GO) enrichment items.

ID	Description	P value	Adjust P value	Gene number	GO items
GO:0062197	Cellular response to chemical stress	$2.20332E-36$	$9.75E-33$	46	Biological process
GO:0010038	Response to metal ion	$1.04408E-35$	$2.31E-32$	46	Biological process
GO:0046677	Response to antibiotic	$5.44269E-34$	$8.03E-31$	43	Biological process
GO:0032496	Response to lipopolysaccharide	$8.0729E-34$	$8.93E-31$	43	Biological process
GO:0097305	Response to alcohol	$1.19658E-33$	$1.06E-30$	38	Biological process
GO:0048545	Response to steroid hormone	$2.14139E-33$	$1.58E-30$	45	Biological process
GO:0002237	Response to molecule of bacterial origin	$4.25534E-33$	$2.69E-30$	43	Biological process
GO:0006979	Response to oxidative stress	$1.67651E-32$	$9.27E-30$	47	Biological process
GO:0000302	Response to reactive oxygen species	$2.14509E-32$	$1.05E-29$	37	Biological process
GO:0031667	Response to nutrient levels	$1.65363E-30$	$7.32E-28$	47	Biological process
GO:0004879	Nuclear receptor activity	$1.2238E-16$	$3.33E-14$	14	Molecular function
GO:0098531	Ligand-activated transcription factor activity	$1.2238E-16$	$3.33E-14$	14	Molecular function
GO:0003707	Steroid hormone receptor activity	$1.51056E-12$	$2.74E-10$	12	Molecular function
GO:0061629	RNA polymerase II-specific DNA-binding transcription factor binding	$1.0407E-11$	$1.42E-09$	21	Molecular function
GO:0140297	DNA-binding transcription factor binding	$2.02886E-11$	$2.21E-09$	23	Molecular function
GO:0001228	DNA-binding transcription activator activity, RNA polymerase II-specific	$5.32777E-11$	$4.35E-09$	25	Molecular function
GO:0001216	DNA-binding transcription activator activity	$5.59254E-11$	$4.35E-09$	25	Molecular function
GO:0019902	Phosphatase binding	$4.84351E-10$	$3.29E-08$	16	Molecular function
GO:0020037	Heme binding	$5.8588E-09$	$3.54E-07$	13	Molecular function
GO:0050661	NADP binding	$7.53723E-09$	$4.10E-07$	9	Molecular function
GO:0045121	Membrane raft	$3.10297E-15$	$5.63E-13$	25	Cellular component
GO:0098857	Membrane microdomain	$3.33964E-15$	$5.63E-13$	25	Cellular component
GO:0098589	Membrane region	$7.90284E-15$	$8.88E-13$	25	Cellular component
GO:0005667	Transcription regulator complex	$4.33831E-10$	$3.66E-08$	22	Cellular component
GO:0031983	Vesicle lumen	$1.59056E-09$	$1.07E-07$	19	Cellular component
GO:0090575	RNA polymerase II transcription regulator complex	$2.17645E-09$	$1.22E-07$	14	Cellular component
GO:0000307	Cyclin-dependent protein kinase holoenzyme complex	$1.03807E-08$	$5.00E-07$	8	Cellular component
GO:1902554	Serine/threonine protein kinase complex	$2.64297E-08$	$1.11E-06$	10	Cellular component
GO:0005741	Mitochondrial outer membrane	$4.65534E-08$	$1.74E-06$	13	Cellular component
GO:0060205	Cytoplasmic vesicle lumen	$5.57446E-08$	$1.88E-06$	17	Cellular component

the loss of MYC and the pharmacological inhibitory effect of ERRα reduced bone loss [49]. The main physiological processes regulated by proteins encoded by the top 10 target genes include inflammatory response, immune response, cell proliferation, differentiation, apoptosis, migration, cell cycle progression, endocrine metabolism, angiogenesis, growth, and nutrition. Based on the above analysis results, it

is also speculated that DHJSD against osteoporosis may play a role through the above process.

The one-to-one correspondence between the top 10 hub genes and the corresponding active compounds contained in DHJSD had been shown using the Sankey diagram. The relative active compounds include MOL000098 (Quercetin), MOL000422 (Kaempferol), MOL000358 (Beta-sitosterol),
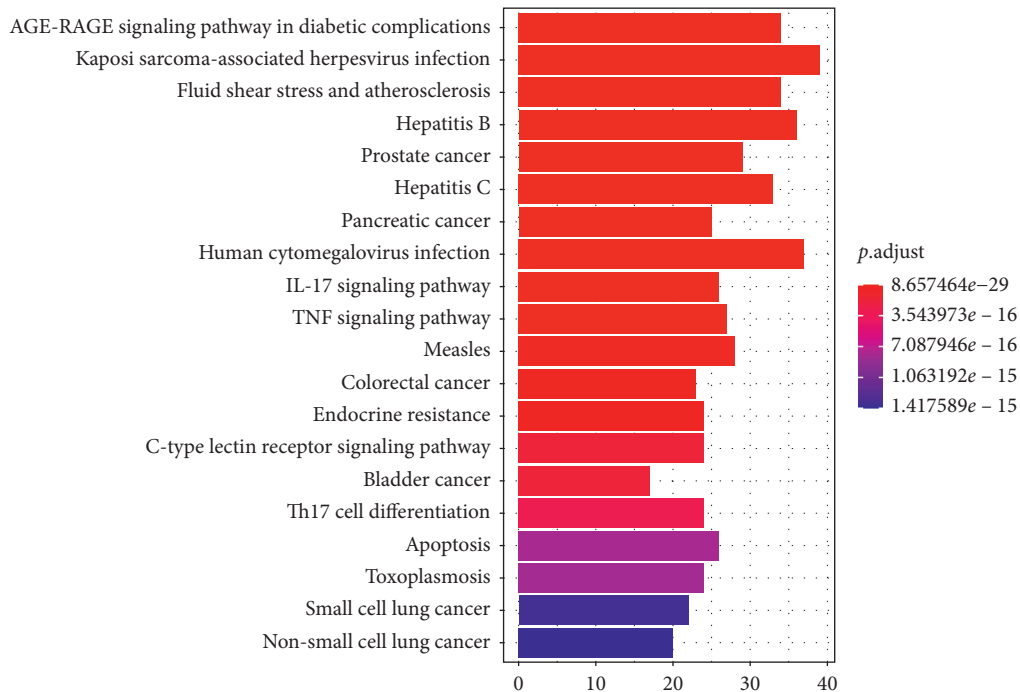
FIGURE 7: Barplot of the top 20 KEGG pathway enrichment items. The color of each bar represents the adjusted *P* value, and the length represents the number of enriched genes.

MOL000173 (Wogonin), MOL002773 (Beta-carotene), MOL002714 (Baicalein), MOL004328 (Naringenin), MOL000392 (Formononetin), MOL001924 (Paeoniflorin), MOL005344 (Ginsenoside Rh2), and MOL009031 (Epiquinidine). Among them, Quercetin targets most central genes. Quercetin is a member of the flavonoid family isolated from onion, apple, grape, tea, and many kinds of Chinese herbal medicines, which seems to have obvious anti-osteoporosis properties [50]. Studies have shown that Quercetin alone or in combination with alendronate could prevent glucocorticoid-induced osteoporosis through its bone formation stimulation [50]. Quercetin promotes bone marrow mesenchymal stem cells (BMSCs) proliferation and osteogenic differentiation, improves the in vitro model of osteoporosis, and provides protection against TNF-α-induced impairment of BMSC osteogenic function [51].

Then, we performed the GO and KEGG pathway enrichment analysis of genes that DHJSD against osteoporosis. Based on the adjusted *P* value from small to large, the top 3 GO-BP terms were mainly enriched in cellular response to chemical stress, response to metal ion, and response to antibiotic. The top 3 GO-CC terms were mainly enriched in membrane raft, membrane microdomain, and membrane region. The top 3 GO-MF terms were mainly enriched in nuclear receptor activity, ligand-activated transcription factor activity, and steroid hormone receptor activity. Based on the adjusted *P* value from small to large, the top 10 KEGG pathways were mainly enriched in AGE-RAGE signaling pathway in diabetic complications, Kaposi sarcoma-associated herpesvirus infection, fluid shear stress, and atherosclerosis, hepatitis B, prostate cancer, hepatitis C, pancreatic cancer, human cytomegalovirus infection, and IL-17

signaling pathway. We searched for osteoporosis in the KEGG pathway database and found that there are ten pathways directly related to osteoporosis and related diseases, including osteoclast differentiation (hsa04380), AGE-RAGE signaling pathway in diabetic complications (hsa04933), Wnt signaling pathway (hsa04310), MAPK signaling pathway (hsa04010), apoptosis (hsa04210), chemokine signaling pathway (hsa04062), T cell receptor signaling pathway (hsa04660), B cell receptor signaling pathway (hsa04662), endocrine and other factor-regulated calcium reabsorption (hsa04961), and mineral absorption (hsa04978). The first eight pathways are in the list of KEGG pathway enrichment analysis we have done. Six of the top 10 hub genes (AKT1, MAPK3, JUN, CASP3, IL6, and VEGFA) are enriched in AGE-AGE signaling pathway in diabetic complications, three of the top 10 hub genes (AKT1, MAPK3, and JUN) are enriched in osteoclast differentiation, eight of the top 10 hub genes (AKT1, MAPK3, VEGFA, JUN, CASP3, EGFR, MYC, and EGF) are enriched in MAPK signaling pathway, two of the top 10 hub genes (JUN, MYC) are enriched in Wnt signaling pathway, four of the top 10 hub genes (AKT1, MAPK3, JUN, and CASP3) are enriched in Apoptosis, two of the top 10 hub genes (AKT1, MAPK3) are enriched in Chemokine signaling pathway, and three of the top 10 hub genes (AKT1, MAPK3, and JUN) are enriched in T cell receptor signaling pathway and B cell receptor signaling pathway.

In addition, the enriched pathways related to the above pathways in the KEGG database include PI3K-Akt signaling pathway (hsa04151; enriched genes: AKT1, IL6, MAPK3, VEGFA, EGFR, MYC, EGF), JAK-STAT signaling pathway (hsa04630; enriched genes: AKT1, IL6, EGFR, MYC, EGF),
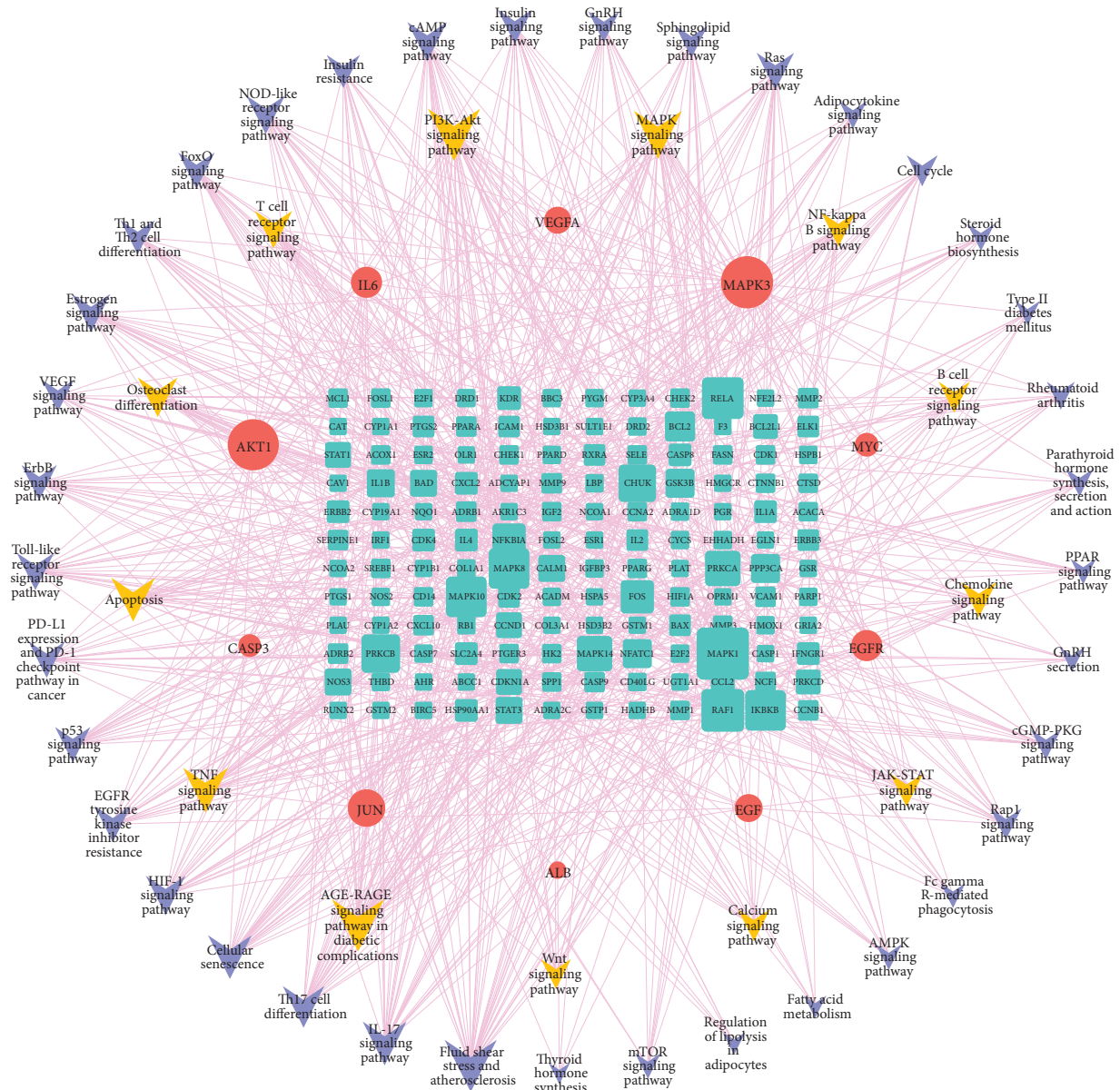
FIGURE 8: "Target genes-pathways" network. The cyan ellipse represents the potential targets of DHJSD against osteoporosis; the red ellipse represents the top 10 hub genes of DHJSD against osteoporosis; the brown arrow represents potential osteoporosis-related pathways; the light blue arrow represents osteoporosis-related pathways. The line between two nodes represents the interaction; the size of each node represents the number of connections. The lines consistent with the color of each hub gene represent the pathways enriched by that gene.

calcium signaling pathway (hsa04020; enriched genes: EGFR, EGF), TNF signaling pathway (hsa04668; enriched genes: AKT1, IL6, MAPK3, JUN, and CASP3), and NF-kappa B signaling pathway (hsa04064). Li et al. [52] found that, through the PI3K-Akt signaling pathway, the knockdown of LNC_000052 could promote BMSCs osteogenesis, proliferation, and migration and inhibit cell apoptosis. Studies have shown that miR-10b could promote osteogenic differentiation and increase bone formation through the TGF-β signaling pathway [53]. In addition, JAK-STAT signaling pathway plays a role in the differentiation of osteoblasts and osteoclasts [54]. Jin et al. [55] found that sclareol prevents bone loss caused by ovariectomy in vivo by

inhibiting NF-κB and MAPK/ERK signaling pathways and inhibits osteoclast production in vitro. Zha et al. [56] found that miR-920 targets HOXA7 through the MAPK signaling pathway to promote the osteogenic differentiation of human bone mesenchymal stem cells. It is well known that there are many pathways that have a large or small relationship with osteoporosis, and these pathways are classified mainly as bone metabolism, inflammatory response, immune response, endocrine system, and cell apoptosis [57].

By mining the database, we obtained the compounds contained in each herb in DHJSD, and then we predicted the potential targets of DHJSD by these compounds, and then we performed KEGG pathway enrichment analysis to obtain

TABLE 4: The enriched 50 possible related pathways of osteoporosis.

ID	Description	P value	Adjust P value	Gene number
hsa04933	AGE-RAGE signaling pathway in diabetic complications	$3.2722E-31$	$8.83495E-29$	34
hsa05418	Fluid shear stress and atherosclerosis	$8.02758E-26$	$6.42442E-24$	34
hsa04657	IL-17 signaling pathway	$2.23263E-21$	$6.69789E-20$	26
hsa04668	TNF signaling pathway	$1.93321E-20$	$5.21968E-19$	27
hsa04659	Th17 cell differentiation	$1.77974E-17$	$3.00331E-16$	24
hsa04210	Apoptosis	$5.07009E-17$	$8.0525E-16$	26
hsa04218	Cellular senescence	$1.70327E-15$	$1.9995E-14$	26
hsa04066	HIF-1 signaling pathway	$4.55414E-15$	$4.72929E-14$	22
hsa01521	EGFR tyrosine kinase inhibitor resistance	$1.19998E-14$	$1.11722E-13$	19
hsa04115	p53 signaling pathway	$3.86218E-14$	$3.36383E-13$	18
hsa05235	PD-L1 expression and PD-1 checkpoint pathway in cancer	$1.25365E-13$	$9.95542E-13$	19
hsa04380	Osteoclast differentiation	$1.52063E-13$	$1.14047E-12$	22
hsa04620	Toll-like receptor signaling pathway	$2.26415E-13$	$1.5283E-12$	20
hsa04660	T Cell receptor signaling pathway	$2.26415E-13$	$1.5283E-12$	20
hsa04012	ErbB signaling pathway	$6.6254E-13$	$4.25919E-12$	18
hsa04151	PI3K-akt signaling pathway	$1.24292E-12$	$7.80436E-12$	34
hsa04370	VEGF signaling pathway	$3.47037E-12$	$1.99361E-11$	15
hsa04915	Estrogen signaling pathway	$6.54943E-12$	$3.60403E-11$	21
hsa04010	MAPK signaling pathway	$6.67413E-12$	$3.60403E-11$	30
hsa04658	Th1 and Th2 cell differentiation	$3.05E-11$	$1.55E-10$	17
hsa04068	FoxO signaling pathway	$1.6511E-10$	$7.96064E-10$	19
hsa04064	NF-kappa B signaling pathway	$2.32207E-10$	$1.09993E-09$	17
hsa04621	NOD-like receptor signaling pathway	$1.2042E-09$	$5.16086E-09$	21
hsa04931	Insulin resistance	$3.58386E-09$	$1.423E-08$	16
hsa04662	B Cell receptor signaling pathway	$5.33879E-09$	$2.08909E-08$	14
hsa04024	cAMP signaling pathway	$5.66891E-09$	$2.1641E-08$	22
hsa04910	Insulin signaling pathway	$1.80579E-08$	$6.58868E-08$	17
hsa04912	GnRH signaling pathway	$2.87106E-08$	$1.03358E-07$	14
hsa04071	Sphingolipid signaling pathway	$1.04592E-07$	$3.62048E-07$	15
hsa04014	Ras signaling pathway	$4.64353E-07$	$1.475E-06$	20
hsa04920	Adipocytokine signaling pathway	$5.07934E-07$	$1.57635E-06$	11
hsa04062	Chemokine signaling pathway	$5.25301E-07$	$1.61172E-06$	18
hsa04110	Cell cycle	$1.11163E-06$	$3.15936E-06$	14
hsa04630	JAK-STAT signaling pathway	$1.15731E-06$	$3.25493E-06$	16
hsa00140	Steroid hormone biosynthesis	$1.30408E-06$	$3.59286E-06$	10
hsa04930	Type II diabetes mellitus	$9.82492E-06$	$2.50258E-05$	8
hsa05323	Rheumatoid arthritis	$1.03843E-05$	$2.62033E-05$	11
hsa04928	Parathyroid hormone synthesis, secretion and action	$3.6295E-05$	$8.67227E-05$	11
hsa03320	PPAR signaling pathway	$6.67976E-05$	0.000155477	9
hsa04020	Calcium signaling pathway	$7.36869E-05$	0.000168606	15
hsa04310	Wnt signaling pathway	$9.54755E-05$	0.000213045	13
hsa04929	GnRH secretion	0.000116074	0.000254797	8
hsa04022	cGMP-PKG signaling pathway	0.000147423	0.000321001	13
hsa04015	Rap1 signaling pathway	0.00041579	0.000863564	14
hsa04666	Fc gamma R-mediated phagocytosis	0.00195976	0.003834313	8
hsa04152	AMPK signaling pathway	0.002019554	0.003922874	9
hsa01212	Fatty acid metabolism	0.002098286	0.003989699	6
hsa04923	Regulation of lipolysis in adipocytes	0.002098286	0.003989699	6
hsa04150	mTOR signaling pathway	0.010773083	0.018409699	9
hsa04918	Thyroid hormone synthesis	0.031361971	0.049810189	5

the potential pathways of action of DHJSD based on these targets. Therefore, the above obtained targets and signaling pathways should be relevant to the functions of the herbs in DHJSD. It has been shown that the therapeutic effect of the herb Du Huo in osteoporotic rats is associated with the activation of Wnt/β-catenin signaling pathway to promote bone formation [58]. Qin Jiao extract showed a better inhibitory effect on adjuvant arthritis rats, which may be related to the inhibition of JAK2/STAT3 signaling pathway [59]. Fu Ling significantly ameliorated renal injury in db/db mice, and the mechanism may be related to the inhibition of p38 MAPK phosphorylation and the activation of PPARγ pathway [60]. These results are consistent with the functional annotations of Du Huo (strengthening bones and reducing back and knee pain), Qin Jiao (dispelling rheumatism), and Fu Ling (strengthening the spleen and
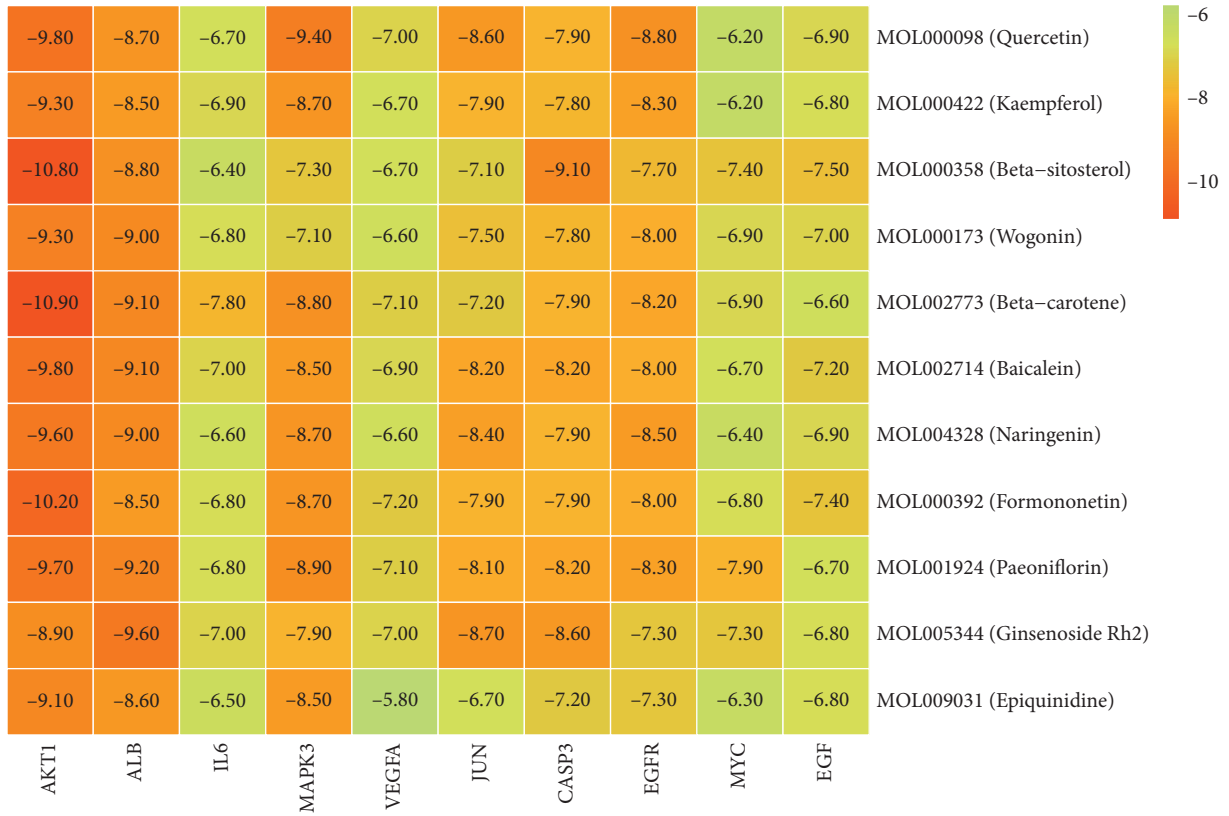
FIGURE 9: Heatmap of the docking scores of the active compounds of DHJSD and the target proteins.
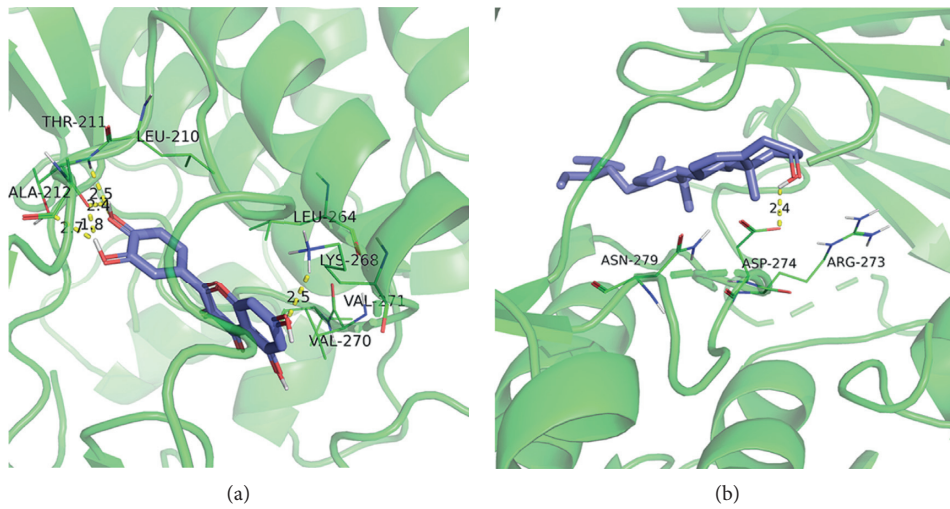

(a)

(b)

FIGURE 10: Continued.

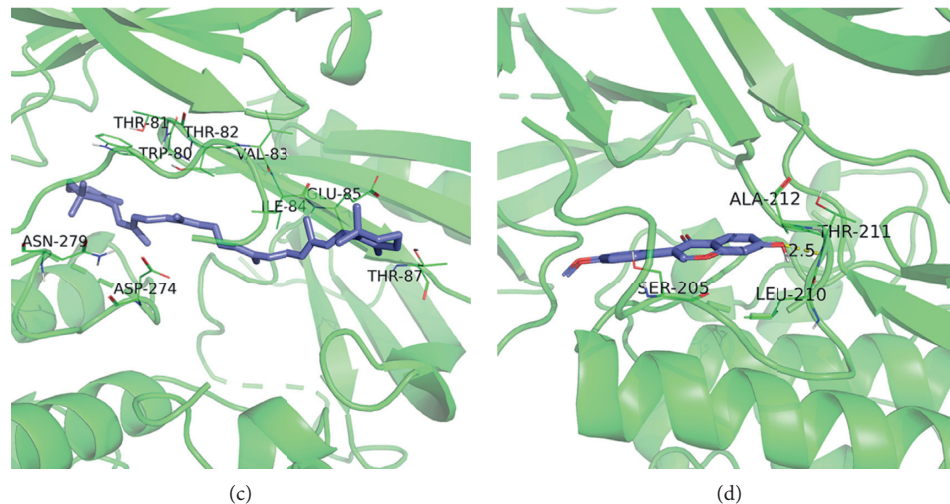(c)   (d)

Figure 10: Molecular docking results of "bioactive compound-hub gene." (a) Quercetin to AKT1; (b) Beta-sitosterol to AKT1; (c) Beta-carotene to AKT1; (d) Formononetin to AKT1.

benefiting the kidney) in TCM theory. The number of studies on the targets and pathways of other herbs for the treatment of osteoporosis is currently very limited, and this becomes our next research direction. By using modern pharmacological methods to explore the specific mechanisms by which DHJSD exerts its therapeutic effects, it is more beneficial to understand and complement TCM theories, and thus to uncover the essence of TCM and find alternative therapies for diseases.

5. Conclusion

By using the network pharmacology approach, we have studied the potential targets of DHJSD and the underlying mechanism of its anti-osteoporosis effect, which has the characteristics of multi-component, multi-target, and multi-pathway. AKT1, ALB, IL6, MAPK3, VEGFA, JUN, CASP3, EGFR, MYC, and EGF may be potential targets of DHJSD in treating osteoporosis. According to the results of enrichment analysis of KEGG pathway, we found pathways closely related to the pathological process of osteoporosis, mainly including AGE-RAGE signaling pathway in diabetic complications, osteoclast differentiation, MAPK signaling pathway, Wnt signaling pathway, PI3K-Akt signaling pathway, JAK-STAT signaling pathway, and TNF signaling pathway. Therefore, this study reveals that the anti-osteoporosis effect of DHJSD may be based on its direct or indirect regulation of the above-mentioned potential targets and pathways. DHJSD may provide a promising direction for future research, so enough relevant experimental research verification is needed, which is very important for revealing its exact regulatory mechanism.

Data Availability

The data used to support the findings of this study are included within the article.

Conflicts of Interest

The authors declare that there are no conflicts of interest regarding the publication of this article.

Acknowledgments

References

[1] H. Zheng, H. Feng, W. Zhang, Y. Han, and W. Zhao, "Targeting autophagy by natural product Ursolic acid for prevention and treatment of osteoporosis," *Toxicology and Applied Pharmacology*, vol. 409, 2020.

[2] J. Li, W. Wang, G Feng et al., "Efficacy and safety of Duhuo Jisheng decoction for postmenopausal osteoporosis: a systematic review and meta-analysis," *Evidence Based Complementary and Alternative Medicine*, vol. 2020, Article ID 6957825, 10 pages, 2020.

[3] J. A. Kanis, "Diagnosis of osteoporosis and assessment of fracture risk," *The Lancet*, vol. 359, no. 9321, p. 1929, 2002.

[4] N. Zhu and J. Hou, "Exploring the mechanism of action Xianlingubao Prescription in the treatment of osteoporosis by network pharmacology," *Computational Biology and Chemistry*, vol. 85, Article ID 107240, 2020.

[5] G. Li, Q. Xu, K. Han, W. Yan, and C. Huang, "Experimental evidence and network pharmacology-based analysis reveal the molecular mechanism of Tongxinluo capsule administered in coronary heart diseases," *Bioscience Reports*, vol. 40, no. 10, 2020.

[6] Y. Zhang, J. Jiang, H. Shen, Y. Chai, X. Wei, and Y. Xie, "Total flavonoids from Rhizoma Drynariae (Gusuibu) for treating osteoporotic fractures: implication in clinical practice," *Drug Design, Development and Therapy*, vol. 11, p. 1881, 2017.

[7] Z. Wu, X. Zhu, C. Xu, Y. Chen, L. Zhang, and C. Zhang, "Effect of Xianling Gubao capsules on bone mineral density in osteoporosis patients," *Journal of Biological Regulators and Homeostatic Agents*, vol. 31, no. 2, p. 359, 2017.

[8] B. Xia, B. Xu, Y. Sun et al., "The effects of Liuwei Dihuang on canonical Wnt/β-catenin signaling pathway in osteoporosis," *Journal of Ethnopharmacology*, vol. 153, no. 1, p. 133, 2014.

[9] N. Wang, H. Xin, P. Xu, Z. Yu, and D. Shou, "Erxian decoction attenuates TNF-α induced osteoblast apoptosis by modulating the akt/nrf2/HO-1 signaling pathway," *Frontiers in Pharmacology*, vol. 10, p. 988, 2019.

[10] W. Xiao, W. Sun, H. Lian, and J. Shen, "Integrated network and experimental pharmacology for deciphering the medicinal substances and multiple mechanisms of Duhuo Jisheng decoction in osteoarthritis therapy," *Evidence Based Complementary and Alternative Medicine*, vol. 2020, Article ID 7275057, 13 pages, 2020.

[11] Z. Xiong, P. Yi, L. Zhang, H. Ma, W. Li, and M. Tan, "Efficacy and safety of modified Duhuo Jisheng decoction in the treatment of lumbar disc herniation: a systematic review and meta-analysis," *Evidence Based Complementary and Alternative Medicine*, vol. 2020, Article ID 2381462, 11 pages, 2020.

[12] Y. Zhang and X. Guan, "Research situation in treatment of orthopedics diseases using Duhuo Jisheng decoction," *Journal of Practical Traditional Chinese Internal Medicine*, vol. 29, no. 4, p. 179, 2015.

[13] W. Liang, X. Li, and C. Li, "The core pathogenesis of postmenopausal osteoporosis-Gu Lou," *Chinese Journal of Gerontology*, vol. 35, no. 18, p. 5333, 2015.

[14] W. Zhang, S. Wang, R Zhang et al., "Evidence of Chinese herbal medicine Duhuo Jisheng decoction for knee osteoarthritis: a systematic review of randomised clinical trials," *BMJ Open*, vol. 6, no. 1, Article ID e008973, 2016.

[15] C.-S. Zheng, X.-J. Xu, H.-Z. Ye et al., "Computational approaches for exploring the potential synergy and polypharmacology of Duhuo Jisheng Decoction in the therapy of osteoarthritis," *Molecular Medicine Reports*, vol. 7, no. 6, p. 1812, 2013.

[16] Z.-C. Liu, Z.-L. Wang, C.-Y. Huang et al., "Duhuo Jisheng Decoction inhibits SDF-1-induced inflammation and matrix degradation in human degenerative nucleus pulposus cells in vitro through the CXCR4/NF-κB pathway," *Acta Pharmacologica Sinica*, vol. 39, no. 6, p. 912, 2018.

[17] J. Zhao, Q. Zha, M. Jiang, H. Cao, and A. Lu, "Expert consensus on the treatment of rheumatoid arthritis with Chinese patent medicines," *The Journal of Alternative and Complementary Medicine*, vol. 19, no. 2, p. 111, 2013.

[18] Y. Shuai, Z. Jiang, Q. Yuan, S. Tu, and F. Zeng, "Deciphering the underlying mechanism of Eucommiae cortex against osteoporotic fracture by network pharmacology," *Evidence Based Complementary and Alternative Medicine*, vol. 2020, Article ID 7049812, 12 pages, 2020.

[19] J. Ru, P. Li, J Wang et al., "TCMSP: a database of systems pharmacology for drug discovery from herbal medicines," *Journal of Cheminformatics*, vol. 6, no. 13, 2014.

[20] K. Tsaioun, B. Blaauboer, and T. Hartung, "Evidence-based absorption, distribution, metabolism, excretion (ADME) and its interplay with alternative toxicity methods," *ALTEX*, vol. 33, no. 4, p. 343, 2016.

[21] S. Sheng, Z. Yang, F. Xu, and Y. Huang, "Network pharmacology-based exploration of synergistic mechanism of guanxin II formula (II) for coronary heart disease," *Chinese Journal of Integrative Medicine*, vol. 27, no. 2, pp. 106–114, 2020.

[22] T. UniProt Consortium, "UniProt: the universal protein knowledge base," *Nucleic Acids Research*, vol. 46, no. 5, p. 2699, 2018.

[23] G. Stelzer, N. Rosen, I Plaschkes et al., "The GeneCards suite: from gene data mining to disease genome sequence analyses," *Current Protocols in Bioinformatics*, vol. 54, pp. 1–30, 2016.

[24] N. Rappaport, M. Twik, I. Plaschkes et al., "MalaCards: an amalgamated human disease compendium with diverse clinical and genetic annotation and structured search," *Nucleic Acids Research*, vol. 45, no. D1, p. D877, 2017.

[25] J. Piñero, J. M. Ramírez-Anguita, J Saüch-Pitarch et al., "The DisGeNET knowledge platform for disease genomics: 2019 update," *Nucleic Acids Research*, vol. 48, no. D1, p. D845, 2020.

[26] Y. Wang, S. Zhang, F Li et al., "Therapeutic target database 2020: enriched resource for facilitating research and early development of targeted therapeutics," *Nucleic Acids Research*, vol. 48, no. D1, p. D1031, 2020.

[27] A. Davis, C. Grondin, R Johnson et al., "Comparative Toxicogenomics database (CTD): update 2021," *Nucleic Acids Research*, vol. 49, no. D1, pp. D1138–D1143, 2020.

[28] J. Amberger and A. Hamosh, "Searching online mendelian inheritance in man (OMIM): a knowledgebase of human genes and genetic phenotypes," *Current Protocols in Bioinformatics*, vol. 58, 2017.

[29] P. Shannon, A. Markiel, O Ozier et al., "Cytoscape: a software environment for integrated models of biomolecular interaction networks," *Genome Research*, vol. 13, no. 11, p. 2498, 2003.

[30] D. Szklarczyk, J. H. Morris, H. Cook et al., "The STRING database in 2017: quality-controlled protein-protein association networks, made broadly accessible," *Nucleic Acids Research*, vol. 45, no. D1, p. D362, 2017.

[31] C. Xu, R. Li, and J. Wu, "Effects of Yuanhu-Zhitong tablets on alcohol-induced conditioned place preference in mice," *Biomedicine & Pharmacotherapy*, vol. 133, Article ID 110962, 2020.

[32] C. Chin, S. Chen, H. Wu, C. Ho, M. Ko, and C. Lin, "cytoHubba: identifying hub objects and sub-networks from complex interactome," *BMC Systems Biology*, vol. S11, 2014.

[33] Gene Ontology Consortium, "The Gene Ontology Consortium: Going forward," *Nucleic Acids Research*, vol. 43, Article ID D1049, 2015.

[34] M. Kanehisa, M. Araki, S Goto et al., "KEGG for linking genomes to life and the environment," *Nucleic Acids Research*, vol. 36, no. Database issue, p. D480, 2008.

[35] G. Yu, L.-G. Wang, Y. Han, and Q.-Y. He, "clusterProfiler: an R package for comparing biological themes among gene clusters," *OMICS: A Journal of Integrative Biology*, vol. 16, no. 5, p. 284, 2012.

[36] O. Trott and A. J. Olson, "AutoDock Vina: improving the speed and accuracy of docking with a new scoring function, efficient optimization, and multithreading," *Journal of Computational Chemistry*, vol. 31, no. 2, p. 455, 2010.

[37] S. Gao, J. Sun, X. Wang, Y. Hu, Q. Feng, and X Gou, "Research on the mechanism of qushi huayu decoction in the intervention of nonalcoholic fatty liver disease based on network pharmacology and molecular docking Technology," *BioMed Research International*, vol. 2020, Article ID 1704960, 12 pages, 2020.

[38] J. Chang, L. Liu, Y. Wang, Y. Sui, H. Li, and L. Feng, "Investigating the multitarget mechanism of traditional Chinese medicine prescription for cancer-related pain by using network pharmacology and molecular docking approach," *Evidence Based Complementary and Alternative Medicine*, vol. 2020, Article ID 7617261, 11 pages, 2020.

[39] I. Hers, E. E. Vincent, and J. M. Tavaré, "Akt signalling in health and disease," *Cellular Signalling*, vol. 23, no. 10, p. 1515, 2011.

[40] A. Mukherjee and P. Rotwein, "Selective signaling by Akt1 controls osteoblast differentiation and osteoblast-mediated osteoclast development," *Molecular and Cellular Biology*, vol. 32, no. 2, p. 490, 2012.

[41] P. F. Giampietro, C. McCarty, B. Mukesh et al., "The role of cigarette smoking and statins in the development of postmenopausal osteoporosis: a pilot study utilizing the Marshfield Clinic Personalized Medicine Cohort," *Osteoporosis International*, vol. 21, no. 3, p. 467, 2010.

[42] R. Wu, J. Ruan, Y Sun et al., "Long non-coding RNA HIF1A-AS2 facilitates adipose derived stem cells (ASCs) osteogenic differentiation through miR-665/IL6 axis via PI3K/Akt signaling pathway," *Stem Cell Research & Therapy*, vol. 9, no. 1, p. 348, 2018.

[43] A. Gupta, S. Upadhyaya, T. Cha, J. Schwab, C. Bono, and S. Hershman, "Serum albumin levels predict which patients are at increased risk for complications following surgical management of acute osteoporotic vertebral compression fractures," *The Spine Journal*, vol. 19, no. 11, p. 1796, 2019.

[44] Y. Yang, X. Zhou, Y Li et al., "CXCL2 attenuates osteoblast differentiation by inhibiting the ERK1/2 signaling pathway," *Journal of Cell Science*, vol. 132, no. 16, 2019.

[45] T. Yu, X. You, H. Zhou et al., "MiR-16-5p regulates postmenopausal osteoporosis by directly targeting VEGFA," *Aging*, vol. 12, no. 10, p. 9500, 2020.

[46] J.-J. Zhao, Z.-F. Wu, Y.-H. Yu, L. Wang, and L. Cheng, "Effects of interleukin-7/interleukin-7 receptor on RANKL-mediated osteoclast differentiation and ovariectomy-induced bone loss by regulating c-Fos/c-Jun pathway," *Journal of Cellular Physiology*, vol. 233, no. 9, p. 7182, 2018.

[47] L. You, W. Gu, L. Chen, L. Pan, J. Chen, and Y. Peng, "MiR-378 overexpression attenuates high glucose suppressed osteogenic differentiation through targeting CASP3 and activating PI3K/Akt signaling pathway," *International Journal of Clinical and Experimental Pathology*, vol. 7, no. 10, p. 7249, 2014.

[48] G. Liu, Y. Xie, J. Su et al., "The role of EGFR signaling in age-related osteoporosis in mouse cortical bone," *The FASEB Journal*, vol. 33, no. 10, p. 11137, 2019.

[49] J. Lorenzo, "The many ways of osteoclast activation," *Journal of Clinical Investigation*, vol. 127, no. 7, p. 2530, 2017.

[50] H. Derakhshanian, M. Djalali, A. Djazayery et al., "Quercetin prevents experimental glucocorticoid-induced osteoporosis: a comparative study with alendronate," *Canadian Journal of Physiology and Pharmacology*, vol. 91, no. 5, p. 380, 2013.

[51] Z. Yuan, J. Min, Y Zhao et al., "Quercetin rescued TNF-alpha-induced impairments in bone marrow-derived mesenchymal stem cell osteogenesis and improved osteoporosis in rats," *American Journal of Translational Research*, vol. 10, no. 12, p. 4313, 2018.

[52] M. Li, R. Cong, L. Yang, L. Yang, Y. Zhang, and Q. Fu, "A novel lncRNA LNC_000052 leads to the dysfunction of osteoporotic BMSCs via the miR-96-5p-PIK3R1 axis," *Cell Death & Disease*, vol. 11, no. 9, p. 795, 2020.

[53] H. Li, J. Fan, L. Fan et al., "MiRNA-10b reciprocally stimulates osteogenesis and inhibits adipogenesis partly through the TGF-β/SMAD2 signaling pathway," *Aging and Disease*, vol. 9, no. 6, p. 1058, 2018.

[54] A. Damerau, T. Gaber, S. Ohrndorf, and P. Hoff, "JAK/STAT activation: a general mechanism for bone development, homeostasis, and regeneration," *International Journal of Molecular Sciences*, vol. 21, no. 23, 2020.

[55] H. Jin, Z. Shao, Q. Wang et al., "Sclareol prevents ovariectomy-induced bone loss in vivo and inhibits osteoclastogenesis in vitro via suppressing NF-κB and MAPK/ERK signaling pathways," *Food & Function*, vol. 10, no. 10, p. 6556, 2019.

[56] J. Zha, X. Wang, and J. Di, "MiR-920 promotes osteogenic differentiation of human bone mesenchymal stem cells by targeting HOXA7," *Journal of Orthopaedic Surgery and Research*, vol. 15, no. 1, p. 254, 2020.

[57] W.-J. Liu, Z.-M. Jiang, Y. Chen et al., "Network pharmacology approach to elucidate possible action mechanisms of Sinomenii Caulis for treating osteoporosis," *Journal of Ethnopharmacology*, vol. 257, Article ID 112871, 2020.

[58] Q. Yao, N. Gao, Y. Ci, and Z. Li, "The therapeutic effect of Angelicae Pubescentis Radix on osteoporosis related to up-regulating Wnt/β-catenin signaling pathway in rats," *Progress of Anatomical Sciences*, vol. 25, no. 5, p. 532, 2019.

[59] L. Yang, W. Lin, and L. Deng, "Function of Gentiana macrophylla Pall on the Regulating JAK2/STAT3 signal pathway in adjuvant arthritis rats," *Clinical Journal of Traditional Chinese Medicine*, vol. 28, no. 6, p. 848, 2016.

[60] J. Li and D. Zhou, "Renal protection action of pachymaran and effects on p38 MAPK/PPAR-γ signaling pathway in db/db mice," *Chinese Journal of Traditional Medical Science and Technology*, vol. 26, no. 3, p. 346, 2019.

Research Article

Mechanism of Modified Danggui Sini Decoction for Knee Osteoarthritis Based on Network Pharmacology and Molecular Docking

Chaoqun Feng [1] **, Min Zhao,** [2] **Leiming Jiang,** [1] **Ziang Hu,** [1] **and Xiaohong Fan** [1]

[1]*Department of Orthopedics, Hospital of Chengdu University of Traditional Chinese Medicine, Chengdu 610075, China*
[2]*Chengdu University of Traditional Chinese Medicine, Chengdu 610075, China*

Correspondence should be addressed to Xiaohong Fan; fanxiaohong@cdutcm.edu.cn

Objective. This study aimed to explore the mechanism of Modified Danggui Sini Decoction in the treatment of knee osteoarthritis via a combination of network pharmacology and molecular docking. *Methods*. The main chemical components and corresponding targets of Modified Danggui Sini Decoction were searched and screened in TCMSP database. The disease targets of knee osteoarthritis were summarized in GeneCards, OMIM, PharmGkb, TTD, and DrugBank databases. The visual interactive network of "drugs-active components-disease targets" was drawn by Cytoscape 3.8.1 software. The protein-protein interaction network was constructed by STRING database. Then, GO function and KEGG pathway enrichment were analyzed by Bioconductor/R, and the pathway of the highest degree of correlation with knee osteoarthritis was selected for specific analysis. Finally, molecular docking was used to screen and verify core genes by AutoDockTools software. *Results*. Seventy-one main components of Modified Danggui Sini Decoction and 116 potential therapeutic targets of knee osteoarthritis were selected. The KEGG pathway and the GO function enrichment analysis showed that the targets of Modified Danggui Sini Decoction in the treatment of knee osteoarthritis were mainly concentrated on PI3K-Akt signaling pathway, TNF signaling pathway, IL-17 signaling pathway, apoptosis signaling pathway, Toll-like receptor signaling pathway, Th17 cell differentiation signaling pathway, HIF-1 signaling pathway, and NF-κB signaling pathway. It mainly involved inflammatory reaction, regulation of apoptotic signaling pathway, cellular response to regulation of inflammatory response, cellular response to oxidative stress, and other biological processes. The molecular docking results showed that ESR1-wogonin, MAPK1-quercetin, RELA-wogonin, RELA-baicalein, TP53-baicalein, TP53-quercetin, and RELA-quercetin have strong docking activities. *Conclusion*. Modified Danggui Sini Decoction has the hierarchical network characteristics of "multicomponent, multitarget, multifunction, and multipathway" in the treatment of knee osteoarthritis. It mainly regulates the proliferation and apoptosis of chondrocytes by regulating the PI3K-Akt signaling pathway and establishes cross-talk with many downstream inflammatory-related pathways to reduce the overall inflammatory response. Meanwhile, HIF-1 expression was used to ensure the normal function and metabolism of knee joint under hypoxia condition, and the above processes play a key role in the treatment of knee osteoarthritis.

1. Introduction

Knee osteoarthritis (KOA) is a common degenerative bone and joint disease, which is caused by the imbalance of degradation synthesis coupling of chondrocytes, extracellular matrix, and subchondral bone under the action of mechanical and biological factors [1]. Among them, articular cartilage damage is the most important pathological change

of KOA, which is mainly mediated by inflammatory reactions, leading to chondrocyte apoptosis and cartilage matrix degradation [2].

Modified Danggui Sini Decoction is a classic prescription of Traditional Chinese Medicine (TCM) in treating KOA. It is composed of Danggui nourishing blood and Guizhi warming meridians, which is combined as the monarch medicine. Baishao helps Danggui to nourish blood

and harmonize nutrient, and Xixin helps Guizhi to warm and dredge blood vessels. It is supplemented with Tongcao, Niuxi, and Duzhong to invigorate kidney and bone, leading meridians to the affected areas. The whole prescription is used for warming yang and dispersing cold, nourishing blood and unblocking pulse, warming without dryness, tonifying without stagnation, and playing the effect of "warming meridians, dispersing cold, nourishing blood, and unblocking pulse" [3]. Previous clinical studies have confirmed that this prescription is safe and effective in the treatment of KOA, but there is still a lack of relevant research on its mechanism [4].

Network pharmacology, based on the discipline concept of "multigene, multitarget, and multidisease," coincides with the medication thinking of TCM and has become a new mode which is suitable for the systematic development of TCM. Based on the network pharmacology, the chemical components of Modified Danggui Sini Decoction were scientifically screened and systematically predicted, and the "drugs-active components-disease targets" interaction network was established. Combined with GO function analysis, KEGG pathway enrichment analysis, and molecular docking technology, the mechanism and scientific connotation of Modified Danggui Sini Decoction in the treatment of KOA were revealed, providing an objective experimental basis for clinical application of TCM treatment of KOA, and providing new ideas and methods for the treatment of orthopedic and traumatology related diseases guided by TCM theory.

2. Data and Methods

2.1. Chemical Components and Targets of Modified Danggui Sini Decoction. Choose TCMSP (https://tcmspw.com/) Database [5], with the oral bioavailability (OB) ≥30% and drug-likeness (DL) ≥0.18 as the screening conditions [6, 7], the constituent herbs of Modified Danggui Sini Decoction were searched in turn, and the main chemical components of the prescription were obtained after supplementing the common components recorded in *Chinese Pharmacopoeia* [8]. Meanwhile, the corresponding targets of the above chemical components were sorted out, and the target genes annotation was completed by selecting the species as "*Homo sapiens*" in UniProt (https://www.uniprot.org/) database.

2.2. Targets Genes of KOA. We selected GeneCards [9], OMIM [10], PharmGKB [11], TTD [12], and DrugBank [13] disease-related databases and searched with "knee osteoarthritis" as the keyword. Among them, the retrieval results of GeneCards database were filtered with "correlation score >1." The related genes of KOA were collected and a Venn map was drawn.

2.3. Potential Targets of Modified Danggui Sini Decoction in the Treatment of KOA. Using R language to match the annotated compound targets and the summarized KOA disease targets, the intersection genes were derived, and the potential targets of Modified Danggui Sini Decoction in

treating KOA were obtained, and a Venn diagram was drawn.

2.4. Construction of Regulatory Network and Protein-Protein Interaction Network. The software of Cytoscape 3.8.1 [14] was used for visual analysis, and the above chemical components and target relationship were imported into the software, and the regulatory network diagram of "drugs-active components-potential therapeutic targets of disease" was drawn, and the color and shape of the visualization grid were adjusted according to different node properties.

The obtained potential therapeutic targets were imported into the STRING (https://string-db.org/) network platform [15], the research species was set as "*Homo sapiens*," the highest reliability (score >0.9) was selected by comprehensive scoring, the discrete targets were hidden, the network diagram of protein-protein interaction (PPI) was constructed, and TSV format file was exported. The TSV file was imported into the software of Cytoscape 3.8.1, and the topological analysis was carried out by CytoNCA plug-in. With the values of betweenness, closeness, degree, eigenvector, and local average connectivity-based method and network greater than the median value, the core gene network was obtained.

2.5. GO Function and KEGG Pathway Enrichment Analysis. Go function analysis and KEGG pathway enrichment analysis were performed using Bioconductor (https://www.bioconductor.org/) platform and R language to analyze the GO function and KEGG pathway enrichment of the potential targets for the treatment of KOA. Through the related scripts, the tables of GO function analysis and KEGG pathway enrichment analysis were derived by R language. In GO function analysis, the top 10 items of biological process (BP), cellular component (CC), and molecular function (MF) were selected for visualization. In KEGG pathway enrichment analysis, the top 30 items were selected for visualization. The barplot was used to draw the histogram, and the bubble was used to make the bubble diagram.

2.6. Molecular Docking. The core genes were selected to find the related drug components in the compound regulatory network as small molecular ligands. The 2D structure information of drug chemical components was downloaded from PubChem (https://www.ncbi.nlm.nih.gov/) platform and converted into the 3D structure by ChemBio3D software, and the energy optimization of MM2 was carried out to complete the preparation of small molecule ligands. The 3D structure of the candidate target proteins was downloaded from PDB (http://www.rcsb.org/) database, and then the protein receptors were prepared after the water molecules and ligands were removed by PyMOL2.4.0 software. Autodocktools software was used to read the receptor files, which were converted to PDBQT format after hydrotreating ion modification. The ligand files were also converted to PDBQT format for saving and then converted into the 2D structure to draw the active pockets. Finally, AutoDock vina

software will be used for molecular docking, and the lowest free energy model is selected for visual analysis.

3. Results

3.1. Main Components of Modified Danggui Sini Decoction and Treatment Targets of KOA. Through TCMSP database, the constituent herbs of Modified Danggui Sini Decoction were searched in turn. After screening by "OB ≥30% and DL≥0.18", we searched the *Chinese Pharmacopoeia* for supplement and got 71 main chemical components of Modified Danggui Sini Decoction, including 3 kinds of Danggui, 7 kinds of Guizhi, 13 kinds of Baishao, 8 kinds of Xixin, 4 kinds of Tongcao, 20 kinds of Niuxi, and 16 kinds of Duzhong (Table 1). A total of 931 target genes were obtained by UniProt gene annotation simultaneously.

Through GeneCards, OMIM, and other disease-related databases, a total of 1812 KOA disease targets were collected (Figure 1). By matching the targets of Modified Danggui Sini Decoction with KOA related targets, one hundred and sixteen cross-genes were derived, which were potential targets of Modified Danggui Sini Decoction in treating KOA (Figure 2).

3.2. Construction of Regulatory Network and PPI Network. Using Cytoscape 3.8.1, the regulatory network of "drugs-active components-disease targets" was drawn (Figure 3). The network consists of 42 chemical component nodes, 116 potential therapeutic targets, and 306 edges. The circular node represents the chemical composition of the drug, and the rectangular node represents the gene target. The size of the visualization node is adjusted according to the degree value of the gene targets. The results showed that the top five components with the highest degree were quercetin (degree = 88), kaempferol (degree = 35), wogonin (degree = 29), baicalein (degree = 19), and beta-sitosterol (degree = 14). It is speculated that these components may be the key active components of Modified Danggui Sini Decoction in treating KOA.

The potential therapeutic targets of Modified Danggui Sini Decoction in the treatment of KOA were imported into the STRING network platform to obtain PPI network diagram (Figure 4). The network contains 103 nodes and 401 edges. After calculating the median value of each parameter, thirty targets were obtained with "betweenness >46.20, closeness >0.21, degree >6, eigenvector >0.05, local average connectivity-based method >2.40, and network >3.10" as the first screening parameters. Similarly, twelve core targets were obtained by the second screening with parameters greater than median value, i.e., "betweenness >7.77, closeness >0.55, degree >8, eigenvector >0.13, local average connectivity-based method >4.14, and network >5.31" (Figure 5, Table 2).

3.3. GO Function and KEGG Pathway Enrichment Analysis. After GO function analysis, a total of 2363 GO entries were obtained ($P < 0.05$), and the top 10 items of BP, CC, and MF were selected for visualization (Figure 6). In the histogram,

the redder the color is, the higher the enrichment degree is and the stronger the possibility of drug target is. According to the results of the biological processes, active components of Modified Danggui Sini Decoction in the human body mainly include response to lipopolysaccharide, response to molecular of bacterial origin, cellular response to chemical stress, response to metal ion, and response to oxidative stress. Cellular components mainly include membrane raft, membrane microdomain, membrane region, vesicle lumen, secretory granule lumen. The molecular functions mainly include nuclear receptor activity, ligand-activated transcription factor activity, protease binding, heme binding, and tetrapyrrole binding. The rich biological functions, to some extent, explain the reason why the same prescription can treat multiple diseases and also lay the foundation for exploring the effective ingredients and searching for signaling pathways.

Through KEGG pathway enrichment analysis, a total of 150 related signal pathways of Modified Danggui Sini Decoction in the treatment of KOA were obtained ($P < 0.05$), and the top 30 items were listed for visual analysis (Figure 7). In the bubble diagram, the abscissa represents the ratio of the gene, the color also reflects the enrichment degree, and the bubble size represents the number of genes. The enrichment pathways mainly include fluid shear stress and atherosclerosis, AGE-RAGE signaling pathway in diabetic complications, kaposi sarcoma-associated herpesvirus infection, human cytomegalovirus infection, PI3K-Akt signaling pathway, hepatitis B, TNF signaling pathway, and IL-17 signaling pathway. The PI3K-Akt pathway, which is closely related to inflammatory response and bone metabolism, is selected as an example (Figure 8). The red labeled nodes are the targets of Modified Danggui Sini Decoction, which indicates that the prescription plays a key role in the PI3K-Akt signaling pathway by regulating marker targets.

3.4. Molecular Docking. In order to further verify the prediction results of the network, and to elaborate the mechanism and scientific connotation of Modified Danggui Sini Decoction as a classic Chinese medicine prescription in the treatment of KOA, quercetin, kaempferol, wogonin, baicalein, and β-sitosterol were selected as the top active components for molecular docking with Jun, TP53, ESR1, MAPK1, and RELA in turn. The binding energy between drug component ligands and target receptors is an important indicator to evaluate the binding capacity. It is generally considered that the docking affinity is stronger when the binding energy is less than −5.0 kcal/mol, and the docking activity is extremely strong when the binding energy is less than −7.0 kcal/mol [16]. From the docking results (Figure 9, Table 3), it was found that ESR1-wogonin, MAPK1-quercetin, RELA-wogonin, RELA-baicalein, TP53-baicalein, TP53-quercetin, and RELA-quercetin had the lower binding energies. In addition, quercetin and wogonin have the largest number of receptors as ligands. It is speculated that Modified Danggui Sini Decoction mainly participates in the treatment of KOA from the above molecular docking process.

TABLE 1: Main chemical components of Danggui Sini Decoction.

| Drug	Meridian tropism	Number of compounds	Part of components
Danggui	Liver, heart, spleen	3	Ferulic acid, beta-sitosterol, stigmasterol
Guizhi	Heart, lung, bladder	7	Beta-sitosterol, taxifolin
Baishao	Liver, spleen	13	Paeoniflorin, beta-sitosterol, kaempferol
Xixin	Heart, lung, kidney	8	Cryptopine, kaempferol
Tongcao	Lung, stomach	4	Sitosterol, tetrapanoside B_qt
Niuxi	Liver, kidney	20	Wogonin, baicalein, kaempferol, quercetin
Duzhong	Liver, kidney	16	Pinoresinol diglucoside, beta-sitosterol
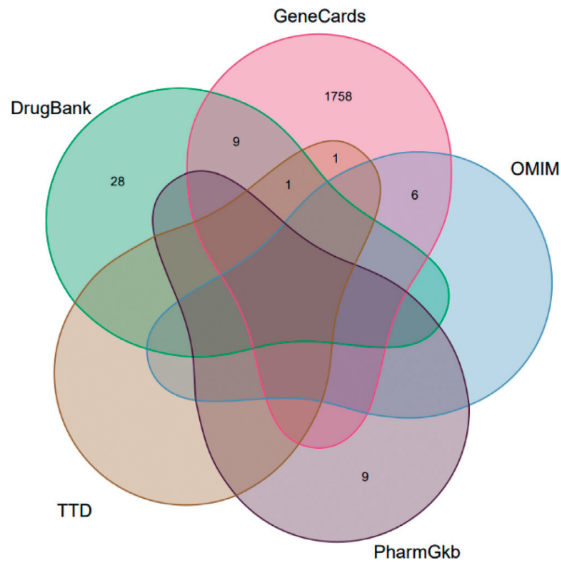
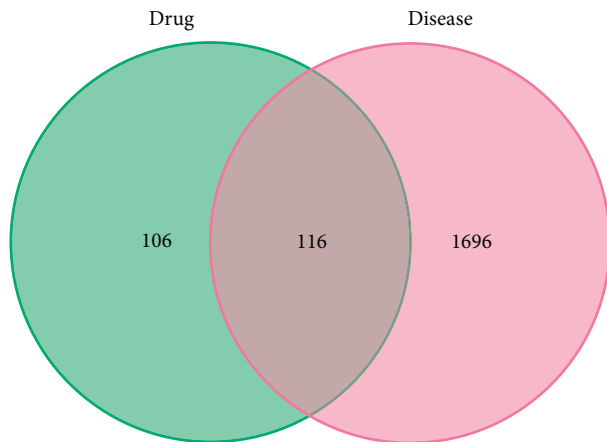FIGURE 1: Venn diagram of KOA disease targets.

FIGURE 2: Venn diagram of Danggui Sini Decoction and KOA targets.

4. Discussion

As a cultural treasure inherited for thousands of years, TCM has accumulated rich clinical experience, especially in the field of Traditional Chinese Medicine prescriptions. With the advancement of the modernization of Chinese herbal medicine, many studies have applied network pharmacology to explore the pharmacological mechanism of herbal medicine and prescription [17–19], and to carry out the

research on the compatibility law and action mechanism of TCM, which also provides new ideas and methods for the scientific development and innovation of Chinese medicine. In order to systematically understand the mechanism of Modified Danggui Sini Decoction in the treatment of KOA, OB and DL were used as the important criteria for drug composition screening, a total of 71 main chemical components were obtained, and 116 potential therapeutic targets were obtained by matching the corresponding drug targets with the KOA disease targets. After further statistical mining, 12 core targets, 2363 GO functional enrichment items, and 150 KEGG related pathways were obtained, which explained that Modified Danggui Sini Decoction has the hierarchical network characteristics of "multicomponent, multitarget, multifunction, and multichannel" in the treatment of KOA.

The classical compatibility theory of TCM emphasizes that the four parts of monarch, minister, adjuvant, and messenger are combined to achieve synergy and minimize toxic and side effects integrally. Among them, the "messenger" mainly provides the effects of guiding the active ingredients to reach the target organs and harmonizing the actions of these agents [20, 21]. In addition, according to modern pharmacology and network biology, the drug mechanism of the TCM rules has been verified from a molecular/system level [7]. In this study, Dazao and Gancao, as the "messenger," did not participate in the direct treatment of the disease. Therefore, in order to avoid bias or redundancy in the results, the two herbs were not included.

4.1. Potential Active Ingredients of Modified Danggui Sini Decoction in Treating KOA. In this study, the top five chemical components with the highest degree were quercetin, kaempferol, wogonin, baicalein, and β-sitosterol. At present, a considerable number of studies have proved that quercetin can significantly inhibit articular chondrocyte apoptosis and delay cartilage degeneration by reducing oxidative stress and endoplasmic reticulum stress, so as to achieve the purpose of treating KOA [22–24]. In addition, kaempferol has obvious anti-inflammatory and therapeutic effects on arthritis by inhibiting inflammatory factors such as IL-1B, NO, and PGE2 [25]. Wogonin can treat osteoarthritis by inhibiting oxidative stress, inflammation, and matrix degradation related to osteoarthritis, and regulating the redox activity of chondrocytes [26]. Baicalein can effectively inhibit the expression of inflammatory factors and slow down chondrocyte apoptosis and cartilage
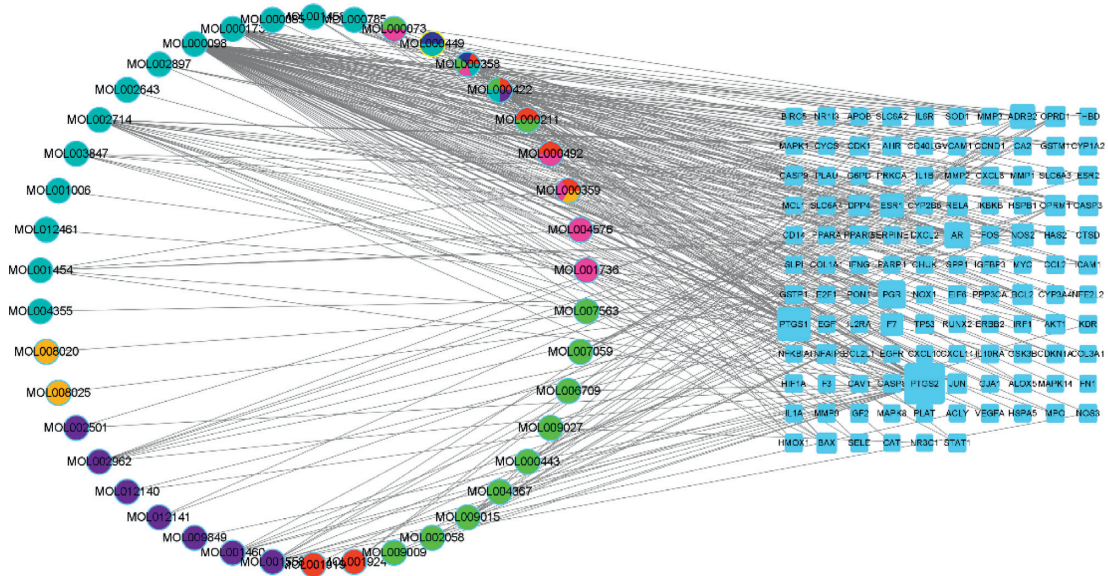
Figure 3: The "drug-active components-disease target" network. *Note.* the pink round is Guizhi, the green one is Duzhong, the red one is Baishao, the purple one is Xixin, the orange one is Tongcao, the cyan one is Niuxi, and the blue one is Danggui.
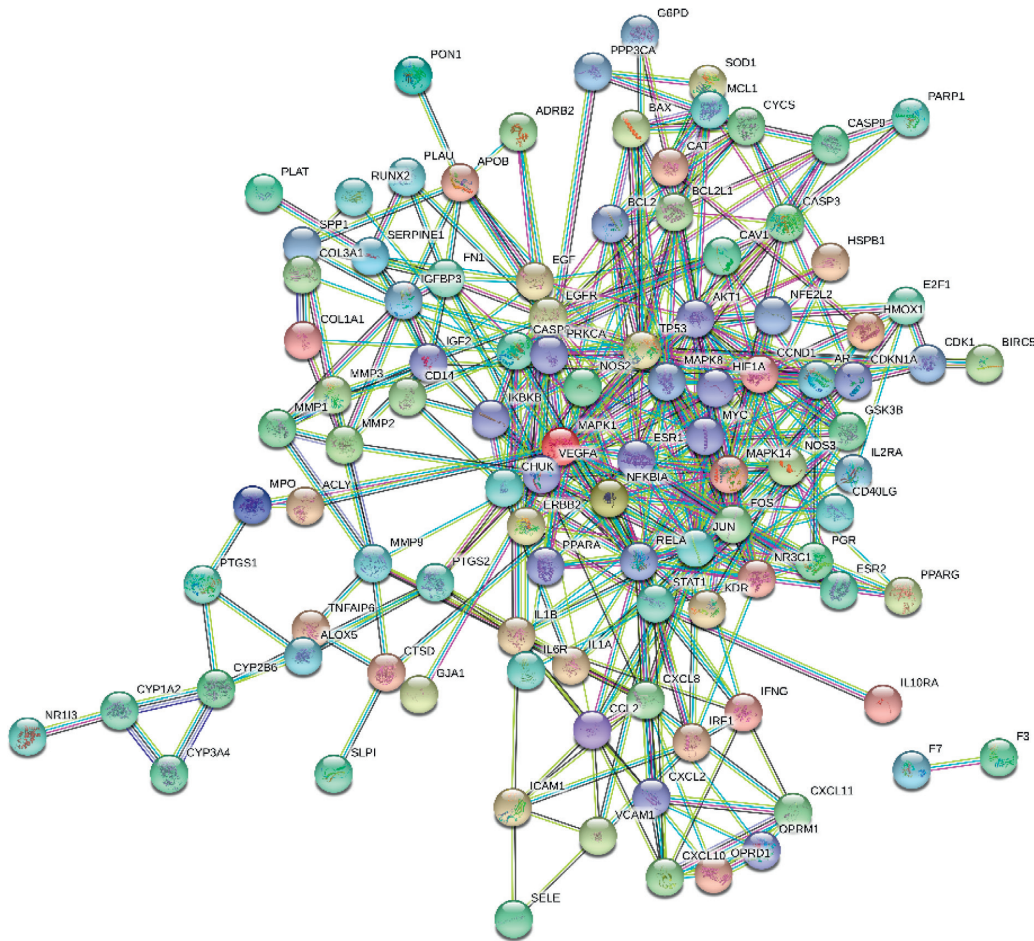

Figure 4: Protein-protein interaction network.

degradation in the treatment of osteoarthritis [27]. β-sitosterol is one of the main components of cell membrane and has an estrogen-like effect. It is known to be effective for hypercholesterolemia, heart disease, immune system regulation, and cancer prevention [28, 29], but there is no treatment research in KOA field.
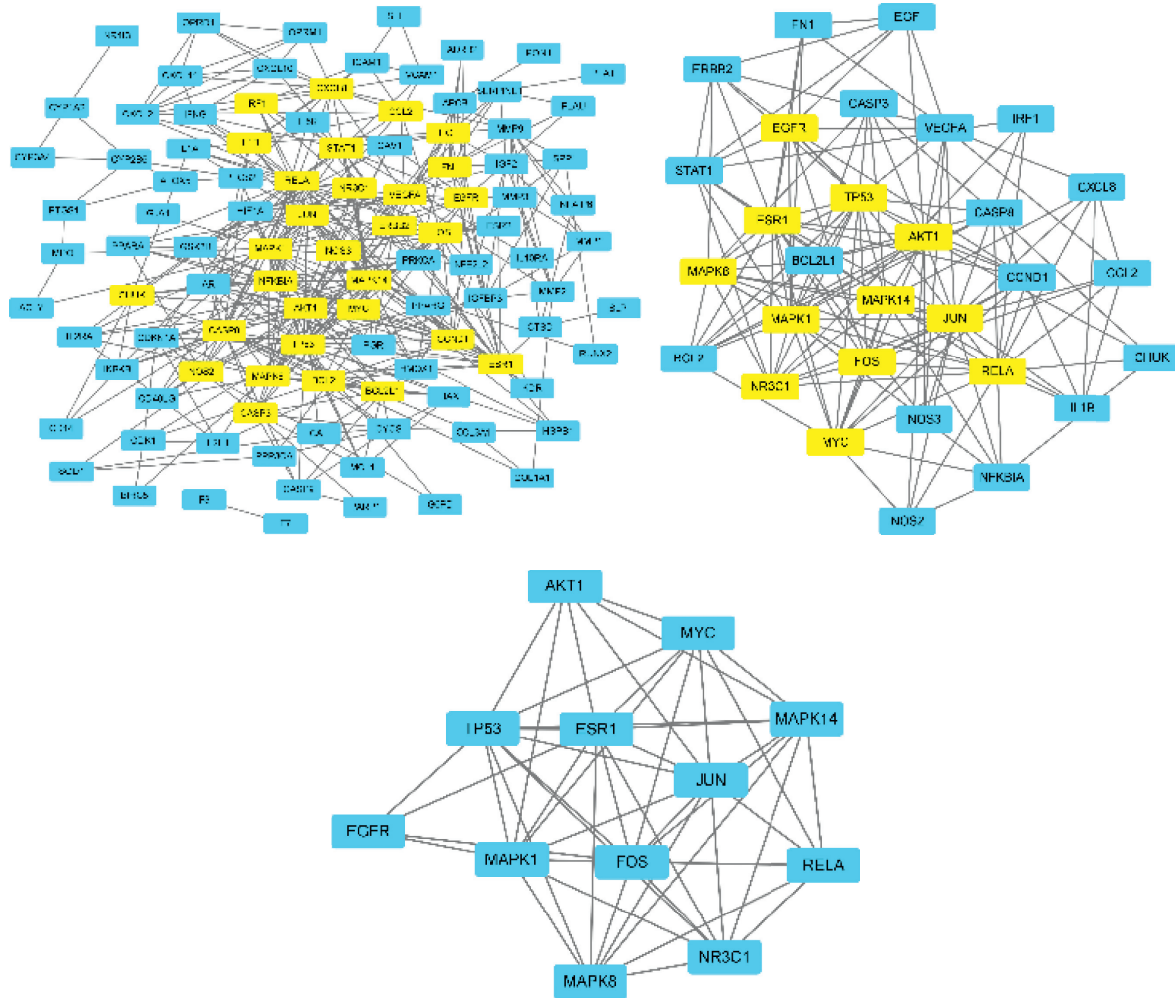
Figure 5: Core genes. *Note.* Yellow nodes are the core genes obtained after screening.

Table 2: Core genes.

Name	Betweenness	Closeness	Degree	Eigenvector	LAC	Network
ESR1	47.50	0.69	16	0.28	7	11.33
MAPK8	22.59	0.63	12	0.23	6	7.68
TP53	53.06	0.71	17	0.30	7.41	12.82
EGFR	14.99	0.57	10	0.16	4.60	6.52
MAPK14	42.57	0.66	14	0.25	5.86	8.35
NR3C1	9.50	0.60	10	0.21	6.20	7.68
MAPK1	61.51	0.69	16	0.28	6.50	10.31
FOS	14.57	0.63	12	0.24	7	8.39
JUN	92.05	0.74	19	0.31	7.16	15.30
MYC	14.59	0.63	12	0.24	6.83	8.99
AKT1	76.72	0.67	15	0.24	4.80	8.17
RELA	71.50	0.67	16	0.24	5.38	10.97

Therefore, the main active components and efficacy of Modified Danggui Sini Decoction are similar to the results of network pharmacology analysis. Meanwhile, it is speculated that β-sitosterol has the value of research and development in anti-KOA treatment.

4.2. *Mechanism Analysis of Modified Danggui Sini Decoction in Treating KOA.* KEGG pathway and GO function enrichment analysis showed that the targets of Modified Danggui Sini Decoction in the treatment of KOA mainly concentrated on PI3K-Akt signaling pathway, TNF signaling
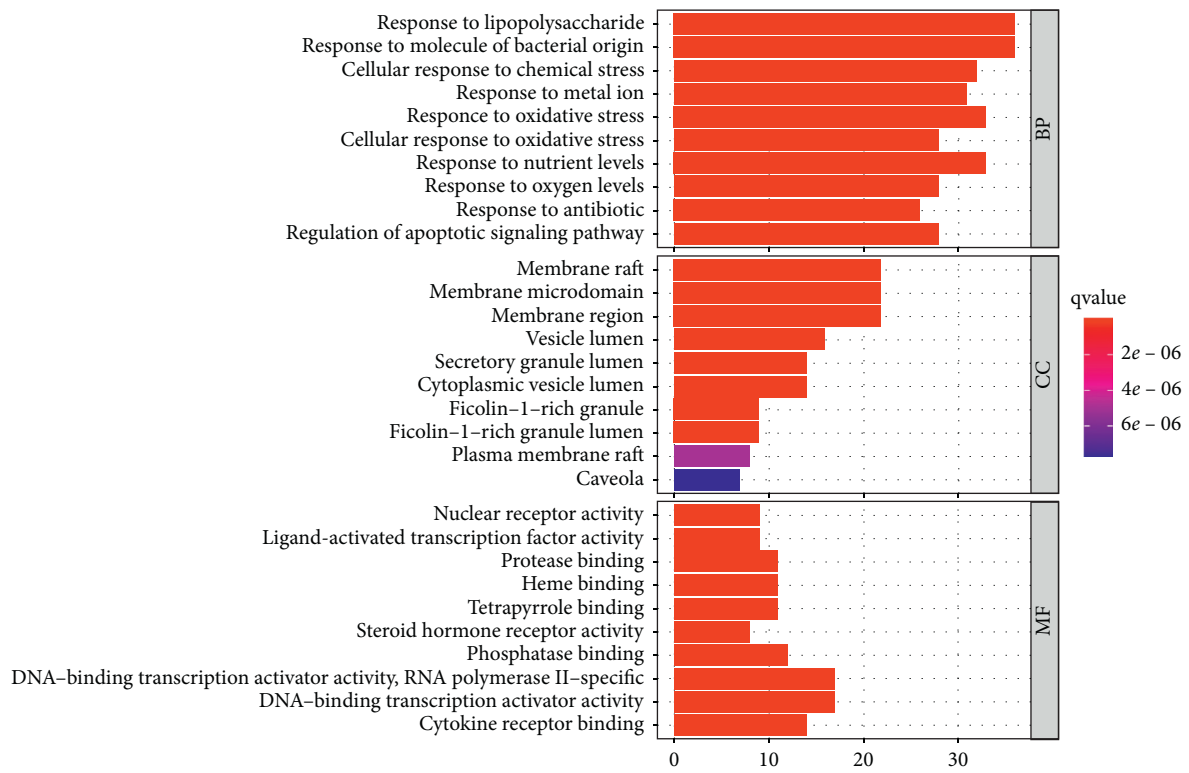
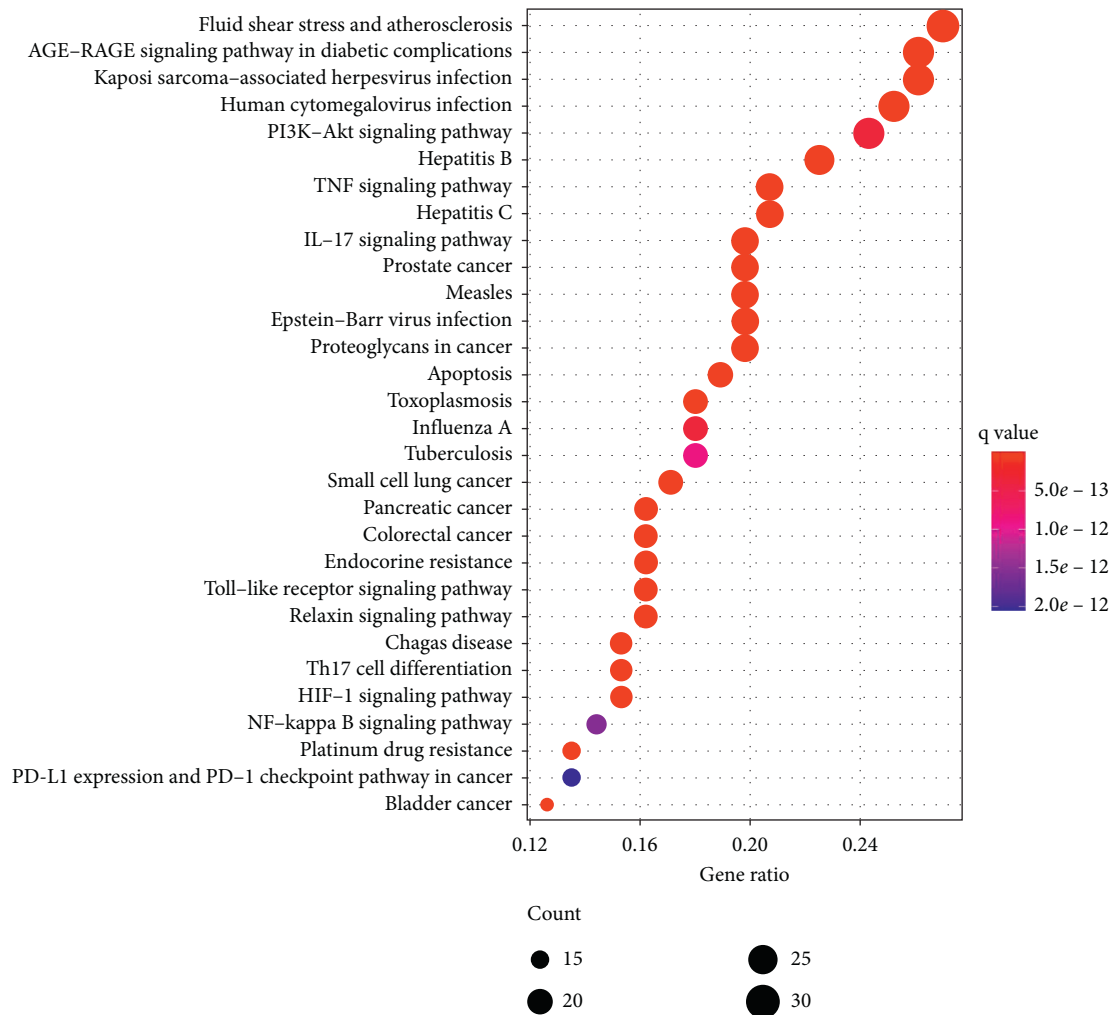Figure 6: Go function analysis.

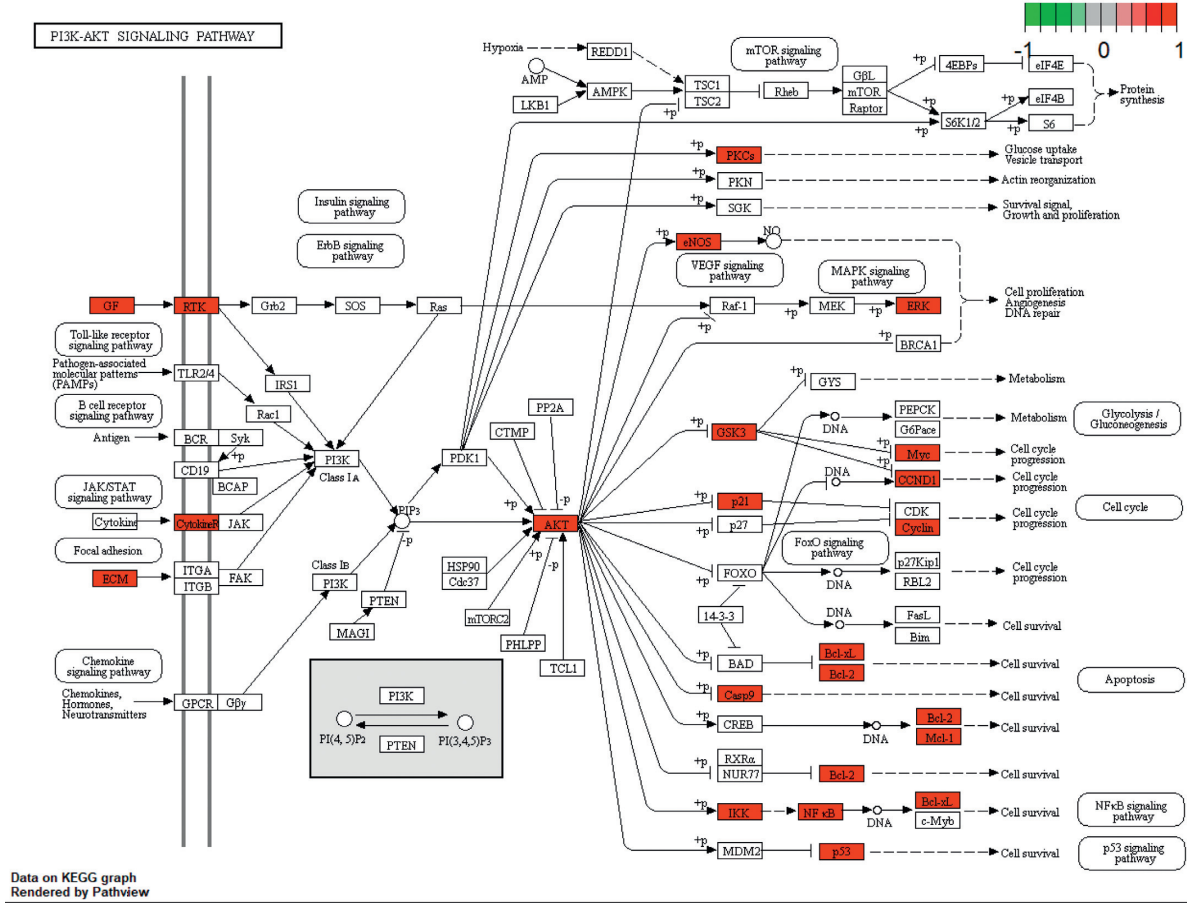Figure 7: KEGG pathway analysis.
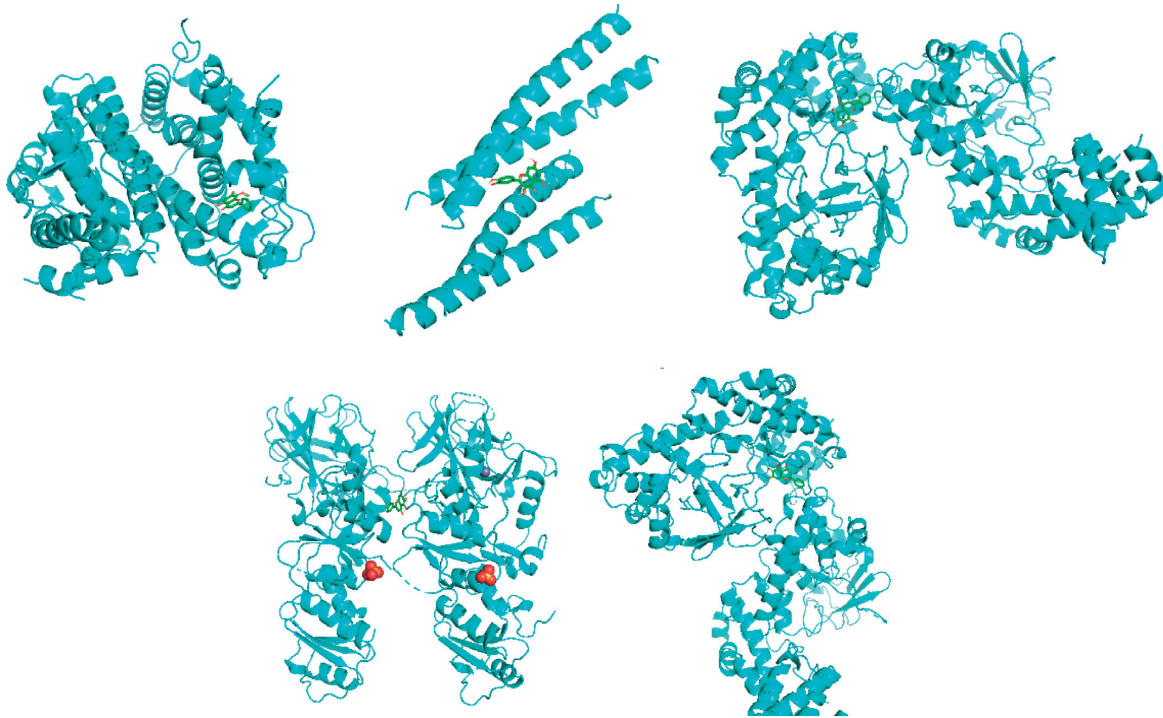
FIGURE 8: PI3K-Akt signaling pathway.

FIGURE 9: Molecular docking. *Note.* A is ESR1-wogonin molecular docking, B is MAPK1-quercetin molecular docking, C is RELA-wogonin molecular docking, D is RELA-baicalein molecular docking, and E is TP53-baicalein molecular docking.

TABLE 3: Molecular docking (unit: kcal/mol).

Molecule name	JUN	TP53	ESR1	MAPK1	RELA
Quercetin	−6.6	−7.2	NA	−8.2	−7.2
Kaempferol	−6.4	NA	NA	NA	−7.1
Wogonin	−6.4	−6.9	−9.0	NA	−7.8
Baicalein	NA	−7.4	NA	NA	−7.6
Beta-sitosterol	−6.7	NA	NA	NA	NA

pathway, IL-17 signaling pathway, apoptosis, Toll-like receptor signaling pathway, Th17 cell differentiation, HIF-1 signaling pathway, and NF-κB signaling pathway. It mainly involves inflammatory reaction, regulation of apoptosis signaling pathway, cell response to chemical stress, cell response to oxidative stress, and other biological processes.

Among them, the PI3K-Akt signaling pathway is an important signal transduction pathway for regulating cell proliferation, differentiation, and apoptosis and promoting related tissue regeneration [30]. Akt can also activate specific downstream targets and interact with NF-κB, mTOR, and P53 pathways. TNF in the tumor necrosis factor signaling pathway is an inflammatory mediator with many biological effects. TNF-α can induce the production of IL-6 and activate the protease that decomposes cartilage and synovium [31]. Activation of Toll-like receptor signaling pathway can release inflammatory factors such as IL and TNF, activate NF-κB in its downstream signaling pathway, and induce apoptosis of articular chondrocytes [32]. As a hypoxia inducible factor, HIF-1 can induce the survival of hypoxic chondrocytes in hypoxic environment by maintaining the hypoxia balance state, which plays an important role in ensuring the normal physiological function and metabolism of knee joint cartilage [33]. In the NF-κB signaling pathway, a variety of upstream signal factors, including TNF, can activate IKK, thus express downstream genes of NF-κB, including MMP-9, P65, and P50, and then produce a cascade of inflammatory reactions and accelerate the decomposition and destruction of articular cartilage [34]. In addition, the IL-17 signaling pathway promotes the expression of inflammatory factors, which leads to the degradation of cartilage matrix. The Th17 signaling pathway can regulate osteoclast differentiation and promote bone resorption [35]. Thus, Modified Danggui Sini Decoction mainly regulates the proliferation and apoptosis of chondrocytes by regulating PI3K-Akt pathway and establishes cross-talk with many downstream inflammatory-related pathways to reduce the overall inflammatory responses. Meanwhile, HIF-1 expression was used to ensure the normal function and metabolism of knee joint under hypoxia condition, so as to play a role in the treatment of KOA.

At present, among the many regulatory pathways involved in KOA, the specific mechanism of some signaling pathways is still unclear, and there may be more complex interactions between the pathways, which jointly participate in the proliferation and apoptosis of chondrocytes, as well as the synthesis and degradation of extracellular matrix. Recent studies have found that the PI3K-Akt-mTOR signaling pathway also plays an important role in the pathogenesis of KOA. mTOR, as another serine/threonine protein kinase

downstream of PI3K-Akt, is closely related to cell apoptosis, autophagy, cell survival, and structural reorganization [36, 37].

In conclusion, the main active components and efficacy of Modified Danggui Sini Decoction are similar to the results of network pharmacology analysis. Meanwhile, it also points out the direction for the follow-up study on the mechanism of Modified Danggui Sini Decoction in the treatment of KOA. This study is only searched through the databases. It did not take into account the clinical dosage, decocting conditions, and other factors brought by the impact. Thus, the next step requires further experimental verification and clinical research.

Data Availability

The datasets used and/or analyzed during the current study are available from the corresponding author on reasonable request.

Disclosure

C. Feng and M. Zhao are co-first authors.

Conflicts of Interest

The authors declare that they have no conflicts of interest.

Authors' Contributions

C. Feng and M. Zhao contributed equally to this paper. C. Feng and M. Zhao designed the study, analyzed the data, and wrote the manuscript. Z. Hu analyzed the data. L. Jiang and X. Fan revised the manuscript. All authors read and approved the final manuscript.

Acknowledgments

Supplementary Materials

Supplementary Table 1: all chemical components of Modified Danggui Sini Decoction. Supplementary Table 2: the results of GO function enrichment analysis. Supplementary Table 3: the results of KEGG enrichment analysis. (*Supplementary Materials*)

References

[1] J. K. Roush, A. R. Cross, W. C. Renberg et al., "Evaluation of the effects of dietary supplementation with fish oil omega-3 fatty acids on weight bearing in dogs with osteoarthritis," *Journal of the American Veterinary Medical Association*, vol. 236, no. 1, pp. 67–73, 2010.

[2] S. Piera, D. Lakshmi, H. Lai Janice et al., "Collagen VI enhances cartilage tissue generation by stimulating chondrocyte proliferation," *Tissue Engineering. Part A*, vol. 21, no. 3-4, pp. 840–849, 2015.

[3] W. Deng and M. Ding, "Clinical study on the treatment of knee osteoarthritis with modified Danggui Sini decoction," *Chinese Herbal Medicine*, vol. 33, no. 5, pp. 840-841, 2010.

[4] Y. Yu, Q. Zhou, X. Fan et al., "Observation of effect of modified Danggui Sini decoction with hot medicated compress of TCM on knee osteoarthritis," *Shanxi Traditional Chinese Medicine*, vol. 33, no. 7, pp. 11-12+16, 2017.

[5] J. Ru, Li Peng, J. Wang et al., "TCMSP: a database of systems pharmacology for drug discovery from herbal medicines," *Journal of Cheminformatics*, vol. 6, no. 1, p. 13, 2014.

[6] X. Xu, W. Zhang, C. Huang et al., "A novel chemometric method for the prediction of human oral bioavailability," *International Journal of Molecular Sciences*, vol. 13, no. 6, pp. 6964–6982, 2012.

[7] W. Tao, X. Xu, X. Wang et al., "Network pharmacology-based prediction of the active ingredients and potential targets of Chinese herbal radix curcumae formula for application to cardiovascular disease," *Journal of Ethnopharmacology*, vol. 145, no. 1, pp. 1–10, 2013.

[8] The State Pharmacopoeia Commission of PR China, *Pharmacopoeia of the People's Republic of China*, vol. 1, pp. 142+177–178, China Medical Science and Technology Press, Beijing, Chuna, 2020.

[9] S. Marilyn, D. Irina, J. Alexander et al., "GeneCards Version 3: the human gene integrator," *Database: The Journal of Biological Databases and Curation*, vol. baq020, 2010.

[10] J. S. Amberger, C. A. Bocchini, F. Schiettecatte, A. F. Scott, and A. Hamosh, "OMIM.org: online Mendelian Inheritance in Man (OMIM), an online catalog of human genes and genetic disorders," *Nucleic Acids Research*, vol. 43, no. D1, pp. D789–D798, 2015.

[11] M. Whirl-Carrillo, E. M. McDonagh, J. M. Hebert et al., "Pharmacogenomics knowledge for personalized medicine," *Clinical Pharmacology & Therapeutics*, vol. 92, no. 4, pp. 414–417, 2012.

[12] Y. Wang, S. Zhang, F. Li et al., "Therapeutic target database 2020: enriched resource for facilitating research and early development of targeted therapeutic," *Nucleic Acids Research*, vol. 48, no. D1, pp. D1031–D1041, 2020.

[13] D. S. Wishart, Y. D. Feunang, A. C. Guo et al., "DrugBank 5.0: a major update to the DrugBank database for 2018," *Nucleic Acids Research*, vol. 46, no. D1, pp. D1074–D1082, 2018.

[14] P. Shannon, A. Markiel, O. Owen et al., "Cytoscape: a software environment for integrated models of biomolecular interaction networks," *Genome Research*, vol. 13, no. 11, pp. 2498–2504, 2003.

[15] S. Damian, A. L. Gable, D. Lyon et al., "STRING v11: protein-protein association networks with increased coverage, supporting functional discovery in genome-wide experimental datasets," *Nucleic Acids Research*, vol. 47, no. D1, pp. D607–D613, 2019.

[16] K.-Y. Hsin, S. Ghosh, and K. Hiroaki, "Combining machine learning systems and multiple docking simulation packages to improve docking prediction reliability for network pharmacology," *PLoS One*, vol. 8, no. 12, p. e83922, 2013.

[17] X. Zhang, W. Chen, G. Tu et al., "Mechanisms of Ertong Huichun Granules in treatment of respiratory virus infection diseases by network pharmacology and molecular docking," *Chinese Traditional and Herbal Drugs*, vol. 51, no. 19, pp. 5010–5018, 2020.

[18] S. Hu, T. Liu, Z. Tong et al., "Study on the mechanism of yupingfeng powder in the treatment of non-small cell lung cancer based on network pharmacology and molecular docking method [J/OL]," *Journal of Hainan Medical University*, vol. 1-17, 2020.

[19] Y. Li, Q. Feng, R. Tan et al., "Molecular mechanism of Eucommia ulmoides active ingredients treating synovitis of knee osteoarthritis: an analysis based on network pharmacology," *Chinese Journal of Tissue Engineering Research*, vol. 25, no. 5, pp. 765–771, 2021.

[20] K. Chan, "Progress in traditional Chinese medicine," *Trends in Pharmacological Sciences*, vol. 16, no. 6, pp. 182–187, 1995.

[21] T.-P. Fan, J.-C. Yeh, K. W. Leung et al., "Angiogenesis: from plants to blood vessels," *Trends in Pharmacological Sciences*, vol. 27, no. 6, pp. 297–309, 2006.

[22] C. Yue, K. Bauerova, B. Stringa et al., "Quercetin reduced inflammation and increased antioxidant defense in rat adjuvant arthritis," *Archives of Biochemistry and Biophysics*, vol. 583, pp. 150–157, 2015.

[23] N. Haleagrahara, S. Miranda-Hernandez, M. A. Alim et al., "Therapeutic effect of quercetin in collagen-induced arthritis," *Biomedicine & Pharmacotherapy*, vol. 90, pp. 38–46, 2017.

[24] K. Feng, Z. Chen, L. Pengcheng, S. Zhang, and X. Wang, "Quercetin attenuates oxidative stress-induced apoptosis via SIRT1/AMPK-mediated inhibition of ER stress in rat chondrocytes and prevents the progression of osteoarthritis in a rat model," *Journal of Cellular Physiology*, vol. 234, no. 10, pp. 18192–18205, 2019.

[25] Z. Zhuang, G. Ye, and B. Huang, "Kaempferol alleviates the interleukin-1β-induced inflammation in rat osteoarthritis chondrocytes via suppression of NF-κB," *Medical Science Monitor*, vol. 23, pp. 3925–3931, 2017.

[26] N. M. Khan, A. Haseeb, M. Y. Ansari, P. Devarapalli, S. Haynie, and T. M. Haqqi, "Wogonin, a plant derived small molecule, exerts potent anti-inflammatory and chondroprotective effects through the activation of ROS/ERK/Nrf2 signaling pathways in human Osteoarthritis chondrocytes," *Free Radical Biology and Medicine*, vol. 106, pp. 288–301, 2017.

[27] X. Zhang, Y. Zhu, X. Chen et al., "Baicalein ameliorates inflammatory-related apoptotic and catabolic phenotypes in human chondrocytes," *International Immunopharmacology*, vol. 21, no. 2, pp. 301–308, 2014.

[28] S. Saeidnia, A. Manayi, R. Gohari A et al., "The story of beta-sitosterol-a review," *European Journal of Medicinal Plants*, vol. 4, no. 5, pp. 590–609, 2014.

[29] Y. H. Ju, L. M. Clausen, K. F. Allred, A. L. Almada, and W. G. Helferich, "β-sitosterol, β-sitosterol glucoside, and a mixture of β-sitosterol and β-sitosterol glucoside modulate the growth of estrogen-responsive breast cancer cells in vitro and in ovariectomized athymic mice," *The Journal of Nutrition*, vol. 134, no. 5, pp. 1145–1151, 2004.

[30] J.-C. Xi, H.-Y. Zang, L.-X. Guo et al., "The PI3K/AKT cell signaling pathway is involved in regulation of osteoporosis," *Journal of Receptors and Signal Transduction*, vol. 35, no. 6, pp. 640–645, 2015.

[31] O. Stannus, G. Jones, F. Cicuttini et al., "Circulating levels of IL-6 and TNF-α are associated with knee radiographic osteoarthritis and knee cartilage loss in older adults," *Osteoarthritis and Cartilage*, vol. 18, no. 11, pp. 1441–1447, 2010.

[32] A. Nair, V. Kanda, C. Bush-Joseph et al., "Synovial fluid from patients with early osteoarthritis modulates fibroblast-like synoviocyte responses to toll-like receptor 4 and toll-like receptor 2 ligands via soluble CD14," *Arthritis & Rheumatism*, vol. 64, no. 7, pp. 2268–6877, 2012.

[33] L. Zhang, L. Zhang, Z. Huang et al., "Increased HIF-1α in knee osteoarthritis aggravate synovial fibrosis via fibroblast-like

synoviocyte pyroptosis," *Oxidative Medicine and Cellular Longevity*, vol. 2019, Article ID 6326517, 11 pages, 2019.

[34] L. Wu, X. Huang, L. Li, H. Huang, R. Xu, and W. Luyten, "Insights on biology and pathology of HIF-1α/-2α, TGFβ/ BMP, wnt/β-catenin, and NF-κB pathways in osteoarthritis," *Current Pharmaceutical Design*, vol. 18, no. 22, pp. 3293–3312, 2012.

[35] K. Sato, A. Suematsu, K. Okamoto et al., "Th17 functions as an osteoclastogenic helper T cell subset that links T cell activation and bone destruction," *Journal of Experimental Medicine*, vol. 203, no. 12, pp. 2673–2682, 2006.

[36] K. Wang, M. Chu, F. Wang et al., "Putative functional variants of PI3K/AKT/mTOR pathway are associated with knee osteoarthritis susceptibility," *Journal of Clinical Laboratory Analysis*, vol. 34, no. 6, p. e23240, 2020.

[37] J.-F. Xue, Z.-M. Shi, J. Zou et al., "Inhibition of PI3K/AKT/ mTOR signaling pathway promotes autophagy of articular chondrocytes and attenuates inflammatory response in rats with osteoarthritis," *Biomedicine & Pharmacotherapy*, vol. 89, pp. 1252–1261, 2017.